UNIVERSITÀ DEGLI STUDI DI NAPOLI 'FEDERICO II'

Scuola Politecnica e delle Scienze di Base

Ph.D. School in Chemical Sciences

XXX Cycle

Molecular olefin polymerization catalysts: applications of molecular design for properties modulation

Francesco Zaccaria

Supervisor:

Prof. Vincenzo Busico

Assessor:

Prof. Francesco Ruffo

Ph.D. School Coordinator:

Prof. Luigi Paduano

2014-2017

Abstract

Olefin polymerization is an industrial sector of huge economic and social impact. In this context, molecular catalysts have drawn much attention since 1990s, as they can be used for the industrial production of advanced polymeric material which are hardly accessible by heterogeneous Ziegler-Natta technology. The growing commercial demand is pushing research toward the identification of novel active species for the synthesis of innovative (co)polymer architectures. Advances in experimental and especially computational technologies foster the ambition of catalyst development *by design*, but the passage from the 'classical' trial-and-error to a fully rational approach is hampered by the complex interactions between all species in the catalytic pool and the many complex subtleties that molecular design has to balance.

This PhD thesis explores several issues related to rational catalyst development, trying to contribute to a more detailed understanding of the polymerization process by a combined experimental and computational approach. The first part of the work deals with the identification of structure/ properties correlations for the selective synthesis of specific products. In particular, **Chapter 2** is dedicated to factors determining reactivity ratios in ethene/α-olefin copolymerization reactions. A suitable computational protocol to accurately reproduce comonomer affinities for a large variety of molecular catalysts is proposed, and utilized to draw tentative conclusions on entropic, electronic and steric effects determining comonomer affinity. Important kinetic considerations on the rate limiting step for chain propagation are provided, potentially explaining the occasionally non-trivial temperature dependence of copolymerization statistics.

Due to the rapidly increasing demand, the production of comonomer (e.g. 1-hexene, 1-octene) feedstock has become an issue of growing relevance

for the polyolefin industry. **Chapter 3** summarizes the work carried out during a three months internship at the Imperial College London (UK), working on chromium-catalyzed ethene oligomerization for the selective production of linear α-olefins (LAOs). The case of bis(benzimidazolyl)amine Cr-catalysts was investigated, providing supporting evidence for a mechanistic and kinetic model explaining alternating distribution of products.

Along with the production of specific polymer architectures, activity and thermal stability are two key catalyst features to be considered in the design of novel active species, which are examined in the second part of this thesis. **Chapter 4** describes a novel chain transfer to solvent process that was recently discovered by our group. This involves CH activation of the toluene solvent by Ti-phosphinimide catalysts, leading to benzyl terminated polypropylenes, and represents a reversible deactivation route being competitive at high temperatures and moderately high pressures. Extensive polymerization and DFT screenings were carried out, aiming at elucidating the mechanism and exploring the scope of this reaction.

Finally, cocatalyst influence on polymerization performance is discussed in **Chapter 5**. Free-trimethylaluminum in commercial MAO solution was effectively trapped by addition of a hindered phenol, allowing to explore the properties of the oligomeric fraction of MAO by NMR spectroscopy. A phosphinimide half-titanocene was used as case study, taking advantage of the presence of a phosphorus atom in the ancillary ligand as spectroscopic probe for ^{31}P NMR. Consequences of the absence of free trialkyl aluminum on the formation of dormant sites are evaluated and connections with the mechanism of chain transfer to solvent are highlighted. This work was carried out in collaboration with the group of Prof. Alceo Macchioni and Prof. Cristiano Zuccaccia at the University of Perugia.

List of abbreviations

<	less than
>	more than
°	degrees
°C	degrees Celsius
Å	Ångstrom
All	Allyl
BBRA	Backbone Rearrangement
BDE	Bond dissociation energy
BIMA	bis(benzimidazolyl)methylamine
Bn	benzyl
BHE	β-H elimination
BHT	2,6-di-*tert*-butyl-4-methylphenol
bht	2,6-di-*tert*-butyl-4-methylphenolate
BHTM	β-H transfer to the monomer
Bn	Benzyl
Calc.	Calculated
CGC	Constrained Geometry Catalyst
Cy	Cyclohexyl
d	doublet
Da	Dalton (atomic mass unit)
DFT	Density Functional Theory
dMAO/BHT	dried MAO/BHT
e.g.	*exempli gratia*
eq.	equivalent(s)
et al.	*et alia*
Exp.	Experimental
FI	Phenoxy-imine (from the Japanese “Fenokishi-Imin”)

h	hours
Hom.	Homolysis
HTE	High Throughput Experimentation
HTC	High Throughput Computation
i.e.	*id est*
INS	insertion
iPP	isotactic Polypropylene
^{i}Pr	*iso*-propyl
HDPE	High Density Polyethylene
ISIP	Inner Sphere Ion Pair
J	coupling constant
K	Kelvin
k	kilo or kinetic constant
L	Litre or ancillary ligand
LAOs	Linear α-olefins
LDPE	Low Density Polyethylene
LLDPE	Linear Low Density Polyethylene
M	Molar concentration (mol/L)
m	multiplet or milli
m-	*meta*-
MAD	Mean Average Deviation
MAO	methylaluminoxane
Me	methyl
MHz	megahertrz
min	minutes
MMAO	Modified Methylaluminoxane
M_n	Number Average Molecular Weight
MW	Molecular Weight

M_w	Weight Average Molecular Weight
MWD	Molecular Weight Distribution
n.d.	not detected
N/A	Not Available
^{n}Bu	*n*-butyl
^{n}Pr	*n*-propyl
o-	*ortho*-
OSIP	Outer Sphere Ion Pair
p	pressure
p-	*para*-
PDI	Polydispersity Index
PCM	Polarized Continuum Model
PEP	*pseudo* Propylene-Ethylene-Propylene sequence
PES	Potential Energy Surface
Ph	Phenyl
PMAO-IP	Polimethylaluminoxane-Improved Performances
P_n	Polymerization Degree
ppm	parts-per-million
q	quartet
QM	Quantum Mechanics
RS	Resting State
RT	Room Temperature
ref.	reference
s	seconds *or* singlet
SBM	Sigma Bond Metathesis
t	triplet
T	Temperature
^{t}Bu	*tert*-butyl

TMA	trimethylaluminum
TiBA	tri-iso-butyl aluminum
TS	Transition State
TTB	trityl borate
UHMWPE	Ultra-High Molecular Weight Polyethylene
Vd+bl	vinylidene + 1-butenyl + 2-butenyl
vs.	*Versus*
ZN	Ziegler-Natta
δ	chemical shift
η	hapto
μ	bridging *or* micro

Acknowledgements

NMR microstructural analysis of polypropylene samples was carried out by Prof. Roberta Cipullo, whose help is gratefully acknowledged. I thank also Ing. Alessio Mingione, Ms Enrichetta Villano, Ms Alessia Napolitano and Mr Geremia Schiano Moriello (from *HTExplore Srl*) for their help in GPC and NMR polymer characterization. Most of the DFT calculations were carried out by using computational facilities at the University of Manitoba, Winnipeg (CA), which were kindly made available by the group of Prof. Peter H. M. Budzelaar.

Additionally, I would like to express my personal, heartfelt gratitude to a number of people. First, I wish to heartily thank my supervisor, Prof. Vincenzo Busico, for his support and guidance over the last (more than) three years. He allowed me freedom to work on projects that fascinated me and also provided direction when I got stuck. His dynamism and frankness has inspired the way I am trying to approach research in chemistry.

Though their name do not appear on the cover of this dissertation, I would like to convey my deepest gratitude to Prof. Roberta Cipullo and Prof. Peter H. M. Budzelaar, who have played different, yet complementary key roles in my scientific education and specifically in the three years of PhD. I was privileged to have them as co-supervisors to pursue the ambition of developing an 'hybrid set' of experimental and theoretical skills.

I am also very grateful to Dr. Christian Ehm for his generous advice concerning this work, daily supervision and constant moral support. His enthusiasm and intellectual contributions were essential in bringing this project to fruition.

I am greatly in debt to all the members of *Laboratory of Stereoselective Polymerization* group (and surroundings) for making the lab a pleasant place to work, and for their silent, everyday assistance and co-operation. To name but a few, I would like to thank Antonio Vittoria and Giuseppe Antinucci, who have

been my companions since the very beginning of my university experience; let's generally say that, despite several evident flaws, they are very nice guys!

During my PhD I spent time in London (UK) and Perugia (I), working in the groups of Prof. George Britovsek, and Proff. Alceo Macchioni and Cristiano Zuccaccia. I warmly thank them and all the members of their groups for their extraordinary kindness and generous contribution of knowledge and experience, as well as for the more informal and pleasant moments we shared.

Finally, this thesis not only marks the end of three years of work, but it also somehow represents the ~~end~~ restart of a personal life cycle. Although it is my strong belief that private things should be kept - indeed - *private*, I think this is a good occasion to make an exception and thank the wonderful people that have decorated my life up to now. I thank my parents, my family: what I am is the result of their love and dedication. To my closest friends - no need for fussy lists, I am sure they know who they are – my warmest gratitude; no personal achievement would have any value without the possibility to share it with them. To my lovely girlfriend, well, this is really our business…

Infine, questa tesi non rappresenta solo la conclusione di tre anni di lavoro, ma - in qualche modo – anche ~~la fine~~ il nuovo inizio di un ciclo di vita personale. Sebbene sia fortemente convinto che gli affari privati debbano essere tenuti – appunto – privati*, credo che questa sia una buona occasione per fare un'eccezione e ringraziare le persone meravigliose che hanno dato colorato la mia vita fino ad oggi. Innanzitutto ringrazio i miei genitori, la mia famiglia tutta: ciò che sono è il risultato del loro amore e dedizione. La mia più profonda gratitudine va ai miei amici più cari - non c'è bisogno di liste fastidiose, sono certo che queste persone sappiano; nessun traguardo personale avrebbe senso senza la possibilità di condividerlo con loro. Alla mia stupenda fidanzata, beh, questo è davvero affar nostro…*

Thank you all.

Table of Contents

Chapter 1

Introduction

1.1 – Industrial production of polyolefins: the role of molecular catalysts

Modern chemical industry largely relies on catalysts, as they serve the needs for highly selective, efficient and environmentally friendly processes.[1-2] In many cases, catalysts are tunable, providing control over efficiency, specificity and selectivity, and the success story of industrial olefin polymerization illustrates this.[3]

Polyethylene was originally commercialized in 1930s by Imperial Chemical Industries (ICI) with the use of a free radical process.[4] The reactor operated under rather harsh reaction conditions (200-300°C and 1000-4000 bar) and the resulting Low Density Polyethylene (LDPE) was a highly branched material with a limited range of properties and applications.[5] The development of metal-catalyzed olefin polymerization signified an enormous step forward in the field, which began in 1950s with the pioneering studies of Nobel laureates Ziegler[6] and Natta.[7] The heterogeneous titanium catalysts they developed led to a variety of linear homo- and co-polymers that dramatically broadened the application range of polyolefins. Industrial plants based on Ziegler-Natta (ZN) technology for the production of isotactic polypropylene (iPP) started operating already in 1957.[3] In the same period, parallel research at the Phillips Petroleum Company in the U.S. had developed chromium-systems for oligo- and polymerization of ethene to produce fuels and linear High Density Polyethylene (HDPE) respectively.[8-9]

Driven by these two breakthroughs, continuous innovations have led the polyolefin industry to be dominated by catalytic processes which currently account for more than 50 wt% of the current global thermoplastics production (estimated around 300 million tons in 2015).[3, 10] Polyolefins are widely differentiated products, ranging from rigid thermoplastics to flexible elastomers

and waxes; they are increasingly replacing critical materials such as steel, glass and ceramics. The origin of this huge commercial success lies in their low cost and outstanding combination of properties, reflecting reliable and versatile production processes.

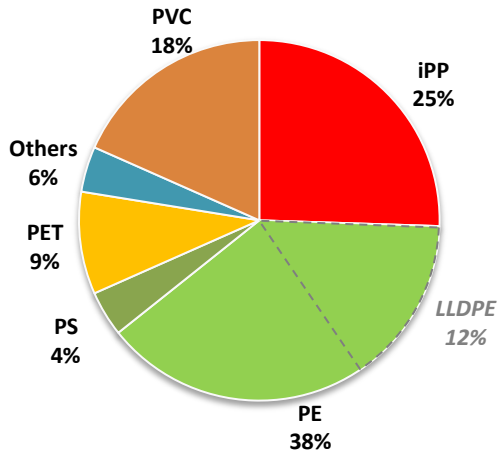

Figure 1.1 – Composition of the major thermoplastics 2014 demand.[11] iPP = isotactic polypropylene; LLDPE = Linear Low Density Polyethylene; PE = polyethylene(s); PS = polystyrene; PET = Polyethyleneterephthalate; PVC = polyvinylchloride.

ZN catalysts are still the workhorse of industrial polyolefin production, and virtually hold a monopoly on the production of iPP, the most common thermoplastic (Figure 1.1).[12] They are generally based on $TiCl_4$ supported on $MgCl_2$ crystals, in combination with organic donors and aluminum alkyls. These relatively cheap systems convert readily available monomers in the final products with 100% atom efficiency, excellent morphology control and extremely high productivities (well above 1 ton of PP per gram of Ti). Solvent-free gas phase reactors can be used under relatively mild conditions (80-110°C, 20-40 bar), further contributing to minimize energy demand for fabrication.

There is still a drive towards further optimization. However, rational engineering of $MgCl_2$ surfaces is made difficult by the limited structural understanding at a molecular level of adsorbed Ti active sites, although some

progress has been made recently.[13-16] While clear correlations are still to be identified, it is known that the choice of donors can serve to tune catalyst selectivity and access specific products, making iPP a versatile material that is successfully applied to packaging, pipes, textiles, lightweight automotive engineering and many other fields.[17] Thanks to these qualities metering of environmental impacts based on Life Cycle Assessment (a tool that quantifies the environmental impacts resulting from the production, use, and disposal of a product or process), listed iPP as the first (and HDPE as the second) polymer in the ranking of sustainability in 2010, despite problems related to recovery, biodegradability and renewability.[18]

In the last few decades, the growing demand for novel commodity plastics has led specialized grades of polyethylene to acquire sizeable market shares. One of the main protagonists of this development is Linear Low Density Polyethylene (LLDPE), which nowadays accounts for ~12% of the global thermoplastic production (Figure 1.1). While radical-produced LDPE is hyper branched, LLDPE is a substantially linear polymer bearing shorter or longer side chains on the polyethylene backbone, which result from the incorporation of an α-olefin like 1-hexene or 1-octene (Figure 1.2). The higher tensile strength, impact and puncture resistance of LLDPE represented a revolutionary innovation for the production of films in the packaging industry.[19]

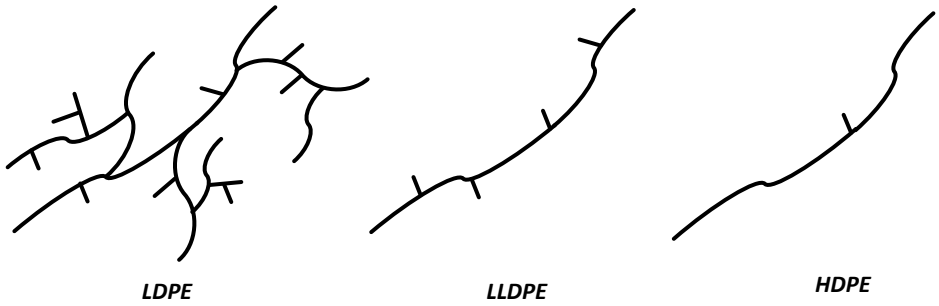

Figure 1.2 – Pictorial comparison between microstructure of LDPE, LLDPE and HDPE.

It should be noted, however, that LDPE has retained a quite important role in the realm of polyolefins. It is still produced under similar conditions to those developed by ICI, because (1) its microstructure is not accessible *via* catalytic routes (yet) and (2) the metal-free process renders the product non-toxic and ideal for food packaging.[3] Furthermore, it is often blended with LLDPE to modulate its processability properties.

Sparsely branched HDPE (Figure 1.2) is largely used for pipes and constructions elements, since it offers several potential advantages over traditional materials like steel, ductile iron and polyvinylchloride (PVC) in terms of durability, chemical and corrosion resistance, range of temperature tolerance, leak avoidance, lightweight and flexibility.[20] Copolymers of ethene with propene (Ethylene-Propylene Rubbers, EPR) and analogous terpolymers with dienes (Ethylene-Propylene-Diene Monomer, EPDM) find applications as rubbers.[19] Ultra-High Molecular Weight Polyethylene (UHMWPE) is also gaining relevance in fibers and biomedicine markets.[21]

The reactivity of active sites in a ZN catalyst can differ noticeably, depending on the chemical surrounding of adsorbed Ti centers (*e.g.* different surfaces on $MgCl_2$ crystals, steric hindrance provided by adsorbed donors, etc.). The multisite nature of heterogeneous ZN systems becomes particularly evident and disadvantageous in copolymerization reactions, due to the different comonomer affinity of the various types of Ti centers. For this reason, they represent only a portion of the ethene-based copolymer production, which largely relies on single-center molecular catalysts.[22]

Thanks to their well-defined structure, molecular catalysts can be more easily tuned and characterized, and generally exhibit single center behavior giving relatively sharp molecular weight distributions (MWD). They allow better control over copolymer microstructure, which is highly desirable for the development of advanced materials; even in cases where the production of

blended polymers in the same reactor is of interest, mixtures of molecular rather than ZN catalysts are often preferable.[10]

Since late 1950s, group IV metallocenes in combination with aluminum alkyls had been known to catalyze olefin polymerization. Initially they served only as molecular models for mechanistic studies.[23-27] Commercial applications were hampered by low productivity and thermal stability, as well as by the more expensive synthesis compared to ZN catalysts. In this context, it should be noted that the price per unit of mass of the most common commodity polyolefins can be as small as ~1.5 times that of monomer feedstock; with such a narrow margin it is only due to the massive production volume of polyolefins that the sector can be profitable, and cheap and highly productive catalysts are essential to guarantee the sustainability of the industry.

In the 1980s, the replacement of conventional aluminum alkyls with methylaluminoxane (MAO) cocatalyst led to improved catalytic activities of several orders of magnitude.[28-31] MAO exhibits quite good solubility properties, and it can also be heterogenized by absorption on supports such as silica or alumina, making molecular catalysts suitable for both solution and gas phase reactors.[32] Its serendipitous discovery sparked a steady growth of molecular olefin polymerization catalysis, which rapidly evolved from questions of academic interest to address notable commercial needs. The possibility to synthesize higher-added-value polymers that were inaccessible with ZN systems, justified the use of slightly more expensive catalyst components.

Catalyst modification is the key to control of polymer architecture.[33-34] The evolution of metallocenes has generated a plethora of different species, for a large part based on ansa-zirconocenes (Figure 1.3a).[35] However, one of the most successful strategies to develop molecular catalysts has been to replace one or both of the Cp-type ligands with different anionic ligands.[36-38] Among these non-metallocene systems, *ansa*-cyclopentadienylamido Ti-complexes

introduced in early 1990s by Dow[39-40] and Exxon[41-42] represented the first class of group IV complexes to attract significant commercial attention. These Constrained Geometry Catalysts (CGC, Figure 1.3b) exhibit remarkable activity, molecular weight and comonomer incorporation capability up to an operating temperature of 160°C, which makes them ideal for the production of LLDPE.[22, 43]

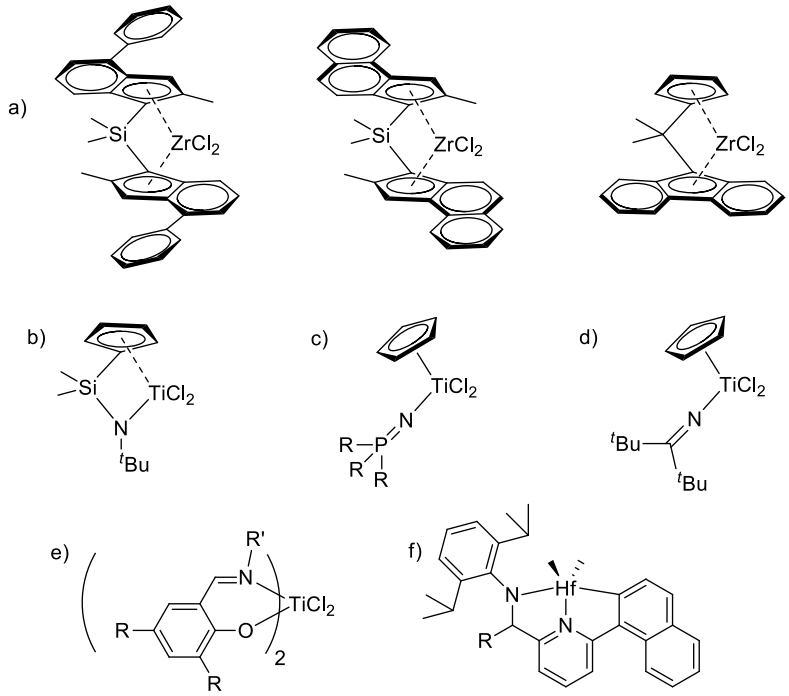

Figure 1.3 – Examples of prototypical metallocenes and non-metallocenes of commercial interest: a) *ansa*-zirconocenes, b) Constrained Geometry, c) phosphinimide, d) ketimide, e) phenoxy-imine and f) pyridylamido catalysts.

Several other non-metallocene systems are currently employed in industry.[37-38, 44] Different from metallocenes, they are often based on Ti, like the phosphinimide half-titanocenes introduced by Teuben in 1978,[45] and further developed as polymerization catalysts by Stephan and co-workers in the late 1990s (Figure 1.3c).[46-48] Currently they are applied to the industrial production

of commodity ethylene/α-olefin copolymers by Nova Chemicals,[49-52] UHMWPE fibers by DSM[53-54] and vinyl norbornene EPDM rubbers by Lanxess (now Arlanxeo).[55] Analogous ketimide complexes were first disclosed by Nova Chemicals [56-57] and then licensed by DSM[58,59] and eventually Lanxess[60] for the production of an advanced EPDM rubber with excellent elastomeric properties (Figure 1.3d).

Although *pseudo*-tetrahedral complexes are by far the most common, interesting examples of octahedral species can be found in the realm of Ti-based catalysts. Phenoxy-imine (also termed FI from the Japanese "Fenokishi-Imin") are versatile systems that allow easy catalyst tuning by modifying the substituents on the phenoxy and imino groups. First reported as Zr-complexes,[61] they were further developed as very active Ti based systems by Mitsui (Figure 1.3e) in the late 1990s.[62-63] They found their most interesting application in combination with Dow pyridylamido Hf-catalysts (Figure 1.3f) for the synthesis of multiblock copolymers with highly crystalline polyethylene and amorphous poly(ethylene-co-1-olefin) blocks.[64] These advanced materials were produced by using the chain shuttling reactions with diethyl zinc, first proposed by the group of Gibson for iron pyridyl–diimine complexes,[65-66] and represent one of the most intriguing current topics in olefin polymerization.[67] This brief overview provides a general picture of how broad the scope of catalyst modification is.

1.2 – Catalyst design

The possibilities to develop novel (co)polymer architectures and the relative commercial demand are conspicuous, but the molecular understanding of polymerization reactions is too limited to fully exploit the potentialities of organometallic catalysts. The Cossee–Arlman mechanism,[68] with adaptations by Brookhart and Green highlighting the role of agostic interactions,[69] is generally accepted as the mechanism for olefin polymerization (Scheme 1.1). Chain propagation occurs *via* a series of migratory insertions and ceases through a termination event, typically β-H elimination to the metal (BHE), β-H transfer to the monomer (BHTM), chain transfer to Al or hydrogenolysis.[70-71]

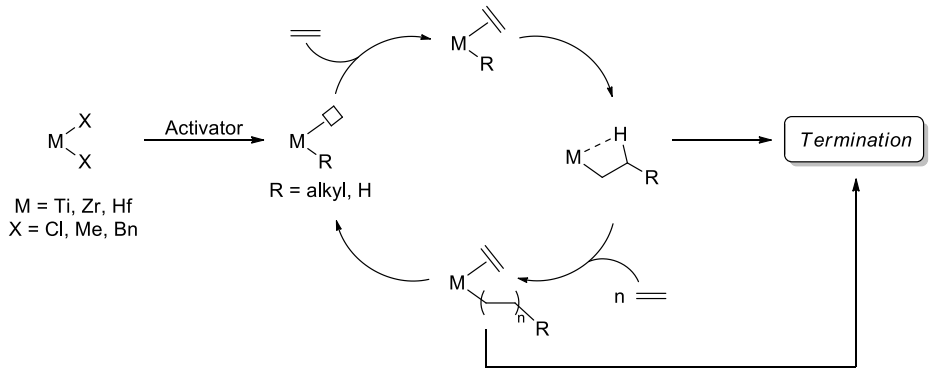

Scheme 1.1 – Simplified ethene polymerization mechanism.

Steric and electronic properties of the active cation are known to control chain growth and to determine its microstructural features. The *design* of novel active species for specific applications would be highly desirable, but rationalizing the many factors determining catalysts performance is extremely difficult. On the one hand, the evolution of High Throughput Experimentation (HTE) technology has enabled rapid empirical screening while reducing cost and preserving accuracy;[72] this is facilitating the *trial-and-error* approach to catalyst discovery and development that has characterized the story of polyolefins since its early stages, and that proved successful in many cases.[73-74] Quantitative

Structure-Activity Relationship (QSAR) database have been often used to identify specific steric and electronic parameters determining catalyst properties, and orient further ancillary ligand modifications,[75-76] but significant improvements are still largely serendipitous.

On the other hand, advances in computational chemistry are offering the possibility to integrate experiments with detailed theoretical models, aiming to fully demystify the polymerization process at a molecular level. This would allow to implement a more *rational* approach to catalyst design, which might represent an extremely powerful tool for advancement in this field.[77-78] The identification of effective and efficient computational methods also offers the chance to prioritize experimental screening *via* initial *in silico* High-Throughput Computation (HTC) of catalysts, thereby offering a green alternative to the conventional workflow in catalyst discovery through reduction of cost-intensive catalyst synthesis and pre-screening.

Molecular mechanics (MM) has been an early and simple tool applied to molecular design.[79] Molecules are described only in terms of nuclei, interacting with each other according to laws of classical physics (typically, harmonic oscillator). These techniques are suitable to explore conformational equilibria and non-bonded interactions, and proved useful to develop simple models for catalyst selectivity.[80-81] The validity of MM modeling strongly depends on the structural parameters used to define the force field, generally deriving from representative bond lengths and angles determined experimentally. For this reason, MM can effectively model minima on the Potential Energy Surface (PES), while it is generally unsuitable to describe bond formation and breakage events typical of chemical reactivity.

Optimization of transition states (TSs) can be more effectively performed using modern electronic structure methods, offering approximate solutions for the Schrödinger equation. These technologies are based on first principles and

do not rely on preconceived ideas of chemical bonding. The possibility to characterize virtually every electronic state of known and unknown molecules comes at the expense of higher computational cost and complexity. The first modeling of olefin insertion based on *ab initio* methods for a metallocene catalyst was reported in 1989 for a cationic bis-Cp titanocene at the HF (Hartree-Fock) and MP2 (Møller-Plesset) level of theory.[82] Since then, quantum mechanical (QM) methodologies have been widely applied to olefin polymerization, and contributed to the evolution of our insight from mostly qualitative mechanistic understanding to more quantitative predictions.[83-85] To name but a few, the groups of Ziegler,[70, 86-90] Morokuma[83-85, 91-92] and Cavallo[81, 93-96] are among those who provided important contributions to this field.

Coupled Cluster methods are known to give highly reliable energy values, and CCSD(T) is still considered to be the 'gold standard' in computational chemistry.[97-98] However, because of the high computational time demand, this method is routinely applicable only to rather small systems. Problems related to the high computational costs, have been often circumvented by using combined QM/MM methods, in which the active pocket was modeled at the QM level and the remaining atoms at the less demanding MM level,[91, 99-101] although the current trend seems to be full QM treatment of complete active species.

In particular, rapid evolution of Density Functional Theory (DFT) has offered the possibility to carry out full QM studies in reasonable time frames on systems that would be unsuitable for classical wave function based methods (DFT scales with systems size ~ N^{2-3}, while CCSD(T) scales ~ N^7; N = number of electrons). DFT is based on Schrödinger like equations, also known as Kohn–Sham equations, which can be treated with a simplified one-electron formalism using the electron density instead of the more complex N-electron wavefunction.[102-103] Several comparative studies have shown that a careful

choice of functional and basis set for a given problem can lead DFT to achieve chemical accuracy (±1 kcal/mol), which is comparable to CCSD(T).[95, 104-105]

This simplified approach is nowadays among the most widely used in modeling of olefin polymerization.[70, 77, 87-88] Static methodologies are by far the most common, although some processes like dissociation equilibria require a molecular dynamics approach.[106]

While significant progress has been made, many questions on the relationship between catalyst structure and properties remain open. The following sections summarize the main achievements and open challenges regarding the understanding of some key aspects of olefin polymerization catalysis.

1.2.1 – Stereoselectivity

The era of catalyst design in olefin polymerization began with the identification of the origins of stereocontrol in propene homopolymerization. The work of Brintzinger and co-workers provided polymerization chemists with the first examples of stereorigid *ansa*-zirconocenes,[107] which were used by Ewen for the unprecedented synthesis of highly isotactic polypropylene by a C_2-symmetric molecular catalysts in 1984.[108] Molecular mechanics calculations led Corradini to propose the 'growing chain orientation mechanism of stereocontrol', according to which the chiral steric bulk surrounding the metal center dictates a preferential orientation to the growing alkyl chain, which in turns 'selects' a certain monomer enantioface *via* non-bonding interactions.[80] This model was initially developed for heterogeneous active sites,[109] and then expanded to molecular catalysts.[81, 93, 110] Especially in cases where the steric bulk of the ancillary ligand is not pronounced enough to orient the growing polymeryl, a 'chain-end' control mechanism has been found to become

competitive, with the chirality of the last polymeryl unit being responsible for stereoselectivity.[108, 111]

Easy correlations between the symmetry of the catalyst and the resulting polypropylene microstructure could be established using Ewen's stereocontrol rules.[112] The simplest cases were iso- and syndioselecivity of C_2- and C_S-symmetric metallocenes that could be easily traced to their homotopic and enantiotopic active sites; the production of hemi-isotactic PP by some C_1-simmetric species could be simply rationalized as well (Figure 1.4).[94]

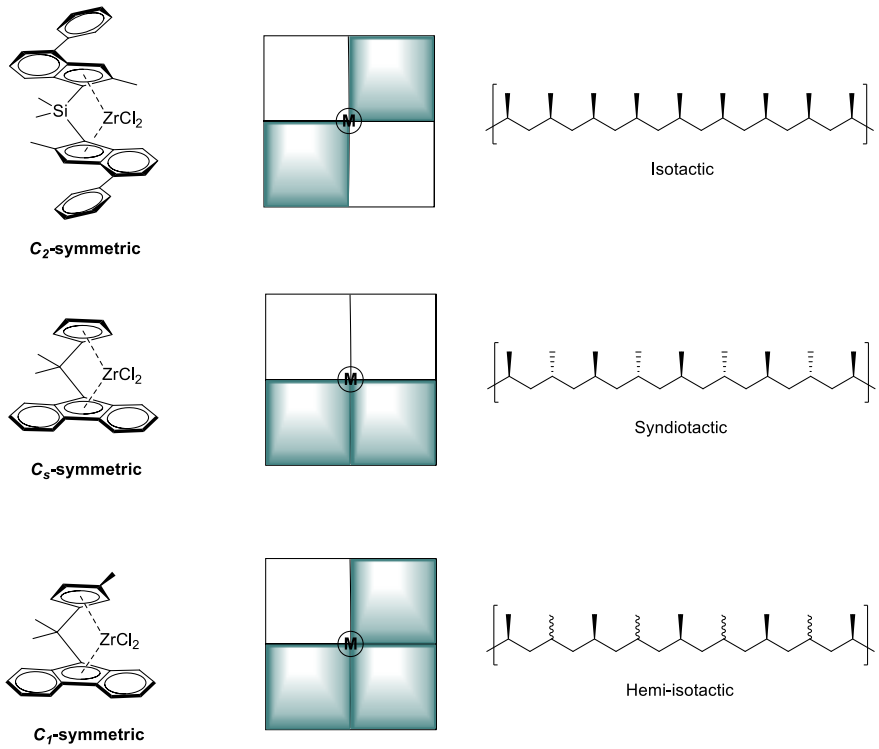

Figure 1.4 – Simple examples of correlations between catalyst symmetry (left), quadrant occupancy (middle) and tacticity of the resulting polypropylenes (right). Grey quadrants correspond to relatively crowded zones.

Advances in polymer characterization (especially by NMR spectroscopy)[113] and catalyst structural amplification soon provided novel

detailed polymer architectures requiring more elaborate interpretation. Instructive cases are the proposed mechanisms of site and chain epimerization that would explain some unexpected observations like the dependence of stereoselectivity on monomer pressure[114-115] and the isoselectivity of some C_1-symmetric metallocenes like [Me_2C(3-*tert*-butyl-C_5H_3)($C_{13}H_8$)]$ZrCl_2$ (C_5H_3 = substituted cyclopentadienyl; $C_{13}H_8$ = fluorenyl).[116-117]

Although highly active and selective metallocenes have been identified, they have never become true competitors for ZN for production of iPP. Along with the aforementioned drawbacks, another limitation of molecular catalysts is that stereoerrors are not confined in small stereoblocks as with ZN systems, but are randomly distributed along the polymer chain. This negatively affects crystallinity of the material, to the extent that for iPPs with equal amounts of stereoerrors the ones produced using ZN catalysts tend to have better mechanical properties than those made using metallocenes or non-metallocenes.[94]

Stereoselectivity is definitely the most studied and understood catalyst property in olefin polymerization, but the evolution of modern DFT[77] and experimental[72] methodologies has continuously fomented the debate on its origins. For instance, recent studies have emphasized the role of agostic[118] and direct ligand-monomer interactions,[119-121] and of monomer coordination itself in determining catalyst selectivity,[122] further emphasizing the subtleties that molecular design has to deal with.

1.2.2 – Molecular weight

Other catalyst features are at least as important as stereoselectivity, but more difficult to control. Molecular weight (MW) capability is given by the relative tendency of the active species to propagate or terminate the polymeryl

chain. Unambiguous identification of the main termination process is an essential prerequisite to model polymer molecular weight. In relatively simple cases, when this has been accomplished, DFT calculations have been reported to successfully reproduce experimental trends, and basic rational strategies for molecular design have been proposed.[70-71, 89, 96, 99, 123-129]

BHTM is a common termination process in absence of transalkylating reagents like trimethylaluminum (TMA) and at relatively high monomer pressures.[70] In cases where it represents the major chain transfer event, comparison with insertion barriers at a computational level is made generally simple by the fact that the two relevant transition states (TSs) have the same molecular composition (Scheme 1.2). The balance between propagation and BHTM can be often tipped toward the former by simply using bulky ancillary ligands that destabilize the sterically demanding six-centered TS for chain transfer to monomer (BHTM-TS in Scheme 1.2) with respect to insertion (INS-TS).[70, 129] It has been noted however that this design principle should not be taken to the extreme.[123, 130]

Getting analogous insight in other termination routes can be more complex. For instance, BHE is a well-understood reaction and optimization of the corresponding TS is often -but not always- an ordinary task for computational chemists. However, direct Gibbs free energy comparison with propagation process is hampered by the different molecularity of the two processes (Scheme 1.2), making prediction of MW much more difficult.[130]

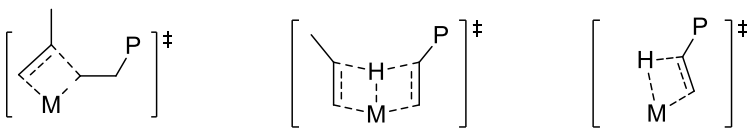

Scheme 1.2 – Comparison between insertion (INS), β-H transfer to the monomer (BHTM) and β-H elimination (BHE) transition states.

A particularly tricky case for molecular weight prediction regards ethene/α-olefin copolymerization. Polymer length in copolymerization is usually appreciably lower than that of the two corresponding homopolymerization reactions,[124, 131] limiting the application range of the resulting material. This has been tentatively traced to β-H transfer to ethene being particularly favored after comonomer insertion.[99, 126, 128, 132] In fact, 2-methyl substitution on bis(indenyl) ansa-zirconocenes is known to yield much longer copolymers, likely since it sterically destabilizes the BHTM process.[126, 133] Nonetheless, quantitative modeling of MW remains challenging.[131]

1.2.3 – Comonomer incorporation

The complexity deriving from the concomitant presence of two (or more) monomers in the polymerization reactor also refers to other aspects of catalyst performance. A topic of primary importance in copolymerization is the relative preference of the active species for insertion of the two competing olefins in the growing alkyl chain. The extent of α-olefin incorporation and its distribution in the polyethylene chain is an important microstructural feature that significantly affects mechanical, optical and many other chemical-physical properties of the material.

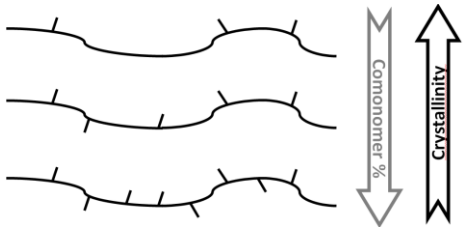

Comonomer (mol%)	Crystallinity (%)
1-2	55-45
2.5-3.5	45-30
>4	<30

Figure 1.5 – Correlation between comonomer content, crystallinity and density of LLDPE. Data from ref. 19.

Calorimetric studies on LLDPE have shown how chain branching can interfere with polymer crystallization, and can therefore be used to tune its melting and rheological behavior (Figure 1.5);[134-136] this aspect is at the origin of the improved processability of LLDPE with respect to HDPE, and of its commercial success. Comonomer content can serve as practical indicator to classify different grades of ethene/α-olefin copolymers differing in morphology, dynamic mechanical response, yielding, and large-scale deformation.[137] The length of side chains was found to affect these properties as well.[138]

Control of the factors determining reactivity ratios in copolymerization is the key to access a variety of tailored polymer architectures and high-performance products. Considerable effort has been put in this direction by academic and industrial researchers, but only a limited level of understanding has been achieved. Initially, most correlations were based on steric considerations, with an open coordination geometry being responsible to coordinate and insert bulky comonomers more easily, but several reports pointed out this is not enough to adequately describe copolymerization behavior.[139-141] Regarding electronic effects, the presence of electron withdrawing groups on indenyl ligands of metallocenes[142] or CGC-type[143] catalysts has often been reported to be beneficial for comonomer incorporation.

High accuracy is needed for computational predictions of copolymerization statistics to be useful. Modeling chain propagation by group IV catalysts is generally challenging, since also subtle effects might be energetically relevant to estimate the typically very low activation energies for olefin insertion. Furthermore, identification of the rate limiting step can be non-obvious; barrier heights for processes like olefin capture or chain rearrangement have been proposed to be comparable with those for monomer insertion.[86, 144-145]

The competition between different monomers makes the task even more arduous. Attempts to model comonomer affinity have provided interesting insights in catalyst reactivity but have not yet been able to quantitatively reproduce them. Missed identification of the correct rate limiting step has been proposed as a potential reason for this lack of success.[131, 146]

1.2.4 – Activity and activators

The production of polymers with desired properties is not the only driving force in the design of molecular catalysts. High activities are also required to develop industrially relevant systems. More insight in activation and deactivation chemistry would be desirable but it is hard to achieve.

Industrial solution processes typically benefit from operating at high pressure and temperature (>120°C). For instance, working close to the polymer melting point reduces polymer aggregation, allows better control of viscosity within the polymerization reactor, and prevents undesirable heat transfer or monomer diffusion limitations. Identifying well-behaved molecular catalysts exhibiting high activity (and molecular weight capability) under such forcing conditions is challenging, due to the increasing number of undesirable side-reactions that can compete with chain propagation at high temperature.[44] Common examples are the formation of metallacycles *via* intramolecular C-H activation of the ancillary ligand,[147-150] α-hydrogen transfer leading to μ-methylene dinuclear species[151-153] and solvent activation.[154-155] Changes in oxidation states, such as reduction of Ti(IV) to Ti(III), are other common deactivation processes that become competitive at high temperatures.[94, 156]

Along with the high reactivity of cationic group IV complexes, major complications arise from the elusive nature of the most widely used cocatalyst for alkene polymerization, namely methylaluminoxane.[31, 157] MAO is typically

obtained by the controlled hydrolysis of trimethyl aluminum (TMA). This results in a dynamic mixture of oligomeric compounds that may differ substantially between samples and over time, hampering an accurate structural characterization.[158] It has become clear from experimental and computational studies that MAO solutions contain a variety of oligomeric $(AlOMe)_n$ cages along with TMA-decorated nanotubes $(AlOMe)_n \cdot (AlMe_3)_m$ in equilibrium with free Al_2Me_6 (TMA dimer).[159-170] This cocatalyst is capable of alkylating typical dichloride precatalysts and generate the coordination vacancy necessary to initiate the catalytic cycle. The thereby generated MAO-derived counterion is poorly coordinating due to charge delocalization over the MAO cage.[158]

The role of free TMA in affecting catalyst performance has been thoroughly investigated. It generally forms rather stable heterodinuclear adducts with transition metal cations (Figure 1.6), which are considered to be the origin for its high alkylating ability and modest abstracting power.[171-175] The connection with chain termination processes *via* chain transfer to aluminum is important as well.[176-178] TMA adducts have often been indicated as plausible dormant sites in olefin polymerization,[176, 179-180] as confirmed by (1) several polymerization studies reporting drops in activity when additional TMA was used [181-182] and (2) the high dissociation energies estimated by NMR[173, 177, 182] and DFT calculations.[105, 176]

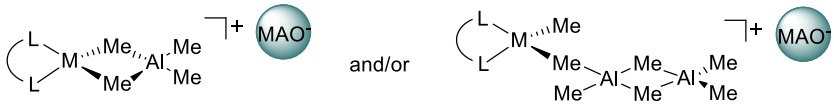

Figure 1.6 – Typical heterodinuclear adducts formed upon addition of TMA-containing MAO solution to M-based (M = Ti, Zr, Hf) precatalysts.

The presence of such highly reactive aluminum alkyl in MAO solutions can be also associated with catalyst decomposition. For instance, Stephan and coworkers have reported NMR evidence for a plausible side reaction between

phosphinimide Ti-complexes and $AlMe_3$, giving Ti-Al-carbide complexes by multiple α-hydrogen activation (Scheme 1.3).[183-184] Analogous reactions have been reported for typical metallocenes as well.[175]

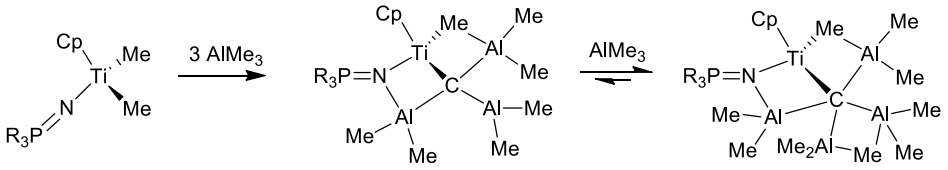

Scheme 1.3 – Plausible catalyst deactivation route *via* reaction with TMA, as reported in ref. 183-184.

This has motivated researchers to develop alternative activators, making the cocatalyst an integral part of catalyst design. Borane and borate-based Lewis acids were identified as potential candidates for the first time in early 1990s by Marks[185] and Ewen.[186] They generally require the precatalyst to be an already alkylated complex; also, a bulky Al-alkyl like triisobutyl aluminum (TiBA) is needed as impurity scavenger.[157] C_6F_5-transfer from perfluorinated borate counterion to the transition metal is one of the most common decomposition routes for these species.[187-192]

Another viable strategy has been to modify methylaluminoxane to remove the TMA component while preserving the desirable properties of this cocatalyst. Some of the most successful examples are MMAO-7 (*Modified Methylaluminoxane-7*) and PMAO-IP (*Polymethylaluminoxane-Improved Performance*). The first is an aluminoxane where part of the methyl groups have been replaced by bulkier and less reactive *n*-octyl groups; the second is an MAO analogue obtained *via* a non-hydrolytic process that yields virtually TMA-free MAO.[157]

Among many other possible modifications of methylaluminoxane,[157-158] one of the simplest and most effective ways to obtain TMA-free MAO solutions is to add a sterically hindered phenol such as 2,6-di-*tert*-butyl-4-methylphenol

(BHT) in a 2:1 molar ratio of free TMA estimated by ^{1}H NMR (usually 30-35% of the total Al).[193] In this way, $AlMe_3$ is converted into the far less reactive $MeAl(bht)_2$ aryloxide complex (bht = 2,6-di-*tert*-butyl-4-methylphenolate). This approach served to demonstrate that the long standing reputation of hafnocenes to be inherently less active than zirconocenes, was simply due to the stronger binding of TMA to Hf.[194] An analogous study on titanocenes has been published recently by using borate activators.[195] Silica has been recently proposed as alternative to BHT to remove aluminum alkyls from MMAO.[196]

The research in this field has led to growing consciousness that accurate description of the active species in polymerization catalysis should include the cocatalyst-deriving counterion,[197] since it can significantly influence catalytic activity and even polymer microstructure.[198] Diffusion NMR studies have experimentally proved that ion pairs and possibly higher aggregates are typically formed in the low polarity solvents used for olefin polymerization.[198-199]

1.2.5 – Perspectives

Olefin copolymerization, and in particular block-copolymerization, are currently among the most studied topics as they broaden applications towards highly profitable fields. The spectacular growth of the market of LLDPE and other ethene-copolymers has posed a problem of 1-alkene comonomer supply, which has expanded the interest of molecular design to the identification of catalytic systems for the selective oligomerization of ethene.[200-201]

Different comonomers attract much attention as well. The production of functionalized polyolefins is one of the most interesting challenges in polymerization catalysts, especially for group IV metals.[202] Incorporation of functionalized olefin in a polyethylene backbone is problematic due to the

generally low tolerance of the active species towards heteroatoms.[203-204] The two most successful strategies consist in 'protecting' the monomer functional group with Lewis acids (*e.g.* modified MAOs)[205-207] or using more tolerant late transition metal catalysts,[208-209] but none of them satisfy all the requirements of productivity, MW and incorporation capabilities to find industrial application, yet. Post-polymerization functionalization is a possible alternative that however suffers from selectivity issues,[210] while quenching with functionalized agents produces at most one functionalized chain-end per active site. Hybrid materials containing non-polyolefin blocks have been synthesized as well.[211]

Finally, cost and thermal stability are two features to keep in mind in the design of novel catalysts. Many extremely interesting catalysts developed on a laboratory scale have failed commercial application simply because their synthesis was based on expensive substrates and/or required a long series of synthetic reactions. Extending the temperature range in which the controlled kinetic properties are exhibited to the high end, is a long-standing challenge for molecular catalysis.

1.3 – Scope of this thesis

This PhD work consists of a combined experimental and computational work aiming at contributing to the *rational design* of molecular olefin polymerization catalysts. A wide variety of approaches has been used to investigate in detail several aspects related to the polymerization mechanism. The experimental part included the synthesis of organometallic precatalysts, their spectroscopic characterization and the exploration of their catalytic properties in olefin polymerization. A detailed NMR study of the reactivity of these complexes and other model compounds activated with modified MAO or trityl borate was carried out for some selected cases. DFT methodologies were widely used to interpret and reproduce in-house generated and/or literature available experimental data. The adopted computational protocol has been recently developed within the *Laboratory of Selective Polymerization* at the University of Naples[104-105] and further refined in the framework of this PhD project. The relative stability of relevant reaction intermediates and TSs is evaluated, and a predictive NMR chemical shift protocol is proposed.

The first part of the thesis (Chapter 2-3) is centered around factors determining selectivity of molecular catalysts, while the second part (Chapter 4-5) explores issues related to their activity and thermal stability. In particular, **Chapter 2** focuses on reactivity ratios in ethene/α-olefin copolymerization. By adopting the aforementioned DFT protocol, we managed to predict comonomer affinities for a variety of metallocenes and non-metallocenes with an unprecedented high accuracy, which allows us to draw tentative conclusions on the role of entropic, electronic, and steric effects determining this important catalyst property. Reaction routes leading to chain growth are carefully analyzed; a novel potential rate limiting step occurring during monomer capture is proposed, providing a plausible explanation for the long-standing difficulties of modeling of relative propagation barriers in copolymerization.

Consequences on kinetics and thermal dependence of copolymerization statistics are discussed.

Chapter 3 summarizes the work carried out during a three-month internship at Imperial College London (UK) working on a copolymerization related issue, such as the production of 1-alkene feedstock as comonomer for LLDPE. Selectivity is of primary importance in ethene oligomerization. The peculiar case of bis(benzimidazolyl)amine (BIMA) chromium catalysts giving alternating distribution of products was investigated. The results provided supporting evidence for the mechanistic and kinetic interpretation proposed by the group of Prof. Britovsek,[212-213] potentially opening new intriguing routes for selectivity tuning in Cr-catalyzed ethene oligomerization.

While exploring the origins of comonomer effects in olefin copolymerization, we got interested in the case of phosphinimide Ti-catalysts. These industrially relevant systems are known to exhibit excellent catalytic properties in homo e copolymerization of ethene,[38] while the very few available reports on α-olefin homopolymerization describe only modest performance with 1-hexene monomer.[47] Trying to get more insight in factors limiting the performance of these catalysts with the simplest α-olefin, propene, we identified a novel chain termination route. **Chapter 4** reports polymerization and DFT studies on this novel chain transfer to solvent process, which involves benzylic CH activation of toluene and leads to benzyl terminated polypropylenes. This reversible deactivation pathway is found to be relevant especially at high temperatures and moderately high pressures (*i.e.* under conditions relatively close to those of commercial solution reactors) and the exploration of its mechanism offers interesting insight in factors determining catalyst decay. The scope of this reaction as a potential tool for catalytic chain end functionalization was explored.

Finally, the important role of cocatalyst is discussed in **Chapter 5.** The chemistry of phosphinimide precatalysts in combination with dried-MAO/BHT was explored by means of NMR spectroscopy, offering an interesting overview of the reactivity of the oligomeric fraction of MAO in absence of free TMA. The presence of a P-atom in the ancillary ligand represented a helpful spectroscopic probe to progressively monitor the activation of typical dichloride complexes by ^{31}P NMR. The main consequences of the choice of TMA-containing commercial MAO *vs.* modified TMA-depleted MAO/BHT cocatalyst on the formation of dormant sites are evaluated, and connections with the mechanism of chain transfer to solvent are discussed. A large part of the NMR experiments was performed during two short visits at the University of Perugia (Italy), in collaboration with Prof. Alceo Macchioni e Prof. Cristiano Zuccaccia.

Chapter 2

Modeling reactivity ratios in ethene/α-olefin copolymerization

A portion of this chapter has appeared in print:

Zaccaria, F.; Ehm, C.; Budzelaar, P. H. M.; Busico, V., Accurate Prediction of Copolymerization Statistics in Molecular Olefin Polymerization Catalysis: The Role of Entropic, Electronic, and Steric Effects in Catalyst Comonomer Affinity. *ACS Catal.* **2017**, *7*, 1512-1519.

Zaccaria, F.; Cipullo, R.; Budzelaar, P. H. M.; Busico, V.; Ehm, C., Backbone rearrangement during olefin capture as the rate limiting step in molecular olefin polymerization catalysis and its effect on comonomer affinity. *J. Polym. Sci. Part A*, **2017**, *55*, 2807-2814.

2.1 - Introduction

The presence of a comonomer in the polymerization mixture is known to induce the so called 'comonomer effect', altering significantly the performance of the catalysts with respect to homopolymerization. Although a few examples of generally small penultimate monomer effects have been reported,[214-217] it is generally accepted that the reactivity of the active species depends on the last inserted olefin.[218]

In such cases, the reactivity of different comonomers towards insertion is described by first-order Markov statistics, employing only two parameters, denoted as r_e and r_c, which correspond to the ratio between homo- and cross-propagation rates:[218]

(2.1) $$r_e = \frac{k_{ee}}{k_{ec}} \quad ; \quad r_c = \frac{k_{cc}}{k_{ce}}$$

Here, *k* is the kinetic constant of the specific insertion reaction indicated by the two subscripts: the first subscript denotes the last *inserted* monomer, while the second refers to the *inserting* one (Scheme 2.1). For instance, k_{ec} is the kinetic constant related to insertion of the comonomer (*c*) after ethene (*e*) (Scheme 2.1). The product $r_e \cdot r_c$ describes the tendency of the catalyst to form *blocky* ($r_e \cdot r_c > 1$), *alternating* ($r_e \cdot r_c < 1$) or *random* ($r_e \cdot r_c \sim 1$) copolymers.

Reactivity ratios can also be expressed in terms of Gibbs free energy differences $\Delta\Delta G^{\ddagger}$ between barrier heights of different insertion modes:

(2.2) $$r_e = \frac{k_{ee}}{k_{ec}} = e^{\frac{\Delta G^{\ddagger}_{ec} - \Delta G^{\ddagger}_{ee}}{RT}} = e^{\frac{\Delta\Delta G^{\ddagger}_{(ec-ee)}}{RT}}$$

(2.3) $$r_c = \frac{k_{cc}}{k_{ce}} = e^{\frac{\Delta G^{\ddagger}_{ce} - \Delta G^{\ddagger}_{cc}}{RT}} = e^{\frac{\Delta\Delta G^{\ddagger}_{(ce-cc)}}{RT}}$$

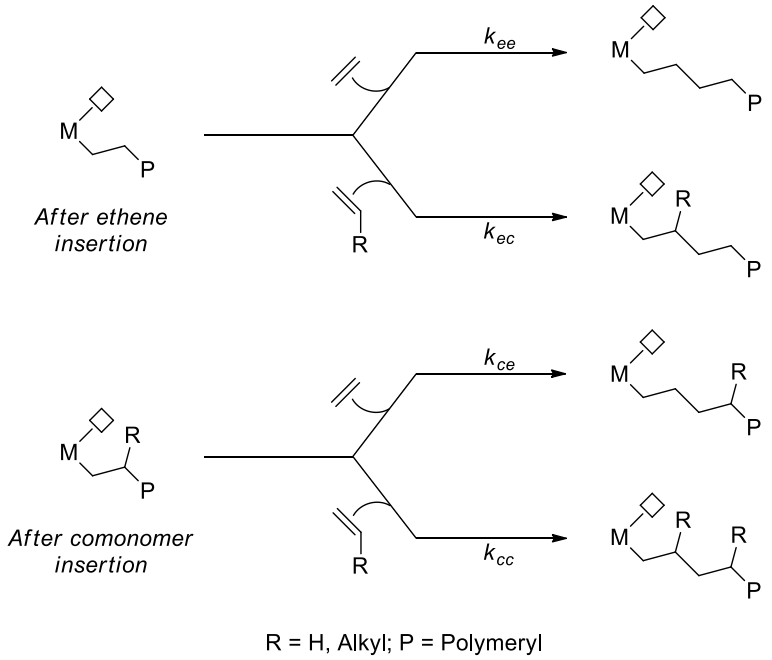

Scheme 2.1 – Possible insertion modes in ethene/α-olefin copolymerization.

The underlying assumption here is that insertion is always rate determining for chain propagation, and that other processes like monomer coordination represent rapid equilibria with respect to chain growth. Therefore, the Curtin-Hammett principle applies and reactivity ratios are solely determined by insertion TS energy differences.[219]

Experimentally, r_e and r_c can be determined *via* different spectroscopic methods (*i.e.* IR or NMR).[217, 220] In cases were several copolymers with different composition are available, they can be calculated by fitting the mole fractions of the two comonomers in the feed and in the polymer according to Mayo and Lewis equation.[221] The *r*-parameters correlate with the slopes of these polymerization curves, which can be affected by relatively large experimental errors in cases where the slopes are steep and the available experimental data are limited (especially at low and high comonomer concentration ratios).[222] Among others, Finemann and Ross have proposed an alternative simplified

approach, which allows the use of data points in the intermediate concentration regimes with reduced uncertainities.[222] However, these graphical methods intrinsically suffer from the relatively strong dependence of reactivity ratios on experimental parameters (especially temperature),[125] which requires the copolymer samples to be produced under rigorously comparable reaction conditions. The applicability of the chosen method through the entire range of feeding compositions spanned should be carefully verified.

An alternative strategy based on ^{13}C NMR microstructural analysis has been proposed by Kakugo[223] and Randall.[224] Statistical analysis of triad distributions provides the probability P_{12} of insertion of monomer *2* after *1*, which correlate to r_e and r_c by the comonomers feeding ratio *X* according to:

(2.4) $$r_e = \frac{P_{ee}}{P_{ec} \cdot X} = \frac{(1-P_{ec})}{P_{ec} \cdot X}$$

(2.5) $$r_c = \frac{P_{cc} \cdot X}{P_{ce}} = \frac{(1-P_{ce}) \cdot X}{P_{ce}}$$

In this case, the major limitations arise from the intricate NMR spectra typically obtained with ethene copolymers, although much progress has been made thanks to high field and high resolution NMR techniques.[217] Another critical point is the accurate determination of *X*, which can be not straightforward in case of gaseous monomers, especially at high temperature.

In order for computational prediction to be useful in catalyst pre-screening, predicted *r* values should not be off by more than a factor of ~2, corresponding to less than 0.5 kcal/mol in $\Delta\Delta G^{\ddagger}$ at 323 K. Early attempts to reproduce/predict reactivity ratios focused on a number of *rac*-dimethylsilylenebis(indenyl) catalysts and significantly overestimated the preference for ethene over propene insertion.[131] The authors tentatively proposed several explanations, regarding the ineffectiveness of the level of theory used (b3-lyp/TZVP//SV(P)) and a potentially oversimplified chemical

model, which did not accounted for solvent and counterion effects. The possibility that processes different from monomer insertion might be kinetically relevant for chain growth was considered as well, especially for the more problematic case of r_c.

More recently, an improved model, including counterion effects in combination with a higher level of theory, led to a better but still not fully satisfying agreement between experiment and theory.[146] The introduction of dispersion corrections rather than anion contributions have been suggested as the key factor for the improvement in accuracy. These conclusions are in line with experimental results showing that going from MAO to other typical weakly coordinating counterion like $[B(C_6F_5)_4]^-$ does not decisively impact comonomer reactivity ratios for *rac*-$Me_2Si(Ind)_2ZrCl_2$.[217] Likewise, solvent polarity was found to play at most a very limited role in determining copolymerization statistics with other monomers.[225]

Recently, research carried out at the *Laboratory of Stereoselective Polymerization* has identified a suitable computational protocol for effective modelling of olefin polymerization related reactions.[104-105, 176, 226-227] In this chapter, we show how this protocol can be successfully applied to the study of reactivity ratios in ethene/α-olefin copolymerization, providing an unprecedented excellent agreement with experimental data. Methodological as well as chemical considerations on the possible rate limiting steps for chain propagation are critically and extensively discussed.

2.2 – Results and Discussion

Calculations were done according to the protocol developed by Ehm et al.,[104-105] which consists of the following steps (see also Section 2.4):

0. the growing polymer chain was modeled by an ^{n}Pr or ^{i}Bu group, corresponding to last inserted units of ethene and propene, respectively;
1. optimization at the relatively low and cost-effective TPSSTPSS/cc-pVDZ-(PP) level;
2. Single point energy calculations at the M06-2X/cc-pVTZ-(PP) level to account for dispersion and solvent corrections (by using the Polarized Continuum Model, PCM).[228]

This computational protocol was benchmarked and refined on an experimental dataset available from the literature. At first, we demonstrated its effectiveness by reproducing r_e parameter for a representative set of molecular catalysts, covering a broad range of structural features and catalytic properties (Figure 2.1):

a. Unbridged Ti, Zr and Hf bis-cyclopentadienyls, which typically exhibit poor comonomer incorporation;[229-230]
b. 11 *ansa*-metallocenes, ranging from poor incorporators (**2-Zr**, **3a-Zr**) to good ones (**4c-Zr**, **4d-Zr**); [131, 217, 229-232]
c. The prototypical CGC (**6-Ti**), an industrially relevant non-metallocene for LLDPE production;[43, 139, 232]
d. Several Ti-based non-metallocenes bearing phenoxy and ketimide ancillary ligands, which are reported to copolymerize ethene and 1-hexene with good activity and molecular weight capability, ranging from quite good (**7-Ti**) to poor (**8c-Ti**) comonomer incorporation.[233-234]

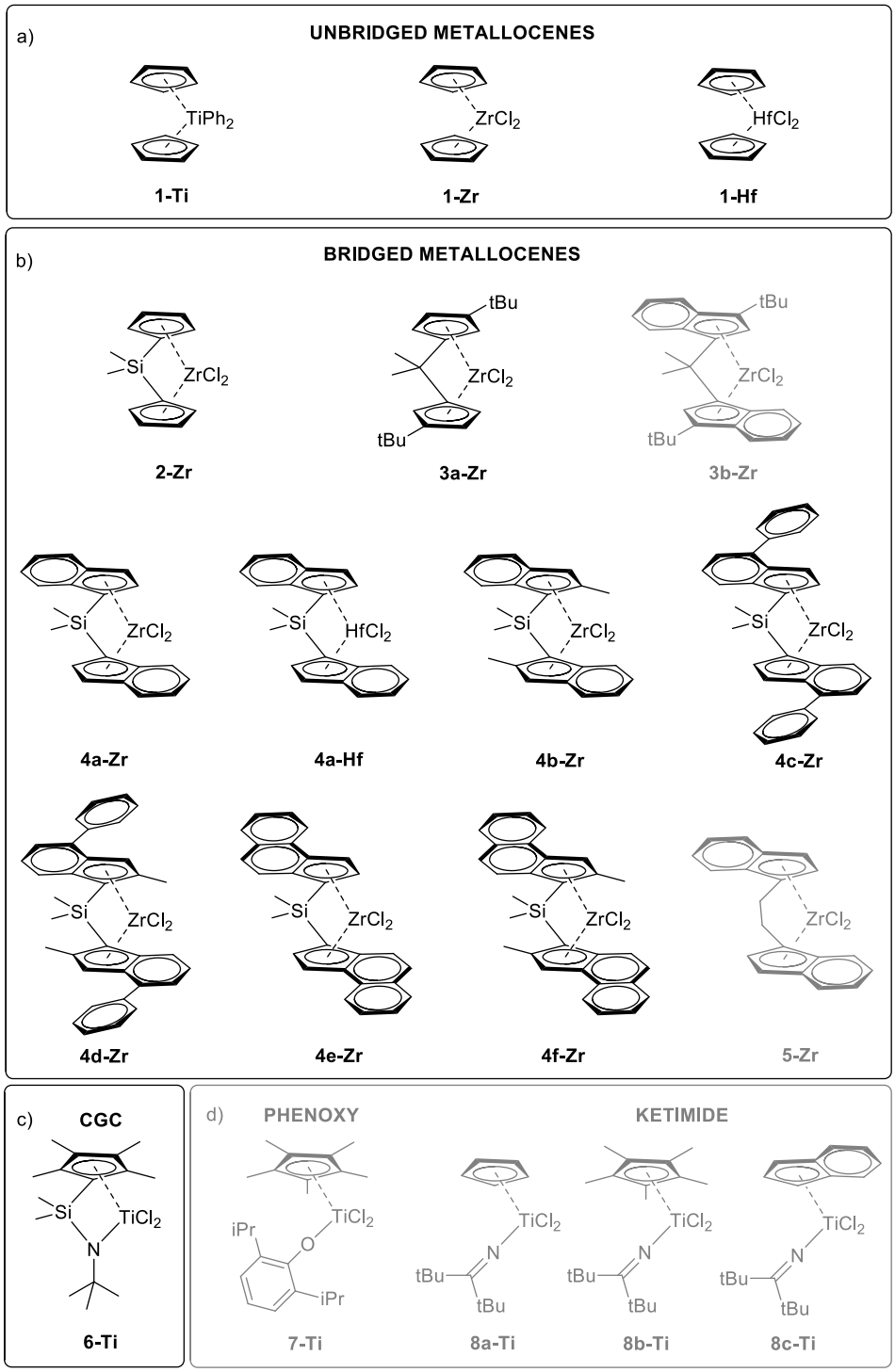

Figure 2.1 - Pre-catalysts included in the modeling of r_e (black + grey) and r_c (black).

Then, we focused on r_c to identify the reasons of its apparently higher complexity. Insertion paths were explored in detail for a subset of catalysts (black structures in Figure 2.1), to examine whether transition states prior to insertion could be kinetically relevant.

2.2.1 – Modeling r_e

2.2.1.1 – Experiment *vs.* computational prediction of r_e

The reactivity ratio r_e indicates the tendency of the catalytic system to incorporate an α-olefin in the homopolyethylene chain. Table 2.1 lists experimental and predicted $\Delta\Delta G^{\ddagger}_{(ec\text{-}ee)}$ values for the selected 19 catalysts (24 different conditions) in copolymerization of ethene with propene or 1-hexene. Experimental r_e values ranging from 1.8 to 48 have been reported. This translates to a Gibbs free energy preference for ethene insertion of 0.4 to 2.5 kcal/mol, *i.e.* only a 2.1 kcal/mol spread, further emphasizing that modelling this process represents a significant challenge due to the high accuracy that is needed.

DFT calculations were performed using the 'naked cation' approximation. Coussens and Linnolahti recently showed that modelling of weakly coordinating anions can be reasonably neglected after the first chain growth step.[146]

$\Delta\Delta G^{\ddagger}_{(ec\text{-}ee)}$ values are computationally reproduced with an average and maximum deviation of only 0.2 and 0.5 kcal/mol respectively, which is in line with expectations for our method[104-105] and represent a remarkably good agreement in this field. In this respect, it should be noted that empirical determination of r_e is nontrivial, and experimental errors in terms of $\Delta\Delta G^{\ddagger}_{(ec\text{-}ee)}$ are often in the order of 0.1 kcal/mol.[217, 229] Linear regression analysis on experimental *vs.* calculated $\Delta\Delta G^{\ddagger}_{(ec\text{-}ee)}$ values for ethene/propene (E/P) copolymerization (entries 1-17, 19-20 in Table 3.1) is reported in Figure 2.2; the

Table 2.1. Experimental[a] and calculated[b] preference ($\Delta\Delta G^{\ddagger}_{(ec\text{-}ee)}$) for ethene over comonomer insertion.

Entry	Catalyst	Comonomer[a]	Solvent	T (K)	r_e	$\Delta\Delta G^{\ddagger}_{(ec\text{-}ee)}$ (kcal/mol)			Ref.
						Exp.	Calc.	Δ	
1	**1-Ti**	Propene	Toluene	323	19.5	1.9	1.8	-0.1	230
2	**1-Zr**	Propene	Toluene	323	48.0	2.5	2.3	-0.2	230
3	**1-Hf**	Propene	Toluene	323	13.5	1.6	1.5	-0.1	229
4	**2-Zr**	Propene	Toluene	323	24.0	2.0	1.7	-0.3	230
5	**3a-Zr**	Propene	Toluene	323	25.6	2.1	1.6	-0.5	229
6	**3b-Zr**	Propene	Toluene	323	14.0	1.7	1.8	0.1	231
7	**4a-Hf**	Propene	Toluene	298	3.0	0.7	0.7	0.0	232
8	**4a-Zr**	Propene	Heptane	323	5.4	1.1	1.0	-0.1	131
9	**4a-Zr**	Propene	Toluene	303	4.5	0.9	0.9	0.0	217
10	**4b-Zr**	Propene	Heptane	323	5.4	1.1	1.3	0.2	131
11	**4b-Zr**	Propene	Toluene	303	4.2	0.9	1.3	0.4	217
12	**4c-Zr**	Propene	Heptane	323	1.8	0.4	0.3	-0.1	131
13	**4d-Zr**	Propene	Heptane	323	2.0	0.5	0.9	0.4	131
14	**4d-Zr**	Propene	Toluene	303	2.5	0.6	0.8	0.2	217
15	**4e-Zr**	Propene	Heptane	323	4.5	1.0	1.2	0.2	131
16	**4f-Zr**	Propene	Heptane	323	4.5	1.0	1.4	0.4	131
17	**5-Zr**	Propene	Toluene	323	6.6	1.2	1.7	0.5	230
18	**6-Ti**	Propene	Toluene	323	1.4	0.2	0.8	0.6[c]	235
19	**6-Ti**	Propene	Toluene	363	3.8	1.0	0.9	-0.1	232
20	**6-Ti**	Propene	Toluene	413	4.3	1.2	1.0	-0.2	232
21	**6-Ti**	1-Hexene	Toluene	293	4.0	0.8	0.5	-0.3	139
22	**7-Ti**	1-Hexene	Toluene	313	2.6	0.6	0.6	0.0	233
23	**8a-Ti**	1-Hexene	Toluene	298	4.5	0.9	0.5	-0.4	234
24	**8b-Ti**	1-Hexene	Toluene	298	5.1	1.0	0.6	-0.4	234
25	**8c-Ti**	1-Hexene	Toluene	298	7.4	1.2	1.0	-0.2	234
							MAD	**0.2**	

[a] Activator: MAO, except for entry 20 (modified MAO, modification not specified in original reference); [b] M06-2X(PCM)/TZ//TPSSTPPSS/DZ; [c] not included in MAD as r_e value differs significantly from entries 19 and 20, for a detailed discussion, see main text. MAD = Mean Average Deviation.

slope and intercept close to 1 and 0 respectively illustrate the high quality of the predictions. Deviations are randomly distributed around zero and comparably small for Ti, Zr and Hf-based systems. In ethene/1-hexene copolymerization r_e appears to be modelled nearly as well as ethene/propene.

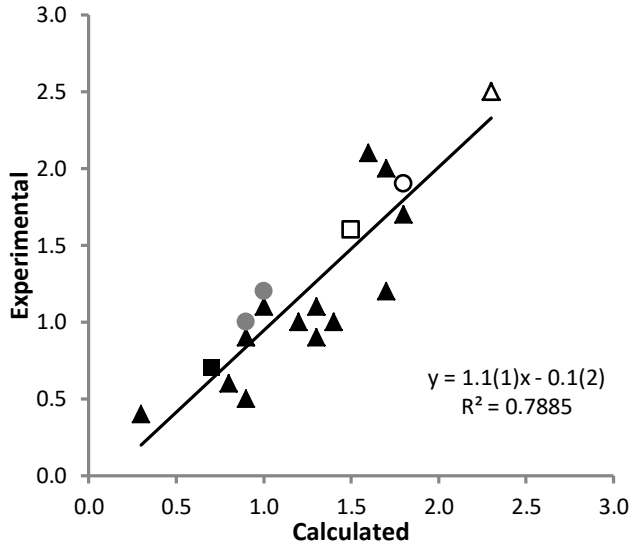

Figure 2.2 - Experimental *vs.* calculated $\Delta\Delta G^{\ddagger}_{(ec\text{-}ee)}$ (kcal/mol, E/P polymerization). Ti species (○), Zr (Δ), Hf (□). Unbridged metallocenes in white, bridged metallocenes in black and CGC in grey. Standard deviations for fitting constants in brackets.

2.2.1.2 - Origins of the improved computational accuracy

The considerable improvement in the prediction of r_e values with respect to earlier attempts[131, 146] can be traced to the choice of method and in particular to electronic energy corrections. The 'tricky' counterion was not included in the modelling, allowing the use of sufficiently large basis sets for final energy evaluation. It was shown earlier that def2-SVP basis set used in previous attempts[146] is not large enough to achieve the accuracy needed, but unfortunately calculations including an anion are not feasible with better basis

sets, yet.[104-105] The good agreement with experiment reported here by adopting the naked cation approach indicates that weakly coordinating anions can be reasonably neglected after the first chain growth step, as recently proposed by Coussens and Linnolahti.[146]

Along with counterion effects, other chemical origins for the disagreement between computational and experimental copolymerization factors have been hypothesized, and generally refer to a shift in rate limiting step to olefin capture or chain rearrangement.[131, 146] As far as r_e is concerned, only conventional insertion transition states (TSs) were considered, and effectively served to reproduce comonomer incorporation. Although locating some of these TSs proved challenging due to the flatness of the Potential Energy Surface (PES) around them, a change in rate limiting step for our catalysts test set appears not to play a role in this case. This further confirms that the accuracy of the data is to be traced to the more accurate computational method.

Dispersion and solvent corrections appear essential to achieve high accuracy. Regarding the former, the group of Maron has reported that entropy and dispersion corrections tend to cancel when calculating relative barriers relevant to olefin polymerization.[236] Conversely, the results presented here indicate that short/medium range dispersion corrections (intrinsic in the M06-2X functional) are crucial to reproduce experimental r_e values. Without dispersion corrections, at the TPSSTPSS/cc-pVTZ-(PP) level of theory, the preference for ethene over propene insertion is vastly overestimated (2-4 kcal/mol), in line with previous observations.[131] Additional Grimme type long range dispersion corrections[237-238] were found not to improve the agreement with experiment any further.

Solvation effects were modelled by the Polarized Continuum Model (PCM).[228] The radar plot Figure 2.3 illustrates their importance by comparing

experimental (blue line), solvent corrected (green) and uncorrected (red) $\Delta\Delta G^{\ddagger}_{(ec\text{-}ee)}$ values. While solvent corrections for silyl-bridged bis(indenyl) metallocenes are small (~0.3 kcal/mol), they can become substantial for other catalyst classes (~0.6 kcal/mol for bis(cyclopentadienyl) metallocenes) or higher olefins (~1.0 kcal/mol in 1-hexene copolymerization), resulting in nearly identical shapes of experimental and solvent corrected lines.

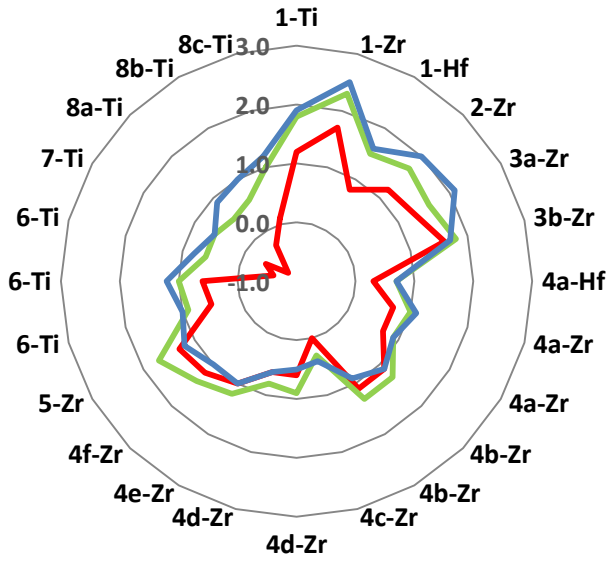

Figure 2.3 - Influence of solvent corrections on predicted *vs.* experimental $\Delta\Delta G^{\ddagger}_{(ec\text{-}ee)}$ (kcal/mol) values. Blue line experimental value, red line uncorrected, green line solvent corrected.

Recently, Coussens and Linnolahti concluded that solvent effects modelled with the PCM do not significantly affect relative insertion barriers for ethene and propene polymerization for a bis(cyclopentadienyl) Zr-catalyst.[146] Our broader test set leads to a slightly different conclusion, in the sense that this appears to be only true with the silyl bridged bis(indenyl) metallocenes **3b** to **5-Zr**. A tentative explanation might be that the more shielding nature of the ancillary ligands mitigates the interactions of the solvent with the active pocket.

Experimentally, the choice of solvent has a small but often detectable effect on copolymerization ratios, with heptane usually giving slightly better co-monomer incorporation than toluene.[225] Our model appears to reproduce this trend (Table 2.2), although the calculated effect is small (<0.1 kcal/mol) and well below our error margins. It appears that agreement with experiment is satisfactory as long as *a* solvent is included.

Table 2.2 - Comparison between $\Delta\Delta G^{\ddagger}_{(ec\text{-}ee)}$ at the M06-2X(PCM)/cc-pVTZ-(PP) level in different solvents (E/P, 323 K, 1 bar).

Entry	Catalyst	$\Delta\Delta G^{\ddagger}_{(ec\text{-}ee)}$ (kcal/mol)*		
		Toluene ε=2.3741	**Methylcyclohexane ε=2.0240**	**Heptane ε=1.9113**
1	**4a-Zr**	1.02	0.98	0.96
2	**4b-Zr**	1.35	1.31	1.30
3	**4d-Zr**	0.93	0.89	0.87

*second significant digit was added to show solvent influence. ε= solvent dielectric constant.

The error margins obtained here in the modelling of r_e appear to be close to the limit of what can be expected from straightforward static DFT calculations. We nevertheless explored options for further improvement. Use in geometry optimization of a better basis set (double-ζ → triple-ζ) or a dispersion-corrected functional (TPSSTPSS → M06-2X) significantly increased computational demands but did not provide significant improvement in accuracy. Additionally, we briefly explored the use of rigid-rotor corrections to entropic contributions. They appear beneficial for a few specific cases (**4a,b-Zr**, *vide infra*) to increase the accuracy of entropy contributions, but the method implemented in Gaussian 09 (Rev. B01) does not work consistently enough to be of use at the moment.

2.2.1.3 – Catalysts comparison: entropic and enthalpic effects on r_e

Comparing the intrinsic copolymerization capabilities of various catalysts based on different literature sources is generally difficult, due to their dependence on experimental conditions. Table 2.2 summarizes the predicted performance of catalysts for E/P copolymerization under a uniform set of conditions (323 K, 1 bar, toluene), allowing a more meaningful comparison. Unbridged metallocenes are predicted to have high r_e, in line with their generally low comonomer incorporation capability, while CGC **6-Ti**, **4a-Hf** and **4c-Zr** are seen to be better incorporators. It has been often proposed in the literature that replacing Zr with Hf increases comonomer affinity of typical metallocenes;[124-125, 128, 239] interestingly, our prediction seem to capture this trend for the couples **1-Zr**/**1-Hf** and **4a-Zr**/**4a-Hf** (entries 14/9 and 5/2 in Table 2.3).

Table 2.3 - Predicted catalysts performance under a uniform set of conditions, ordered by increasing r_e.*

Entry	Abbreviation	$\Delta\Delta H^{\ddagger}_{(ec\text{-}ee)}$	$T\Delta\Delta S^{\ddagger}_{(ec\text{-}ee)}$	$\Delta\Delta G^{\ddagger}_{(ec\text{-}ee)}$	Calculated r_e
1	**4c-Zr**	-1.1	-1.4	0.4	1.8
2	**4a-Hf**	-0.4	-1.2	0.8	3.4
3	**6-Ti**	0.1	-0.7	0.8	3.5
4	**4d-Zr**	-0.6	-1.5	0.9	4.3
5	**4a-Zr**	-0.2	-1.3	1.0	4.9
6	**4e-Zr**	0.0	-1.2	1.2	6.6
7	**4b-Zr**	0.3	-1.1	1.3	8.2
8	**4f-Zr**	0.3	-1.1	1.4	8.7
9	**1-Hf**	0.1	-1.4	1.5	10.4
10	**3a-Zr**	0.2	-1.4	1.6	12.1
11	**5-Zr**	0.6	-1.1	1.7	13.1
12	**2-Zr**	0.5	-1.2	1.7	14.1
13	**3b-Zr**	0.4	-1.4	1.8	16.5
14	**1-Ti**	0.4	-1.4	1.8	16.5
15	**1-Zr**	0.5	-1.8	2.3	36.0

*Ethene/propene copolymerization, 323 K, toluene solvent.

Figure 2.4 graphically shows a breakdown of the predicted free energy difference $\Delta\Delta G^{\ddagger}$ (green line) into enthalpic ($\Delta\Delta H^{\ddagger}$, blue line) and entropic ($T\Delta\Delta S^{\ddagger}$, red line) contributions (Table 2.3), allowing a tentative analysis of trends that influence catalyst performance.

Trends in $\Delta\Delta G^{\ddagger}$ are dominated by enthalpy, while $T\Delta\Delta S^{\ddagger}$ barely changes and oscillates around an average value of -1.25 kcal/mole. $\Delta\Delta H^{\ddagger}$ can be positive or negative, *i.e.* the *enthalpic* preference for ethene or propene insertion can switch, depending on the catalyst.

With respect to metallocenes, it appears that the bis-cyclopentadienyl system **1-Zr** has similarly high preference for ethene as the more open *ansa*-analogue **2-Zr**. Bis-benzindenyl systems like **4e** and **4f** have a reduced enthalpic preference for ethene compared to **1-Zr** and **2-Zr**, while bis-indenyl systems like **4a**, **4c** and **4d** even show an enthalpic preference for propene. The trend in electron donation of aromatic system Ind~BenzInd<Cp is inversely proportional to the preference for propene, in agreement with the experimental observation that electron withdrawing substituents increase comonomer affinity.[44]

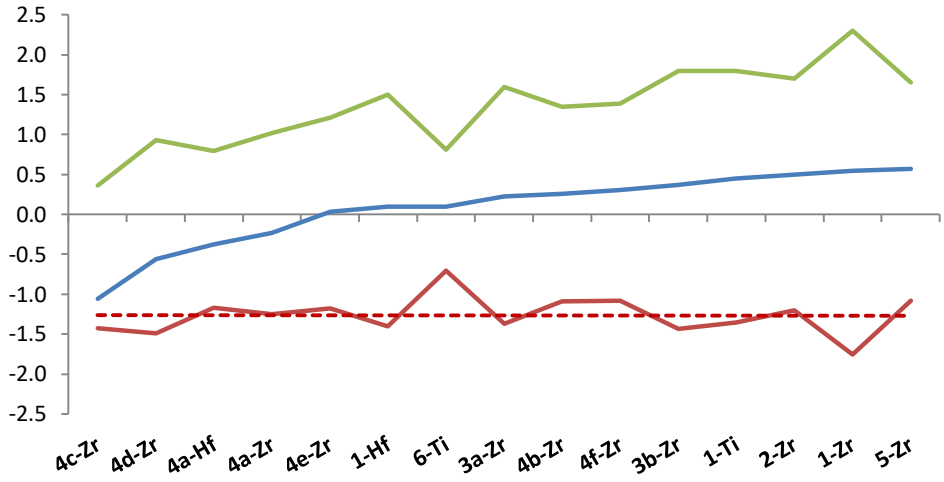

Figure 2.4 - Calculated entropy ($T\Delta\Delta S^{\ddagger}_{(ec\text{-}ee)}$, red line) and enthalpy ($\Delta\Delta H^{\ddagger}_{(ec\text{-}ee)}$, blue line) contributions (kcal/mol) to $\Delta\Delta G^{\ddagger}_{(ec\text{-}ee)}$ (green line) for E/P copolymerization (323 K, solvent toluene).

Methyl substitution at the 2-position of the indenyl or benzindenyl fragment (which enhances molecular weight) is calculated to decrease the enthalpic preference for propene (**4a** *vs.* **4b**, **4c** *vs.* **4d** and **4e** *vs.* **4f**) while hardly affecting the entropic contributions. The resulting increase of $\Delta\Delta G^{\ddagger}_{(ec\text{-}ee)}$ is within the accuracy of the method for the **4e**/**4f** couple (0.2 kcal/mol), but larger for the couples **4a**/**4b** (0.3 kcal/mol) and **4c**/**4d** (0.6 kcal/mol). Including free rotor corrections would yield a net difference for the **4a**/**4b** couple of 0.0 kcal/mol, in agreement with experimental observations (Entries 8-11, Table 2.1). Finally, introduction of a phenyl group at the 4-position of the benzindenyl fragment, which enhances stereoselectivity, also enhances the enthalpic preference for propene (**4a** vs. **4c** and **4b** vs. **4d**).

$T\Delta\Delta S^{\ddagger}$ is always negative, *i.e.* favouring ethene insertion. Of the average value of -1.25 kcal/mol (323 K, toluene), half is due to the different symmetry numbers σ of ethene and propene (σ = 4 for ethene and 1 for every other species in the present work; this is basically the statistical factor). The rotational entropy of a molecule in the gas phase contains the term $-R\ \ln(\sigma)$, which becomes $-0.67\ RT\ \ln(\sigma)$ in our case since we use entropy values scaled by 0.67 (see Section 2.4 for details). This symmetry term corresponds to -0.60 kcal/mol for ethene at 323K, favouring ethene insertion since we are comparing $[G^{\ddagger}_{INS,(M\text{-}propene)} + G_{(ethene)}]$ with $[G^{\ddagger}_{INS,(M\text{-}ethene)} + G_{(propene)}]$.

We tentatively attribute the other half to a tighter transition state for insertion of propene than of ethene. Propene insertion TSs are later than ethene insertion TSs; C…C and M…C distances are about 0.1 Å shorter than the corresponding ones for ethene and the C=C bond is 0.05 Å more elongated. The methyl rotation vibrational mode in propene insertion TSs is blue shifted with respect to that of the free olefin (Table 2.4), which also points to some congestion at the TS.

Table 2.4 – Calculated frequency ν of the propene methyl rotation in propene insertion TS.

Entry	Catalyst	ν (cm^{-1})
1	**1-Ti**	257
2	**1-Zr**	251
3	**2-Zr**	234
4	**4a-Zr**	242
5	**6-Ti**	229
6	**Propene**	211

As can be seen from Figure 2.4, unusually small $T\Delta\Delta S^{\ddagger}$ for CGC catalyst **6-Ti** (-0.7 kcal/mol) and high $T\Delta\Delta S^{\ddagger}$ for **1-Zr** (-1.8 kcal/mol) were obtained. Some caution is required in interpreting these numbers since even small errors in low-frequency modes can easily cause 'noise' in final $\Delta\Delta G^{\ddagger}$ estimation.

However, **6-Ti** is known to be a very good comonomer incorporator, which would not be predicted with a 'normal' entropic contribution. Therefore, the unexpected $T\Delta\Delta S^{\ddagger}$ value for this system is likely to be real, and possibly due to the sterically open active site reducing difference in congestion between ethene and propene insertion TS.

It should be noted here that literature r_e values for **6-Ti** reported by different authors[232, 235] appear to be somewhat inconsistent. The difference of 0.8 kcal/mol between entry 18 (T = 323 K) and 19 (T = 363 K) in Table 2.1 translates to an entropy difference of 20 cal mol^{-1} K^{-1} between ethene and propene insertion, but the difference of 0.2 kcal/mol between entry 19 (T = 363 K) and 20 (T = 413 K) leads only to an entropy contribution of 4 cal mol^{-1} K^{-1}. In principle, such discrepancy could be explained by a change in rate limiting step occurring around 363 K. Our calculated r_e agrees with a small entropy contribution (ref. 232), which also correlates with the success of CGC type catalysts at high process temperatures.

If the unusually negative $T\Delta\Delta S^{\ddagger}$ value for **1-Zr** is also real, it might be due to the incoming propene monomer interfering with free Cp movement: the

preferred geometry for ethene insertion has perfectly eclipsed Cp rings, but in propene insertion a distortion towards a staggered arrangement is visible (Figure 2.5). Indeed, we found multiple ethene insertion TSs for ethene for **1-Hf**. The closer the insertion geometry approaches eclipsed conformation, the larger the $T\Delta\Delta S^{\ddagger}$ difference between ethene and propene insertion TSs. This difference vanishes for bridged system which is reflected by the lower $T\Delta\Delta S^{\ddagger}$ for **2-Zr** compared to **1-Zr**.

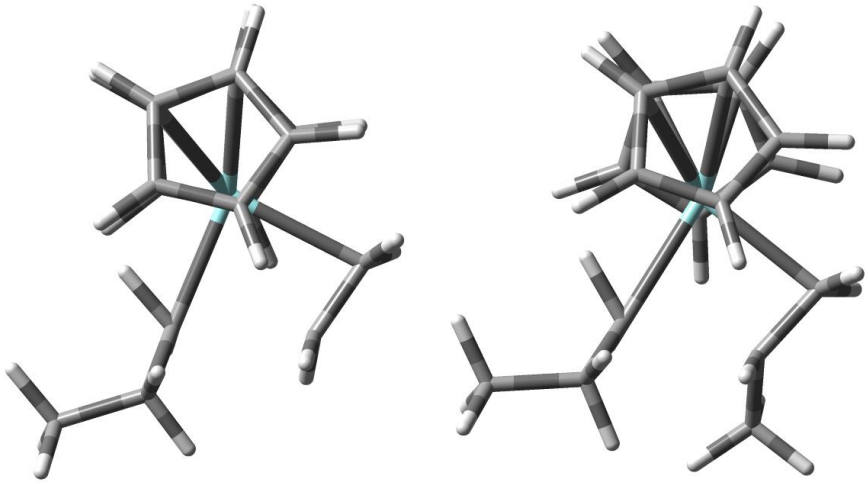

Figure 2.5 - Ethene (right) *vs*. propene (left) insertion TS in M-^{n}Pr for **1-Zr**.

2.2.2 – Modeling r_c

2.2.2.1 – Possible rate limiting steps in copolymerization

Modeling of r_c based on straightforward competing insertion TSs yielded much higher average deviations than those obtained for r_e. Since the *r*-parameters are determined by the relative rates of incorporation of two different olefins, we considered the possibility that the kinetically relevant steps for ethene and comonomer incorporation are different.[131, 146]

Few examples of systematic studies on temperature dependence of copolymerization parameters can be found in the literature. Mühlhaupt et al. has reported *T*-dependent r_e and r_c values for copolymerization of ethene and 1-octene using $Me_2Si(2\text{-}MeBenz[e]Ind)_2ZrCl_2$ (**4f-Zr**, Figure 2.1).[240-241] The data allows extrapolation of an approximate entropy contribution to $\Delta\Delta G^{\ddagger}_{(ce\text{-}cc)}$ of ~13 cal mol^{-1} K^{-1}. The authors explained this observation with solution-enthalpy of gaseous ethene in the solvent.

Lu et al. reported r_e and r_c for ethene/propene copolymerization using $Me_2Si(2\text{-}Me\text{-}4\text{-}Ph\text{-}Ind)_2ZrCl_2$ (**4d-Zr**) at 313, 333 and 353 K.[242] From 313 to 333 K, *S* = 12-18 cal mol^{-1} K^{-1} can be estimated, while *S* = 2-5 cal mol^{-1} K^{-1} from 333 to 353 K; r_c appears to be more temperature dependent than r_e in their data. Assuming competing insertion TS for both monomers, we showed that entropy contribution to r_e amounts to 2-5 cal mol^{-1} K^{-1} over a wide range of catalysts. The changing entropy contribution in Lu's data, if real, indicates a shift in rate limiting step for one monomer around ~ 333 K, possibly involving a reaction step with reduced entropic penalty (12-18 kcal/mol) with respect to insertion but clearly not a unimolecular process as this would require 30-40 cal mol^{-1} K^{-1}.

This prompted us to investigate different rate determining steps for chain propagation. The subset of catalysts considered is analogous to but slightly smaller than the one used for r_e. A variety of bridged and unbridged

metallocenes was included, along with the archetypal CGC (black structures in Figure 2.1).

Analysis of experimental trends suggests that the extent of ligand substitution effects can be different for r_e and r_c. Bis-cyclopentadienyl systems are poor incorporators, characterized by a high r_e (13.5 to 48.0) and a very low r_c (0.015 to 0.074, see also Table 2.5).[229-230] Bis-indenyl derivatives show better incorporation. However, while **4a-Zr** and **4b-Zr** have much lower r_e (5.4) than bis-cyclopentadienyl systems, r_c is only moderately better (0.05 to 0.08). 4-Ph substitution of the indenyl fragment improves r_c (**4a-Zr**: 0.08, **4c-Zr**: 0.98) much more than r_e (**4a-Zr**: 5.4, **4c-Zr**: 1.8). Bis-benzindenyl systems also show a much improved r_c (~0.3) but r_e barely changes (**4a-Zr**: 5.4, **4e/f-Zr**: 4.5).[131]

Several possible rate limiting steps have been discussed in the literature:[131] (a) insertion, (b) olefin capture, (c) rotation of the growing alkyl chain, (d) rotation of the olefin and (e) solvent and/or anion effects (which we exclude here based on the same consideration discussed earlier for r_e). Extensive screening of agostic olefin complexes and connected TSs for **4a-Zr** did not reveal any potentially limiting TS for alkyl chain or olefin rotation (c-d).

Capture (b) is generally difficult to model, since it represents a barrierless process on the PES. However, the entropic penalty generates a barrier on the 'free energy surface', making capture potentially relevant for kinetics. While exploring monomer uptake pathways, we noted that different β-agostic complexes differing in the M-olefin distance can be observed, depending on the catalyst. Their role will be explained in the following, trying to highlight the potential connection with kinetics of chain propagation.

2.2.2.2 - Bis-Cp systems: insertion/insertion competition after propene insertion

Bis-cyclopentadienyl metallocenes are among the simplest and best understood class of polymerization catalysts.[85, 87-88, 92, 243-244] Entries 1-5 of Table 2.5 show that their experimental r_c are effectively reproduced by calculations under the assumption of insertion competition in the M-^{i}Bu bond being rate limiting for both ethene and propene.

Table 2.5 - Experimental[a] and calculated[b] preference ($\Delta\Delta G^{\ddagger}_{(ce\text{-}cc)}$) for ethene over comonomer insertion. r_e given for comparison. In kcal/mol.

Entry	Cat.	Solv.	T (K)	r_e	r_c	$\Delta\Delta G^{\ddagger}_{(ce\text{-}cc)}$ (kcal/mol)				BVol (%)[c]	Ref
						Exp.	Calc. INS	Calc. BBRA	Δ		
ethene *vs.* propene insertion											
1	**1-Ti**	Hept	323	19.5	0.015	-2.7	-2.4	N/A	0.3	66.5	230
2	**1-Zr**	Hept	323	48.0	0.015	-2.7	-2.7	N/A	0.0	62.3	230
3	**1-Hf**	Hept	323	13.5	0.041	-2.1	-2.1	N/A	0.0	62.4	229
4	**2-Zr**	Hept	323	24.0	0.029	-2.3	-2.5	N/A	-0.2	62.1	230
5	**3-Zr**	Hept	323	25.6	0.074	-1.4	-1.8	N/A	-0.4	-	229
6	**4a-Zr**	Hept	323	5.4	0.08	-1.6	-2.3	(-2.9)	-0.7	65.1	131
7	**4b-Zr**	Hept	323	5.4	0.05	-1.9	-2.4	(-3.8)	-0.5	67.2	131
ethene backbone rearrangement *vs.* propene insertion											
8	**4c-Zr**	Tol	323	1.8	0.98	0.0	(-1.4)	0.0	0.0	-	131
9	**4d-Zr**	Tol	323 343	2.0	0.88 0.44[d]	-0.1 -0.7	(-1.2)	-0.7 -0.9	0.2	68.4	131
10	**4e-Zr**	Tol	323	4.5	0.29	-0.8	(-2.6)	-1.3	-0.5	65.4	131
ethene backbone rearrangement *vs.* propene backbone rearrangement											
11	**4f-Zr**	Tol	323	4.5	0.35	-0.7	(-2.5)	-1.3	-0.5	67.6	131
12	**6-Ti**	Hept	363	3.8	0.38	-0.7	(-2.6)	-1.0	-0.3	62.5	232
								MAD	**0.3**		

[a] Activator: MAO; [b] M06-2X(PCM)/TZ//TPSSTPPSS/DZ; [c] buried volume, taken from ref. 96; [d] second r_c value for **4d-Zr** taken from ref. 126. Calc. INS = including only insertion TS; Calc. BBRA = including BBRA when relevant. N/A = BBRA TS nonexistent. Tol = toluene, Hept = heptanes. MAD = Mean Average Deviation.

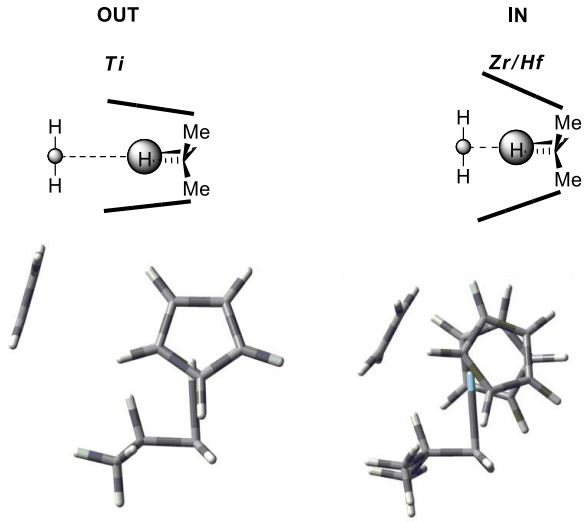

Figure 2.6 - Cis β-agostic ^{i}Bu/ethene complex for Cp_2M systems. Average M-C_{ethene} distances Ti: 4.89 Å, Zr: 2.84 Å, Hf: 2.83 Å. $Cp_{centroid}$-M-$Cp_{centroid}$ angles: Ti 136°, Zr 129°. Top: schematic side view along the C=C axis, small grey circle carbon atom(s) of ethene, large grey circle central metal. Bottom: Optimized structure (top view).

Nonetheless, it is very instructive to inspect the cis β-agostic olefin capture complexes for **1-Ti**, **1-Zr** and **1-Hf** (Figure 2.6). The monomer is only loosely captured in the second coordination sphere of the metal for titanocene **1-Ti** (*out* structure, Ti-C_{ethene} 4.89 Å), while it is neatly tucked into the first coordination sphere for **1-Zr** and **1-Hf** (*in* structure, M-C_{ethene} ~2.84 Å). This can be easily rationalized considering that the stability of the π-complex is dominated by the accessible surface area of the metal,[87] which is rather small for Ti and larger for Zr and Hf.

The Cp rings in **1-Ti** are eclipsed while they are staggered and more bent towards each other in **1-Zr** and **1-Hf**. In difference to olefin coordination to Cp_2ZrMe^+,[244] the monomer is coordinated symmetrically (near equivalent M-C_1 and M-C_2 olefin bonds) in all three cases.

In these small and highly symmetric systems, a symmetric monomer approach following the path of least steric hindrance seems to be preferred

and we find only a single olefin capture local minimum in each case: *in* for **1-Zr** and **1-Hf**, and *out* for **1-Ti** where there is not enough space for direct olefin coordination. Insertion TS for all three systems are geometrically close to the *in* structure. We hypothesized that in more highly substituted and less symmetric systems the preferred approach path might also be less symmetric, so that both *in* and *out* cis β-agostic olefin complexes might exist and that the connecting TS could become rate limiting.

2.2.2.3 - Indenyl based metallocenes and CGC: backbone Induced changes in the rate limiting step after propene insertion

Indeed, we were able to locate two cis β-agostic olefin structures and the TS connecting them for all Zr indenyl metallocenes and for CGC **6-Ti.** Figure 2.7 provides a schematic representation of the process. Olefin capture initially leads to the *out* structure or capture complex; then, an opening motion of the catalyst backbone allows the monomer to enter the first coordination sphere of the metal, resulting in the β-cis agostic *in* structure.

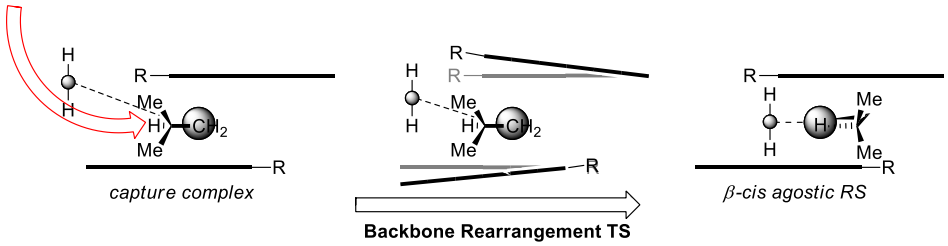

Figure 2.7 - Schematic representation of the two cis β-agostic *i*Bu/ethene complexes, asymmetric approach vector of olefin and the BBRA TS connecting both for indenyl type metallocene systems. Olefin shown in front view.

This rearrangement does not only involve the *iso*-butyl chain, but consists in a 'breathing motion' of the indenyl fragments and/or rotation of the

2-methyl substituent. No indication for ring slippage or haptotropic rearrangements could be found.[245-247] We call this process backbone rearrangement (BBRA) to emphasize that the movement in the TS resembles an opening of the catalyst mouth, and to distinguish it from the capture TS that connects the naked cation with dissociated olefin to the capture complex. A true capture TS likely only exists on the Gibbs free energy surface (not on the potential energy surface) and can thus only be computed using -for example- molecular dynamics.

Concerning ethene, the BBRA TS is always competitive (within ±2 kcal/mol) with the actual insertion TS (INS). For Zr indenyl systems at 323 K, the rate limiting step depends on the ligand, changing from ethene INS (**4a-Zr** and **4b-Zr)** to ethene BBRA (**4c-Zr** to **4f-Zr)**. As an example, Figure 2.8 shows the free-energy profile for **4f-Zr**.

Propene INS barriers are usually higher than the ones for ethene. As a result, insertion is predicted to be rate limiting for **4a-Zr** to **4e-Zr** (0.4 to 3.2 kcal/mol above BBRA for propene); only for the most hindered Zr-indenyl system (**4f-Zr**) is BBRA predicted to have a higher barrier than INS. For the constrained-geometry system **6-Ti**, BBRA is limiting for both ethene and propene.

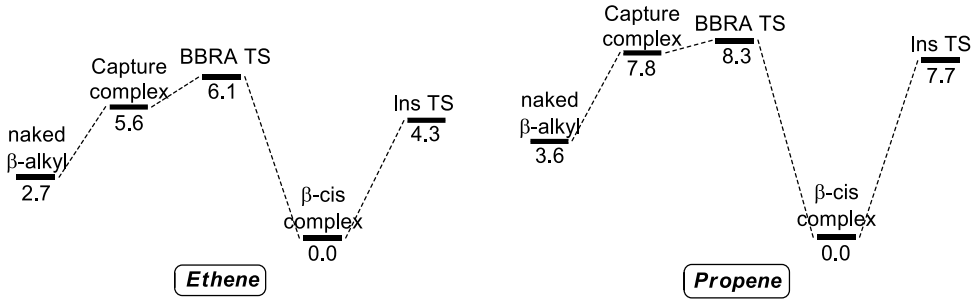

Figure 2.8 - Relative free energy profile (kcal/mol, 323 K, heptane) for ethene (top) and propene (bottom) insertion into the Zr-^{i}Bu bond in **4f-Zr**.

BBRA is part of the monomer uptake pathway; at the insertion TS virtually all the entropic two-to-one particle penalty has been paid, as opposed to roughly 2/3 of it at the BBRA stage. This more favorable entropic term is compensated by the 3-4 kcal/mol higher enthalpic barrier for BBRA. The true capture TS has to be earlier than BBRA, and therefore have an even smaller entropy penalty; thus, a substantial enthalpy contribution (far away from the catalyst) would be necessary for it to become kinetically relevant. Although we cannot exclude it, we find this rather unlikely.

2.2.2.4 - Experiment *vs*. computational prediction of r_c

Experimentally, r_c values of the 12 catalysts studied range from 0.015 (poor incorporation) to 0.98 (very good incorporation). This translates to a $\Delta\Delta G^{\ddagger}_{(cc\text{-}ce)}$ preference for ethene insertion of 2.7 to 0.0 kcal/mol. Compared to the copolymerization factor r_e, r_c usually has larger experimental error margins of up to ± 0.4 kcal/mol (see Table 2.5 and references therein).

Table 2.5 shows predicted r_c values (as $\Delta\Delta G^{\ddagger}$) separated into systems where according to calculations INS/INS is rate limiting (**1-Ti/Zr/Hf**, **2-Zr**, **3-Zr**, **4a-Zr**, **4b-Zr**), systems where ethene BBRA competes with propene INS (**4c-Zr**, **4d-Zr**, **4e-Zr**) and systems where BBRA is rate limiting for both monomers (**4f-Zr** and **6-Ti**). The MAD is good if BBRA is factored in (0.3 kcal/mol) and comparable to that obtained with r_e. Solvent corrections are essential also in this case, especially for those systems where BBRA is rate limiting (Figure 2.9).

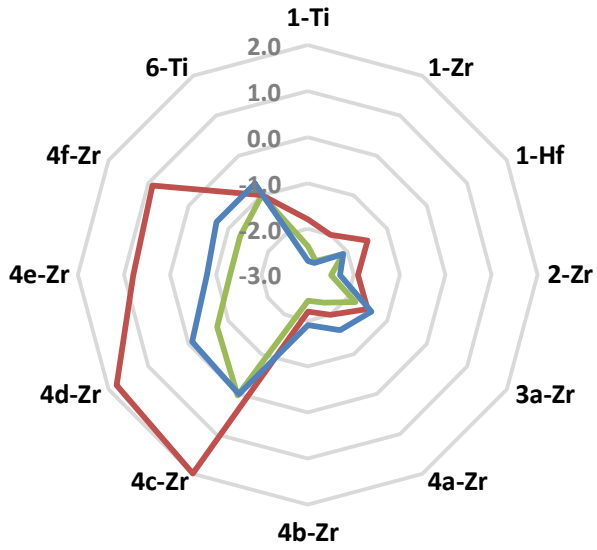

Figure 2.9 - Influence of solvent corrections on predicted *vs.* experimental $\Delta\Delta G^{\ddagger}_{(ce\text{-}cc)}$ (kcal/mol) values. Blue line experimental value, red line uncorrected, green line solvent corrected.

2.2.2.5 – Catalyst comparison: entropic and enthalpic effects on r_c

Trends in enthalpic and entropic contribution to $\Delta\Delta G^{\ddagger}_{(ce\text{-}cc)}$ are graphically reported in Figure 2.10 for all metallocene systems under a uniform set of conditions (323 K, heptane). We did not include the only post-metallocene **6-Ti** here, as it belongs to a different class of catalysts and it is unclear whether results for this species are representative.

We found earlier for r_e that $T\Delta\Delta S^{\ddagger}_{(ec\text{-}ee)}$ shows modest variations around an average value of -1.25 kcal/mol at 323 K, favoring ethene insertion. Likewise, for those systems where r_c is determined by INS/INS competition, we now find a fairly constant entropic contribution $T\Delta\Delta S^{\ddagger}_{(ce\text{-}cc)}$ of roughly +1.5 kcal/mol (favoring ethene). The same interpretation based on the symmetry term $-RT\ln(\sigma)$ might apply in this case. The enthalpic contribution $\Delta\Delta H^{\ddagger}$ is small for these catalysts (-1.0 to -0.5 kcal/mol) but consistently favors ethene. The increased

steric bulk of the *iso*-butyl chain with respect to *n*-propyl is probably the origin of the enhanced preference for the smaller ethene monomer.

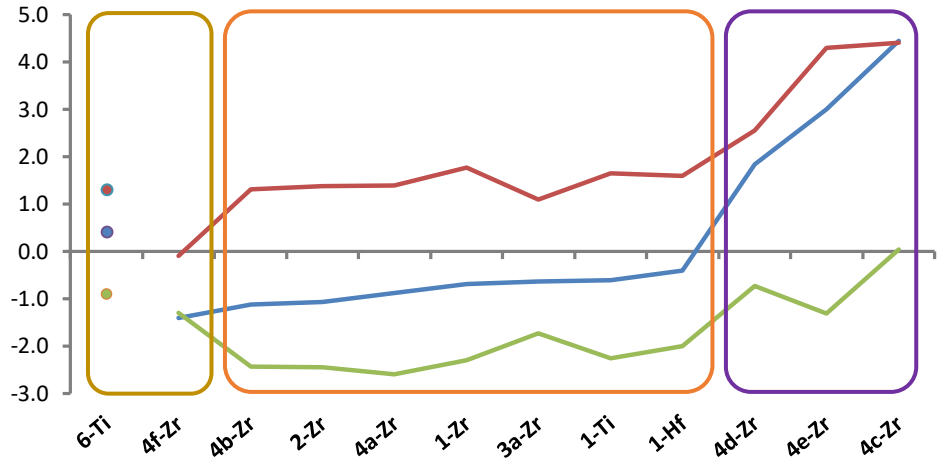

Figure 2.10 - Calculated entropy ($T\Delta\Delta S^{\ddagger}_{(ce\text{-}cc)}$, red line) and enthalpy ($\Delta\Delta H^{\ddagger}_{(ce\text{-}cc)}$, blue line) contributions (kcal/mol) to $\Delta\Delta G^{\ddagger}_{(ce\text{-}cc)}$ (green line) in E/P copolymerization (323 K, solvent heptane). Brown rectangle BBRA/BBRA, orange insertion/insertion, violet BBRA/insertion competition.

Conversely, $T\Delta\Delta S^{\ddagger}_{(ce\text{-}cc)}$ is close to zero for BBRA/BBRA competition, reflecting that transition states for ethene and propene BBRA are comparably loose; the $\Delta\Delta H^{\ddagger}$ contribution is also small here. Entropy differences for BBRA/BBRA are lower than for insertion/insertion competition also in the case of **6-Ti**.

Larger effects are seen for the three BBRA/INS competition cases. The entropic contribution favors ethene (BBRA) over propene (insertion), which likely is due to the 'looser' character of the capture TS. However, enthalpy in this case favors propene, and the enthalpy/entropy compensation results in final $\Delta\Delta G^{\ddagger}_{(ce\text{-}cc)}$ values that are only about 1.5 kcal/mol less negative than for the INS/INS case.

The identification of BBRA as potential rate limiting step in copolymerization might provide an interesting insight in steric effects

determining comonomer incorporation. As pointed out before, it has been demonstrated that a more open catalyst mouth does not necessarily imply an easier comonomer insertion.[139] Table 2.5 shows buried volume values for most catalysts in this study, taken from recent work by the groups of Cavallo and Talarico.[96] The trend in buried volume does not follow the trend in BBRA barriers, in line with the above considerations.

However, it might be possible to rationalize the role of steric bulk remote from the active pocket in determining propagation kinetics. For instance, the catalyst pair **4a-Zr**/**4e-Zr** exhibit the same buried volume, since the additional steric bulk of the benzindenyl fragment is located far from the metal center. Therefore, while this change in ligand backbone has negligible effects on the relative insertion barriers (tight TS structures), olefin approach to the metal is affected by the presence of the additional steric crowding, leading to increased BBRA barriers. Indeed, predicted ethene/propene competition at the insertion TS stage yield no difference in $\Delta\Delta G^{\ddagger}_{(ce\text{-}cc)}$ between these two systems, while including BBRA enables us to reproduce the higher propene affinity of **4e-Zr** (Table 2.5).

Analogous reasoning can be applied to the couple **1-Ti/6-Ti**. Although CGC is 'more open' than bis-Cp titanocene, opening of the active pocket of the catalyst by replacing a Cp ring of **1-Ti** with a bridged amido moiety leads to the appearance of two stable olefin coordination structures (*in* and *out*) and the connecting BBRA TS becomes rate limiting.

2.2.2.6 - Temperature dependence of r_c

In cases where both exist, we found that INS and BBRA TS are always close in energy. The balance between them can be tuned with temperature, resulting in kinetic regime crossovers. The BBRA TS has a higher entropy (and a

less favorable enthalpy) than insertion, so increasing the temperature stabilizes it and hence tends to make INS rate limiting. This shift in rate limiting step can occur both for ethene and propene, and therefore three kinetic regimes and two crossover points are typically possible for r_c (Table 2.6). $\Delta\Delta S^{\ddagger}$ is the largest for cases in the BBRA/INS regime, so these are also the cases where r_c varies most strongly with temperature. Conversely, r_c will be almost *T*-independent in the temperature range where BBRA is rate limiting for both ethene and propene.

Table 2.6 - Rate limiting step competition and entropy influence (cal mol^{-1} K^{-1}) for r_c.

T	Rate limiting for ethene	Rate limiting for propene	Approx. $\Delta\Delta S$ (cal mol^{-1} K^{-1})
Low	BBRA	BBRA	~0
Intermediate	BBRA	INS	~10
High	INS	INS	~4

Table 2.7 - Predicted $\Delta\Delta G^{\ddagger}_{(ce\text{-}cc)}$ at different temperatures and rate limiting step changes.

Catalyst	223 K		273 K		323 K		373 K	
	r. l.	$\Delta\Delta G^{\ddagger}$	r. l.	$\Delta\Delta G^{\ddagger}$	r. l.	$\Delta\Delta G^{\ddagger}$	r. l.	$\Delta\Delta G^{\ddagger}$
4a-Zr	*/I	-2.1	I/I	-2.3	I/I	-2.6	I/I	-2.9
4b-Zr	I/I	-2.0	I/I	-2.2	I/I	-2.4	I/I	-2.6
4c-Zr	B/B	0.7	B/B	0.7	B/I	0.0	B/I	-0.6
4d-Zr	B/B	-0.5	B/B	-0.5	B/I	-0.7	B/I	-1.1
4e-Zr	B/I	-0.2	B/I	-0.7	B/I	-1.3	B/I	-2.0
4f-Zr	B/B	-1.4	B/B	-1.3	B/B	-1.3	B/B	-1.3
6-Ti	B/B	-0.5	B/B	-0.7	B/B	-0.9	B/B	-1.0

r. l. = rate limiting, B/B = BBRA/BBRA competition, I/I = insertion/insertion competition, B/I =BBRA/insertion competition. *BBRA and insertion have equal barrier heights. Solvent = heptane.

Temperature dependence and switches in rate limiting step were computationally explored for catalysts **4a-Zr** to **6-Ti** in the range from 223 to 373 K (Table 2.7). Catalysts **4a-Zr** and **4b-Zr** show only INS/INS competition, while **4c-Zr** and **4d-Zr** show BBRA/BBRA competition between 223 and 273 K but crossover to BBRA/INS competition at higher temperatures. Predictions for

4d-Zr are in nice agreement with experiment, which implied a switch in rate limiting step around 333 K.[242] In the BBRA/INS regime, incorporation decreases rapidly with increasing temperature (2-fold over only 50 K for **4c-Zr**). Finally, **4f-Zr** shows BBRA/BRRA competition even up to 373 K and incorporation increases with increasing temperature (10-fold over 150 K).

2.3 – Concluding remarks

In this Chapter we presented a highly reliable computational protocol (MAD: 0.2 kcal/mol) to reproduce the copolymerization parameter r_e for several metallocene and non-metallocene catalysts. An appropriate modeling of dispersion and solvent corrections seems to be the origin of the improved agreement between experiment and theory with respect to previous attempts.

The high accuracy of the method allowed to analyze enthalpic and entropic contributions to comonomer affinity. For instance, the results suggest that the commercial success of CGC is at least in part due to an exceptionally small entropic contribution, whereas for *ansa*-metallocenes as **4a-Zr** to **4f-Zr** enthalpic factors appear to be more important. The present computational protocol reaches an accuracy needed for a computational hit-or-miss approach and could aid in the development of HTC tools for *in silico* prescreening of ethene/α-olefin copolymerization catalysts.

The same straightforward DFT protocol can be applied to the modeling of the more intricate r_c parameter, provided that the olefin capture process is included in the model. We proposed that Backbone rearrangement (opening of the active site of the catalyst to accommodate the incoming olefin) can become competitive with insertion. For both ethene and propene, BBRA can be important even at elevated temperatures, especially for ethene insertion after propene insertion. The identification of this new potentially rate limiting step for chain propagations allows to computationally reproduce *T*-dependence of reactivity ratios and the effect of steric bulk remote from the active pocket.

Although BBRA could also play a role in the competition for insertion after ethene insertion (r_e), calculating only insertion TS appears to yield results accurate enough for predictive purposes. This is not the case for r_c, and it appears likely that each catalysts class will require careful analysis of the whole olefin incorporation path if accurate estimates of r_c are desired. The added

complexity of having to search for capture transition states on a flat potential energy surface makes HTC prescreening for copolymerization less straightforward than one might hope for.

2.4 –Computational Part

All geometries were fully optimized by using the Gaussian 09 software package[248] in combination with the OPTIMIZE routine of Baker[249250] and the BOpt software package.[251] Insertion transition states were located by direct optimization from a suitable initial geometry. In more complex cases, *e.g.* backbone rearrangement, we used either the *Synchronous Transit-Guided Quasi-Newton* (STQN) Method, developed by H. B. Schlegel and coworkers[252-253] (Opt=QST2 or QST3) or a relaxed potential energy scan (as implemented in Gaussian 09) to arrive at a suitable transition state guess, followed by a optimization using OPTIMIZE.

Following the protocol proposed in ref. 104, all relevant minima and transition states were fully optimized at the TPSSTPSS level[254] of theory employing correlation-consistent polarized valence double-ζ (Dunning) basis sets,[255-261] from the EMSL basis set exchange library,[262-263] with cc-pVDZ-(PP) quality and accompanying small core pseudopotential for Zr and Hf.[264-267]

All calculations were performed at the standard Gaussian 09 quality settings [Scf=Tight and Int(Grid=Fine)]. All structures represent either true minima (as indicated by the absence of imaginary frequencies) or transition states (with exactly one imaginary frequency corresponding to the reaction coordinate). Final single-point energies were calculated at the M06-2X level of theory[268] employing triple-ζ Dunning basis sets.[255-261] Solvent effects were included with the polarizable continuum model approach (PCM) at this stage.[228] Selected optimizations in solvent revealed no significant differences. Convergence criteria were not relaxed with the exception of propene BBRA in **6-Ti** (TOLG 0.0002 instead of 0.0001). This approximation should not cause significant error, as all BBRA TS are located on a plateau of the potential energy surface. For further discussion see Ref. 90.

For additional verification, a few modifications of the above standard protocol were explored. Several alternative functionals were tested for single-point energy corrections (M11, B3PW91-D3, TPSSh-D3, PBE0-D3) and gave results comparable to M06-2X.[269] Selected optimizations including a solvent model revealed no significant differences in geometries.

Enthalpies and Gibbs free energies were obtained from TZ single-point energies and thermal corrections from the TPSSTPSS/cc-pVDZ-(PP) vibrational analyses. Entropy corrections were scaled by a factor of 0.67 to account for decreased entropy in the condensed phase. [270-272] To limit entropy increase, low frequencies were adjusted to value ≥10 cm^{-1}. To account for the last inserted monomer effect, we modelled insertion of olefin using *n*-propyl and *iso*-butyl as polymeryl chain models for insertion after an ethene and propene last-inserted unit. Only primary insertions were considered.

Chapter 3

Selectivity in chromium catalyzed ethene oligomerization: the case of BIMA catalysts giving alternating LAOs distributions

3.1 - Introduction

Ethene oligomerization giving Linear α-Olefins (LAOs) has become a topic of growing interest for both industry and academia.[273-276] The discovery of the so-called 'nickel-effect' by Ziegler in mid 1950s, shed light on the catalytic ability of Ni to produce 1-butene.[277,278,279] Since then, many oligomerization catalysts based on late transition metals have been developed,[274] with the Brookhart-type diazadiene (DAD)[280-281] and the Shell Higher Olefin Process (SHOP, Figure 3.1)[275] systems being some of the most prominent examples.

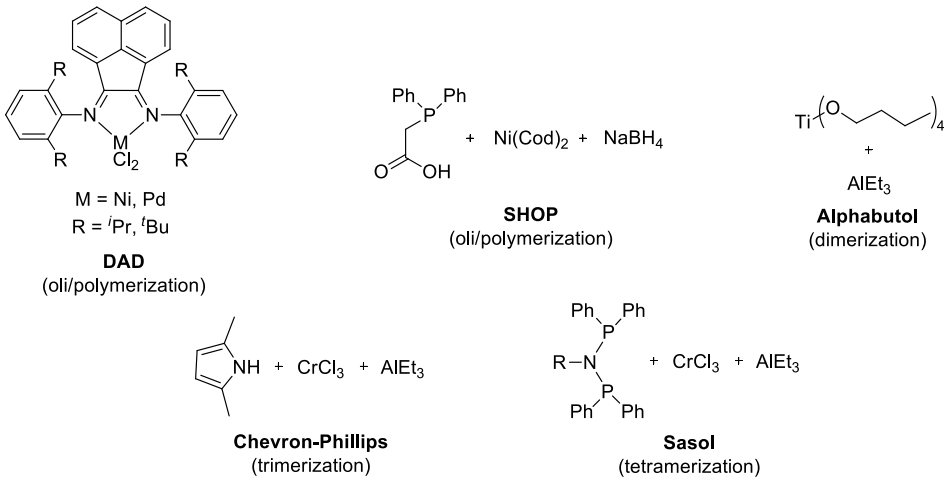

Figure 3.1 – Notable examples of oligomerization catalysts.

These systems generally give Schultz-Flory distributions of oligomers in the range C_4-C_{20}, and operate by the same Cossee-Arlman mechanism that olefin polymerization is based on.[68] Starting from a Ni-hydride complex, olefin coordination and migratory insertion lead to a linear chain growth, which typically terminates *via* β-H elimination (BHE, Scheme 3.1a). In fact, what differentiates Ni-based oligomerization from group IV polymerization catalysis is mostly the higher propensity of late transition metal to undergo BHE, yielding lower MW products and maximizing olefinic chain ends. Generally, a

pronounced steric bulk round Ni metal center is required in order to favor chain growth beyond 1-butene.[274, 280-281] An important issue with late transition metals is chain walking, which leads to branched polymers and/or undesirable internal olefins.[280, 282-285]

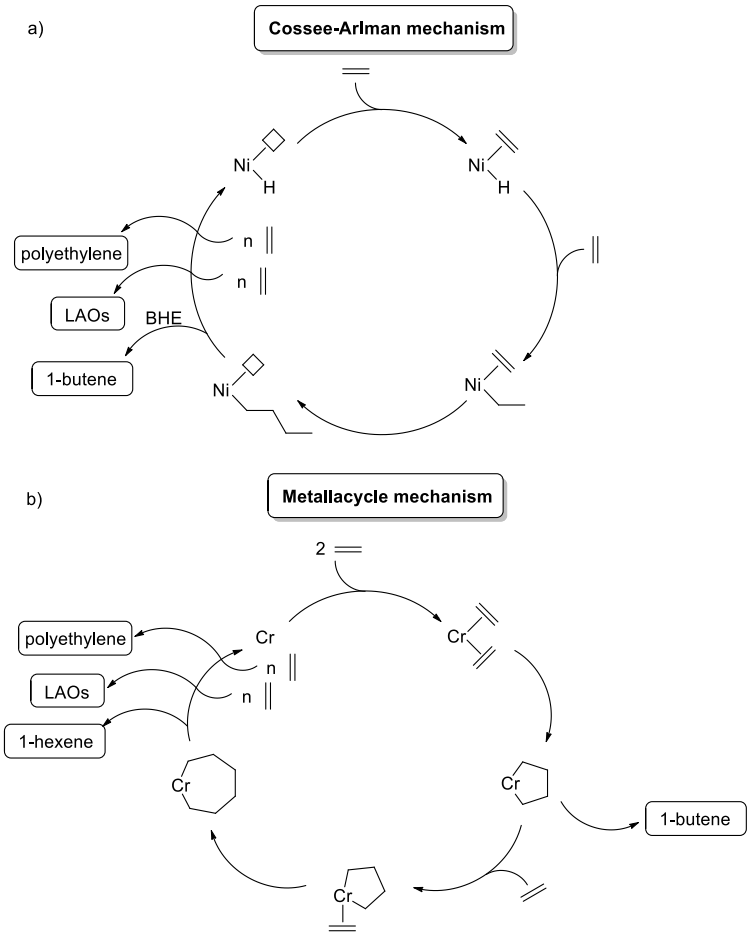

Scheme 3.1 – Schematic comparison between Cossee-Arlman (linear chain growth) and metallacycle mechanism for ethene oligomerization.

It should be noted, however, that also group IV systems are known to oligomerize ethene in some cases where chain termination is particularly favorable. One of the most notable examples is the IFP/Sabic Alphabutol process based on Ti-alkoxides and triethyl aluminum (Figure 3.1).[286-288]

In the last few years, promising systems based on chromium have drawn much attention as well.[200-201] They were initially inspired by modifications of the heterogeneous Phillips catalysts; Manyik *et al.* first reported the high propensity of some Cr systems to co-produce ethylene oligomers and polymers in 1967.[289] More recently, Chevron-Phillips has commercialized a homogeneous pyrrole-based Cr-catalyst for ethene trimerization,[290-291] while another very interesting system based on PNP ligands for selective tetramerization has been proposed by Sasol (Figure 3.1).[292]

Chromium catalysts operate by a different mechanism, first proposed in 1977[293] and then refined by Briggs in 1989.[294] The catalytic cycle initiates with double ethylene coordination to the metal center, followed by oxidative coupling to form a chromacyclo-pentane; insertion of further monomer units leads to expansion of the metallacycle, which eventually can reductively eliminate giving an α-olefin (Scheme 3.1b).[295] Chain termination processes are similar but different from those of the Cossee-Arlman mechanism, as schematically reported in Scheme 3.2. The three most common routes are (a) β-H transfer to Cr followed by C-H reductive elimination, (b) a concerted mechanism involving β-H transfer to $C_{\alpha'}$, or (c) β-H transfer to coordinated monomer and 'back' β-H transfer to $C_{\alpha'}$.[295] It is generally accepted that a Cr(I)/Cr(III) redox couple is involved.[296-299] This mechanism is well established for trimerization reactions, while it is still debated for tetra- and oligomerization.[200, 295] In many cases, metallacycle and Cossee-Arlman mechanisms can be easily distinguished by deuterium labeling studies.[294, 300-301]

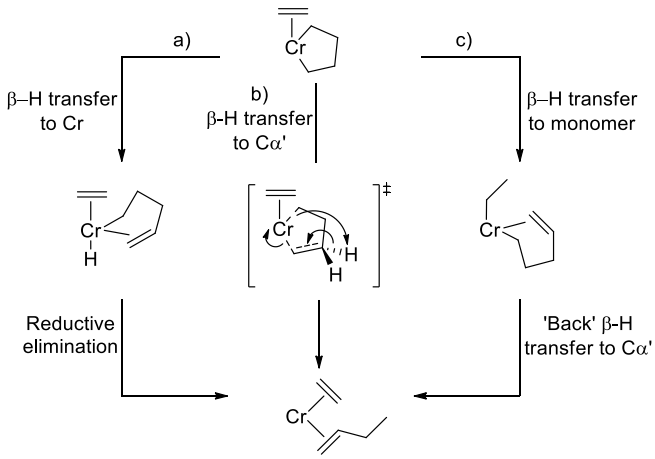

Scheme 3.2 – Most common chain termination processes for metallacycle mechanism.

The relative stabilities of the various metallacycles determine the competition between chain propagation and termination. In many cases, H-transfer reactions are particularly favored for 7- to 9-membered rings, which explains why Cr-catalysts are largely used for selective tri- and tetramerization of ethene.[200] However, several other systems easily grow much larger metallacycles up to formation of polyethylene chains; Schultz-Flory distributions are generally obtained in these cases.[300, 302-303]

Along with some applications as intermediates for the production of detergents and lubricants, the main commercial interests for LAOs focus on C_4-C_8 oligomers as comonomers for LLDPE.[200] Consequently, controlling catalysts selectivity to access a specific oligomer fraction is a top priority for ethene oligomerization in order to avoid an expensive product purification step. A large variety of LAOs distributions can be obtained by modifying catalysts structure and experimental conditions.

In 2006, the group of Gibson introduced the first bis(benzimidazolyl)methylamine (BIMA) Cr(III)-complex in the realm of homogeneous oligomerization precatalysts (Figure 3.2). Upon activation with MAO, this system gives a very peculiar alternating distributions of LAOs (Figure

3.3), in which oligomers obtained from an odd number of ethylene units (*e.g.* 1-hexene, 1-decene) are less abundant than those with an even number (*e.g.* 1-octene, 1-dodecene).[304] Although this kind of distribution is not of immediate commercial relevance, rationalizing the processes originating it would be of great interest to gain insight in selectivity tuning in ethene oligomerization.

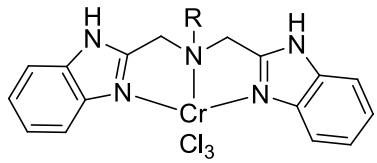

9-R

Figure 3.2 - Bis(benzimidazolyl)amine (BIMA) Cr-catalysts

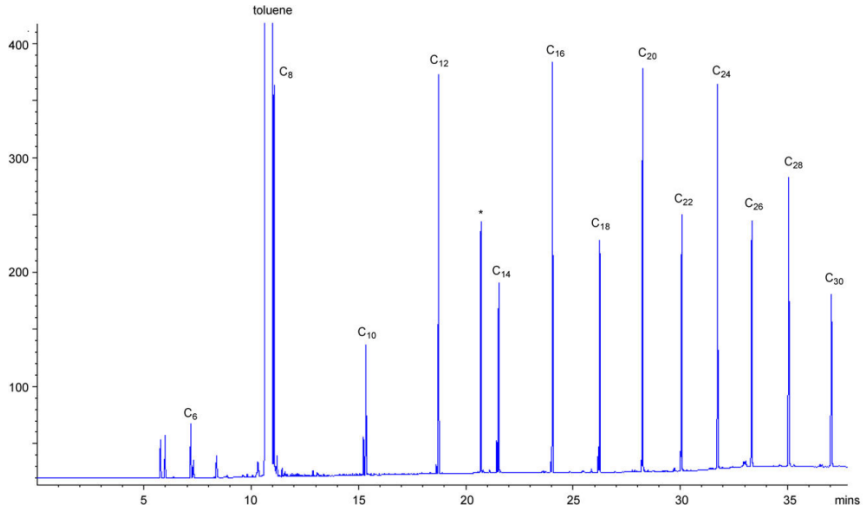

Figure 3.3 – GC trace showing alternating molecular weight distribution of LAOs obtained with **9-Me**/MAO; taken from ref. 304.

The group of Britovsek has recently proposed an interpretation of these results based on an expanded metallacycle mechanism, involving a competition between single and double insertion of ethylene.[213] This mechanistic and kinetic model would also explain other intriguing observations, such as the aforementioned high selectivity of PNP catalysts for 1-octene.[212, 305-306]

The same group has carried out an extensive screening of differently substituted BIMA-catalysts and various reaction conditions, which provided an interesting insight in the chemistry of these systems.[307] In the framework of a three-month internship in the Britovsek group at Imperial College London (UK), this PhD work has contributed to provide supporting experimental evidence for the proposed double insertion mechanism. At first, the dependence of linear α-olefin (LAOs) distribution on ethylene pressure was investigated for two representative catalysts: **9-Me** and **9-H**. Secondly, the effect of external donors in the polymerization mixture was explored and the synthesis of the analogous [NPN] phosphine ligand was attempted.

3.2 – Results and Discussion

Figure 3.4 shows a comparison between typical Schultz-Flory (a) and alternating (b) LAOs distributions, obtained with bis-(benzimidazole)pyridine and BIMA Cr-complexes respectively.[213] It is instructive to comment on the different metallacycle mechanisms these two systems operate by, and how this translates to the different distribution of products.

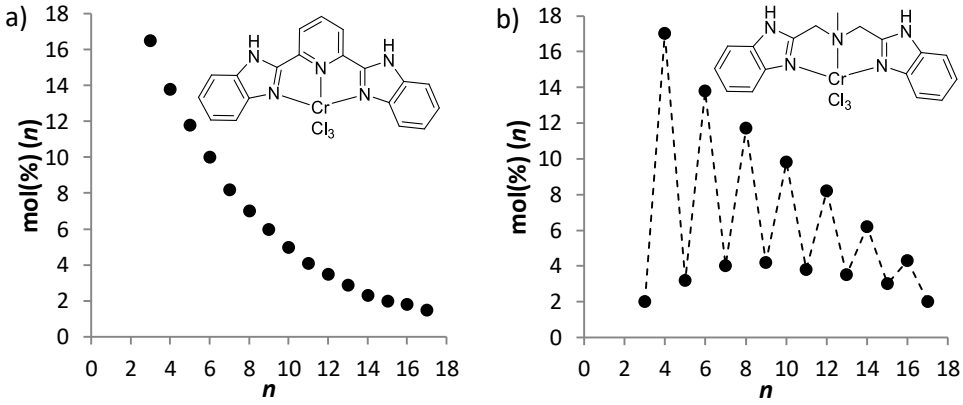

Figure 3.4 – Comparison between (a) Schultz-Flory and (b) alternating LAOs distributions. *n* = number of ethylene units in the oligomer. Data from ref. 213.

Chain growth by bis-(benzimidazole)pyridine catalyst occurs *via* 'classical' metallacycle mechanism (Scheme 3.3a); we can define α as the probability of single ethylene insertion in the growing metallacycle and consequently (1-α) as the probability of chain termination. Both α and (1-α) are roughly constant for all the differently sized cycles.

The resulting LAOs distribution can be mathematically described *via* 1st order recurrence relations, in which each oligomer fraction (T_{n+1}, n = number of ethylene units) is related to the previous one (T_n) by the probability of insertion α, according to Formula 3.1. This represents a simplified mathematical

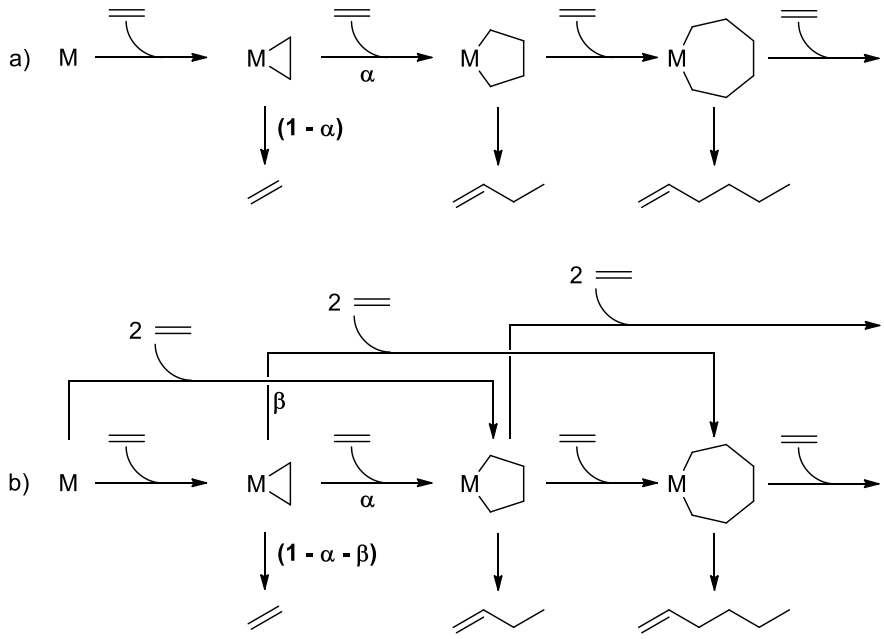

Scheme 3.3 – Pictorial comparison between metallacycle mechanism *via* (a) single and (b) competing single and double ethylene insertion. Adapted from ref. 213.

expression to describe Schultz-Flory distributions (Figure 3.4a), alternative to the one first proposed by Flory in 1936.[308]

(3.1) $$T_{n+1} = \alpha \cdot T_n$$

In the case of BIMA catalysts, an additional route is possible, in which two ethylene units are coordinated to Cr at the same time and insertion of the first triggers insertion of the second one (Scheme 3.3b).[212-213, 307] The probability of this double insertion is defined as β, and therefore (1-α-β) is the one for chain termination. Analogous mechanisms have already been debated for Ziegler-Natta[309-310] and metallocene catalysts.[311] These competing propagation processes entail that each oligomer fraction (T_{n+2}) is related to previous one (T_{n+1}) by α, and the one before (T_n) by β, as in equation 3.2:

(3.2) $$T_{n+2} = \alpha \cdot T_{n+1} + \beta \cdot T_n$$

This 2nd order recurrence relation allows description of alternating LAOs distribution of the type reported in Figure 3.4b. In this case, this formalism is much simpler, since the one developed by Schultz and Flory would give very complicated equations.[212-213, 307]

The β/α ratio is an effective parameter to describe the relative preference for double *vs.* single ethylene insertion, as already reported in the literature.[307] In the following we will mostly refer to this quantity to evaluate the induced changes in LAOs distribution.

Insertion probabilities α and β can be calculated by fitting experimental LAOs. The general solution of recurrence relation takes the form of Equation 3.3, whereby $c_{1,2}$ and $r_{1,2}$ are related to α and β as described in ref. 213.

(3.3) $$mol\,(n) = c_1 r_1^{\,n} + c_2 r_2^{\,n}$$

This equation formally corresponds to the sum of (a) an exponential decay function $c_1 r_1^{\,n}$ with a positive decay parameter r_1, and (b) an alternating exponential decay function $c_2 r_2^{\,n}$ with a negative parameter r_2 (Figure 3.5).[213] The c_1/c_2 ratio gives an indication of the extent of alternation.

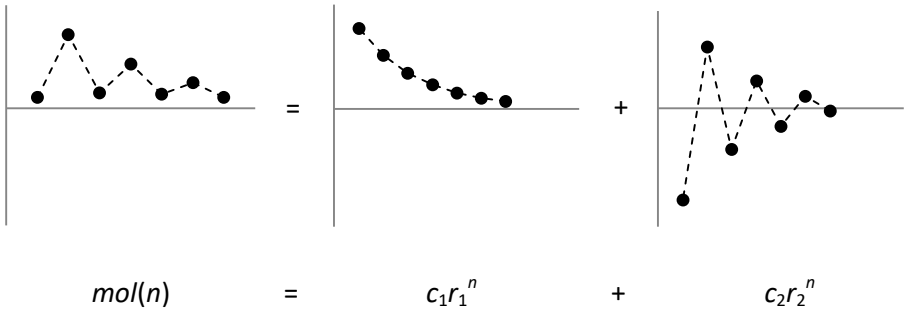

Figure 3.5 – Pictorial representation of Eq. 3.3.

Regarding the experiments described below, data fitting analysis was performed using the C_8-C_{32} LAOs fraction (*i.e.* n = 4 to 16). 1-hexene (n=3) was excluded from the fitting since it appeared to be an outlier, being slightly more

abundant than expected from calculated distributions. This might indicate some deviation from constant α and β probabilities in the early stages of metallacycle growth, which could be traced to the relative stability of chromacyclo-heptane and higher metallacycles.

It should be noted that the above description of alternating distribution is only a very simplified version of the comprehensive model developed by the Britovsek group. A more detailed mathematical and chemical discussion is beyond the scope of this work, but can be found in several publications[212-213, 298, 304-307] and in the PhD thesis of Dr. Craig T. Young from Imperial College London.[312]

3.2.1 – Pressure dependence of LAOs distribution

Recently published results described the pressure dependence of the β/α ratio for the representative BIMA catalyst **9-Hex** (Hex = *n*-hexyl).[307] According to the proposed kinetic model, this dependence can be mathematically described by Equation 3.4, whereby the constants g_1 and g_2 originate from a combination of rate constants involved for the various reactions.[312] However, experimental observations in the range 1 to 4 bar (Figure 3.6) were not enough to discriminate between this relation and a more simple linear dependence of the type described by Equation 3.5.

(3.4) $$\frac{\beta}{\alpha} = \frac{P_{Et}}{g_1 + g_2 P_{Et}}$$

(3.5) $$\frac{\beta}{\alpha} = g P_{Et}$$

The first goal of this work was to expand the pressure range, trying to get experimental evidence for the expected drop of β/α at $p < 1$ bar. Based on the structure/activity database available,[307] the selected case studies were **9-Me** and **9-H**. The former exhibits a remarkable catalytic activity -which is especially desirable to get reasonable LAO yields also at low monomer pressure- and a

marked alternating distribution. On the other hand, **9-H** is only moderately active but gives a peculiar gentle alternating distribution, which might indicate an interesting 'borderline' kinetic regime.

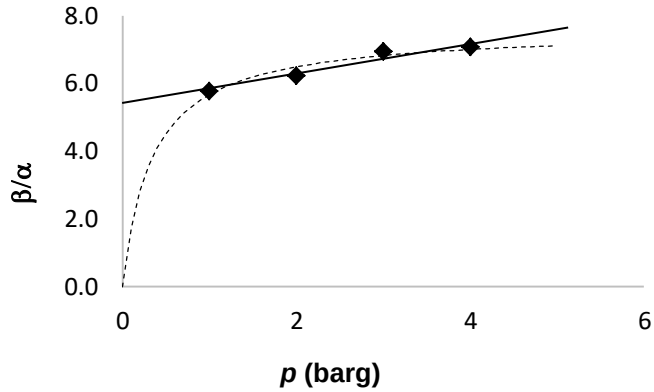

Figure 3.6 – Dependence of β/α on ethylene pressure for **9-Hex**, showing fitted curves according to Formula 1 (dashed) or 2 (full). Data from ref. 307.

Oligomerization runs were carried out by keeping all experimental parameters constant, only varying monomer partial pressure in the range 0.3-4.0 bar. The liquid fractions were analysed by FID-GC and generally consisted of C_6–C_{38} LAOs. The amount of each oligomer was quantitatively determined using 2,2,4,4,6,8,8-heptamethylnonane as internal standard. The overall amount of soluble LAOs generally accounts for up to 27 wt % of the total product, with the remaining part being solid polyethylene. Ethene and 1-butene in the gas phase were not quantified.

3.2.1.1 - 9-Me: supporting evidence for the expected dependence of β/α on monomer pressure

The first catalyst screened was **9-Me** (Table 3.1). The dependence of β/α on ethylene pressure reflects the different reaction order of single and double

insertion mechanism with respect to ethylene concentration. Double insertion requires that two rather than one ethylene units are coordinated to the Cr-center at the same time, and therefore is expected to have an higher order than single insertion.[212] Experimentally, this can be observed by comparing the pressure dependence of 1-hexene and 1-octene yields in mmol on pressure, as reported in Figure 3.7. The former olefin is obtained *via* single ethylene insertion in chroma-cyclopentane and appears to have an approximately 1st order linear dependence on p_{Et}; on the other hand, 1-octene is mostly generated by double insertion in chroma-cyclopentane and clearly shows a higher order dependence on ethylene pressure.

This implies that increasing ethylene concentration favours double at the expenses of single ethylene insertion. Indeed, Table 3.1 shows that when going from 0.3 to 4.0 bar of ethylene, the probability β increases from 0.30 to 0.65, while α decreases from 0.51 to 0.14. Interestingly, the probability of chain termination (1-α-β) remains constant through the entire pressure range explored, which is in line with the mechanistic hypothesis of the main termination process being intramolecular β-H transfer (Scheme 3.2a-b).[307]

Table 3.1 - Pressure dependence of LAO distribution with **9-Me**/MAO.[a]

Entry	*p*[b]	Activity[c]	liquid wt %	∑mmol(n)[d]	α	β	1-α-β	β/α	c2/c1	R^2 [e]
1	4.0	58329	23	10.49	0.14	0.65	0.20	4.57	0.87	0.996
2	3.0	69420	16	6.90	0.15	0.65	0.20	4.26	0.80	0.997
3	2.0	55672	14	3.13	0.17	0.63	0.20	3.64	0.82	0.996
4	1.0	62807	14	1.78	0.21	0.60	0.20	2.86	0.80	0.997
5	0.7	30455	16	0.48	0.21	0.55	0.24	2.59	0.43	0.996
6	0.5	37797	17	0.57	0.26	0.53	0.20	2.03	0.34	0.993
7	0.3	36228	8	0.14	0.43	0.39	0.18	0.90	0.56	0.997

[a] Conditions: 50 nmol cat., 50 °C, MAO (5mmol), toluene 200 mL, 1h; [b] Ethene pressure in bar; [c] Activity in g $mmol^{-1}$ h^{-1} bar^{-1}; [d] Experimental total amount of LAOs n = 3-16; [e] R^2 signifies the goodness of fit of the calculated values compared with the experimental data.

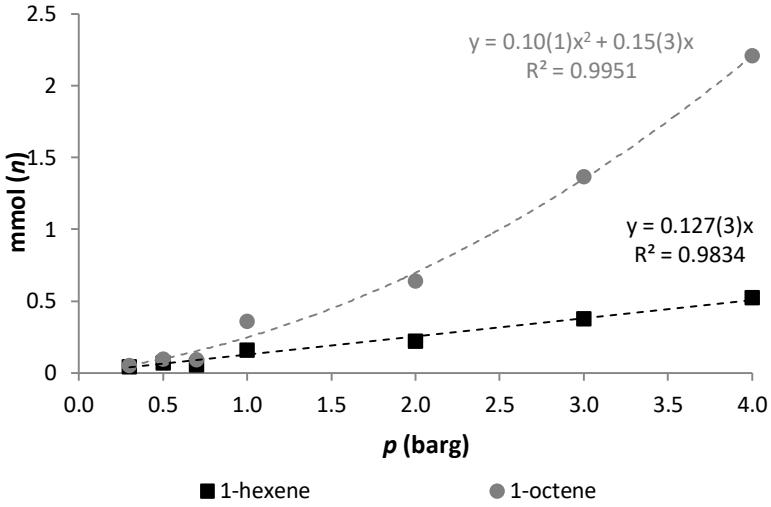

Figure 3.7 – Dependence of 1-hexene (black squares) and 1-octene (grey circles) yields (mmol) on ethylene pressure for **9-Me**. Trend lines reported assuming 1st and 2nd order dependence for 1-hexene and 1-octene, respectively. Standard deviations for fitting constants in brackets.

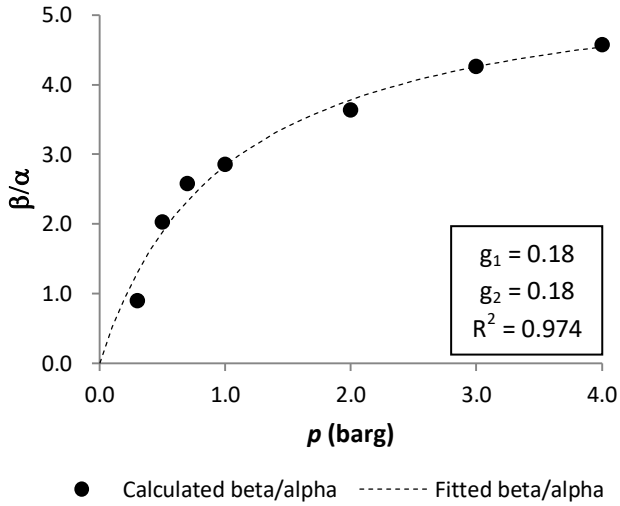

Figure 3.8 – Dependence of β/α on ethylene pressure for **9-Me** (see Table 3.1).

The resulting β/α *vs. p* plot is reported in Figure 3.8. Experimental data are nicely described by a pressure dependence of the type of Formula 3.4, and provided supporting experimental evidence for the proposed mechanistic and kinetic model leading to alternating distribution. Furthermore, these

observations show how monomer pressure can be used as practical experimental handle to tune the selectivity of the catalyst in ethylene oligomerization.

It has to be noted here, that even if we do *not* exclude 1-hexene from the fitting, experimental observations are in quite good agreement with expectations. Indeed, β/α drops below 1 bar and rapidly reaches a plateau at higher pressures (R^2 = 0.939, rather than 0.974 excluding 1-hexene).

3.2.1.2 - 9-H: *p*-induced switch from 2nd to 1st order distributions

Details of the oligomerization experiments with **9-H** are reported in Table 3.2. In this case, activity is roughly one order of magnitude lower than **9-Me**, and higher amounts of catalyst were required especially at 0.5 and 0.3 bar. Analogous trends of α and β are observed; termination probabilities (1-α-β) are roughly independent of pressure and quite close to those obtained with **9-Me**.

Table 3.2 - Pressure dependence of LAO distribution with **9-H**/MAO.[a]

Entry	*p*[b]	Activity[c]	liquid wt %	∑mmol(n)[d]	α	β	1-α-β	β/α	c2/c1	R^2 [e]
1	4.0	3866	27	1.64	0.22	0.53	0.25	2.40	0.34	>0.999
2	3.0	3315	20	0.93	0.27	0.50	0.23	1.87	0.47	0.999
3	2.0	4190	20	1.03	0.29	0.50	0.21	1.70	0.46	0.999
4	1.0	5860	26	0.35	0.45	0.34	0.21	0.77	0.70	0.991
5	0.7	7364	16	0.20	0.53	0.28	0.19	0.52	1.34	0.998
6[f]	0.5	5752	17	0.29	nearly Schultz-Flory					
7[g]	0.3	7606	27	1.24	nearly Schultz-Flory					

[a] Conditions: 150 nmol cat., 50 °C, MAO (5mmol), toluene 200 mL, 1h; [b] Ethene pressure in bar; [c] Activity in g $mmol^{-1}$ h^{-1} bar^{-1}; [d] Experimental total amount of LAOs n = 3-16; [e]R^2 signifies the goodness of fit of the calculated values compared with the experimental data, [f]300 nmol cat.; [g]600 nmol cat.

As stated before, **9-H** exhibits a rather gentle alternating distribution and generally the effect of decreasing ethylene pressure is to suppress the

alternation. Interestingly, when we explored the pressure dependence of β/α on monomer concentration with **9-H** we observed a switch in LAOs distribution from 2nd order at high pressures to roughly 1st order/Schultz-Flory distribution at low pressure, as schematically shown in Figure 3.9.

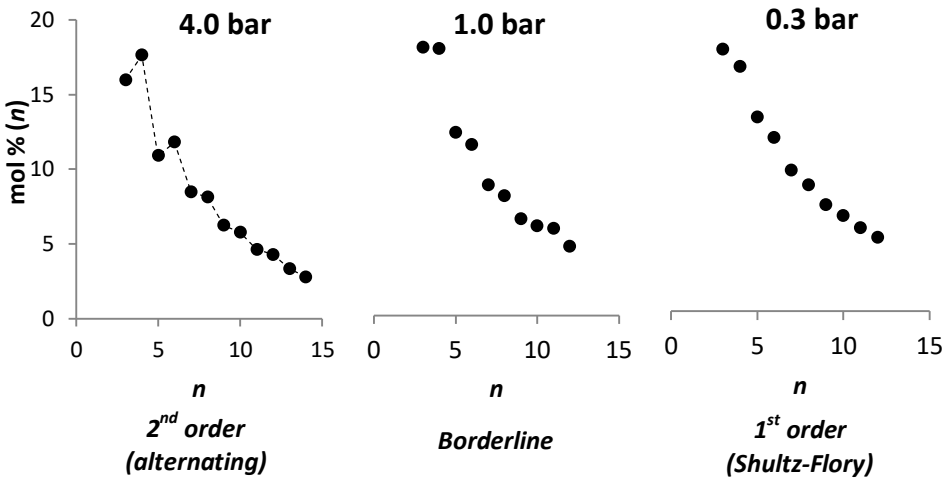

Figure 3.9 – Representative LAOs distributions at different ethylene pressure obtained with **9-H**.

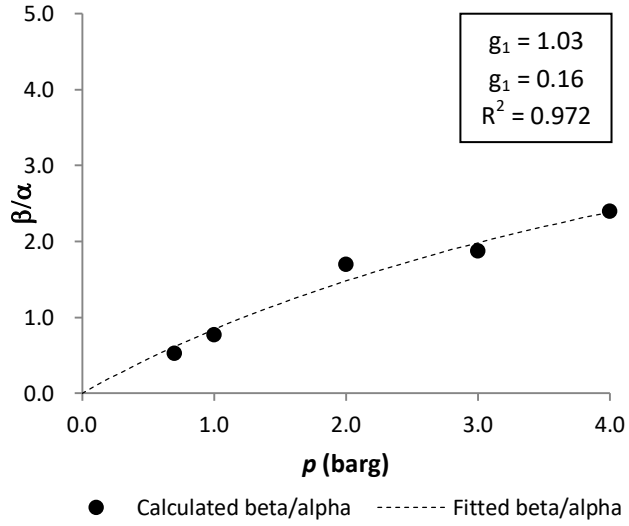

Figure 3.10 – Dependence of β/α on ethylene pressure for **9-H** (see Table 3.2).

For those distributions that are close to a Schultz-Flory regime (0.5 and 0.3 bar), no reliable α and β probabilities can be obtained, and therefore they are excluded from the β/α *vs.* P_{C2} plot reported in Figure 3.10. In this case, g_1 is much higher than g_2, entailing that the trend line is much closer to a linear dependence than for **9-Me**. Thus, **9-H** represents another interesting example of selectivity tuning by controlling ethylene pressure.

3.2.2 - Effect of external donor on alternating distribution

It has been shown for the case of Cr-PNP catalysts that the presence of coordinating anions or additional donors on the ancillary ligand backbone favours single with respect to double insertion mechanism.[305] Here we tried to get analogous experimental evidence for the BIMA catalysts by adding an external donor such as triphenylphosphine to the polymerization mixture.

9-Me was selected as a case study. The polymerization procedure was the same used for the previous experiments, with the only difference being that a known amount of PPh_3 in toluene was added to the catalyst/MAO solution straight before injection in the polymerization reactor. Experimental details are reported in Table 3.3.

Table 3.3 – Effect of PPh_3 on LAO distribution with **9-Me**/MAO.[a]

Entry	PPh_3/Cr[b]	Activity[c]	liquid wt %	∑mmol(n)[d]	α	β	1-α-β	β/α	c2/c1	R^2 [e]
1	0	58329	23	10.49	0.14	0.65	0.20	4.57	0.87	0.996
2	1	14988	20	2.19	0.20	0.57	0.23	2.88	0.93	0.997
3	3	13336	25	1.80	0.16	0.58	0.26	3.70	0.81	0.999

[a]Conditions: 4 bar ethylene, 50 nmol cat., 50 °C, MAO (5mmol), toluene 200 mL, 1h; [b]mol/mol; [c]Activity in g $mmol^{-1}$ h^{-1} bar^{-1}; [d]Experimental total amount of LAOs n = 3-16; [e]R^2 signifies the goodness of fit of the calculated values compared with the experimental data.

Addition of PPh_3 leads to a reduced activity due to catalyst poisoning, and affects LAOs distribution. Figure 3.11 graphically shows the dependence of

α, β and β/α on the amount of external donor. As expected, going from 0 to 1 equivalent of PPh_3, β drops from 0.65 to 0.57, while α increases from 0.14 to 0.20. Further addition of donor (up to 3 eq.) barely affects β, while α slightly decreases. Interestingly, termination probability always increases with the amount of phosphine.

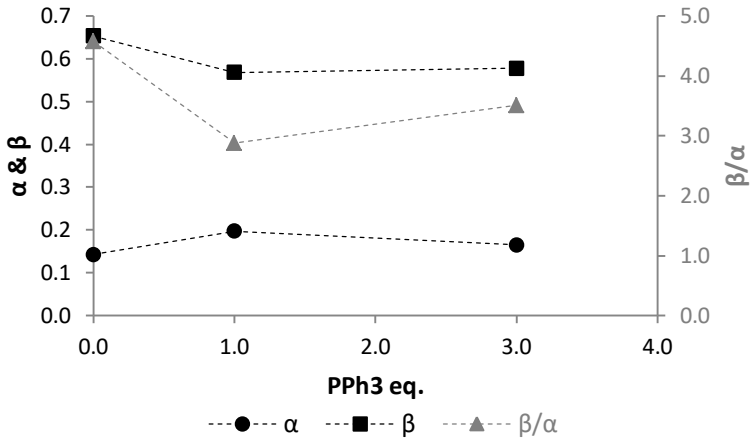

Figure 3.11 - Dependence of α, β and β/α on the amount of external donor for **9-Me**.

These observations are in line with the mechanistic hypothesis of competing single and double insertion mechanisms. The latter requires a higher number of coordinated ethylene units (*i.e.* of coordination sites involved in the metallacycle growth) and therefore is more affected by the presence of competing external donors than the single insertion mechanism (Figure 3.12).

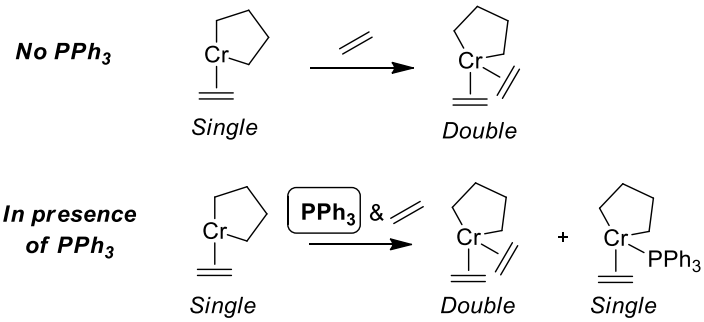

Scheme 3.4 – Schematic representation of the competition between ethene and PPh_3 for coordination to Cr, favoring single coordination mechanism.

3.2.3 - Synthesis of BIMP ligands

The nature of the central donor atom of BIMA-type ligands is known to affect the properties of the resulting catalysts decisively.[307, 313] Along with differently substituted amines, ether and thioether groups have been screened in ethene oligomerization, generally leading to reduced activity.[307] The replacement of the classical amine donor with the analogous group 15 phosphine donor is potentially very interesting, but it has never been reported. In the last part of the visit at Imperial College London, the synthesis of such P-based bis(benzimidazolyl)phosphine ligand (BIMP, Figure 3.12) was attempted.

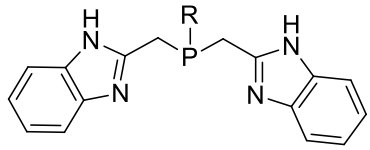

BIMP ligand

Figure 3.12 - Bis(benzimidazolyl)phosphine ligands.

Typically, BIMA ligands are synthesized by reaction of benzenediamine with a suitable iminodiacetic acid in ethylene glycol. Unfortunately, this procedure cannot be used with the corresponding P-based dicarboxylic acid (Scheme 3.5a) since the high reaction temperatures required (190°C) would lead to undesirable oxidation of P(III) to P(V). A potential alternative route might be the reaction of a benzimidazole Zn-alkyl with an appropriate dichloroalkyl phosphine (Scheme 3.5b), but the presence of the acidic NH on the benzimidazole might lead to self-decomposition of the Zn-compound. Therefore, the introduction of a protecting group for NH was required, and our choice fell on the carboxybenzyl group (Cbz, Scheme 3.5c).

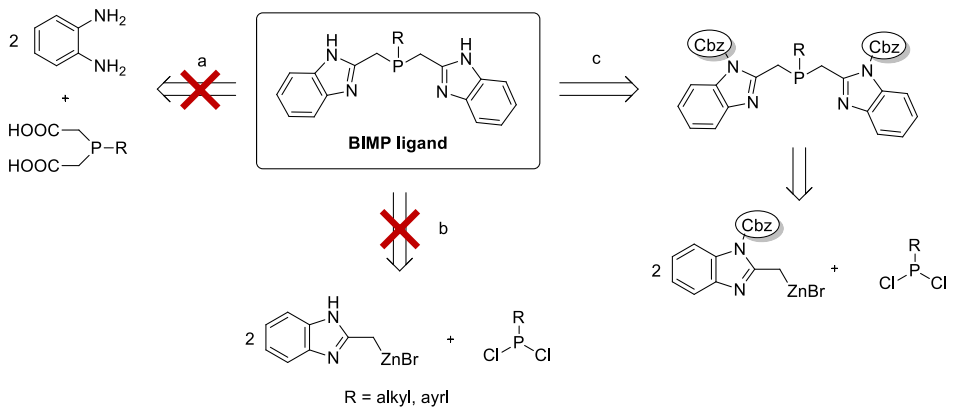

Scheme 3.5 – Possible synthetic routes to BIMP ligands.

The complete synthetic strategy is reported in Scheme 3.6. Alcohol **a** was selected as easily available starting material.[307] Reaction with benzyl chloroformate selectively leads to the protected alcohol **b**, which in turn is reacted with PBr_3 giving bromide **c**. Both reactions proceed with high yields (80 and >99% respectively).

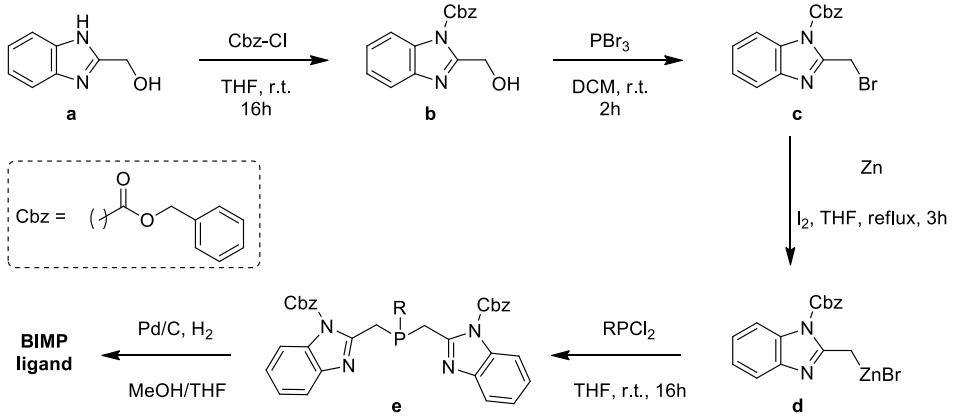

Scheme 3.6 – Proposed synthetic strategy for BIMP ligand.

The Zn-alkyl **d** could be generated *in situ via* reaction of **c** with activated Zn powder which was then reacted with a dichloro phosphine to give the protected ligand **e**. Initially, we wanted to synthesize a BIMP ligand with R

being a *n*-alkyl, such as *n*-butyl, since these species are expected to be the most interesting based on the comparison with analogous BIMA catalysts. The synthesis of $BuPCl_2$ was attempted by direct reaction of PCl_3 with BuLi,[314] which unfortunately gives the monochloride phosphine Bu_2PCl preferentially even in presence of excess PCl_3 (2 eq.). Therefore, a step-wise preparation was attempted by reacting phosphorus trichloride with lithium diisopropylamide to obtain bis(amido)phosphine **f**,[315] followed by alkylation with BuLi and regeneration of the P-Cl bonds with HCl in Et_2O (Scheme 3.7). These reactions gave surprisingly low yields that made it practically impossible to isolate reasonable amounts of pure **g**.

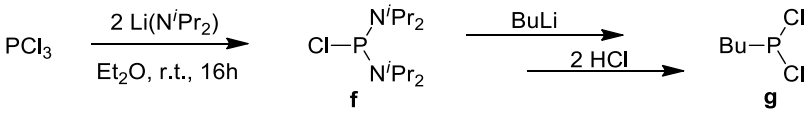

Scheme 3.7 - Synthetic strategy for $RPCl_2$.

In the very final part of the project, the effectiveness of the synthetic proposal was evaluated by using commercially available dichlorophenyl phosphine. The reaction to prepare the protected ligand **e** gave a mixture of at least three different P-containing species (based on ^{31}P NMR), but the available time was not enough to identify a suitable purification strategy. Further attempts to synthesize BIMP ligand are currently on-going in the Britovsek Group.

3.3 – Concluding remarks

Pressure dependence of alternating LAOs distribution with **9-Me** is in line with the predicted correlation based on the assumption of competing single and double insertion mechanism. Pressure was seen to be a practical experimental parameter to tune selectivity. The case of **9-H** is particularly illustrative in this respect since going from 4.0 to 0.3 bar implies a shift from second to first order distribution.

External donors in the polymerization mixture leads to a decrease of the β/α ratio, in line with the aforementioned mechanistic hypothesis. A synthetic strategy for a bis(benzimidazolylmethyl)phosphine ligand (BIMP) was proposed and preliminary explored.

3.4 – Experimental Part

3.4.1 - Materials and Methods

Oligomerization and other air sensitive reactions were carried out under nitrogen using Schlenk or glove box techniques. Toluene was dried by passing through a column packed with commercially available Q-5 catalyst (13 % Cu(II) oxide on Al_2O_3). Other solvents were dried over sodium wires (THF) or CaH_2 (DCM), distilled and stored over 4Å molecular sieves. All solvents were thoroughly deoxygenated before use. NMR spectra were recorded at 298K using Bruker DRX-400 MHz, AV-400 MHz, AV-500 MHz spectrometers. The ^{1}H NMR and ^{13}C NMR chemical shifts were referenced to the residual protio impurity and ^{13}C signal of the deuterated solvent, respectively. To describe the multiplicity of the signals, the following abbreviations are used: s, singlet; bs, broad singlet; d, doublet; bd, broad doublet; dd, double doublet; t, triplet; dt, double triplet; m, multiplet. BIMA complexes, [304, 307] alcohol **a**[304, 307] and phosphine **f**[315] were synthesized according to literature procedures.

3.4.2 – General oligomerization procedure

BIMA precatalysts (4 mmol) were dissolved in 3mL of 10 wt % commercial MAO solution. The resulting green mixture was diluted with a known amount of toluene to give a solution with a suitable catalyst concentration. The preparation of such activated catalyst solution is necessary due to the substantial insolubility of **9-R** in toluene and the very low amount of catalyst loading used in polymerization. These mixtures were carefully stored under nitrogen at -15°C for up to one week, and different aliquots were used in the various experiments. It has been previously observed that they show no

significant loss of activity when stored at low temperatures for up to two weeks,[307] as further confirmed by our observations.

A mechanically stirred pressure reaction flask was filled with toluene (200 mL) and a suitable amount of MAO (5 mmol) as impurity scavenger. The system was warmed up to 50°C in a water bath. An aliquot of activated catalyst solution was injected in the reactor and the desired partial pressure of ethene was applied rapidly (see Tables 3.1-3.3). After vigorously stirring for 1h, the reaction was terminated by turning off the ethylene supply and promptly cooling down to 0°C. Excess unreacted monomer was vented off. A known amount of GC standard (2,2,4,4,6,8,8-heptamethylnonane) was added to the reaction mixture, and a small sample of liquid phase filtered through neutral alumina to be analysed by FID-GC. The remaining polymer product was precipitated by the addition of methanol/HCl, filtered and dried in a vacuum oven.

3.4.3 – Synthetic procedures

Benzyl 2-(hydroxymethyl)-1H-benzo[d]imidazole-1-carboxylate, **b**. Benzyl chloroformate (30 mmol, 4.3 mL) and triethylamine (39 mmol, 5.3 mL) were sequentially added dropwise to a stirred suspension of alcohol **a** (30 mmol, 4.4 g) in dry THF (150 mL) at 0°C. After 15 min, the suspension was allowed to warm to room temperature and stirred for 16h. The mixture was concentrated under vacuum and extracted three times with DCM/water. The combined organic layers were dried over $MgSO_4$, and the volatiles removed under vacuum to give a white solid (7g, 85% yield).

^{1}H NMR (400 MHz, $CDCl_3$): 9.96 (s, 1H, OH), 7.79 (m, 1H, aromatic CH), 7.47 (m, 1H, aromatic CH), 7.39 (bs, 5H, aromatic CH), 7.31 (m, 2H, aromatic CH), 5.45 (s, 2H, -CH_2-), 5.23 (s, 2H, -CH_2-) ppm. ^{13}C NMR (100 MHz, $CDCl_3$): 155.5, 147.9,

142.7, 134.6, 133.6, 128.9, 128.7, 128.4, 123.8, 122.6, 120.0, 111.1 (aromatic C), 70.5 (-CH_2-), 63.3 (-CH_2-) ppm.

Benzyl 2-(bromomethyl)-1H-benzo[d]imidazole-1-carboxylate, **c**. Phosphorus tribromide (22 mmol, 2.1 mL) was added to a stirred solution of **b** in DCM (150mL) over a period of 10 min. The resulting mixture was shielded from light and stirred for 1h. The reaction was then quenched by cooling down to 0°C and adding saturated NH_4Cl solution in water (100 mL). The solid precipitate was filtered and washed with water and DCM, to obtain highly pure product (6 g, quantitative yield).

^{1}H NMR (400 MHz, MeOD): 7.83 (m, 2H, aromatic CH), 7.67 (m, 2H, aromatic CH), 7.40 (m, 5H, aromatic CH), 5.71 (s, 2H, -CH_2-), 5.29 (s, 2H, -CH_2-) ppm. ^{13}C NMR (100 MHz, MeOD): 134.9, 130.9, 128.4, 128.2, 126.6, 113.7, 105.1, 70.6 (-CH_2-), 59.2 (-CH_2-) ppm.

Chapter 4

Thermally stable Ti-catalysts: insight into reversible decomposition via Ti-C bond homolysis and its use as a potential chain-end functionalization tool

A portion of this chapter has appeared in print:

Ehm, C.; Cipullo, R.; Passaro, M.; Zaccaria, F.; Budzelaar, P. H. M.; Busico, V., Chain Transfer to Solvent in Propene Polymerization with Ti Cp-phosphinimide Catalysts: Evidence for Chain Termination via Ti–C Bond Homolysis. *ACS Catal.* **2016**, *6*, 7989-7993.

4.1 - Introduction

Ti(IV)-based complexes bearing cyclopentadienyl (Cp) and phosphinimide ancillary ligands (Figure 4.1) are one of the most successful examples of commercialized polymerization catalysts.[46-48]

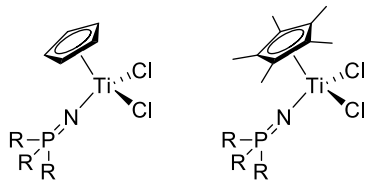

10 (R = Ph) **10'** (R = Ph)
11 (R = Cy) **11'** (R = Cy)
12 (R = ^{t}Bu) **12'** (R = ^{t}Bu)

Figure 4.1 – Phosphinimide catalysts.

The phosphinimide ancillary ligand is characterized by almost linear P-N-Ti geometry, leading to a conical shape that resembles that of a Cp ring (Figure 4.2) but offers several potential advantages.[46-48] First, the ease of synthesis from the readily available phosphines allows for an easier structural amplification and tuning of steric and electronic properties. Secondly, while the steric bulk of Cp-ligand is relatively close to the Ti-center, the presence of the P=N fragment keeps the bulky tri-substituted phosphine far from the metal. In this way, a more open catalyst's mouth is obtained, while the ancillary ligand still provides an efficient shielding of the metal center; the sum of these two features offer potential advantages in terms of activity with respect to bis-Cp titanocenes. Finally, the presence of a phosphorus atom in the ligand backbone represents a helpful spectroscopic handle, as further discussed in Chapter 5.

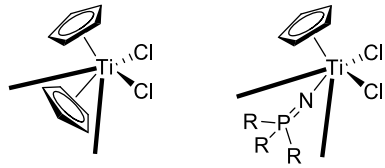

Figure 4.2 – Steric analogy of bis(cyclopentadienyl) and phosphinimide complexes.

The major commercial applications of these catalysts lie in the field of olefin co-polymerization and UHMWPE production.[38] Their catalytic performance are remarkable both in solution[51] and gas-phase reactors.[52, 316] Copolymers with narrow MWD can be obtained,[317] although many applications have been found for systems giving broad distributions as well.[52, 316]

It is interesting to highlight the catalytic properties of these species in homopolymerization. Early reports describe ethylene homopolymerization performances at 25°C and 1 bar. Cp-complexes with R = Cy (**11**) and ^{i}Pr give low activity (40-50 g_{PE} $mmol^{-1}$ h^{-1}) and broad molecular weight distributions (MWD) if activated by MAO, likely due to catalyst modification by free trimethylaluminum (TMA) contained in commercial MAO.[47-48] Much higher productivities and monomodal MWD can be obtained with bulkier and more shielding ancillary ligands (*e.g.* **12**/MAO: 652 Kg_{PE} mol^{-1} h^{-1}) and/or using molecular trityl-borate (TTB) activators (*e.g.* **11**/TTB: 231 Kg_{PE} mol^{-1} h^{-1}).[46-48, 318] Analogous results in ethylene homopolymerization at higher temperatures can be found in the patent literature. High productivities and thermal stability up to 160°C are reported, often with TTB or modified methylaluminoxane such as MMAO-7 or PMAO-IP as activators.[49, 319]

The behavior of these systems in α-olefin homopolymerization has rarely been covered in the literature and it is limited to 1-hexene monomer. The very few examples available describe rather modest activity and molecular weight capability. For instance, polyhexene with M_n of less than 2 kDa was obtained with **12** at 25°C.[47]

We wanted to explore the polymerization performance of this class with the simplest α-olefin, propene, being particularly interested in identifying the chain termination processes limiting MW. Interestingly, we observed that when polymerizing propene at high temperatures (>80°C) with these species, a sizable fraction of benzyl terminated chains is obtained. This results from

catalytic C-H activation of the toluene solvent and subsequent benzyl incorporation in the polymer chain, which represents an unprecedented chain transfer to solvent reaction we wanted to study in more detail.[320]

The initial screening of catalysts and experimental conditions was carried out by MSc. Miriana Passaro during her Master Thesis in the *Laboratory of Stereoselective Polymerization*. Experimental results were combined with DFT calculations by Dr. Christian Ehm and a tentative mechanistic interpretation was proposed.[321] The key points of this background are critically described in Sections 4.1.1 and 4.1.2. In this project, the study was expanded by a combined experimental and computational approach, aiming at further elucidating the mechanism and exploring the scope of this reactivity.

4.1.1 – Chain transfer to toluene solvent

MAO/BHT was selected as cocatalyst to explore the properties of phosphinimide complexes in propylene polymerization, while avoiding undesirable side reactions with TMA.[183-184] Typically, these catalysts give atactic, glue-like and colorless polypropylenes, whose microstructural properties were determined by high-resolution ^{1}H and ^{13}C NMR, and Gel Permeation Chromatography (GPC). The polydispersity Index (PDI) is generally close to 2, indicating single-site behavior. The initial focus was on the representative catalyst **10'** (Cp*, R = Ph), whose X-ray structure and polymerization performance were reported for the first time by our group.[320]

Among the preliminary combinations of pressure and temperature explored, the most satisfactory results were obtained at 110°C and 1 bar (Entry 1, Table 4.1 and 4.2). Although this reactivity was observed also at lower temperature (80°C; Entry 2, Table 4.1 and 4.2), these experiments required

much lower pressures, leading to unsatisfactory productivity and reproducibility.

Table 4.1 – Catalysts performance in propene polymerization at high temperature: selection of initial results reported in ref. 321.[a]

Entry	Catalyst	T (°C)	*p* (bar)	Activity[b]	M_n[c] (kDa)	M_w[c] (kDa)	P_n	PDI	Chains/Met.[d]
1	**10'**	110	1.0	112	7.0	19	167	2.7	32
2	**10'**	80	0.13	20	5.3	10	126	1.9	1
3	**Cp*TiCl$_3$**[e]	80	0.5	13	23	112	537	4.9	1

[a] 25 μmol catalyst, MAO/BHT cocatalyst, Al/Ti 400, toluene 200mL, 120 min, MeOH/HCl quenching; [b] in Kg_{PP} mol^{-1} bar^{-1} h^{-1}; [c] by GPC characterization; [d] assuming 100% active Ti; [e] 80°C and 0.5 bar represent the most forcing conditions we could identify to get reasonable activity with **Cp*TiCl$_3$**.

Table 4.2 – Microstructure and chain-end analysis by ^{13}C NMR characterization relative to the experiments of Table 4.1.[a]

Entry	2,1	3,1	PEP	$^{n}Bu_A$	$^{n}Bu_B$	Σ[b]	^{n}Pr[c]	^{i}Bu	Bn	Vd+bl[d]	Allyl	%Bn[e]
1	7.2	0.5	0.4	0.5	0.2	8.6	<0.3	0.2	0.2	0.07	0.04	>31
2	4.1	1.2	0.5	0.5	0.5	6.8	<0.3	0.4	0.35	0.08	0.05	>32

[a] Chain ends and regioerrors are given in units of mol %; [b]Sum of regioerrors, Σ = 2,1 + 3,1 + PEP + $^{n}Bu_A$ + $^{n}Bu_B$; [c] conservative estimate as ^{n}Pr chain ends overlap with regioerrors; [d] Vd+bl = vinylidene + 1-butenyl + 2-butenyl; [e] percentage of benzylated polymer chains, %Bn = 2*Bn/($^{n}Bu_A$ + $^{n}Bu_B$ + ^{n}Pr + ^{i}Bu + Bn + Vd + bl + Allyl).

Benzyl terminated polymer chains were unambiguously identified by ^1H and ^{13}C NMR microstructural analysis of polypropylene samples (Figure 4.3). Low amounts of benzyl chain ends are usually obtained when using dibenzyl precatalysts, since the first monomer insertion occurs in the cationic monobenzylated active species. However, typical dichloride precursors are used here and the only source of benzyl groups is the toluene solvent. Several examples of solvent activation by highly reactive group IV cationic complexes have been reported before, but they generally lead to inactive species.[154-155] In our case instead, C-H activation does not necessarily kill the active species but

leads to solvent incorporation in the polymer chain. No tolyl chain ends are observed, indicating selective benzylic CH activation.

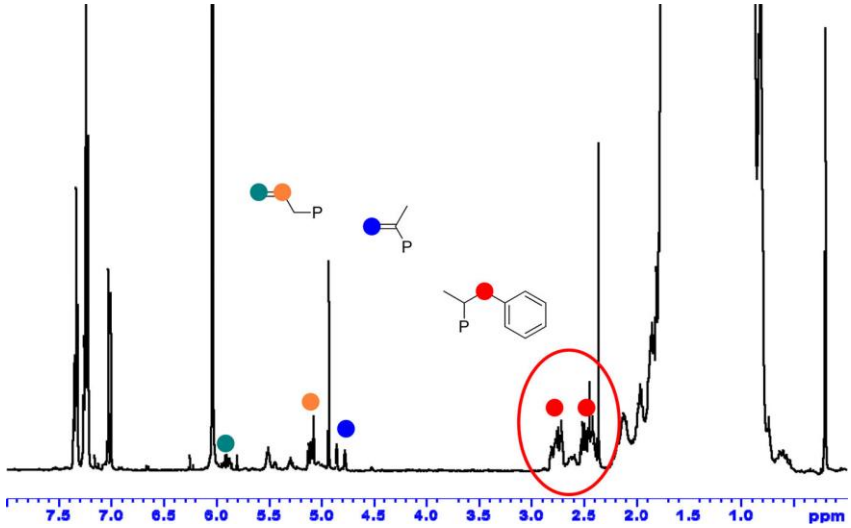

Figure 4.3 - ^{1}H NMR showing benzylic chain ends (red circles) and olefinic chain ends (blue, orange, and green circles); chemical shifts are shown in units of ppm.

If we consider the optimal experiment at 110°C and 1 bar, we find that about 32 polymer chains are produced per metal atom in the optimistic assumption of 100% Ti-centers being active (Entry 1, Table 4.1). Of these, 31% are benzylated chains, *i.e.* each Ti generates ~10 benzyl terminated polymers. This points to solvent incorporation in the polypropylene chain being a catalytic process, especially if we consider that in reality only a small fraction of the precatalysts (a reasonable guess for Ti being 5-10%)[182, 320, 322] is generally active under polymerization conditions.

When using different cocatalysts like dried MAO, the catalytic activity of **10'** drops by more than an order of magnitude and no benzylated chains are obtained.[321] To verify that trace amounts of the **Cp*TiCl$_3$** precursor used for the synthesis of phosphinimide precatalysts are not the actual responsible species for such peculiar reactivity, comparative experiments were performed; they

clearly showed that **Cp^*TiCl_3** gives rather different and *non*-benzylated polymers (Entry 3, Table 4.1).

Regarding the other chain terminations, the amount of unsaturated chain ends is surprisingly low with respect to saturated ones. The former are generally obtained *via* β-H transfer to the coordinated monomer (BHTM) or *via* β-H elimination (BHE). In such cases, vinylidene groups are obtained starting from primary Ti-polymeryl, while 1- or 2-butenyl fragments are obtained after secondary insertion (Scheme 4.2).[71] Only traces of butenyl chain ends are observed in our case.

Saturated chain ends can be either branched (^{i}Bu) or linear (^{n}Bu or ^{n}Pr) fragments, typically originating from (1) propene insertion in Ti-H or Ti-^{n}Pr bonds (obtained after BHE and BHTM respectively), (2) chain transfer to aluminum, or (3) hydrogenolysis in presence of H_2 (or any other acidic quenching agent, Scheme 4.2).[94, 113] Among the saturated chain terminations *n*-butyls predominate, with two different structures: $^{n}Bu_A$ formed *via* a 1,2−1,2−2,1, and unusual $^{n}Bu_B$, which we tentatively trace to a 2,1−1,2−2,1 monomer sequence (Figure 4.4a).[323] No hydrogen was fed to the reactor, while the addition of BHT traps TMA and suppresses transalkylation reaction to Al.[193] The latter assumption is confirmed by oxygen quenching experiments,[324] showing no OH-labelled end groups therefore excluding that a significant amount of chains are transferred to aluminum. Consequently, aliphatic chain ends should only derive from chain reinitiation, following BHTM or BHE,[94] but they vastly outnumber olefinic chain ends. In other words, saturated chain ends always exceed 50% of the total and, consequently, at least some of them must originate from an unidentified different mechanism, which might be connected to benzyl chain end formation.

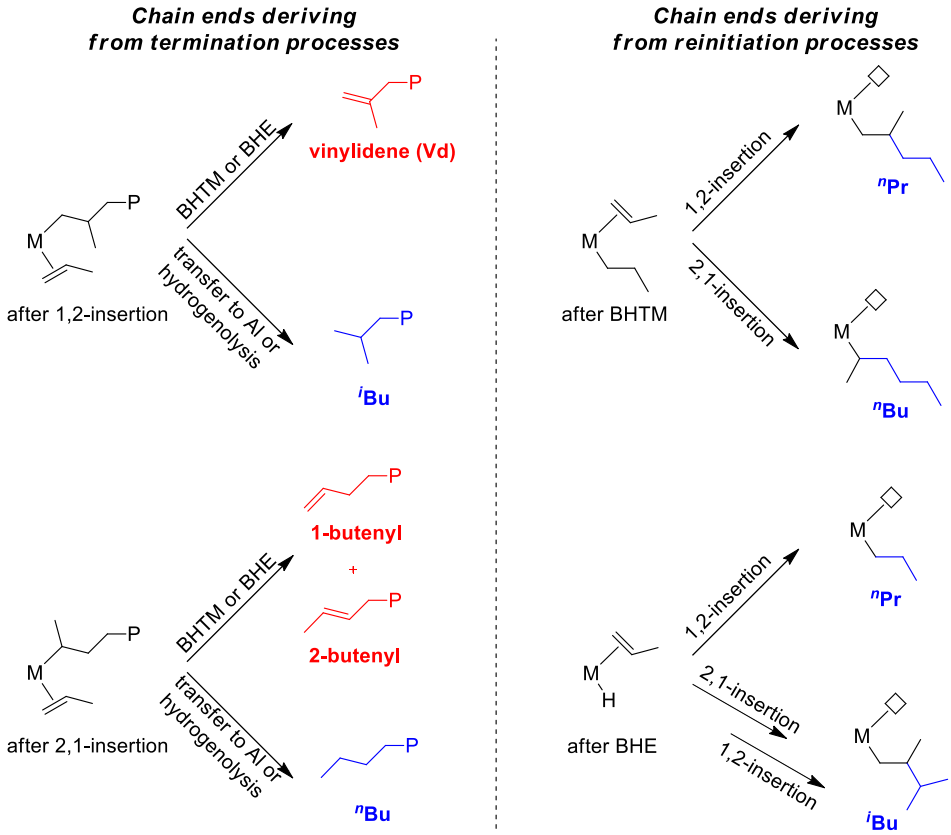

Scheme 4.2 – Schematic representation of the main processes giving unsaturated (red) and saturated (blue) chain ends.

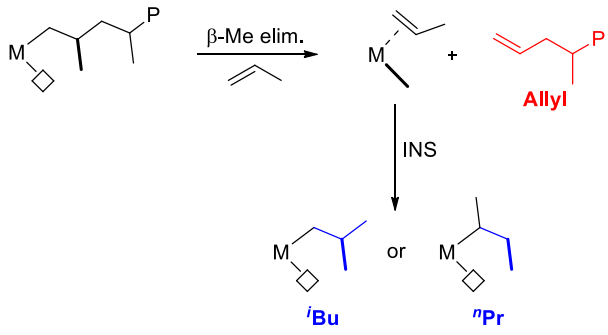

Scheme 4.3 – Generation of allyl polymer tail (red) and *iso*-butyl or *n*-propyl head (blue) *via* β-Me elimination and subsequent chain reinitiation.

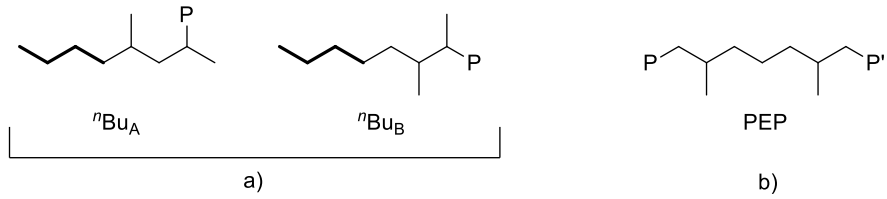

Figure 4.4 – Two types of nBu chain ends and 'pseudo' PEP triad observed with phosphinimide catalysts.

Finally, it should be noted that we found a small but detectable amount of rather unusual allyl terminations. They can be obtained *via* β-Me elimination,[325-326] which produces PP chains initiated by *iso*-butyl or *n*-propyl, and terminated by the allyl groups (Scheme 4.3).[94] Interestingly, a potential alternative source of allyl chain ends might be chain transfer to monomer *via* CH activation of the CH_3 of propene rather than of toluene, but we cannot easily discriminate these two cases at this stage.

The dominant propene insertion mode is 1,2-insertion. However, insertion into secondary metal polymeryl bonds appears to be relatively facile (Table 4.2), as observed previously for some sterically open CGC and late-transition-metal catalysts.[327-329] Regioerrors consisting of 2,1 and 3,1 units can be found, with the latter originating from 2,1-insertion and subsequent isomerization and reinsertion.[94] Indeed, we observed "pseudo PEP" triads, which mimic authentic ones formed in propene/ethene copolymerization and can be ascribed to a 2,1−3,1−1,2 monomer sequence in the present case (Figure 4.4b).

4.1.2 – The mechanistic proposal

Two alternative mechanisms for benzylic CH activation were explored by DFT, namely 1) σ-bond metathesis (SBM) from the growing chain and 2) radical pathway involving Ti-C homolysis.[320] The study, carried out on a model catalyst

(Cp, R = Me), compared barriers for SBM with those of the various insertion modes and more typical termination processes (*i.e.* BHTM and BHE), and tried to estimate the relative ease of Ti-C homolysis.[320-321] Conclusions point to barriers for SBM being too high to represent a competitive termination process, while the alternative homolysis pathway seems to a more feasible option.[226] Clear observation of green color during polymerization experiments is indicative of the presence of Ti(III) species, in line with this interpretation.

It has been observed that very weak Ti-C bond can be obtained under polymerization conditions. For instance, in the case of bis-cyclopentadienyl $Cp_2Ti(n\text{-alkyl})^+$ cation, Ti-C Bond Dissociation Energies (BDE) are predicted to comparable to those of typical O-O bonds in organic peroxides like $(^tBuO)_2$.[226] This implies that practically at each stage of chain growth there is a potential competition between propagation and homolytic Ti-C bond cleavage.

As pointed out before, ^{n}Bu chain ends are largely dominant, indicating that the leading termination event is linked to Ti-*sec*-alkyl species. Indeed, several elements contribute to making chain termination *via* homolysis especially competitive after secondary insertion.[226] Comparison of few available experimental BDE for sterically crowded $Ti(neopentyl)_4$ and less hindered $Ti(CH_2SiMe_3)_4$ (47.3 and 60.5 kcal/mol respectively)[330] shows that steric effects have a strong influence on Ti-C BDE. In this respect, *sec*-alkyls bound to Ti after 2,1-insertion introduce a marked steric strain around the metal center, which weakens the Ti-C bond with respect to corresponding Ti-*n*-alkyl. Moreover, the steric hindrance of Ti-*sec*-alkyl fragments limits the degree of possible agostic interactions, further destabilizing the alkyl complex.

Olefin π-coordination requires considerable additional space around the metal. Typically, this implies a switch from β-agostic to less favorable (from a BDE perspective) α- or non-agostic structures. These space issues are especially marked for secondary alkyl chains and milder for β-substituted or

unsubstituted primary polymeryl. Moreover, they are practically absent for the Ti(III)-product $\mathbf{L_xL_yTi(propene)}^{\cdot+}$, which is consequently more stabilized by the olefin than the parent Ti(IV)-R cation. Thus, monomer coordination favors homolysis since it stabilizes the reaction product more than the starting alkyl, and this effect is particularly evident after secondary insertion. Other ligands including coordinating solvents and/or counterions should favor homolysis in a similar manner. Finally, considering relative stabilities of alkyl anions (primary > secondary) and radicals (secondary > primary), Ti-C bond cleavage after 2,1-insertion would transform a relative unstable secondary anion in a relatively stable secondary radical.

Based on the above considerations, a tentative mechanism was proposed, as reported in Scheme 4.4. After secondary insertion, homolysis of the Ti-C bond (Scheme 4.4A) gives a polymerization inactive Ti(III) species and a polymeryl radical. The latter quickly abstracts an H atom from a benzylic C-H bond of toluene and an *n*-butyl terminated chain is obtained (B). The resulting benzyl radical can then recombine with the Ti(III) cation (C), regenerating a Ti(IV) species that can initiate chain growth by insertion of propylene in the Ti-Bn bond (D). BHT from MAO/BHT cocatalyst might take part in the mechanism thanks to its radical stabilizer properties, and possibly play a crucial role if organic radicals escape the solvent cage.

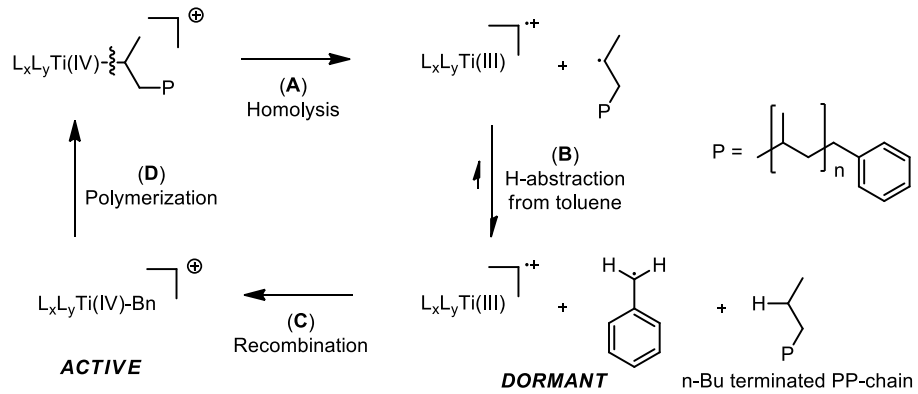

Scheme 4.4 – Proposed mechanism for chain transfer to solvent.

A similar mechanism has been reported by Piers and co-workers for activation of chloro- and bromo-benzene solvents by phosphinimide Ti-hydride **12'-H$^+$**.[331-332] The thermodynamic product of the reaction between **12'-H$^+$** and C_6H_5X at 4 bar H_2 pressure is the corresponding **12'-X$^+$** halocation (X = Cl, Br). In this case, it was possible to clearly discriminate the alternative σ-bond metathesis pathway, which becomes kinetically favorable at lower H_2 pressure and leads to a β-haloaryl cation *via* aromatic C-H activation.[332] In the same paper, the group of Piers also reported activation of toluene-d_8 by **12'-H$^+$** in absence of H_2 overpressure. The deuterated benzyl cation **12'-Bn$^+$** was identified as one of the main products and, although the mechanism was not fully elucidated, the authors suggested that benzylic C-H activation should *not* occur *via* σ-bond metathesis since the tolyl complex would be expected in this case.[332] This exemplifies how broad and complex the chemistry of phosphinimide complexes can be.

Attempts to clarify the mechanism of chain transfer to solvent, incorporate more-interesting chain ends and test different catalysts are reported in the following sections.

4.2 – Results and Discussion

In the framework of this doctoral project, we focused on polymerization experiments carried out at 110°C, as working at high temperatures should facilitate homolysis and it is more interesting to evaluate catalyst thermal stability under industrially relevant conditions. Initially, we tried to optimize other experimental parameters, such as monomer pressure and reaction time, to identify a standard set of reaction conditions. Then, different catalysts, solvents and activators were screened to identify factors determining relative preference for insertion *vs.* homolysis, and the ability to incorporate benzyl chain ends. Experimental results were integrated with DFT modeling, providing supporting evidence for the radical mechanism.

Tables 4.3a-c represent the 'master tables' of this Chapter that summarize all polymerization experiments described in here. Further tables in the following sections provide details for selected groups of polymerization experiments, retaining the experiment numbering of the master tables. Experiments 101 to 104 are taken from ref. 321 for comparison.

The employed computational protocol is analogous to the one described in Chapter 2, the only differences being that (1) the optimization step was carried out using the density fitting approximation (Resolution of Identity, RI),[333-336] and (2) all problems involving species in the doublet state were calculated without PCM solvent corrections.[228]

Table 4.3a – Catalyst performance in propene polymerization at high temperature: master table of experimental conditions for all the experiments carried out in this project.[a]

Exp.	Catalyst	Solv.	T (°C)	*p* (bar)	Cocatalyst	Al/ Ti	AlR_3/ BHT[b]	*t* (min)	Cat. µmol	Act.[c]
1	**10'**	Tol.	110	0.3	MAO/BHT	400	1:2	120	25	5
2	**10'**	Tol.	110	3.0	MAO/BHT	400	1:2	120	37	491
3	**10'**	Tol.	110	1.0	MAO/BHT	400	1:2	15	25	208
4	**10'**	Tol.	110	1.0	MAO/BHT	400	1:2	30	25	236
5	**11'**	Tol.	110	1.0	MAO/BHT	400	1:2	15	25	368
6	**12'**	Tol.	110	1.0	MAO/BHT	400	1:2	15	25	Olig.
7	**10**	Tol.	110	1.0	MAO/BHT	400	1:2	15	25	192
8	**11**	Tol.	110	1.0	MAO/BHT	400	1:2	15	25	208
9	**12**	Tol.	110	1.0	MAO/BHT	400	1:2	15	25	160
10	**Cp_2TiCl_2**	Tol.	110	1.0	MAO/BHT	400	1:2	15	25	4.8
11	**CGC**	Tol.	110	1.0	MAO/BHT	400	1:2	15	25	88
12	**FI**	Tol.	110	1.0	MAO/BHT	400	1:2	15	25	-
13	**FI**	Tol.	70	1.0	MAO/BHT	400	1:2	15	25	32
14[d]	**10'**	Tol.	110	1.0	$B(C_6F_5)_3$/ TiBA/BHT	25	1:1	15	25	144
15[d]	**10'**	Tol.	110	1.0	TTB/ TiBA/BHT	25	1:1	15	25	226
16[d]	**10'**	Tol.	110	1.0	$B(C_6F_5)_3$/ MAO/BHT	400	1:2	15	25	228
17	**10'**	Tol.	110	1.0	MAO/BHT	400	1:1	15	25	-
18	**10'**	Tol.	110	1.0	MAO/BHT	400	1:3	15	25	192
19	**10'**	Tol.	110	1.0	MAO/BHT	400	1:5	15	25	96
20[e]	**10'**	EB	110	1.0	dMAO/BHT	400	1:2	15	6	18
21[e]	**10'**	F-tol.	120	1.5	dMAO/BHT	400	1:2	15	6	27
22[e]	**10'**	F-tol.	90	0.5	dMAO/BHT	400	1:2	15	6	54
23[e]	**10'**	F-B/tol[f]	110	1.0	MAO/BHT	400	1:2	15	6	25
101*	**10'**	Tol.	110	0.5	MAO/BHT	400	1:2	120	25	15
102*	**10'**	Tol.	110	1.0	MAO/BHT	400	1:2	120	25	112
103*	**Cp^*TiCl_3**	Tol.	80	0.5	MAO/BHT	400	1:2	120	25	13
104*,[e]	**10'**	Mesityl.	110	1.0	dMAO/BHT	400	1:2	120	25	40

[a] *V* = 200mL, MeOH/HCl quenching; [b] AlR_3 = $AlMe_3$ (in MAO) or Al^iBu_3; [c] Activity in Kg_{PP} mol^{-1} bar^{-1} h^{-1}; [d] precatalyst reacted with molecular activator prior to injection in the polymerization reactor, Ti/B 1:1.1; [e] *V* = 50mL; [f] 50 v/v %. * taken from ref. 321. TiBA = tri-*iso*-butylaluminum; TTB = $[Ph_3C][B(C_6F_5)_4]$. Tol. = toluene; EB = ethylbenzene; F-tol. = 4-fluorotoluene; Mesityl. =

Mesitylene; F-B = ortho-difluorobenzene; CGC = Constrained Geometry Catalyst, FI = phenoxy-imine catalyst; dMAO/BHT = dried-MAO/BHT.

Table 4.3b – Catalyst performance in propene polymerization at high temperature: master table of GPC polymer characterizations for relevant experiments.

Exp.	M_n[c] (kDa)	M_w[c] (kDa)	P_n	PDI
1	2.2	3.6	52	1.6
2	8.2	16	195	2.0
3	2.8	5.7	67	2.1
4	3.0	7.2	71	2.4
5	0.6	1.2	14	1.9
7	6.3	15	151	2.4
8	3.0	6.0	72	2.0
9	2.4	4.4	57	1.9
10	17	42	404	2.5
11	3.5	6.8	83	2.0
13	1.5	1.7	35	1.1
14	3.5	6.3	83	1.8
15	3.3	7.0	79	2.1
16	2.9	6.1	70	2.1
18	2.5	4.9	59	2.0
19	1.9	3.6	45	1.9
20	3.9	8.0	93	2.0
21	2.3	4.8	55	2.1
22	2.7	6.0	64	2.2
23	3.0	6.0	71	2.0
101	4.3	7.5	102	1.7
102	7.0	19	167	2.7
103	23	112	537	4.9
104	3.3	7.0	79	2.1

Table 4.3c – Catalyst performance in propene polymerization at high temperature: master table of NMR polymer characterizations for relevant experiments.[a]

Exp.	2,1	3,1	PEP	$^{n}Bu_A$	$^{n}Bu_B$	Σ[b]	^{n}Pr[c]	^{i}Bu	Bn	Vd+bl[d]	Allyl	%Bn[e]
1	2.2	3.4	0.6	0.8	1.2	8.2	<0.5	1.6	0.3	0.17	0.5	>12
2	8.2	0.44	0.49	0.3	0.1	9.5	<0.2	0.25	0.11	0.015	0.045	>22
3	3.0	2.8	0.44	0.9	0.9	8.0	<0.7	1.0	0.5	0.14	0.36	>22
4	4.6	1.5	0.6	0.8	0.7	8.2	<0.8	0.7	0.38	0.1	0.16	>21
5	n.d.	1.9	n.d.	1.1	0.5	3.5	<0.7	8.2	1.1	0.02	1.4	>17
7	8.9	n.d.	n.d.	0.2	n.d.	9.1	<0.4	0.4	0.1	0.17	n.d.	>16
8	4.5	0.4	0.3	0.4	0.6	6.2	<1.0	1.2	0.23	0.31	0.07	>12
9	5.7	1.3	0.5	0.8	0.8	9.1	<1.1	1	0.22	0.37	0.25	>10
14	4.3	1.5	0.7	0.5	0.4	7.4	<1.0	0.5	n.d.	0.5	0.16	n.d.
15	4.6	2.3	0.8	0.6	0.6	8.9	<1.0	0.7	0.06	0.15	0.3	>4
16	3.8	2.1	0.4	0.7	0.7	7.7	<0.9	0.8	0.19	0.28	0.25	>10
18	4.2	1.8	0.8	0.8	0.5	8.1	<0.8	0.7	0.3	0.12	0.19	>17
19	4.6	1.3	0.4	0.8	0.7	7.8	<0.8	0.5	0.2	0.09	0.16	>12
20	5.7	0.9	0.4	0.5	0.5	8.0	<0.8	0.4	0.05	0.13	0.11	>4
21	4.6	1.8	0.35	0.5	0.5	7.7	<1.5	0.5	n.d	0.9	0.16	-
22	4.8	0.7	0.4	0.4	0.3	6.6	<1.1	0.4	n.d	0.61	0.14	-
23	3.9	2.3	1.1	0.7	0.8	8.8	<1.1	0.7	0.03	0.24	0.18	>2
101	4.1	2.1	0.6	0.7	0.7	8.2	<0.4	0.7	0.25	0.18	0.22	>16
102	7.2	0.5	0.4	0.3	0.2	8.6	<0.3	0.2	0.2	0.07	0.04	>31
104	4.6	1.4	n.d.	0.9	0.6	7.4	<0.5	0.4	0.8	0.13	n.d.	>50

[a] Chain ends and regioerrors are given in units of mol %; [b] Sum of regioerrors, Σ = 2,1 + 3,1 + PEP + $^{n}Bu_A$ + $^{n}Bu_B$; [c] conservative estimate as ^{n}Pr chain ends overlap with regioerrors; [d] Vd+bl = vinylidene + 1-butenyl + 2-butenyl; [e] percentage of benzylated polymer chains, %Bn = 2*Bn/($^{n}Bu_A$ + $^{n}Bu_B$ + ^{n}Pr + ^{i}Bu + Bn + Vd + bl + Allyl).

4.2.1 - Identification of standard polymerization conditions

4.2.1.1 – Pressure dependence

The first experimental parameter we wanted to systematically investigate was monomer pressure. Table 4.4 and 4.5 summarize polymerization experiments at 110°C and four different propene loadings. While experiments at $p \leq 1$ bar can be easily performed in a Pyrex flask, the one at 3 bar requires a steel autoclave reactor.

Table 4.4 – Catalyst performance in propene polymerization at high temperature: pressure dependence.[a]

Exp.	p (bar)	Activity[b]	M_n[c] (kDa)	M_w[c] (kDa)	P_n	PDI	Chains/Met.[d]
1	0.3	5	2.2	3.6	52	1.6	1
101*	0.5	15	4.3	7.5	102	1.7	4
102*	1.0	112	7.0	19	167	2.7	32
2[e]	3.0	491	8.2	16	195	2.0	90

[a] 25 µmol catalyst **10'**, 110°C, MAO/BHT cocatalyst, Al/Ti 400, toluene 200mL, 120 min, MeOH/HCl quenching; [b] in Kg_{PP} mol^{-1} bar^{-1} h^{-1}; [c] by GPC characterization; [d] assuming 100% active Ti; [e] 37 µmol catalyst, toluene 300 mL. * taken from ref. 321.

Table 4.5 – Microstructure and chain-end analysis by ^{13}C NMR characterization relative to the experiments of Table 4.4.[a]

Exp.	2,1	3,1	PEP	$^{n}Bu_A$	$^{n}Bu_B$	Σ[b]	^{n}Pr[c]	^{i}Bu	Bn	Vd+bl[d]	Allyl	%Bn[e]
1	2.2	3.4	0.6	0.8	1.2	8.2	<0.5	1.6	0.3	0.17	0.5	>12
101	4.1	2.1	0.6	0.7	0.7	8.2	<0.4	0.7	0.25	0.18	0.22	>16
102	7.2	0.5	0.4	0.3	0.2	8.6	<0.3	0.2	0.2	0.07	0.04	>31
2	8.2	0.4	0.49	0.3	0.1	9.5	<0.2	0.25	0.11	0.015	0.045	>22

[a] Chain ends and regioerrors are given in units of mol %; [b] Sum of regioerros, Σ = 2,1 + 3,1 + PEP + $^{n}Bu_A$ + $^{n}Bu_B$; [c] conservative estimate as ^{n}Pr chain ends overlap with regioerrors; [d] Vd+bl = vinylidene + 1-butenyl + 2-butenyl; [e] percentage of benzylated polymer chains, %Bn = 2*Bn/($^{n}Bu_A$ + $^{n}Bu_B$ + ^{n}Pr + ^{i}Bu + Bn + Vd + bl + Allyl).

The sum of regioerrors remains practically constant throughout the explored pressure range, but its composition changes. Termination after 2,1-

insertion (giving ^{n}Bu chain ends, Table 4.5) becomes less probable at increasing propene pressure; consequently, further propagation is favored leading to a growth of internal 2,1-units and polymer MW.

The amount of benzyl chain ends seems to be affected by the variation of monomer concentration. In the range 0.3 to 1.0 bar, %Bn increases with *p* from 12 to 31%, while it drops to 22% at 3 bar (Table 4.5). Although a clear dependence on monomer pressure could not be identified, it is remarkable to observe that benzyl chain ends formation represents a competitive process also at rather high pressures, *i.e.* under experimental conditions close to those of commercial solution reactors. Anyway, for additional experiments in this study we preferred to work at 1 bar for practical reasons and because we were generally interested in maximizing the amount of benzyl terminated polymers.

4.2.1.2 – Time dependence

In the initial stages of this project, low pressure experiments required relatively long polymerization times of 2 hours to get reasonable polymer yields. Once more convenient experimental conditions at 110 °C and higher pressure had been identified, we tried to evaluate the effect of reduced reaction time. Along with some practical advantages, shorter experiments might also be more representative of the catalyst behavior especially in terms of productivity, since it is reasonable to expect a marked kinetic decay at high temperature after such long polymerization times.

Indeed, productivity increases up to >200 Kg_{PP} mol^{-1} bar^{-1} h^{-1} (Table 4.6), but also an effect on polymer microstructure is observed. Internal 2,1-units increase with increasing polymerization time, at the expense of 3,1-units, PEP sequences and terminal ^{n}Bu groups. Chain end composition remains similar up to 30 min, while ~50% more benzylated chains are observed at 120 min.

Table 4.6 – Catalyst performance in propene polymerization at high temperature: time dependence.[a]

Exp.	*t* (min)	Activity[b]	M_n[c] (kDa)	M_w[c] (kDa)	P_n	PDI	Chains/Met.[d]
3	15	208	2.8	5.7	67	2.1	19
4	30	236	3.0	7.2	71	2.4	39
102*	120	112	7	19	167	2.7	32

[a] 25 µmol catalyst **10'**, 110°C, 1 bar, MAO/BHT cocatalyst, Al/Ti 400, toluene 200mL, MeOH/HCl quenching; [b] in Kg_{PP} mol^{-1} bar^{-1} h^{-1}; [c] by GPC characterization; [d] assuming 100% active Ti. * taken from ref. 321.

Table 4.7 – Microstructure and chain-end analysis by ^{13}C NMR characterization relative to the experiments of Table 4.6.[a]

Exp.	2,1	3,1	PEP	$^{n}Bu_A$	$^{n}Bu_B$	Σ[b]	^{n}Pr[c]	^{i}Bu	Bn	Vd+bl[d]	Allyl	%Bn[e]
3	3.0	2.8	0.4	0.9	0.9	8.0	<0.7	1.0	0.5	0.14	0.36	>22
4	4.6	1.5	0.6	0.8	0.7	8.2	<0.8	0.7	0.38	0.1	0.16	>21
102	7.2	0.5	0.4	0.3	0.2	8.6	<0.3	0.2	0.2	0.07	0.04	>31

[a] Chain ends and regioerrors are given in units of mol %; [b] Sum of regioerrors, Σ = 2,1 + 3,1 + PEP + $^{n}Bu_A$ + $^{n}Bu_B$; [c] conservative estimate as ^{n}Pr chain ends overlap with regioerrors; [d] Vd+bl = vinylidene + 1-butenyl + 2-butenyl; [e] percentage of benzylated polymer chains, %Bn = 2*Bn/($^{n}Bu_A$ + $^{n}Bu_B$ + ^{n}Pr + ^{i}Bu + Bn + Vd + bl + Allyl).

The most notable changes are found in polymer MW. Going from 15 to 120 min reaction time, P_n increases from 67 to 167 and MWD become gradually broader, indicating a steady deviation from Schultz-Flory regime (Table 4.6). In particular, a PDI of 2.1 at 15 min (Exp 3, Table 4.6) clearly indicates single site behavior, while PDI of 2.7 at 120 min is somewhat too high to be compatible with a perfectly monomodal distribution (Exp. 102).

A plausible explanation might be that inevitable catalyst decomposition at high temperature generates another polymerization active species yielding higher MW polymers. The longer the polymerization proceeds, the more the second active species accumulates and becomes relevant in determining the product composition. A drift in monomer pressure under such relatively forcing

conditions might be another plausible origin. Reincorporation of unsaturated macromonomers is a debated process that has been reported to lead to long chain branched polymers in some cases, and it becomes more likely at increasing concentration of polymer chains (*i.e.* at longer reaction time).[22]

Although the effect on MWD is not dramatic in our case, it still represents a non-negligible indication of some multi-site behavior, which led us to prefer 15 min as the standard reaction time for the following experiments.

4.2.2 – The screening

4.2.2.1 – Phosphinimide catalysts tuning

Six phosphinimide catalysts were tested under the standard set of conditions, which is 1 bar/110 °C/15 min, and interesting trends in polymer microstructure were observed. We explored some ligand variations, including Cp *vs.* Cp* ligands, and different aromatic (Ph) and alkyl (Cy and ^{t}Bu) phosphines (Figure 4.1). The synthesis of the precatalysts is straightforward (Scheme 4.5). Based on established protocols,[318, 320] the trimethylsilyl ligand precursors **Lig(R)-TMS** are easily obtained *via* solvent-free Staudinger reaction of N_3SiMe_3 with a suitable phosphine, and subsequently reacted with Cp or Cp*-titanium trichloride in toluene to obtain typical dichloride precatalysts in high yields.

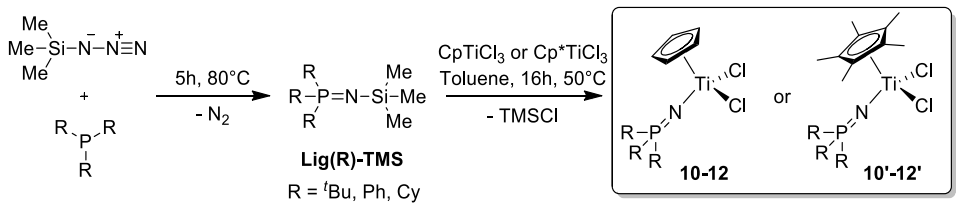

Scheme 4.5 – Synthesis of phosphinimide Ti-complexes.

Table 4.8 – Catalyst performance in propene polymerization at high temperature: ligand variations.[a]

Exp.	Catalyst	Cp *vs.* Cp*	R	Activity[b]	M_n[c] (kDa)	M_w[c] (kDa)	P_n	PDI	Chains/Met.[d]
3	**10'**	Cp*	Ph	208	2.8	5.7	67	2.1	19
5	**11'**	Cp*	Cy	368	0.6	1.2	14	1.9	153
6	**12'**	Cp*	^{t}Bu			*Oligomers*			
7	**10**	Cp	Ph	192	6.3	15	151	2.4	8
8	**11**	Cp	Cy	208	3.0	6.0	72	2.0	17
9	**12**	Cp	^{t}Bu	160	2.4	4.4	57	1.9	17

[a] 25 µmol catalyst, 110°C, 1 bar, MAO/BHT cocatalyst, Al/Ti 400, 15 min, toluene 200mL, MeOH/HCl quenching; [b] in Kg_{PP} mol^{-1} bar^{-1} h^{-1}; [c] by GPC characterization; [d] assuming 100% active Ti.

Table 4.9 – Microstructure and chain-end analysis by ^{13}C NMR characterization relative to the experiments of Table 4.8.[a]

Exp.	2,1	3,1	PEP	^{n}Bu$_A$	^{n}Bu$_B$	Σ[b]	^{n}Pr[c]	^{i}Bu	Bn	Vd+bl[d]	Allyl	%Bn[e]
3	3.0	2.8	0.4	0.9	0.9	8.0	<0.7	1.0	0.5	0.14	0.36	>22
5	1.9	n.d.	n.d.	1.1	0.5	3.5	<0.7	8.2	1.1	0.02	1.4	>17
7	8.9	n.d.	n.d.	0.2	n.d.	9.1	<0.4	0.4	0.1	0.17	n.d.	>16
8	4.5	0.4	0.3	0.4	0.6	6.2	<1.0	1.2	0.23	0.31	0.07	>12
9	5.7	1.3	0.5	0.8	0.8	9.1	<1.1	1	0.22	0.37	0.25	>10

[a] Chain ends and regioerrors are given in units of mol %; [b] Sum of regioerrors, Σ = 2,1 + 3,1 + PEP + ^{n}Bu$_A$ + ^{n}Bu$_B$; [c] conservative estimate as ^{n}Pr chain ends overlap with regioerrors; [d] Vd+bl = vinylidene + 1-butenyl + 2-butenyl; [e] percentage of benzylated polymer chains, %Bn = 2*Bn/(^{n}Bu$_A$ + ^{n}Bu$_B$ + ^{n}Pr + ^{i}Bu + Bn + Vd + bl + Allyl).

Good productivities, monomodal MWD and non-negligible amounts of benzylated chains are obtained for all catalysts, except for **12'** that produces only oligomers (Table 4.8 and 4.9). Activity is only somewhat affected by the nature of ancillary ligands. **11'** is the most active species, giving the highest formal amount of chains per metal as well.

To discuss polymer microstructure, we refer to Table 4.10, which contains processed data from Table 4.8 and 4.9 to highlight trends in the following quantities:

- P_n = (M_n / $MW_{propene}$);
- *Sum of regioerrors, Σ(mol %)* = (2,1 + 3,1 + PEP + $^{n}Bu_A$ + $^{n}Bu_B$);
- *% Terminal 2,1 units* = [100 * ($^{n}Bu_A$ + $^{n}Bu_B$)/(2,1 + $^{n}Bu_A$ + $^{n}Bu_B$)]
- *% Chains with Bn end* = [2 * Bn/($^{n}Bu_A$ + $^{n}Bu_B$ + ^{n}Pr + ^{i}Bu + Bn + Vd + bl + Allyl)];
- *% Chains with saturated end* = [2 * ($^{n}Bu_A$ + $^{n}Bu_B$ + ^{n}Pr + ^{i}Bu)/($^{n}Bu_A$ + $^{n}Bu_B$ + ^{n}Pr + ^{i}Bu + Bn + Vd + bl + Allyl)];
- *% Chains with unsaturated end* = [2 * (Vd + bl + Allyl)/($^{n}Bu_A$ + $^{n}Bu_B$ + ^{n}Pr + ^{i}Bu + Bn + Vd + bl + Allyl)].

Molecular weight strongly depends on substitution patterns of both ancillary ligands, with bulkier groups leading to shorter polymers. The fact that **12'** only yields oligomeric products is consistent with the above trends in MW. Indeed, considering that **11'** already gives a P_n of only 14, very short oligomers deriving from the replacement of Cy with bulkier ^{t}Bu are in line with expectations.

A specific experiment was necessary to prove the production of oligomers at 110°C with **12'**. Major complications arise from the typical quenching procedure that consists in interrupting the monomer supply, venting the reactor and rapidly adding an acidic methanol solution. Venting the reactor at such high temperature might lead to the evaporation of the propene oligomers (*e.g.* the boiling point of propene dimer 4-methyl-1-pentene is 53-54°C), while cooling down the reactor before venting would not allow an easy discrimination between reaction products obtained at 110°C and at lower temperatures. Preliminary experiments showed that **12'** produces non-benzylated polymers at 50°C and 1 bar with productivities of about 20 kg mol^{-1} h^{-1} bar^{-1}. Therefore, before venting the reactor, we rapidly connected it to a cold trap at -78°C, and then followed the usual quenching procedure at 110°C while trapping the hot vapors (see Section 4.4.3 for experimental details). NMR

analysis of the condensed vapors and of a concentrated aliquot of the polymerization mixture showed that oligomers are formed and also benzyl chain ends are detected. Quantitative microstructural considerations are hampered by the difficulties in isolating a representative sample of pure oligomers.

Table 4.10 – Summary of the main polymer features deriving from data analysis of Table 4.8 and 4.9.

	P_n		
	Ph	*Cy*	*^{t}Bu*
Cp	151	72	57
*Cp**	67	14	Olig.

	Sum of regioerrors, Σ (mol %)		
	Ph	*Cy*	*^{t}Bu*
Cp	9.1	6.3	9.3
*Cp**	8.4	4.9	-

	% Terminal 2,1 units		
	Ph	*Cy*	*^{t}Bu*
Cp	2	18	22
*Cp**	38	46	-

	% Chains with Bn end		
	Ph	*Cy*	*^{t}Bu*
Cp	16	12	10
*Cp**	22	17	-

	% Chains with saturated end		
	Ph	*Cy*	*^{t}Bu*
Cp	157	168	163
*Cp**	156	161	-

	% Chains with unsaturated end		
	Ph	*Cy*	*^{t}Bu*
Cp	27	20	27
*Cp**	22	22	-

Catalyst abbreviations: **10**, Cp/Ph; **11**, Cp/Cy; **12**, Cp/^{t}Bu;**10'**, Cp*/Ph;**11'**, Cp*/Cy; **12'**, Cp*/^{t}Bu.

The overall sum of regioerrors decreases when using Cp* rather than Cp ligand, likely due to the higher steric bulk of the former disfavoring secondary insertion mode, while no clear correlation can be established with the P-substituents (Table 4.10). Interestingly, if we consider the amount of regioerrors leading to *n*-butyl chain ends rather than internal 2,1 units, we observe an analogous trend in steric hindrance of *both* ancillary ligands, as previously highlighted for MW (% Terminal 2,1 units, Table 4.10). The bulkier the ancillary ligands, the higher the amount of terminal rather than internal regioerrors. In the case of **11'**, a percentage close to 50% terminal regioerrors indicate that no more than one internal 2,1-unit per polymer chain is found on

average. If the above trend holds also for **12'**, we might even conclude that nearly every regioerror leads to chain termination.

This trend can be rationalized by considering the competition between chain propagation and termination after secondary insertion. We have shown earlier that termination after 2,1-insertion likely proceeds *via* homolysis, and that steric crowding facilitates this process. The observed trends in % Terminal 2,1 units and MW are in line with this mechanistic hypothesis.

If the above considerations are correct, the percentage of terminal regioerrors provides an experimental indication of the relative probability of insertion in and homolysis of the Ti-*sec*-alkyl bond. Therefore, we tentatively tried to estimate the relative barriers for these propagation and termination processes by DFT and to compare them with this experimental parameter. Modeling of the Ti(IV)-C bond cleavage giving separated Ti(III) and polymeryl radical P$^{\cdot}$ is not straightforward, since it is associated with a monotone increase of energy on the PES. Indeed, the Gibbs free energy barrier for this process is mostly due to the fact that much of the Ti–C bonding is lost before the 1→2 particle entropy increase is gained.[226] Based on evaluations by Peters and Scott[337] and according to ref. 226, we assume a constant 8 kcal/mol barrier above the two radical fragments for all the six phosphinimide catalysts.

The trend in % Terminal 2,1 regioerrors is in nice agreement with the predicted $\Delta\Delta G^{\ddagger}_{(Hom.\text{-}INS,\ Ti\text{-}iPr)}$ (Figure 4.5), as increasing relative barriers for homolysis correspond to lower percentages of terminal regioerrors, providing another supporting indication for our mechanistic interpretation. Experimental data for **12'** are not available, but the aforementioned trends suggest that an easier termination after 2,1 insertion than for **11'** is expected, in agreement with computational predictions.

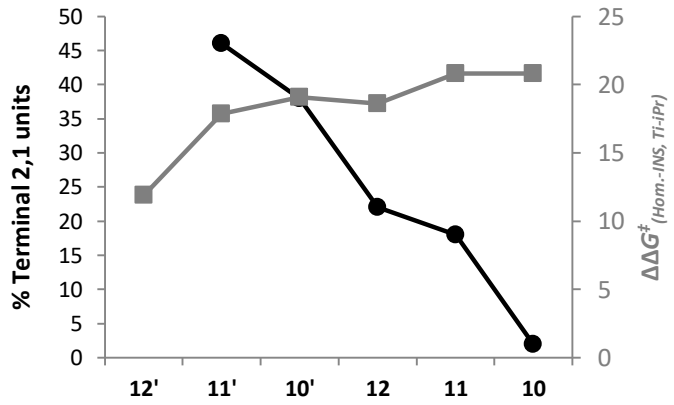

Figure 4.5 – Comparison between trends in experimental % Terminal 2,1 units and calculated $\Delta\Delta G^{\ddagger}_{(hom,\text{-}INS,\ Ti\text{-}iPr)}$ after 2,1 insertion at 383K in kcal/mol (M06-2X/TZ//RI-TPSSTPSS/DZ, gas phase). $\Delta\Delta G^{\ddagger}$ estimated under the assumption of constant 8 kcal/mol homolysis barrier, as $G_{(LxLyTi(propene)+\cdot)} + G_{(iPr\cdot)} - G_{(insertion)}$ + 8 kcal/mol, according to ref. 226. Datapoints ordered according to decreasing experimental % Terminal 2,1 units.

It should be emphasized here that we refer to the general relative trends and that minor deviations between experiments and theory are expected. Regarding the experimental data, the underlying assumption is that isomerization of Ti-*sec*-alkyl bond giving 3,1 units represents a minor process that should not affect the competition between insertion and homolysis of Ti-*sec*-alkyl significantly. Concerning computational predictions, it has been shown earlier that calculating absolute trends for $\Delta\Delta G^{\ddagger}_{(Hom.\text{-}INS,\ Ti\text{-}iPr)}$ would require to include the anion in every calculation,[226] which exceeds our current computational capacities. Gibbs free energy differences reported in here were therefore calculated within the naked cation approximation, which should still provide reliable qualitative relative trends. Predicted $\Delta\Delta G^{\ddagger}_{(Hom.\text{-}INS,\ Ti\text{-}iPr)}$ are in the range of 12-21 kcal/mol, *i.e.* much higher than those estimated experimentally between 0.2 and 3 kcal/mol; however, counterion effects have been predicted to account for up to 20 kcal/mol for the specific case of BF_4^-,[226] which are in the

same order of magnitude of our discrepancy. Further consideration on counterion effects are discussed in Section 4.2.2.3.

Regarding the percentage of benzylated chains, Cp* catalysts **10'** (22%) and **11'** (17%) give slightly higher solvent incorporation than Cp-analogues **10** (16%) and **11** (12%), while less bulky P-substituents lead to more benzylated chains (Ph > Cy > ^{t}Bu) (Table 4.10). Rationalizing variations in the amount of benzyl chain ends is complex, since chain transfer to solvent is not only dependent on the ease of homolysis but also on the probability of H abstraction from toluene, Ti(III)/benzyl radical recombination and chain reinitiation (Scheme 4.4).

The aforementioned trend in calculated $\Delta\Delta G^{\ddagger}_{(Hom.\text{-}INS,\ Ti\text{-}iPr)}$ (Figure X1), does not correlate with the experimental amount of solvent incorporation. For instance, **10'** gives the highest percentage of benzyl chain ends (22%) but it is predicted to be one of the least prone to give Ti-C homolysis. This suggests that the ease of Ti-*sec*-alkyl bond cleavage is not the main parameter determining solvent incorporation.

The probability of H abstraction from toluene should be catalyst independent, since the Ti-species is not directly involved in the reaction between the polymeryl radical and the solvent molecule. Likewise, the ease of organic radical recombination should be virtually the same for all the catalysts screened, since concentration of all the components of the catalytic pool was kept constant, while recombination of organic and metal radical might be somewhat different. For instance, Piers and co-workers reported that Cp-containing Ti(III) cations can dimerize, giving homodinuclear species containing bridged phosphinimide ligands (Figure 4.6).[331] Formation of these species should be more difficult when using bulky Cp* ligands, but it could still compete with chain transfer to solvent after Ti-C homolysis. These Ti(III) dimers represent inactive species that can accumulate during polymerization

experiments, and might be responsible for the green color observed. Quantifying the effects of this side reaction is difficult; however, if there was a significantly different tendency of the six phosphinimide catalysts to dimerize under the high-dilution polymerization conditions, this should probably be reflected by a much larger effect on activity than the one we observe.

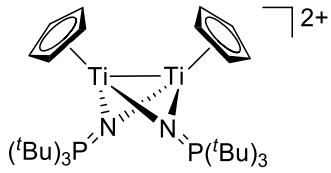

Figure 4.6 – Dimers reported by the group of Piers for CpTi(III) phosphinimide complexes.[331]

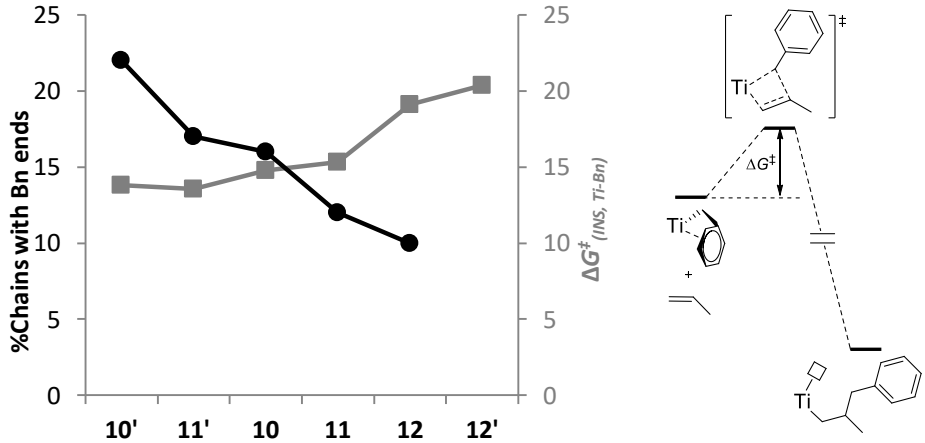

Figure 4.7 - Comparison between trends in experimental %benzylated chains (black circles) and calculated $\Delta G^{\ddagger}_{(INS,\ Ti\text{-}Bn)}$ (grey squares) barriers for propene insertion in Ti-Bn bonds at 383K in kcal/mol (M06-2X(PCM)/TZ//RI-TPSSTPSS/DZ). Insertion barriers are calculated with respect to the η^2 benzyl cation. Datapoints ordered according to decreasing %Bn. No experimental data available for **12'**, although %Bn should be >0 (see main text).

We estimated the ease of chain reinitiation by calculating insertion barriers in Ti-Bn bonds with respect to the naked cation with η^2-coordinated benzyl. Experimental trend in the percentage of benzyl chain ends seems follow

the calculated $\Delta G^{\ddagger}_{(INS,\ Ti\text{-}Bn)}$, with higher barriers corresponding to lower incorporation (Figure 4.7).

Furthermore, we evaluated the competition between insertion and homolysis of the Ti-Bn bond, and found that the experimental percentage of benzylated chains nicely correlates with the $\Delta\Delta G^{\ddagger}_{(Hom.\text{-}INS,\ Ti\text{-}Bn)}$ as well (Figure 4.8). The easier the homolysis, the lower the amount of benzylated chains. These results point to chain reinitiation being the key step determining benzyl chain end formation, with the barrier heights for insertion and/or the ease of homolysis of the Ti-Bn bond limiting the amount of solvent incorporation. It should be noted here that homolysis of the Ti-Bn might favor other competitive routes, such as the aforementioned dimerization of Ti(III) species.

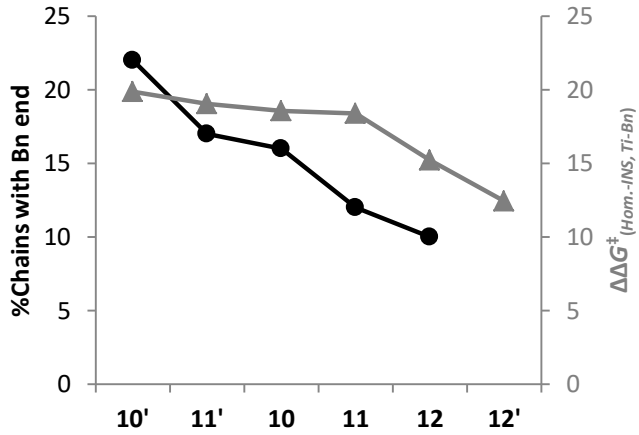

Figure 4.8 - Comparison between trends in experimental %benzylated chains (black circles) and calculated relative barriers for propene insertion and Ti-Bn homolysis $\Delta\Delta G^{\ddagger}_{(\text{Hom.-}INS,\ Ti\text{-}Bn)}$ (grey triangles) at 383K in kcal/mol (M06-2X(PCM)/TZ//RI-TPSSTPSS/DZ). Datapoints ordered according to decreasing %Bn. No experimental data available for **12'**, although %Bn should be > 0 (see main text).

For all the catalysts studied, the percentage of chains bearing a saturated chain end is well above 100%, meaning that more than 50% of all chains have aliphatic head and tail (Table 4.10). The case of **11'** is particularly indicative.

Under the assumption of 100% active metal, this catalyst produces 153 chains/Ti, of which at least 61% have only saturated chain ends. This means that each Ti center produces ~93 fully aliphatic polymer chains. The most obvious explanation would be a dominant termination process *via* chain transfer to Al, but we can rule this out due to the presence of BHT, as previously discussed. The generation of such unusually high amounts of saturated chain ends seems to be linked to the reactivity leading to chain transfer to solvent. The low amount of unsaturated chain ends suggests that BHTM and/or BHE play only a limited role.

Finally, based on the above considerations and on DFT calculations (Figure 4.5), among the phosphinimide complexes in our test set, homolysis is expected to be particularly easy for **12'**. This prompted us to explore chain transfer to solvent also in ethene polymerization with this catalysts under analogous conditions to those described here for propene. In ethene polymerization, only primary Ti-alkyls are expected, which should be less prone to give homolytic Ti-C bond cleavage than Ti-*sec*-alkyls, as previously discussed. A preliminary experiment at 1 bar and 110°C showed that a sizable amount of benzyl chain ends is produced also in ethene homopolymerization (~69%). Broad MWD (PDI = 8.0) and very high activity (1357 kg mol^{-1} h^{-1} bar^{-1}) suggest that the experiment was likely carried out under diffusion kinetic regime, which hamper any quantitative consideration. Phosphinimide complexes are known to polymerize ethene with remarkably high activity,[38, 49, 319] and monomer concentration under our conditions might have been too low to run a controlled experiment. Nevertheless, this preliminary observation seems to prove the generality of the chain transfer to solvent process and that homolysis can be a competitive reaction pathway also with primary alkyls. In the continuation of this project we preferred to focus on propene polymerization,

although the above results with ethene monomer certainly represents a potential new starting point for further interesting studies.

4.2.2.2 – Different catalyst classes

Several Ti-based catalysts with ligand backbones other than phosphinimide groups were tested as well. Along with **Cp^*TiCl_3** that was already mentioned in Section 4.1.1, we included the simplest metallocene **Cp_2TiCl_2**, the prototypical CGC and a phenoxyimide (FI) catalysts (Figure 4.9).

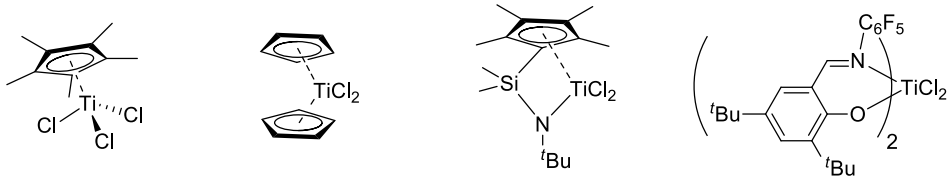

Cp^*TiCl_3 **Cp_2TiCl_2** **CGC** **FI**

Figure 4.9 – Non-phosphinimide catalysts studied.

Under polymerization conditions analogous to those used for phosphinimide catalysts (Table 4.11), none of these species produces benzylated polymers. **Cp_2TiCl_2** exhibits very low activity at 110°C and 1 bar, in line with previously observed rapid deactivation above 50°C.[338] Furthermore, this catalyst produces polymers with no detectable amounts of 2,1-units. These observations might be rationalized assuming that practically every 2,1-insertion leads to Ti(IV) reduction to Ti(III) because of homolysis, in agreement with previously reported DFT calculations.[226] In this case, however, radical decomposition is not followed by chain reinitiation as for phosphinimide catalysts, since no benzyl chain ends are found. Therefore, we tried to verify if our hypothesis on factors determining the extent of solvent incorporation applies also in this case. DFT calculations predict an insertion barrier in the Ti-

Bn bond $\Delta G^{\ddagger}_{(INS,\ Ti\text{-}Bn)}$ of 20.0 kcal/mol, which is comparable to the one of **12** that produces 10% benzylated chains under analogous conditions (Section 4.2.2.1). However, in the case of **Cp_2TiCl_2**, homolysis of the Ti-Bn bond seems to be particularly easy and even favored with respect to insertion, as a $\Delta\Delta G^{\ddagger}_{(Hom.\text{-}INS,\ Ti\text{-}Bn)}$ of -0.6 kcal/mol is found computationally. This is likely due to the higher steric hinderance close to the metal center provided by the Cp rather than phosphinimide ligands, which significanlty favors homolysis. Furthermore, it seems to confirm our tentative conclusion on chain reinitiation being the limiting step for benzyl chain ends formation.

Table 4.11 – Catalyst performance in propene polymerization at high temperature: different catalyst classes.[a]

Exp.	Catalyst	T (°C)	*p* (bar)	Activity[b]	M_n[c] (kDa)	M_w[c] (kDa)	P_n	PDI
103*	**Cp^*TiCl_3**	80	0.5	13	23	112	537	4.9
10	**Cp_2TiCl_2**	110	1.0	4.8	17	42	404	2.5
11	**CGC**	110	1.0	88	3.5	6.8	83	2.0
12	**FI**	110	1.0	-	-	-	-	-
13	**FI**	70	1.0	32	1.5	1.7	35	1.1

[a] 25 µmol catalyst, MAO/BHT cocatalyst, Al/Ti 400, toluene 200mL, 15 min, MeOH/HCl quenching; [b] in Kg_{PP} mol^{-1} bar^{-1} h^{-1}; [c] by GPC characterization. * taken from ref. 321, 2h.

CGC is known to be highly thermally stable and indeed gives rather good yields at 110°C; the polypropylene obtained with this catalyst has the typical microstructure deriving from BHTM or BHE being the dominant termination process. Finally, FI catalysts are known to propagate *via* 2,1 insertion modes.[62] The high frequency of secondary insertion should trigger homolysis, but PDI of 1.1 at 70°C indicates that practically no chain transfer/termination mechanism is operative under our conditions, *i.e.* that the polymerization is *pseudo*-living. Higher temperatures however yielded no polymer. In conclusion, it is necessary to emphasize that only a limited number of tests for each additional catalyst

were performed and conditions optimal for chain end functionalization might have been missed.

4.2.2.3 – The role of cocatalyst

The role of the co-catalyst seems to be crucial for chain transfer to solvent. As mentioned above, the effect of the cocatalyst-derived counterion on the ease of homolysis has been theoretically explored only for the case of BF_4^-,[226] *i.e.* a particularly 'sticky' anion which is poorly representative of those used in olefin polymerization. From a computational point of view, methylborate deriving from Ti-Me abstraction by $B(C_6F_5)_3$, is the simplest case of a typical counterion in olefin polymerization, due to its well-defined molecular nature and the B-Me group that allows to locate it easily around the cationic Ti-complex with the methyl pointing towards the metal center.[188, 339] Identifying realistic models for MAO-based anions is especially tricky,[146, 164-165] while it is difficult to identify the correct location and orientation for the highly symmetric pentafluorophenylborate obtained from $[Ph_3C][B(C_6F_5)_4]$ (trityl borate, TTB).[146, 340]

Therefore, we focused on $[MeB(C_6F_5)_3]^-$. Due to the complexity and computational time demand of modeling of the counterion, we preliminary explored its interaction with a model phosphinimide catalyst bearing Cp and $[Me_3PN]^-$ ancillary ligands (Figure 4.10).

The presence of methyl borate seems to dramatically favor homolysis with respect to insertion, as the $\Delta\Delta G^{\ddagger}_{(Hom.-\ INS,\ Ti\text{-}iPr)}$ drops from 19.7 in the case of the naked cation to only 3.1 kcal/mol with $[MeB(C_6F_5)_3]^-$. This value is quite reasonable for a sterically open species like our model complex. Interestingly, for the least sterically hindered phosphinimide catalyst we screened (**10,** *i.e.* Cp, R = Ph), we estimate an experimental $\Delta\Delta G^{\ddagger}_{(Hom.-\ INS,\ Ti\text{-}iPr)}$ of exactly 3.0 kcal/mol,

indicating that our computational predictions is able to capture the expected range of relative Gibbs free energy differences.

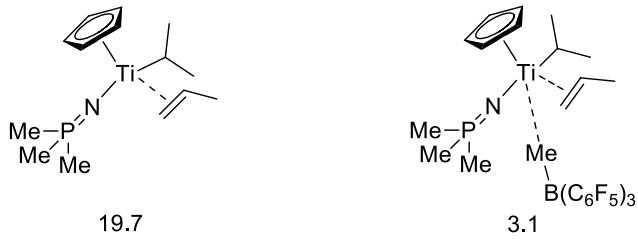

19.7 3.1

Figure 4.10 – Evaluation of counterion effect on the ease of homolysis for a model phosphinimide precatalyst bearing Cp and $[Me_3PN]^-$ ancillary ligands. Numbers are $\Delta\Delta G^{\ddagger}_{(Hom.-\ INS,\ Ti-iPr)}$ in kcal/mol at 383 K, calculated at the M06-2X(PCM)/TZ//RI-TPSSTPSS/DZ level.

The effect of BF_4^- has been previously estimated to be around 20 kcal/mol,[226] which is comparable to the one we predict here for $[MeB(C_6F_5)_3]^-$ approaching 17 kcal/mol. Methylborate is generally considered more coordinating than MAO-derived anions and $B(C_6F_5)_4^-$,[157, 339] but the difference between these three species is relatively small compared to the by far more 'sticky' tetrafluoroborate. Therefore, we expect that the effect of the three typical weakly coordinating anions for olefin polymerization on $\Delta\Delta G^{\ddagger}_{(Hom.-\ INS,\ Ti-iPr)}$ should be quite similar.

We tried to explore this hypothesis experimentally, by comparing the polymerization performance of the case study **10'** with MAO/BHT cocatalyst and with typical molecular activators such as $B(C_6F_5)_3$ and TTB (Exp. 3 and 14-15, Table 4.12 and 4.13). Bulky trialkyl aluminum, such as Al^iBu_3 (TiBA), are typical impurity scavengers used in combination with boranes and borates. Due to the undesirable reactivity of phosphinimide catalysts towards free aluminum alkyls,[183-184] we preferred to modify TiBA with BHT as well. An Al/BHT ratio of 1:1 is enough to prevent undesired reactions, since *iso*-butyl are much bulkier than methyl groups of TMA. While high Al/Ti ratio are necessary with MAO, it is

generally advisable not to use large amounts of TiBA due to its purely Al-alkyl nature. An Al/Ti ratio of 25 (*i.e.* [Al] = 3 mM) was used in these experiments.

Table 4.12 – Catalyst performance in propene polymerization at high temperature: different activators.[a]

Exp.	Cocatalyst	Al/Ti	AlR_3/ BHT	Activity[b]	M_n[c] (kDa)	M_w[c] (kDa)	P_n	PDI	Chains/ Met.[d]
3	MAO/BHT	400	1:2	208	2.8	5.7	67	2.1	19
14[e]	$B(C_6F_5)_3$/TiBA/BHT	25	1:1	144	3.5	6.3	83	1.8	10
15[e]	TTB/TiBA/BHT	25	1:1	226	3.3	7.0	79	2.1	17
16[e]	$B(C_6F_5)_3$/MAO/BHT	400	1:2	228	2.9	6.1	70	2.1	26

[a] 25 μmol **10'**, 110°C, 1 bar, 15 min, toluene 200mL, MeOH/HCl quenching; [b] in Kg_{PP} mol^{-1} bar^{-1} h^{-1}; [c] by GPC characterization; [d] assuming 100% active Ti; [e] *dimethyl* precatalyst reacted with molecular activator prior to injection in the polymerization reactor, Ti/B 1:1.1. TiBA = tri-*iso*-butylaluminum; TTB = $[Ph_3C][B(C_6F_5)_4]$; AlR_3 = $AlMe_3$ (in MAO) or Al^iBu_3.

Table 4.13 – Microstructure and chain-end analysis by ^{13}C NMR characterization relative to the experiments of Table 4.12.[a]

Exp.	2,1	3,1	PEP	^nBu_A	^nBu_B	Σ[b]	^nPr[c]	^iBu	Bn	Vd+bl[d]	Allyl	%Bn[e]
3	3.0	2.8	0.4	0.9	0.9	8.0	<0.7	1.0	0.5	0.14	0.36	>22
14	4.3	1.5	0.7	0.5	0.4	7.4	<1.0	0.5	n.d.	0.5	0.16	n.d.
15	4.6	2.3	0.8	0.6	0.6	8.9	<1.0	0.7	0.06	0.15	0.3	>4
16	3.8	2.1	0.4	0.7	0.7	7.7	<0.9	0.8	0.19	0.28	0.25	>10

[a] Chain ends and regioerrors are given in units of mol %; [b] Sum of regioerrors, Σ = 2,1 + 3,1 + PEP + ^nBu_A + ^nBu_B ; [c] conservative estimate as ^nPr chain ends overlap with regioerrors; [d] Vd+bl = vinylidene + 1-butenyl + 2-butenyl; [e] percentage of benzylated polymer chains, %Bn = 2*Bn/(^nBu_A + ^nBu_B + ^nPr + ^iBu + Bn + Vd + bl + Allyl).

Reducing $\Delta\Delta G^{\ddagger}_{(Hom.-\ INS,\ Ti\text{-}iPr)}$ should translate to an higher amount of *n*-butyl chain ends with respect to internal regioerrors, and lower MW, as a result of the easier chain termination after secondary insertion. However, the percentage of terminal 2,1-units and P_n remain practically constant going from TTB to $B(C_6F_5)_3$/TiBA/BHT cocatalyst, while variations close to the experimental accuracy are found for MAO/BHT (Table 4.14).

Activity is barely affected (Table 4.12), although a strict comparison between MAO and molecular activators is generally not possible, due to their different chemical nature and the different dichloride *vs.* dimethyl precatalyst used. It has been proposed that interactions of the more coordinating $[MeB(C_6F_5)_3]^-$ counterion with respect to $B(C_6F_5)_4^-$ might have a detrimental effect on activity,[339] but this effect seems to be rather small and close to the experimental uncertainty in our case (Exp. 14-15, Table 4.12). The fact that activity, *n*-butyl chain ends and MW are substantially independent from the cocatalyst is in nice agreement with our hypothesis, suggesting that homolysis is comparably favored with respect to insertion in Ti-*sec*-alkyls as far as one of the typical weakly coordinating anions for olefin polymerization is considered.

Table 4.14 – Summary of the main polymer features deriving from data analysis of Table 4.12 and 4.13.

P_n			**Sum of regioerrors, Σ (mol %)**			**% Terminal 2,1-units**		
	MAO/ BHT	TiBA/ BHT		*MAO/ BHT*	TiBA/ BHT		*MAO/ BHT*	TiBA/ BHT
MAO/ BHT	67	-	*MAO/ BHT*	8.4	-	*MAO/ BHT*	38	-
$B(C_6F_5)_3$	70	83	*$B(C_6F_5)_3$*	8.0	7.6	*$B(C_6F_5)_3$*	27	17
TTB	-	79	*TTB*	-	9.2	*TTB*	-	21

% Chains with Bn end			**% Chains with saturated end**			**% Chains with unsaturated end**		
	MAO/ BHT	TiBA/ BHT		*MAO/ BHT*	TiBA/ BHT		*MAO/ BHT*	TiBA/ BHT
MAO/ BHT	22	-	*MAO/ BHT*	156	-	*MAO/ BHT*	22	-
$B(C_6F_5)_3$	10	n.d.	*$B(C_6F_5)_3$*	162	157	*$B(C_6F_5)_3$*	28	43
TTB	-	4	*TTB*	-	170	*TTB*	-	26

At the same time, it should be noted that the nature of the cocatalyst has a quite notable effect on chain end composition. No benzylated chains are found with $B(C_6F_5)_3$/TiBA/BHT as cocatalyst, while only 4% is obtained with TTB (Table 4.14). With respect to MAO/BHT (that gives a much higher percentage of

solvent incorporation of 22%), the drop of benzyl chain ends with $B(C_6F_5)_3$ is compensated by an increase of unsaturated chains ends (up to 43% unsaturated chains), even though they remain well below the saturated ones. This suggests that BHTM and BHE are somewhat more competitive in this case. Both unsaturated and especially saturated terminations increase in the case of TTB.

These considerations on the counterion effect might represent a further indication of the mechanism of chain transfer to solvent being radical and not SBM. If the assumption of comparably loose interactions with the counterion is correct, SBM should give roughly the same amount of benzyl chain ends in all the cases explored, since the capability of the cationic Ti complex to activate the toluene solvent should be unaffected. Conversely, in the case of the proposed radical mechanism, we have previously discussed that the extent of solvent incorporation depends on the ease of Ti-C homolysis, radical recombination and chain reinitiation, and the nature of the active cation is not the only variable determining the balance between them. For instance, the probability of radical recombination might be dependent on the nature and concentration of the cocatalyst, especially if it includes a radical stabilizer such as BHT. This would explain why cocatalyst effects on polymer chain ends can be different from those on activity and other polymer microstructural features, although fully rationalizing these observations is difficult at this stage.

We tried to obtain some more experimental evidence for the aforementioned hypothesis by performing a competitive experiment in which $B(C_6F_5)_3$ was used in combination with MAO/BHT (Exp. 16, Table 4.12 and 4.13). The borane activator was reacted with **10'** before injection in the MAO/BHT-containing polymerization reactor to ensure methyl abstraction from the Ti-precatalyst by the borane not MAO. The results in terms of activity, MW capability and regioselectivity are in line with expectations (*i.e.* minor

differences with respect to other cocatalyst systems), and a sizable amount of benzyl chain ends is observed (10%).

Therefore, with respect to Exp. 14 ($B(C_6F_5)_3$/TiBA/BHT), we observe that replacing TiBA/BHT with MAO/BHT seems to be the key to allow chain transfer to solvent also in the presence of $[MeB(C_6F_5)_3]^-$, as benzyl chain ends grow from 0 to 10%. An analogous effect has been reported previously when dried MAO/BHT was used in place of dried MAO.[321] Whether this enhancing effect is due to the higher amount of BHT used or to the nature of MAO/BHT itself being particularly suitable to promote this reactivity remains an open question at this stage.

We tried to preliminary explore the role of BHT by screening the influence of various $AlMe_3$/BHT ratios on catalyst performances (Table 4.15 and 4.16). We observed that the phosphinimide system stays active as long as at least 2 eq. of BHT per TMA are added (Exp. 3). Lower amounts (1 eq., Exp. 17) might be not enough to effectively trap TMA, leading to catalyst deactivation.[47] Higher amounts of BHT (3 to 5 eq., Exp. 18-19) lead to a steady decrease of activity, either because the part of the phenol that does not react with TMA represents a poison for the catalyst or because the phenol reacts with the MAO clusters reducing the amount of available acidic sites necessary to activate the catalyst.

Table 4.15 – Catalyst performance in propene polymerization at high temperature: different Al/Ti and BHT/Ti ratios, and catalyst concentration.[a]

Exp.	$AlMe_3$/ BHT	Activity[b]	M_n[c] (kDa)	M_w[c] (kDa)	P_n	PDI	Chains/Met.[d]
17	1:1	-	-	-	-	-	-
3	1:2	208	2.8	5.7	67	2.1	19
18	1:3	192	2.5	4.9	59	2.0	19
19	1:5	96	1.9	3.6	45	1.9	13

[a] 25 µmol, 110°C, 1 bar, MAO/BHT cocatalyst, Al/Ti 400, 15 min, toluene 200mL, MeOH/HCl quenching; [b] in Kg_{PP} mol^{-1} bar^{-1} h^{-1}; [c] by GPC characterization; [d] assuming 100% active Ti.

Table 4.16 – Microstructure and chain-end analysis by ^{13}C NMR characterization relative to the experiments of Table 4.15.[a]

Exp.	2,1	3,1	PEP	$^{n}Bu_A$	$^{n}Bu_B$	Σ[b]	^{n}Pr[c]	^{i}Bu	Bn	Vd+bl[d]	Allyl	%Bn[e]
3	3.0	2.8	0.4	0.9	0.9	8.0	<0.7	1.0	0.5	0.14	0.36	>22
18	4.2	1.8	0.8	0.8	0.5	8.1	<0.8	0.7	0.3	0.12	0.19	>17
19	4.6	1.3	0.4	0.8	0.7	7.8	<0.8	0.5	0.2	0.09	0.16	>12

[a] Chain ends and regioerrors are given in units of mol %; [b] Sum of regioerrors, Σ = 2,1 + 3,1 + PEP + $^{n}Bu_A$ + $^{n}Bu_B$; [c] conservative estimate as ^{n}Pr chain ends overlap with regioerrors; [d] Vd+bl = vinylidene + 1-butenyl + 2-butenyl; [e] percentage of benzylated polymer chains, %Bn = 2*Bn/($^{n}Bu_A$ + $^{n}Bu_B$ + ^{n}Pr + ^{i}Bu + Bn + Vd + bl + Allyl).

MW and regioerrors are barely affected by the different $AlMe_3$/BHT ratio, as expected, while small but detectable trends in chain ends composition are observed (Table 4.16). In particular, higher amounts of BHT seem to favor saturated chain end formation and reduce benzylated and unsaturated ones, indicating that BHT is somehow involved in the process, possibly *via* trapping of polymeryl radicals.

4.2.2.4 – Incorporation of different solvents and potential chain end functionalization

We tried to explore the scope of this new reaction with solvents different from toluene. Some analogous aromatic solvents such as mesitylene and ethylbenzene were tested, along with heteroatom containing 4-fluorotoluene (Table 4.17 and 4.18). MAO/BHT solutions were dried in this case, and the resulting white solid used as cocatalyst in order not to have toluene impurities in the polymerization mixture (see also Chapter 5).

Remarkably high amounts of benzylated chains (up to 50%) are obtained with mesitylene solvent. BDE for benzylic C-H bonds of toluene and mesitylene are very similar,[330] and would not justify such a marked increase of benzylated chains. Rather, a plausible explanation might be related to the higher viscosity

of mesitylene, which could limit the mobility of the radicals and favor recombination with Ti(III).

Table 4.17 – Catalyst performance in propene polymerization at high temperature: different solvents.[a]

Exp.	Solvent	T (°C)	*p* (bar)	Activity[b]	M_n[c] (kDa)	M_w[c] (kDa)	P_n	PDI	Chains/ Met.[d]
3	Toluene	110	1.0	208	2.8	5.7	67	2.1	19
104*	Mesitylene[e]	110	0.8	40	3.3	7.0	79	2.1	19
20	Ethylbenzene	110	1.0	18	3.9	8.0	93	2.0	9
21	4-F-toluene	120	1.5	27	2.3	4.8	55	2.1	35
22	4-F-toluene	90	0.5	54	2.7	6.0	64	2.2	20
23	F-benz/toluene[f]	110	1.0	25	3.0	6.0	71	2.0	17

[a] 6 µmol catalyst, dried MAO/BHT cocatalyst, Al/TI 400, 15 min, solvent 50mL, MeOH/HCl quenching; [b] in Kg_{PP} mol^{-1} bar^{-1} h^{-1}; [c] by GPC characterization; [d] assuming 100% active Ti; [e] 120 min; [f] 50 v/v %, MAO/BHT as cocatalyst. * taken from ref. 321. 4-F-toluene = 4-fluorotoluene; F-benz = ortho-difluorobenzene.

Table 4.18 – Microstructure and chain-end analysis by ^{13}C NMR characterization relative to the experiments of Table 4.17.[a]

Exp.	2,1	3,1	PEP	$^{n}Bu_A$	$^{n}Bu_B$	Σ[b]	^{n}Pr[c]	^{i}Bu	Bn	Vd+bl[d]	Allyl	%Bn[e]
3	3.0	2.8	0.4	0.9	0.9	8.0	<0.7	1.0	0.5	0.14	0.36	>22
104	4.6	1.4	n.d.	0.9	0.6	7.4	<0.5	0.4	0.8	0.13	n.d.	>50
20	5.7	0.9	0.4	0.5	0.5	8.0	<0.8	0.4	0.05	0.13	0.11	>4
21	4.6	1.8	0.3	0.5	0.5	7.7	<1.5	0.5	n.d	0.9	0.16	-
22	4.8	0.7	0.4	0.4	0.3	6.6	<1.1	0.4	n.d	0.61	0.14	-
23	3.9	2.3	1.1	0.7	0.8	8.8	<1.1	0.7	0.03	0.24	0.18	>2

[a] Chain ends and regioerrors are given in units of mol %; [b] Sum of regioerrors, Σ = 2,1 + 3,1 + PEP + $^{n}Bu_A$ + $^{n}Bu_B$; [c] conservative estimate as ^{n}Pr chain ends overlap with regioerrors; [d] Vd+bl = vinylidene + 1-butenyl + 2-butenyl; [e] percentage of benzylated polymer chains, %Bn = 2*Bn/($^{n}Bu_A$ + $^{n}Bu_B$ + ^{n}Pr + ^{i}Bu + Bn + Vd + bl + Allyl). *taken from ref. 321.

According to previous work, SBM is predicted to be easier from Ti-H than from Ti-alkyl.[320-321] BHTM and BHE termination processes are typically responsible for generating equal amounts of Ti-H species and unsaturated chain ends. In this case, the amount of benzyl chain ends vastly outnumber

unsaturated ones, indicating that the amount of Ti-H formed during polymerization is not enough to justify formation of benzyl chain ends. This points to SBM from Ti-H being not a relevant reaction pathway.

Ethylbenzene only give 4% benzylated polymers. This finding is quite expected since H abstraction from the benzylic CH_2 (path a in Scheme 4.6) should be easier than from aliphatic CH_3 (path b) and lead to secondary carbon bound to Ti. Chain reinitiation by insertion in the Ti-secondary C bond should be more difficult compared to the primary one obtained with toluene. Furthermore, homolysis of secondary Ti-C bonds is easier and could limit chain reinitiation, as previously discussed for Ti-Bn.

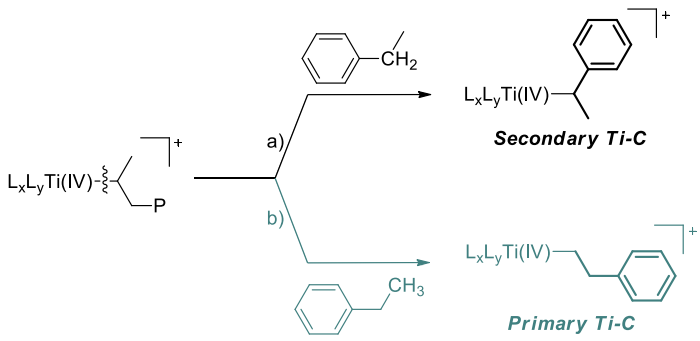

Scheme 4.6 – Comparison between (a) benzylic CH_2 and (b) aliphatic CH_3 activation of ethylbenzene leading to secondary a primary Ti-C respectively.

Regarding heteroatom containing aromatic solvents, preliminary experiments showed that low activity and no benzyl chain ends are observed when using 2- and 4-chlorotoluene.[321] Since the C-Cl could be easily attacked by radicals, we investigated the more inert 4-fluorotoluene (Exp. 23-24). Although also in this case no benzylated polymers are obtained, we tried to draw some tentative conclusion on what hampers functionalized toluene incorporation.

About 50% of the total chains have fully saturated head and tail, suggesting that the reactivity associated to chain transfer to solvent is not completely ceased (Table 4.18). Since C-H BDE for fluorotoluene is slightly

smaller than toluene,[330] solvent activation should be at least similarly easy in the two cases. If this is true, a more difficult propene insertion in the Ti-(4-F-Bn) bond rather than generation of Ti-(4-F-Bn) itself might be the explanation for the absence of functionalized chains. We explored this hypothesis by DFT for the specific case of **10'**, by comparing relative barriers for insertion with respect to the benzyl olefin complex or naked cation with dissociated propene (Figure 4.11a-b), but found only negligible differences for Ti-Bn *vs.* Ti-(4-F-Bn).

Another possibility might be that activation of 2-fluorotoluene impurities leads to a dormant Ti-(2-F-Bn) cation, due to interactions between Ti and the ortho-fluorine atom. Indeed, insertion barriers are predicted to be slightly higher than for Ti-Bn, but not high enough to justify the complete absence of fluorobenzyl chain ends (Figure 4.11c). Likewise, $\Delta\Delta G^{\ddagger}_{(Hom.\text{-}INS)}$ is predicted to be only 1 kcal/mol lower for substituted rather than unsubstituted toluene (19.8 kcal/mol for Ti-Bn; 18.9 kcal/mol for Ti-(4-F-Bn); 18.8 kcal/mol for Ti-(2-F-Bn)).

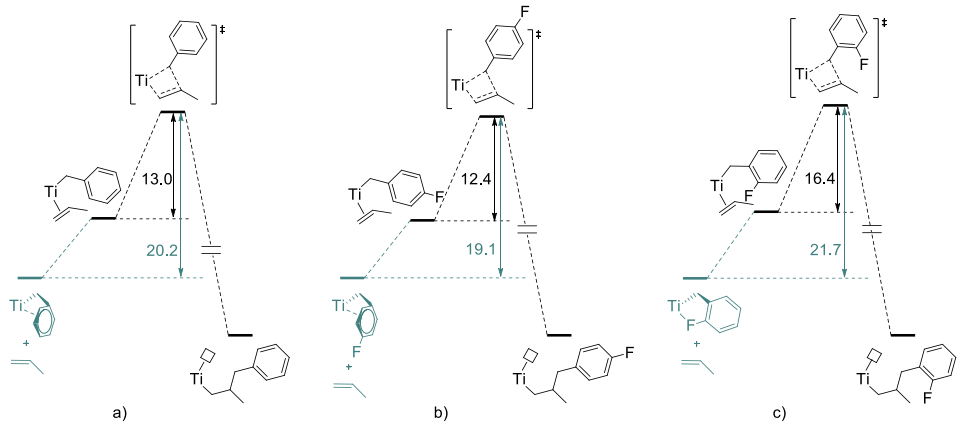

Figure 4.11 – Comparison between DFT calculated (M06-2X/TZ//RI-TPSSTPSS/DZ, gas phase, 383K) insertion barrier heights for chain reinitiation in **10'** a) Ti-Bn, b) Ti-(4-F-Bn) and c) Ti-(2-F-Bn) bond. Numbers are Gibbs Free Energy differences in kcal/mol.

Finally, aromatic C-F activation might be a competitive side reaction hampering incorporation of benzyl chain ends. A polymerization experiment in a 50 v/v% mixture of toluene and *ortho*-difluorobenzene was performed under the aforementioned standard set of reaction conditions 1 bar/110 °C/15 min (Exp. 25, Table 4.17). In this way, we tried to evaluate the effect of the presence of an aromatic C-F containing solvent on incorporation of benzyl chain ends. Only traces of benzylated polymers were obtained, suggesting that the presence of the fluorine atom might be detrimental for chain transfer to solvent. It should be noted, however, that the drop of benzyl chain ends might be simply due to the lower concentration of toluene. Further studies would be necessary to discriminate between these two effects.

4.3 – Concluding Remarks

In this Chapter, we described an unprecedented chain transfer to solvent process in propene homopolymerization by Ti-phosphinimide catalysts, representing a competitive chain termination process at high operating temperatures. It involves activation of the toluene solvent and subsequent formation of benzylated polymer chain ends, and represents an interesting example of reversible catalyst deactivation.

The proposed mechanism consists of a radical route involving homolysis of the Ti(IV)-polymeryl bond, benzylic H abstraction from toluene by the polymeryl radical, recombination of the resulting benzyl radical with the Ti(III) species, and finally chain reinitiation by insertion of propene in the so formed Ti(IV)-Bn bond. This process is expected to be particularly favored after 2,1-monomer insertion due to the weaker Ti-C bond compared to primary Ti-alkyls, and offers an interesting insight in the role of regioerrors in α-olefin polymerization and on factors determining the thermal stability of Ti-based molecular catalysts. Chain transfer to solvent was found to be a relevant reaction pathway at high temperatures and moderately high pressures, and could potentially be applied to the catalytic synthesis of chain end functionalized polyolefins. Furthermore, a preliminary experiment showed that this reactivity is observed also in ethene homopolymerization, proving the generality of the process.

Polymerization and computational screening allowed to highlight interesting trends in polymer microstructure and draw tentative mechanistic conclusions. We started by tuning the phosphinimide catalysts by modifying the R-substituents on phosphorus and replacing Cp* with Cp ligands. Trends in MW and % Terminal 2,1 units (empirical parameter to estimate the competition between chain propagation and termination after 2,1-insertion) follow that in steric hindrance of the ancillary ligands, with bulky groups favoring chain

termination, as expected based on steric effects on the Ti-C BDE. Indeed, a quite nice correlation between the experimental number of regioerror per chain and the $\Delta\Delta G^{\ddagger}_{(Hom.\text{-}INS,\ Ti\text{-}iPr)}$ estimated by DFT was found.

Sizable amounts of benzyl chain ends are obtained with all the phosphinimide catalyst studied, and they correlate with the calculated insertion barriers of propene insertion in the Ti(IV)-Bn bond and especially $\Delta\Delta G^{\ddagger}_{(Hom.\text{-}INS,\ Ti\text{-}Bn)}$. These preliminary conclusions indicate that the extent of solvent incorporation in the polypropylene chain for different catalysts under analogous reaction conditions is mostly dependent on the ease of chain reinitiation rather than Ti-polymeryl homolysis.

Exploration of cocatalyst effects for the representative case study **10'** indicates that catalyst activity, MW capability and regioselectivity are barely affected by the nature of the counterion. Interestingly, only chain end composition varies going from MAO/BHT to borane and borate activators. The former observation points to rather weak interactions between the cationic Ti-complex and the counterion (*i.e.* the reactivity of the active species is not influenced by the nature of the cocatalyst), while the latter clearly indicates that the amount of benzylated chains follows the trend $B(C_6F_5)_3$/TiBA/BHT (n.d.) < TTB/TiBA/BHT (4%) < MAO/BHT (22%). These effects can be hardly rationalized under the assumption of chain transfer to solvent occurring *via* SBM, since the aforementioned negligible effect of the counterion should be reflected by a constant percentage of solvent incorporation as well. Conversely, according to our mechanistic proposal, formation of benzylated chains also depend on factors other than the reactivity of the active species itself, such as the probability of radical recombination. For instance, this can be influenced by the nature and the concentration of cocatalyst, especially if it includes a radical stabilizer like BHT.

Supporting evidence for this mechanistic hypothesis are provided. Firstly, in the presence of the same $[MeB(C_6F_5)_3]^-$ counterion, **10'** is found give no or 10% benzylated chains depending on whether $B(C_6F_5)_3$ activator is used in combination with TiBA/BHT (Al/Ti 25:1, Al^iBu_3/BHT 1:1) or MAO/BHT (Al/Ti 400:1, $AlMe_3$/BHT 1:2), respectively. Secondly, the amount of benzyl chain ends is affected by the variation of $AlMe_3$/BHT, pointing to the phenol being somehow involved in the mechanism. Anyways, a fully consistent interpretation of the role of catalyst is complex and it has not been found, yet.

Attempts to incorporate the toluene solvent also with other typical Ti-catalysts and to explore the scope of this reaction as a potentially chain end functionalization tool were unsuccessful. In both cases, however, we believe that the radical reactivity leading to chain transfer to solvent is not necessarily ceased, but simply competing processes hamper chain reinitiation. For instance, in the case of **Cp_2TiCl_2**, we propose that the ease of homolysis of Ti-Bn compared to insertion is responsible for the missing generation of benzyl chain ends.

In conclusion, the study provided interesting insight in this unprecedented reactivity of cationic Ti-complexes, but the molecular understanding of the process is still at its early stages. Nevertheless, it should be emphasized that, if the above explanation for benzyl chain ends formation is correct, this new reactivity represents an important step forward in the understating of several aspects related to olefin polymerization catalysis:

1) It emphasizes the importance of 2,1-insertions on catalyst stability, since they not only represent an inconvenience (*i.e.* regioerrors, often formation of dormant sites)[94] but also pose a significant 'stress test' for the catalyst;[226]
2) It is symptomatic of the weak metal-carbon bond obtained under polymerization conditions;

3) It demonstrates that homolysis and subsequent formation of Ti(III) species do not necessarily represent an irreversible catalyst deactivation pathway;
4) It represents an unprecedented synergy of Ti(IV) polymerization activity, Ti(IV)/Ti(III) oxidation state changes and purely organic radical chemistry;
5) It opens a potential new catalytic route to chain-end functionalized polyolefin.

On the one side, further studies should be oriented to fully elucidate the mechanism, by providing definitive proof for the radical route and demystifying the origin of the abnormal percentage of saturated chain ends. On the other side, increasing the amount of toluene incorporation and including heteroatom containing solvents might significantly broaden the potential applications of this reaction. Considering that benzyl chain end formation is observed both with ethene and propene, it would be interesting to explore it in copolymerization reactions. This might have direct connections with the commercial applications of phosphinimide catalysts, and possibly offer novel elements to explore the so-called 'comonomer effect'. In the next Chapter, we report NMR studies on the reactivity of **12'** with dried-MAO/BHT and, among other topics, some more mechanistic indications on chain transfer to solvent are discussed.

4.4 – Experimental Part

4.4.1 – Materials and methods

All manipulations of air-sensitive compounds were conducted under argon or nitrogen using Schlenk techniques and/or MBraun LabMaster 130 glove boxes. Chemicals reported in Table 4.19 were used as received, unless stated otherwise.

Table 4.19 - Chemicals used in this Chapter work.

Chemical	***Supplier***
tri-tert-butylphosphine (95%)	Acros Organics
triphenylphosphine (99%)	Sigma Aldrich
tricyclohexylphosphine (97%)	Sigma Aldrich
azidotrimethylsilane (97%)	Acros Organics
Cyclopentadienyl titanium trichloride	Stream Chemicals
Pentamethylcyclopentadienyl titanium trichloride	Stream Chemicals
Methylaluminoxane (MAO) 10 wt % in toluene	Chemtura
2,6-di-tert-butyl-4-methyl-phenol (BHT, ≥99.0%)	Sigma Aldrich
Propene*	Rivoira

* Purified by passing it through a mixed-bed activated-Cu/A4-molecular-sieves column

Toluene and heptane were purchased from Romil and purified by passing them through a mixed-bed activated-Cu/A4-molecular-sieves column in an MBraun SPS-5 unit (final concentration of O_2 and H_2O < 1 ppm). 4-fluotoluene (Alpha Aesar), mesitylene and ethylbenzene (Sigma Aldrich) were purified by passing them over activated silica, degassed and stored over 4Å molecular sieves. Deuterated solvents were purchased from Armar Chemicals, dried over CaH_2, distilled, freeze-pump-thaw degassed and stored over 4Å molecular

sieves. Precatalyst were prepared according to previously established protocols.[318, 320]

NMR measurements of organic and organometallic compounds were performed at 298 K using a Bruker DRX spectrometer (400 MHz for ^{1}H). ^{1}H NMR spectra were referenced to the residual protons of the deuterated solvent used (δ = 7.16, C_6D_6); ^{13}C NMR spectra were referenced internally to the D-coupled ^{13}C resonances of the NMR solvent (δ = 128.00, C_6D_6); ^{31}P NMR spectra were externally referenced to H_3PO_3. To describe the multiplicity of the signals, the following abbreviations are used: s, singlet; bs, broad singlet; d, doublet; bd, broad doublet; dd, double doublet; t, triplet; dt, double triplet; m, multiplet.

NMR polymers characterization was performed by using a Bruker Avance spectrometer (400 MHz for ^{1}H) equipped with a 5mm high temperature cryoprobe, operating on 50 mg mL^{-1} solutions in tetrachloroethane-1,2-d_2 at 393 K. The specific parameters for the measurements were as follows:

- ^{1}H NMR: 90° pulse; 2 s acquisition time; 10 s relaxation delay; 200 transients; 8.0 kHz spectral width; 32K time domain data points.
- ^{13}C NMR: 45° pulse; 2.3 s acquisition time; 5.0 s relaxation delay; 2-10K transients; 14 kHz spectral width; 64K time domain data points.

GPC experiments were carried out with a Freeslate Rapid GPC setup, equipped with a set of 2 mixed-bed Agilent PLgel 10 µm columns and a Polymer Char IR4 detector. The setup consists of a sample dissolution station for up to 48 samples in ~6 mL magnetically stirred glass vials. Pre-weighed polymer amounts (typically 2.5 to 5 mg) were dissolved in proper amounts of orthodichlorobenzene (ODCB) containing 0.40 g L^{-1} of 2,6-di-tert-butyl-4-methyl-phenol stabilizer, so as to obtain solutions at a concentration of 0.5 to 1.0 mg

mL^{-1}. After 4 h at 150°C under gentle stirring to ensure complete dissolution, the sample array was transferred to a thermostated bay at 145°C, and the samples were sequentially injected into the column line at 145°C and a flow rate of 1.0 ml min-1. In post-trigger delay operation mode, the analysis time is 12 min per sample. Calibration was carried out with the universal method using 10 monodisperse polystyrene samples (M_n between 1.3 and 3700 KDa).

4.4.2 – Synthetic procedures

Ligand precursors, **Lig(R)-TMS**. PR_3 phosphine (4 mmol) and N_3SiMe_3 (6 mmol) were added to a pressure tight Schlenk flask and stirred at 80°C for 4 hours. The rotaflo stopcock of the flask was opened at regular intervals to release N_2 pressure from the reaction environment. A colorless solution was initially obtained. The product precipitated as a white solid and the excess azide was removed under vacuum. Recrystallization from saturated toluene solution at -30°C afforded the pure product in high yields (80 to 96 %).

Lig(Ph)-TMS. ^{1}H NMR (400 MHz, C_6D_6): 7.74 (m, 6H, aromatic CH), 7.04 (m, 9H, aromatic CH), 0.38 (s, 9H, Si-CH_3) ppm. ^{31}P NMR (161 MHz, C_6D_6): -0.99 ppm.

Lig(Cy)-TMS. ^{1}H NMR (400 MHz, C_6D_6): 1.96-1.00 (m, 30H, C_6H_{10}), 0.44 (s, 9H, Si-CH_3) ppm. ^{31}P NMR (161 MHz, C_6D_6): 17.17 ppm.

Lig(^{t}Bu)-TMS. ^{1}H NMR (400 MHz, C_6D_6): 1.16 (d, $^{1H\text{-}31P}$J = 12.4 Hz, 27H, CCH_3), 0.41 (s, 9H, Si-CH_3) ppm. ^{31}P NMR (161 MHz, C_6D_6): 32.43 ppm.

Precatalysts, **10-12** and **10'-12'.** A solution of Cp or Cp*$TiCl_3$ (1mmol) in toluene (10 mL) was added dropwise to solid ligand precursor **Lig(R)-TMS** while stirring. The resulting mixture was stirred at 80°C for 16 hours. The completeness of the reaction was verified by ^{31}P NMR spectroscopy. After cooling down to room temperature, the solution was filtered thorough celite

and dried under vacuum. The resulting solid was redissolved in toluene and recrystallized at -30°C to obtain the pure product in high yields (45 to 80%).

10'. ^{1}H NMR (400 MHz, C_6D_6): 7.81 (m, 6H, aromatic CH), 7.01 (m, 9H, aromatic CH), 2.10 (s, 15H, Cp-CH_3) ppm. ^{13}C NMR (100 MHz, C_6D_6): 132.6 (d, JPC = 10.5 Hz, aromatic CH), 131.7 (d, JPC = 2.9, aromatic CH), 128.5 (d, JPC = 12.5 Hz, aromatic CH), 128.0 (quaternary C), 126.5 (quaternary C), 12.8 (Cp-CH_3). ^{31}P NMR (161 MHz, C_6D_6): 1.83 ppm.

11'. ^{1}H NMR (400 MHz, C_6D_6): 2.30 (s, 15H, Cp-CH_3), 2.04-1.00 (m, 30H, C_6H_{10}) ppm. ^{31}P NMR (161 MHz, C_6D_6): 26.2 ppm.

12'. ^{1}H NMR (400 MHz, C_6D_6): 2.20 (s, 15H, Cp-CH_3), 1.25 (d, 27H, CCH_3) ppm. ^{31}P NMR (161 MHz, C_6D_6): 45.1 ppm.

10. ^{1}H NMR (400 MHz, C_6D_6): 7.66 (m, 6H, Ph), 6.96 (m, 9H, Ph), 6.20 (s, 5H, Cp) ppm. ^{31}P NMR (161 MHz, C_6D_6): δ 2.17.

11. ^{1}H NMR (400 MHz, C_6D_6): 6.48 (s, 5H, C_5H_5), 1.91-0.90 (m, 30H, C_6H_{10}) ppm. ^{31}P NMR (161 MHz, C_6D_6): 28.5 ppm.

12. ^{1}H NMR (400 MHz, Tol-d_8): 6.46 (s, 5H, Cp), 1.12 (d, 27H, CCH_3) ppm. ^{31}P NMR (161 MHz, Tol-d_8): 45.0 ppm.

4.4.3 – Polymerization procedure

4.4.3.1 – Standard polymerizations in toluene

Propene homopolymerizations were carried out in a 300 mL magnetically stirred jacketed Pyrex reactor with three necks; one with a 15 mm SVL cap housing a silicone rubber septum; another with a 30 mm SVL cap; the last one with a two-way Rotaflo® tap connected to the Schlenk manifold and the propene cylinder. Operating under nitrogen, the reactor was charged with 200 mL of dry toluene, 6.0 mL of MAO commercial solution (or 0.1 mL of TiBA) and

an appropriate amount of 2,6-di-tert-butyl-4-methyl-phenol (BHT). The resulting solution was stirred gently at room temperature for 1 hour in order to allow the reaction between free-TMA and BHT.

The reactor was then thermostated at 110 °C and saturated with propene at the desired partial pressure while stirring vigorously. The appropriate amount of precatalyst (and borane or borate activator, if necessary) was dissolved in 1-2 mL of neat toluene and injected in the reactor to initiate the polymerization reaction. The reaction was then stopped by turning off the propene supply, venting the reactor and quenching with a 95:5 v/v methanol/HCl (aq, conc.) solution. The resulting polymer was coagulated with 300 mL of the same acidic solution, decanted and vacuum-dried at 50°C. Details of experimental conditions can be found in Table 4.3.

4.4.3.2 –Polymerizations in solvents other than toluene

Propene homopolymerizations in solvents different from toluene were carried out in a 150 mL magnetically stirred jacketed Pyrex reactor analogous to the one described in Section 4.3.3.1. At first, dried-MAO/BHT was prepared by adding the necessary amount of MAO to a 5-10 mL solution of BHT in toluene. After stirring for 1 hour, the solution was dried under vacuum to obtain a white solid.

The reactor was then charged with 50 mL of the desired solvent and dried-MAO/BHT. From this point on, the same polymerization procedure reported above was followed.

4.4.3.3 – Oligomerization with 12’

The same procedure described in Section 4.4.3.1 was followed, except for the quenching step. In order to avoid massive evaporation of the oligomeric products, the polymerization was stopped by turning off the propene supply, venting the reactor and bubbling air in the polymerization mixture, while condensing the vented vapors in a cold trap at -78°C.

The polymerization solution immediately turned purple. After cooling it down to room temperature, the liquid was filtered through alumina to remove the inorganic components and obtain a yellowish solution, which was concentrated under vacuum to about 4 mL. ^{1}H NMR of an aliquot of this solution showed that it mostly consisted of toluene solvent, which was let evaporate gently at room temperature for 24h. The resulting yellow liquid (100mg) was characterized by NMR.

Only traces of product could be found in the condensed vapors, which practically consisted of toluene.

Chapter 5

NMR study of activation and deactivation routes of Ti-catalysts in combination with $AlMe_3$-free MAO/BHT co-catalysts

5.1 - Introduction.

Activity in molecular olefin polymerization catalysis is not only determined by propagation barriers. Rather, productivity of a given catalyst is often dependent on the active fraction of metal centers *x** and the formation of 'dormant' or inactive species.[179-180, 324, 341-344] The choice of the cocatalyst is often crucial in determining the performances of a polymerization catalyst, as in the case of the unexpected reversible homolysis described in Chapter 4.

While insight in activation and deactivation chemistry can lead to significant improvements of catalyst performance, it is rather difficult to achieve. Methylaluminoxane is one of the most widely used cocatalyst in olefin polymerization;[158] demystifying its structure and properties represents one of the biggest challenges for molecular design and catalyst development. MAO can be used in combination with both dichloride or dialkyl precatalysts, since it can act as both alkylating and abstracting agent. It is generally accepted that abstraction can occur by a tricoordinated aluminum of oligomeric $(AlMeO)_n$,[345-348] although an alternative mechanism involving transfer of $AlMe_2^+$ (generated by interaction of TMA with MAO cages) has been proposed.[178, 322, 349-350] A large excess of MAO is usually needed to obtain the active alkyl cation quantitatively.[157, 164]

The chemistry of the TMA component of MAO is relatively easy to explore. Its molecular nature and the possibility to react pure commercial TMA with transition metal precatalysts have been widely exploited for structural characterization and mechanistic investigations, both experimentally[174, 176-178, 182, 350-352] and computationally.[105, 164, 176, 345, 347]

Activation experiments with oligomeric TMA-free MAO are much less common. Typically, in these cases TMA is *physically* removed by drying commercial MAO solutions under vacuum (b.p. Al_2Me_6: 125 °C),[353-355] but this procedure does not always lead to quantitative removal of TMA.[180, 182, 356]

Drying process and temperature variations can affect the structure of MAO as well, further illustrating the complexity of the system.[158, 346, 357-358] *Chemical* modification by addition of BHT has proven to be extremely effective in trapping TMA,[182, 193-194] but this approach has been rarely applied to NMR activation studies.[356]

In order to gain further insight in the reactivity of phosphinimide complexes, we explored the behavior of a prototypical dichloride precatalysts in presence of *dried*-MAO/BHT (dMAO/BHT). ^{31}P NMR represented a helpful spectroscopic handle to monitor the evolution of the system from progressive addition of cocatalyst to polymerization of a model α-olefin, namely 1-hexene. The results presented in here provide a general picture of the activation chemistry of the oligomeric fraction of MAO, separate from the widely debated role of free-TMA, and allows to draw tentative conclusions on the nature of its acidic sites. Comparison of dichloride to dimethyl, dibenzyl and diallyl species as well as DFT modelling (NMR chemical shifts and stability of activated species) allowed a tentative assignment of species observed upon activation. Connections with the mechanism of chain transfer to solvent described in Chapter 4 are proposed. A large part of the NMR experiments was carried out at the University of Perugia during two visits in the group of Prof. Alceo Macchioni and Prof. Cristiano Zuccaccia, who closely collaborated with us on this project.

5.2 – Results and Discussion.

The phosphinimide complex bearing Cp* and *tert*-butyl substituted phosphinimide ligand (**12'-X_2**) was selected as case study (Figure 5.1). This precatalyst is known to be especially suitable for activation studies, due to the stability of the corresponding cationic species.[331-332, 359-361] For instance, the group of Piers reported one of the first examples of stable Ti(IV) hydrides **12'-H^+**, by activating the dimethyl precursor **12'-Me_2** in presence of H_2.[331-332] The chemistry of **12'-H^+** in aromatic solvents has already been summarized in Section 4.1.2 and exemplifies the wide and complex reactivity of phosphinimide complexes. Precatalysts featuring different phosphine groups (*e.g.* PCy_3 or PPh_3) and especially Cp ancillary ligands lead to fast catalyst deactivation upon reaction with MAO or borate activators at room temperature, hampering accurate structural characterization.

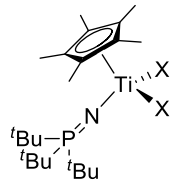

12'-X_2

X = Cl, Me, Bn, All

Figure 5.1 – Phosphinimide complexes studied.

Due to the high reactivity and poor solubility of catalytic ion pairs, NMR activation experiments are often carried out at quite low temperatures and in halogenated solvents.[173, 177-178] In our case, instead, we could easily work at 298 K or even higher temperatures; a low polarity solvent as toluene-d_8 was used, which is representative of those typically employed in polymerization catalysis.

In general, interpretation of ^1H and ^{13}C NMR spectra containing precatalyst and large amounts of MAO is made difficult by the intense and

broad peaks of aluminum compounds, especially at high Al to metal ratios. The presence of a large variety of resulting transition metal-species having similar chemical shifts and BHT adds further complexity (Figure 5.2). Phosphinimide Ti-catalysts represent a fortunate case in this respect, since the P atom of the ancillary ligand can be used as a convenient spectroscopic probe for speciation of the system, even at high Al/Ti ratios.

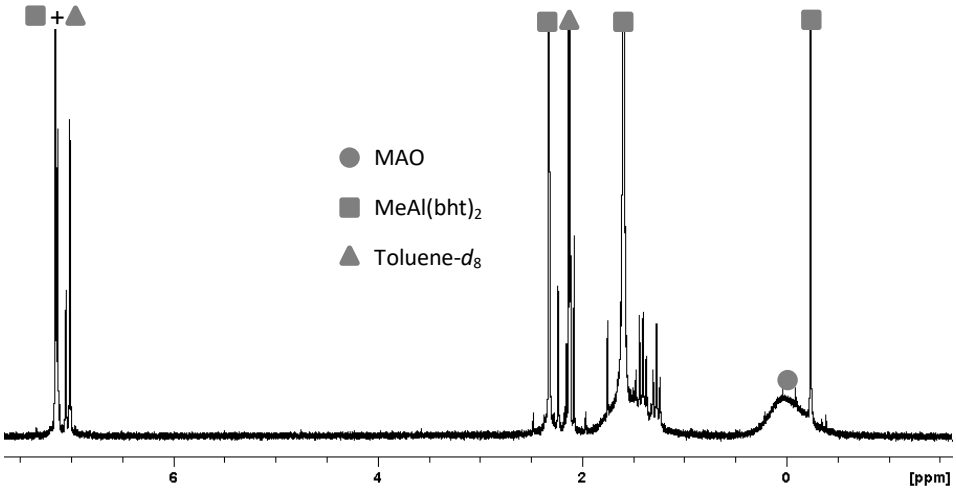

Figure 5.2 – Typical ^{1}H NMR spectrum obtained by reaction of **12'-Cl$_2$** with dMAO/BHT at Al/Ti ~40, showing the complexity of the spectrum in presence of large quantities of Al-based clusters and MeAl(bht)$_2$.

Identification of activation products was facilitated by comparison with model species, obtained by reacting the precatalyst **12'-X$_2$** with trityl borate activator ([Ph$_3$C][B(C$_6$F$_5$)$_4$], TTB). The use of TTB greatly simplifies the spectra, as it can be used in lower (stoichiometric) amounts and gives much sharper peaks than MAO. Moreover, its molecular nature allows a more selective synthesis of cationic products, allowing us to build a spectroscopic database that can be used for the speciation of complex reaction mixtures.

The employed computational protocol is analogous to the one described in Chapter 4. The GIAO method[362-365] at the TPSSTPSS level in combination with

basis sets optimized for this method (aug-cc-pVTZ-J basis set[366-370] for Ti and IGLO-III[371-372] for all other atoms) was used for ^{31}P NMR chemical shift predictions.

5.2.1 - Preparation and properties of *dried*-MAO/BHT (dMAO/BHT)

An MAO/BHT solution in toluene was prepared according to ref. 193 and subsequently dried under vacuum to remove the toluene solvent. This *dried*-MAO/BHT (dMAO/BHT, approximate formula $[(AlOMe)_x{\cdot}MeAl(bht)_2]_n$ with x~2) white powder was used as cocatalyst for NMR as well as for polymerization experiments with solvents different from toluene (see Section 4.2.2.4). BHT reacts preferentially with TMA, yielding monomeric Al-bis(phenolate) species, although modification of oligomeric MAO cannot be excluded.[356] It is known that addition of phenol tends to homogenize the behavior of different MAO solutions.[182]

The phenolate complex $MeAl(bht)_2$ is soluble in saturated hydrocarbons and can be selectively removed from MAO. It has to be noted here that $MeAl(bht)_2$ has been occasionally proposed as 'heuristically useful' molecular model to study methyl abstracting capabilities of oligomeric MAO, since it contains a tricoordinate aluminum bound to a methyl group and two oxygen atoms. However, it was observed that it is a far less efficient abstractor than MAO (and TMA), likely due to the steric hindrance of the di-*tert*-butyl phenolate ligands;[172] its contribution to the activation chemistry of dichloride complexes should be negligible.

5.2.2 – Activation of phosphinimide complexes.

Figure 5.3 shows a comparison of ^{31}P NMR spectra of **12'-Cl$_2$** /dMAO/BHT mixtures at increasing Al/Ti ratios and after addition of 1-hexene. Please note that Al/Ti ratios refer only to the oligomeric fraction $(AlOMe)_n$ contained in dMAO/BHT.

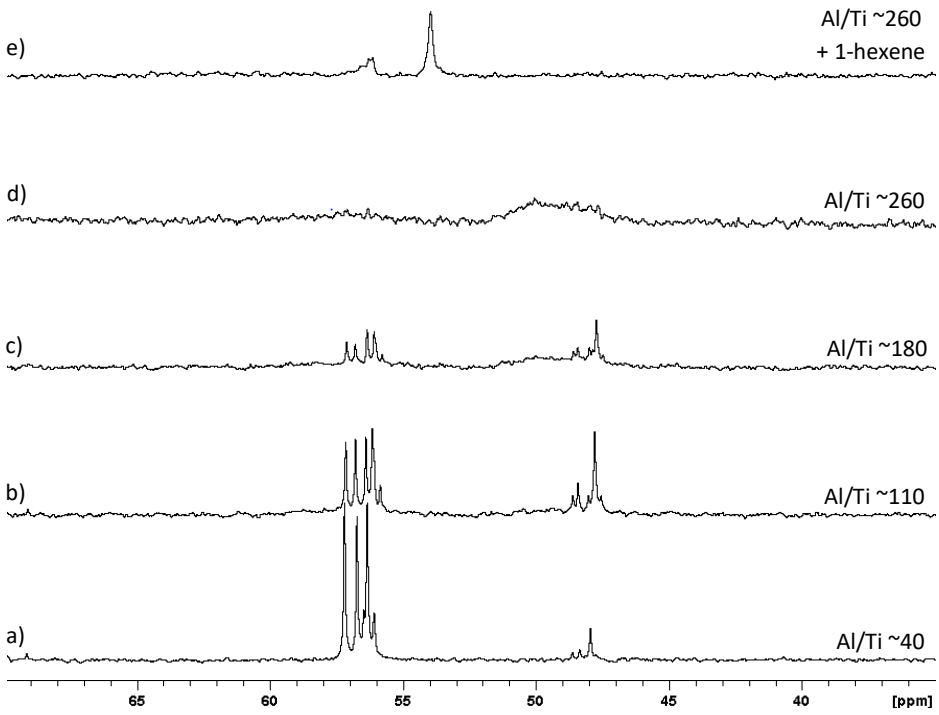

Figure 5.3 – Overall comparison between ^{31}P NMR (tol-d_8, 298 K) spectra of **12'-Cl$_2$** + dMAO/BHT reaction mixture at different Al/Ti ratios (298 K, toluene-d_8).

At low Al/Ti ratio (ca. 40, Figure 5.3a) two groups of peaks around 48 and 56 ppm are observed. While increasing the amount of dMAO/BHT, the peaks around 48 ppm increase at the expense of those at 56 ppm (Figure 5.3b), with a broad signal between 46.4 and 51.6 ppm becoming evident at Al/Ti ~180 (Figure 5.3c). Finally, only two broad peaks at 46.4-51.6 and 54.6-60.5 ppm are obtained at Al/Ti ~260 (Figure 5.3d). Interestingly, the addition of 1-hexene to

the NMR tube simplifies the spectrum, giving reasonably sharp signals at 54.0 and 57.2-55.5 ppm (Figure 5.3e). Speciation of the various reaction mixtures was made possible by extensive 1D and 2D NMR characterization, as well as by comparison with independently synthesized compounds and DFT modeling, as described below.

5.2.2.1 - Low Al/Ti ratios: partial alkylation and abstraction leading to homodinuclear adducts

Addition of MAO to the dichloride precursor **12'-Cl_2** initiates the activation process. At relatively low Al/Ti ratios the amount of MAO is not enough to quantitatively alkylate the precatalyst and convert it in the unsaturated active species, resulting in a mixture of neutral or cationic compounds bearing Ti-Cl and/or Ti-Me fragments.

In fact, at Al/Ti~40 (Figure 5.3a) we observe several chlorinated and partially methylated homodinuclear adducts of the type Cp*LTiCl-(μ-Cl)-TiClCp*L (**13-Cl_3^+**) and Cp*LTiMe-(μ-Cl)-TiClCp*L or Cp*LTiMe-(μ-Cl)-TiMeCp*L (**13-Me/Cl^+,** with L=NP^tBu_3), as described in Scheme 5.1. These dimeric compounds result from the stabilizing interaction between the neutral species (**12'-Cl_2**, **12'-Me_2** and **12'-ClMe)**, and the corresponding cationic complexes (**12'-Cl^+** and **12'-Me_2^+**) obtained after addition of cocatalyst.

Analogous homodinuclear species have already been reported for other catalyst classes activated with commercial MAO, but only as minor components. Heterodinuclear adducts with free TMA are generally much more stable (especially at high Al/Ti ratios)[173, 177, 350, 373-374] and can be found even when using dried MAO (*i.e.* physically removing TMA, without addition of BHT).[180, 356] Here, we do not observe any signal related to Ti-(μ-Me)-Al, proving the effectiveness of TMA removal by reaction with an hindered phenol.

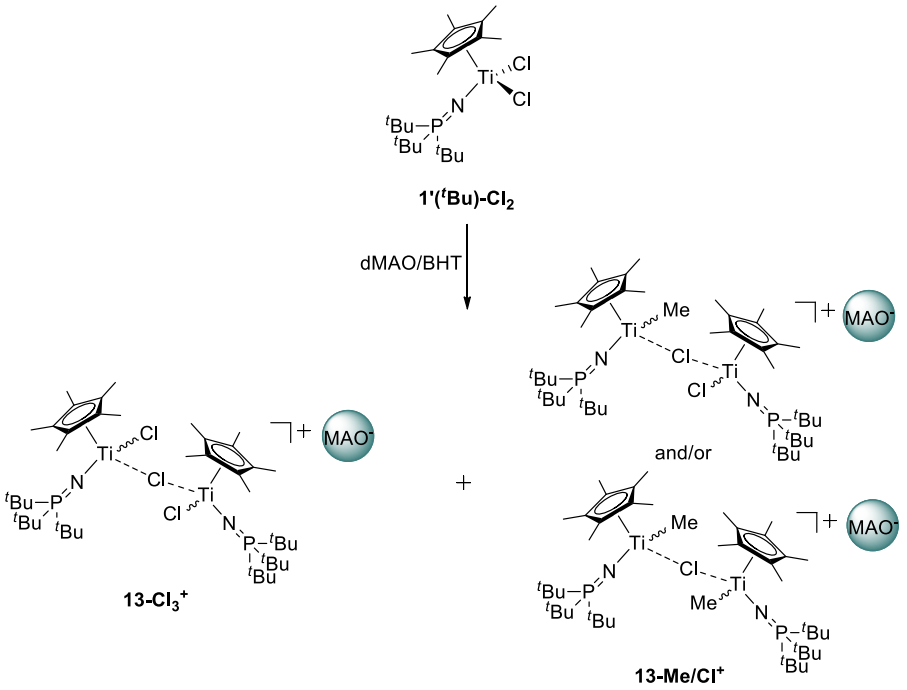

Scheme 5.1 – Major species obtained at low Al/Ti ratios.

This spectroscopic interpretation has been confirmed by comparison with the independently synthesized compounds with TTB. The fully methylated dimers **13-Me$_3^+$** can be easily prepared by reacting the dimethyl precursor **12'-Me$_2$** with only half an equivalent of TTB (Scheme 5.2a); chloride containing dimers **13-Cl$_3^+$** and **13-Me/Cl$^+$** can be prepared accordingly by reacting appropriate amounts of dimethyl and dichloride precursors with TTB, taking advantage of Ti-Me/Cl scrambling (Scheme 5.2b-c).

This strategy allowed detailed characterization of these well-defined species with borate counterion, which served to elucidate the composition of the more complex reaction mixtures obtained with dMAO/BHT. Comparison of ^{31}P NMR spectra of dimers obtained with TTB and dMAO/BHT (Al/Ti~40) is particularly illustrative in this respect (Figure 5.4). The major signals observed with dMAO/BHT around 56 ppm correspond to **13-Cl$_3^+$** species, while **13-Me/Cl$^+$**

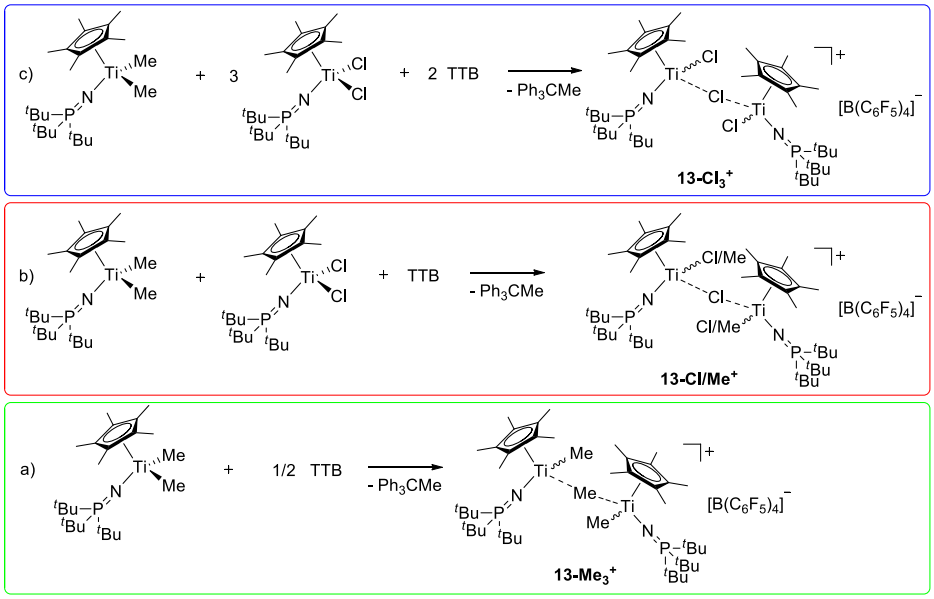

Scheme 5.2 – Synthesis of homodinuclear dimers by reaction with TTB.

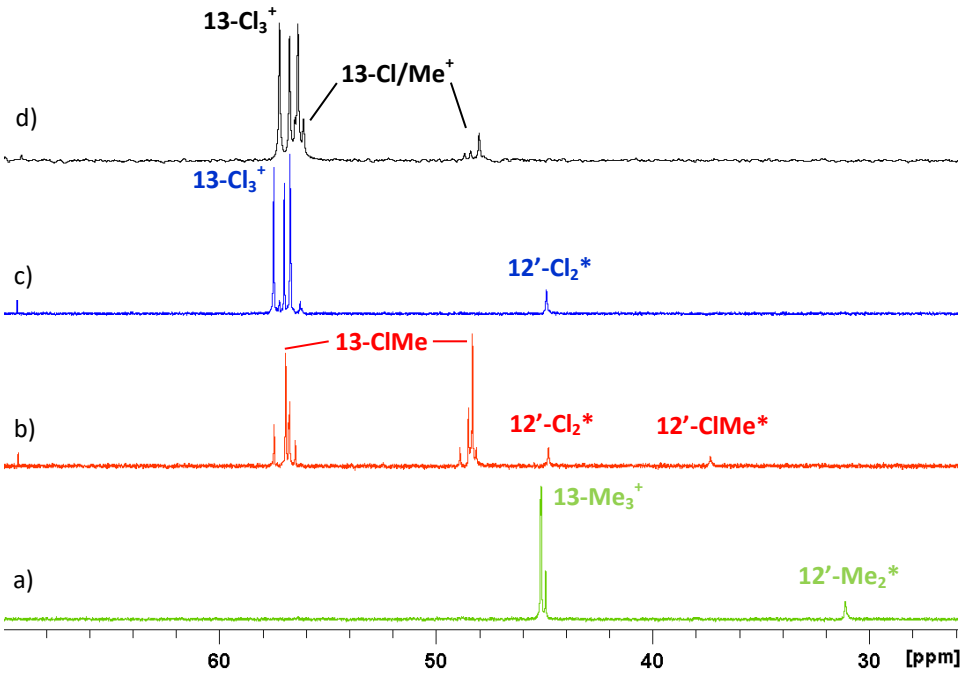

Figure 5.4 - Comparison between ^{31}P NMR (tol-d_8, 298 K) spectra of (a) **12'-Me$_2$ + ½·TTB,** (b) **12'-Cl$_2$** + **12'-Me$_2$** + **TTB,** (c) **12'-Me$_2$ + 3·12'-Cl$_2$ + 2·TTB** and (d) **I-Cl$_2$** + dMAO/BHT (Al/Ti ~40, see also Figure 5.3a) reaction mixture. See Scheme 5.2 for comparison. *Observed due to slight excess precursors with respect to TTB.

can be found at 48.0-48.7 ppm and as a second set of peaks coinciding with **13-Cl_3^+** around 56 ppm (as further confirmed by ^1H-^{31}P heterocorrelation experiments). No signals related to dichloride precursor **12'-Cl_2**, mono- or di-methylated neutral species **12'-ClMe** and **12'-Me_2**, nor fully methylated dimers **13-Me_3^+** are observed. Small differences in chemical shift are likely due to the different counterion (MAO^- *vs.* $B(C_6F_5)_4^-$). The minor species appearing at 69 ppm is still to be identified. ^1H and ^{13}C NMR characterization are in line with these conclusions; furthermore, ^1H and ^{13}C resonances for the bridging and terminal methyl groups are consistent with similar homodinuclear species based on *ansa*-cyclopentadienyl amido Ti-complexes reported in the literature under analogous conditions.[150]

The presence of multiple peaks for each type of dimer can be traced to the *rac* and *meso* diastereoisomers and (up to) four rotamers thereof, since rotation around the bridging group is sterically hindered by bulky Cp* and P^{t}Bu$_3$ groups.[359, 361] The relative stability of the various isomers was explored by DFT modeling and 2D NMR. The eight possible configurations are schematically reported in Figure 5.5; for each of those, the X-Z groups can be a methyl or a chloride group.

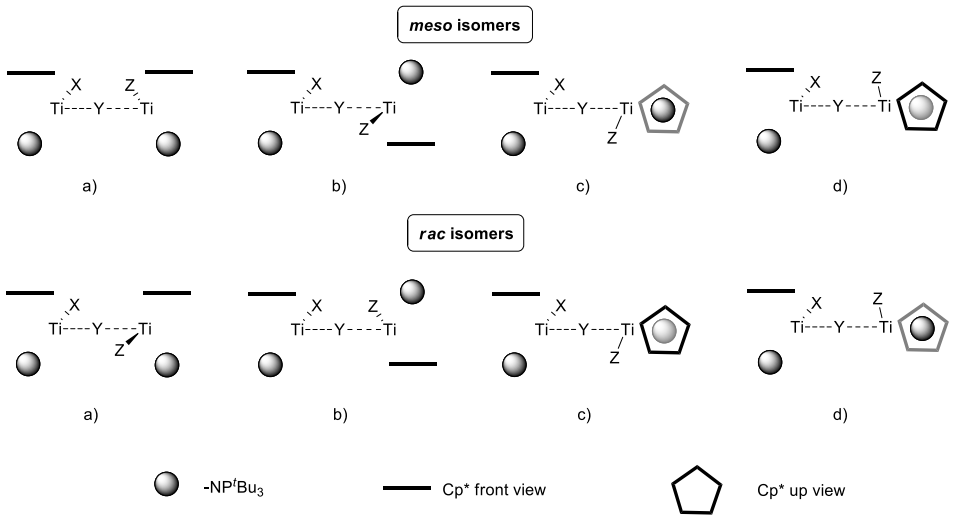

Figure 5.5 – Schematic representation of homobinuclear adducts isomers. X, Y, Z = Cl or Me.

Table 5.1 – Dissociation energies for **13** and comparison between calculated and predicted ^{31}P NMR chemical shift. Predicted δ are internally referred to **12'-Cl_2**.

Entry	Abbreviation	Isomer	X	Y	Z	Relative diss. Δ*G**	Calc. ^{31}P δ (ppm)	Exp. ^{31}P δ (ppm)	Δδ (ppm)
1	**P^{t}Bu$_3$**						65.1	62.3	2.8
2	**O=P^{t}Bu$_3$**						67.5	69.9	-2.4
3	**Me$_3$Si-NP^{t}Bu$_3$**						26.2	32.4	-6.2
4	**12'-Cl_2**						44.8	44.8	0.0[a]
5	**12'-Cl^+**						78.2	N.A.[b]	-
6	**12'-Me_2**						30.5	31.1	-0.6
7	**12'-Me^+**						55.6	55.7	-0.1
8	**12'-MeCl**						37.2	37.3	-0.1
9	**12'-All_2**						35.0	34.2	0.8
10	**12'-All^+**						63.5	55.1[c]	8.4[d]
11	**12'-Bn_2**						36.8	35.2	1.6
12	**12'-Bn^+**						58.7	55.2	3.5
13		**meso c/d**	**Cl**	**Cl**	**Cl**	**0.0**	**60.9; 62.3**	**56.7; 57.5**[e]	**4.2; 4.8**
14		rac c	Cl	Cl	Cl	0.1	61.0; 62.0 (61.5)[f]	57.0[e]	4.0; 5.0 (4.5)[f]
15	**13-Cl_3^+**	rac d	Cl	Cl	Cl	2.9	58.6; 57.6		
16		rac b	Cl	Cl	Cl	14.7	59.6; 59.9		
17		meso b	Cl	Cl	Cl	15.4	61.1; 62.6		
18		**meso c**	**Me**	**Cl**	**Cl**	**0.0**	**51.4; 61.1**		
19		rac c	Me	Cl	Cl	0.7	52.5; 60.0		
20		meso d	Cl	Cl	Me	1.8	52.1; 60.6		
23		rac d	Me	Cl	Cl	2.0	49.0; 59.3		
21		rac c	Cl	Me	Cl	6.0	54.4; 61.1		
22	**13-Me/Cl^+**	meso c/d	Cl	Me	Cl	6.1	53.3; 61.7	*56.4-57.4;*	
24		meso b1	Cl	Cl	Me	8.4	52.8; 59.5	*48.1-48.9*	
25		rac b	Me	Cl	Cl	10.9	52.6; 59.8		
26		meso b2	Me	Cl	Cl	12.0	52.4; 61.4		
27		meso b	Cl	Me	Cl	14.0	51.7; 61.4		
28		rac d	Cl	Me	Cl	14.2	56.3; 50.7		
29		rac b	Cl	Me	Cl	14.9	58.2; 51.2		
30		**meso c/d**	**Me**	**Cl**	**Me**	**0.0**	**51.2; 51.7**		
31		rac c	Me	Cl	Me	0.9	50.7; 51.2		
32	**13-Me/Cl^+**	rac d	Me	Cl	Me	1.1	48.9; 50.5	*56.4-57.4;*	
33		rac c	Me	Me	Cl	4.4	47.2; 54.2	*48.1-48.9*	
34		meso c	Me	Me	Cl	4.9	44.1; 51.7		

Table 5.1 (continued) – Dissociation energies for **13** and comparison between calculated and predicted ^{31}P NMR chemical shift. Predicted δ are internally referred to **12'-Cl$_2$**.

Entry	Abbreviation	Isomer	X	Y	Z	Relative diss. Δ*G**	Calc. ^{31}P δ (ppm)	Exp. ^{31}P δ (ppm)	Δδ (ppm)
35		meso d	Cl	Me	Me	5.7	45.7; 47.5		
36		meso b	Me	Cl	Me	6.8	51.2; 52.9		
37		meso b2[g]	Me	Me	Cl	7.2	50.8; 53.3	*56.4-57.4;*	
38	**13-Me/Cl$^+$**	rac d	Me	Me	Cl	8.3	50.8; 48.7	*48.1-48.9*	
39		meso b1[g]	Cl	Me	Me	8.8	50.3; 51.4		
40		rac b	Me	Cl	Me	9.2	52.4; 53.1		
41		rac b	Me	Me	Cl	16.1	52.9; 51.7		
42		**rac c**	**Me**	**Me**	**Me**	**0.0**	**44.4; 50.3** (47.3)[f]	**44.9**	**0.5; 5.4** (2.4)[f]
43		meso c/d	Me	Me	Me	0.7	44.4; 49.9	45.2; 45.1	0.7; 4.8
44	**13-Me$_3$$^+$**	meso b[g]	Me	Me	Me	4.8	42.9; 49.9		
45		rac d	Me	Me	Me	6.5	48.2; 43.2		
46		rac b	Me	Me	Me	11.5	45.7; 52.2		
								MAD	*2.8 ppm*
								(MAD considering averages)	*2.6 ppm*

Dimers 13 are grouped according to their chemical composition and ordered according to their relative stability. Most stable configuration for each group of dimers in **bold**, least stable ones in grey. Quantitative comparison between calculated and experimental NMR chemical shifts for **13** include only fully assigned dimers; experimental chemical shift ranges are provided in the other cases. [a]reference; [b]Not Available; [c]15 vol/vol % dichlorobenzene-d_8; [d]excluded from Mean Average Deviaton (MAD) since the optimized allyl conformation might not be the most stable one (see main text); [e]assuming analogous experimental distribution as for **13-Me**$^+$ (see main text); [f] considering the average between the two redicted chemical shifts for the symmetric isomer (see main text); [g]attempted optimization of *meso* **b** structures led to a configuration that closely resembles *meso* **c-d**. *Gibbs free energies difference in kcal/mol, calculated at the M06-2X(PCM)/TZ//RI-TPSSTPSS/DZ level.

According to DFT calculations, staggered isomers **c-d** (Figure 5.5) represent the most stable configurations for all the dimers. Attempts to optimize **a**-type rotamers failed, likely because this configuration maximizes the steric repulsion between ancillary ligands. Likewise, optimization of **b**-type species inevitably entails a small rotation around the bridging Y group, and in

some cases only a local minimum that closely resembles type **c** and **d** structures was found (Table 5.1, entries 37, 39, 44). Nevertheless, slightly staggered isomers obtained starting from of molecular arrangements of type **b** represent high energy configurations, generally being up to 12 kcal/mol less stable than **c** and **d** (Table 5.1). Thus, we mainly focused on staggered isomers **c**-**d**, and explored all the possible combinations for **13-Cl$_3$$^+$**, **13-Me/Cl$^+$** and **13-Me$_3$$^+$**.

In the simple cases of **13-Cl$_3$$^+$** (X=Y=Z=Cl) and **13-Me$_3$$^+$** (X=Y=Z=Me), *meso* rotamers **c** and **d** are enantiomers, while *rac* rotamers **c** are predicted to be 3 to 6 kcal/mol more stable than **d** (compare entries 14-15 and 42-45, Table 5.1). The difference in energy between the two predicted most stable diasteroisomers *meso* **c/d** and *rac* **c** is small and below 1 kcal/mol for both **13-Cl$_3$$^+$** and **13-Me$_3$$^+$**. However, there is a substantial difference between these species from a spectroscopic point of view: the chemical environment experienced by terminal X and Z groups in the *rac* isomers **c** is the same (*i.e.* X and Z are magnetically equivalent, as for *rac* **d**), while this is not the case for the *meso* analogues (X and Z are magnetically distinct).

Indeed, the spectroscopic region of the terminal methyl groups bound to Ti is especially diagnostic to determine adduct configurations experimentally. ROESY NMR experiments show that the reaction of dimethyl precursor **12'-Me$_2$** with low amounts of dMAO/BHT gives two similarly abundant major species **13-Me$_3$$^+$**, one *asymmetric* and one *symmetric* (Figure 5.6). In particular, the *asymmetric* dimer features a bridged μ-Me at -0.69 ppm and two non-equivalent 'terminal' Ti-Me fragments: the first Ti-Me (0.60 ppm) is spatially close to two P^{t}Bu$_3$ groups and one Cp*, while the second (0.71 ppm) is close to one P^{t}Bu$_3$ and two Cp*. Conversely, the *symmetric* species (μ-Me at -0.61 ppm) features two equivalent Ti-Me groups (0.61 ppm).

The corresponding NOESY experiment of **12'-Me$_2$** with ½ eq. of TTB shows an analogous cross-peak pattern with minor differences in chemical shift

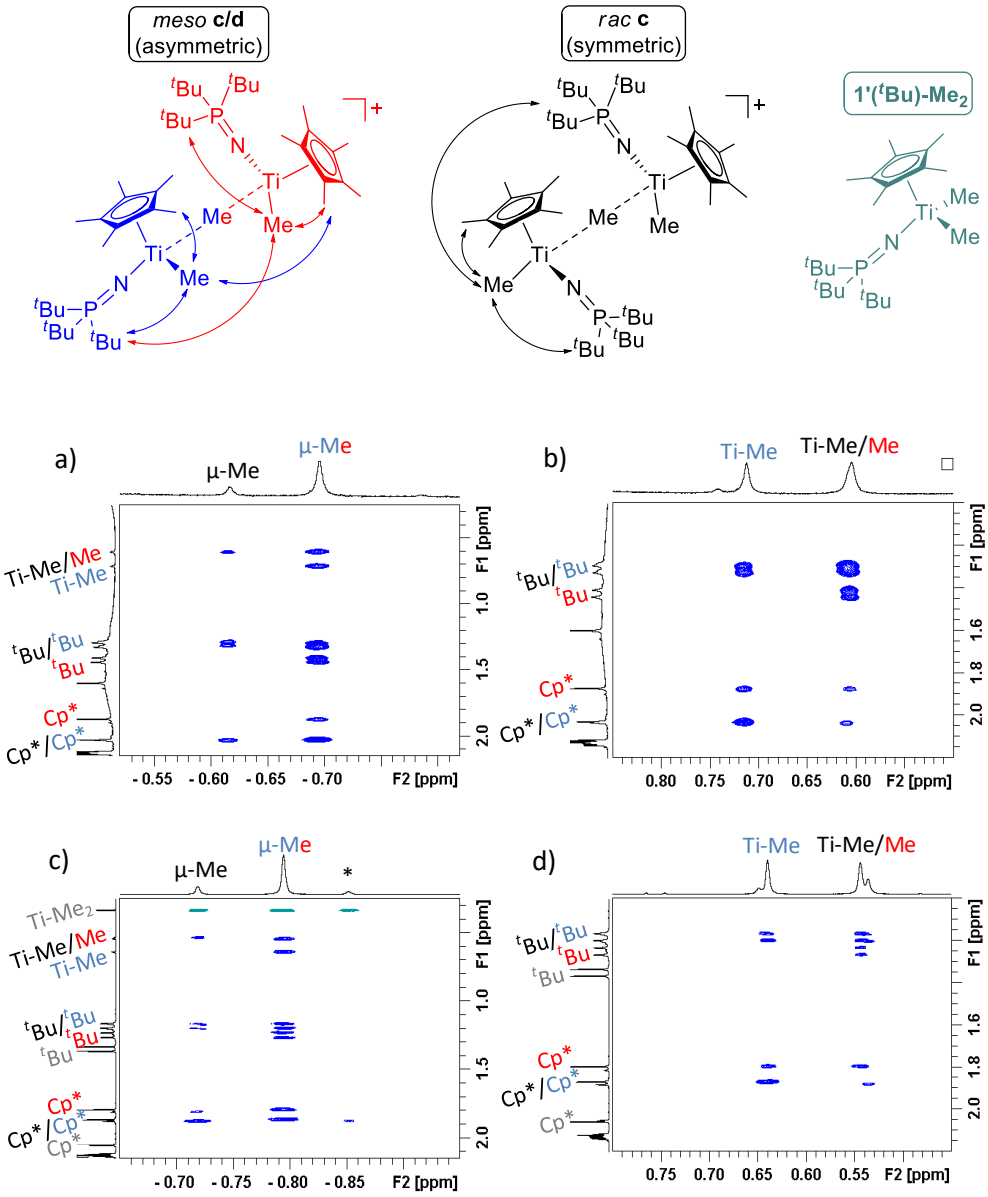

Figure 5.6 – Top: predicted most stable configuration for **13-Me$_3^+$** obtained starting from **12'-Me$_2$**; arrows highlight NOE contacts for terminal Ti-Me. Bottom: ROESY maps (tol-d_8, 298 K) showing relevant couplings for (a) μ-Me and (b) Ti-Me protons for **12'-Me$_2$** + dMAO/BHT reaction mixture and analogous NOESY maps for (c) μ-Me and (d) Ti-Me protons for **12'-Me$_2$** + ½ TTB. MeAl(bht)$_2$ was extracted with pentane to simplify the spectra. *Minor unidentified **13-Me$_3^+$** isomer.

(Figure 5.6c,d). Moreover, both μ-methyl groups appear to be in chemical exchange with excess **12'-Me$_2$** precursors (0.34 ppm), as expected. No exchange peaks are found between different **13-Me$_3^+$** isomers. It might be that the exchange rate between two **13-Me$_3^+$** dimers is lower than the abovementioned one between **13-Me$_3^+$** and excess **12'-Me$_2$**, and probably too low to be detectable on the NMR timescale.

Thus, the relative abundance of these two isomers and their NMR structural characterization are in line with the theoretical prediction of *meso* (asymmetric) and *rac* (symmetric) **c**-**d** configurations being the most stable for **13-Me$_3^+$**. In this case, *rac* isomers **c** and **d** cannot be distinguished experimentally since the signals of the two *tert*-butyl and Cp* groups may coincide, but DFT predicts the **c**-configuration to be preferred (Figure 5.7).

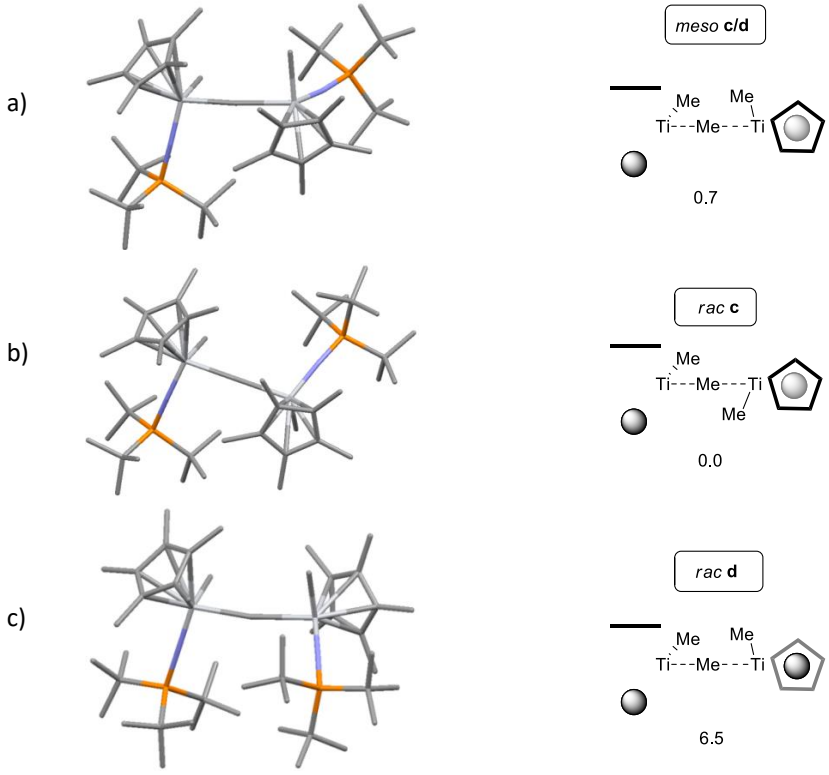

Figure 5.7 – Optimized geometries for the predicted most stable asymmetric (*meso*) and symmetric (*rac*) dimers **13-Me$_3^+$**. Hydrogen omitted for clarity. Numbers are relative dissociation Gibbs free energies in kcal/mol, calculated at the M06-2X(PCM)/TZ//RI-TPSSTPSS/DZ level.

Relative stabilities of analogous chloride containing dimers **13-Cl_3^+** and **13-Me/Cl^+** are predicted to be similar (Table 5.1), but it is more difficult to obtain clear experimental evidence in this case due to the absence of diagnostic methyl groups in **13-Cl_3^+** and the many possible Ti-Me/Cl combinations for **13-Me/Cl^+**. The pattern of ^{31}P NMR peaks observed for **13-Cl_3^+** and their relative integrals are in line with the hypothesis of a symmetric and asymmetric isomer being the most stable, as discussed for **13-Me_3^+**. No signals compatible with bridging μ-Me in chloride containing dimers can be found, in agreement with computational predictions (compare for instance entries 18-20 *vs.* 21-22 and 30-32 *vs.* 33-35 in Table 5.1) and previous observations.[173, 350] Regarding mixed adducts **13-Me/Cl^+,** in the case of different Ti-X and Ti-Z groups, both *meso* and *rac* structures **c** and **d** are non-equivalent. The difference between the two *meso* configurations is generally within 2 kcal/mol (entries 18 *vs.* 20 and 34 *vs.* 35, Table 5.1), while it is up to 4 kcal/mol for *rac* analogues (entries 19 *vs.* 23 and 33 *vs.* 38).

Experimental indication for a strong binding between the two subunits of the homodinuclear adducts was obtained by performing competing experiments with tris(pentafluorophenyl)borane as activator. The methyl borate $[MeB(C_6F_5)_3]^-$ counterion deriving from activation with $B(C_6F_5)_3$ interacts with the transition metal cation much more strongly than analogous $[B(C_6F_5)_4]^-$, typically yielding zwitterionic products of the type L_2TiMe-(μ-Me)-$B(C_6F_5)_3$. It has been shown that these zwitterionic species are more stable than homodinuclear adducts in the case of zirconocene catalysts.[339] Here instead, we observe that reaction of **12'-Me_2** with 0.5 eq. of borane preferentially gives the same type of dimers observed with TTB, further denoting their stability.

DFT prediction of NMR chemical shifts is generally in good agreement with experimental observations, further confirming our spectroscopic interpretation. All the relevant species were screened, including the neutral

precursors **12'-X_2** and their corresponding cations, as well as phosphinimide ligand precursor Me_3Si-NP^tBu_3 and associated species P^tBu_3 and $O{=}P^tBu_3$.

The first group of species in entries 1-12 (Table 5.1) includes ligand building blocks and well-defined monomeric species; agreement between theory and experiment is good, emphasizing the reliability of the DFT method. Relatively large deviations were only obtained for **12'-All$^+$**, where the correct orientation of the allyl group and its potential steric interaction with the Cp* ligand remains to be identified, and mixtures of deuterated solvents had to be used (*vide infra*).

In the case of homodinuclear adducts (entries 13-46), comparisons between predicted and observed chemical shift is more complicated due to the variety of species that can be obtained, especially for **13-Me/Cl**. Calculations are generally able to reproduce the effect of dimer formation and replacement of chlorides with methyls, occasionally overestimating the difference between two P atoms of the same adduct especially when Y = Me (Figure 5.5). For instance, in the case of the two expected most stable structures for **13-Me_3^+** (entries 42-43, Table 5.1) we can see that while one of the two predicted chemical shifts (44.4 ppm) is in good agreement with experiments, the other (50.3 and 49.9 ppm) is at slightly lower fields than DFT predicts. Interestingly, structural analysis of optimized geometries shows that in the case of **13-Me_3^+** (and generally of methyl bridged dimers) the μ-Me tends to be closer to one of the two Ti-centers of the adduct, while μ-Cl are generally symmetrically positioned between the metal atoms. It seems that DFT predicts a persisting charge separation between neutral dimethyl and cationic monomethyl subunits of μ-Me adducts, and a more equally distributed positive charge for μ-Cl dimers. Therefore, a plausible explanation for the larger deviations with **13-Me_3^+** might be a rapid exchange on the NMR timescale of the bridging methyl between the two Ti-centers that cannot be easily reproduced with static DFT

methodologies. Considering average values for the two phosphorus atoms of the symmetric *rac* **c** isomers for **13-Me$_3^+$** gives a deviation of 2.4 ppm, which is in line with the Mean Average Deviation (MAD) of 2.8 ppm (2.6 ppm when considering average values for **13-Me$_3^+$** and **13-Cl$_3^+$**). Despite this improvement, maximum deviations up to 6 ppm are probably too high for the method to be suitable for accurate predictive purposes, especially for species like **13**.

5.2.2.2 - Increasing Al/Ti ratios: alkylation and formation of ISIP with MAO

Further addition of MAO leads to progressive conversion of chlorinated **13-Cl$_3^+$** to partially methylated dimers **13-Me/Cl$^+$**. At the same time, a broad peak between 46.4 and 51.6 ppm appears at Al/Ti ~110 (Figure 5.8a) and grows further at Al/Ti ~180 (Figure 5.8b). Finally, at Al/Ti ~260 (Figure 5.8c) no sharp peaks can be seen anymore and only two broad signals are found at 46.4-51.6 (major) and 54.6-60.5 (minor) ppm. Corresponding ^{1}H NMR spectra confirm that all dimers have disappeared.

We ascribe these broad signals to the presence of Inner Sphere Ion Pairs (ISIP) between monomeric Ti-cations and MAO.[197] The broadness of the peaks is likely due to the heterogeneous nature of MAO that can interact with transition metal complexes *via* different sites on different $(AlOMe)_n$ clusters.[178]

Based on chemical shift considerations, the two broad peaks of Figure 5.8c are tentatively assigned to the ISIP formed with cations bearing Ti-Cl (54.6-60.5 ppm) or Ti-Me (46.4-51.6 ppm) fragments, as schematically shown in Figure 5.9. Corresponding reaction of dMAO/BHT with **12'-Me$_2$** gives a single broad peak at 46.4-51.6 ppm, in line with this interpretation. Ion pairs of the type **14-Me** appear to be more abundant than **14-Cl**. Although the incomplete conversion to **14-Me** at relatively high Al/Ti ratios points to dMAO/BHT being a

modest alkylator, our results further confirm that MAO is capable to alkylate and activate dichloride precatalysts quite effectively, even in absence of free trimethyl aluminum.[180, 193]

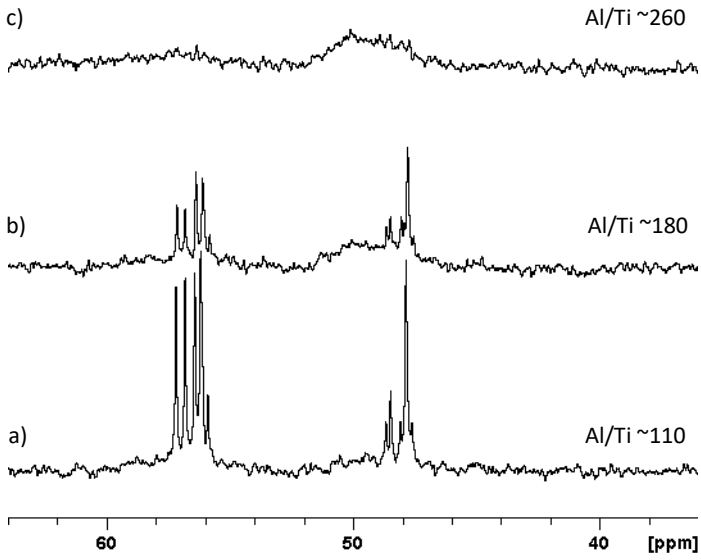

Figure 5.8 – Details of the ^{31}P NMR (tol-d_8, 298 K) spectra at Al/Ti ratios between 110 and 260. See also Figure 5.3c-e.

14-Cl
54.6-60.5 ppm

14-Me
46.4-51.6 ppm

Figure 5.9 – Schematic representation of inner sphere ion pairs between phosphinimide cationic complexes and MAO, and corresponding experimental ^{31}P NMR chemical shifts.

We also tried to computationally model **14-Me** and **14-Cl**. In order to do so, we chose the simplest feasible models reported in the literature to reproduce interaction of a cationic Ti-complex with tri-coordinated Al and bridged oxygen atom on MAO clusters,[163, 165, 348] which are shown in Figure 5.10 for the representative case of **14-Cl**. The interaction with an Al-center can occur *via* μ-Cl (Figure 5.10a) or μ-Me (Figure 5.10b). Oxygen bound ISIPs (Figure 5.10c) are predicted to be significantly more stable than the others (entries 1-2 *vs.* 3 and 4-5 *vs.* 6, Table 5.2), as also previously observed.[163, 165, 178, 345, 375]

Table 5.2 – Comparison of ion pairs **14** in terms of relative dissociation energies and of calculated *vs.* experimental chemical shifts (Figure 5.8). Predicted δ are internally referred to **12'-Cl_2** (see Table 5.1).

Entry	Abbreviation	Ti-*X*-MAO	Relative dissociation Δ*G* (kcal/mol)	Calculated ^{31}P δ (ppm)	Experimental ^{31}P δ (ppm)
1		**O**	0.0	44.1	
2	**14-Cl**	**Cl**	0.4	47.5	46.4-51.6
3		**Me**	13.9	47.2	
4		**O**	1.4	51.7	
5	**14-Me**	**Me**	0.1	54.3	54.6-60.5
6		**Cl**	14.6	54.2	

Gibbs free energies calculated at the M06-2X(PCM)/TZ//RI-TPSSTPSS/DZ level.

Our simplistic model is obviously not suitable for reproducing experimental shape of NMR peaks. Indeed, it is rather difficult to account for all the possible conformers with similar energies on different MAO clusters that are the presumed origin for such broadness.[165] However, data in Table 5.2 indicate that our model seems to capture the range of expected resonances for **14-Me** and **14-Cl** and the relative difference between them. Further considerations on the acidic sites on MAO can be found in the following sections.

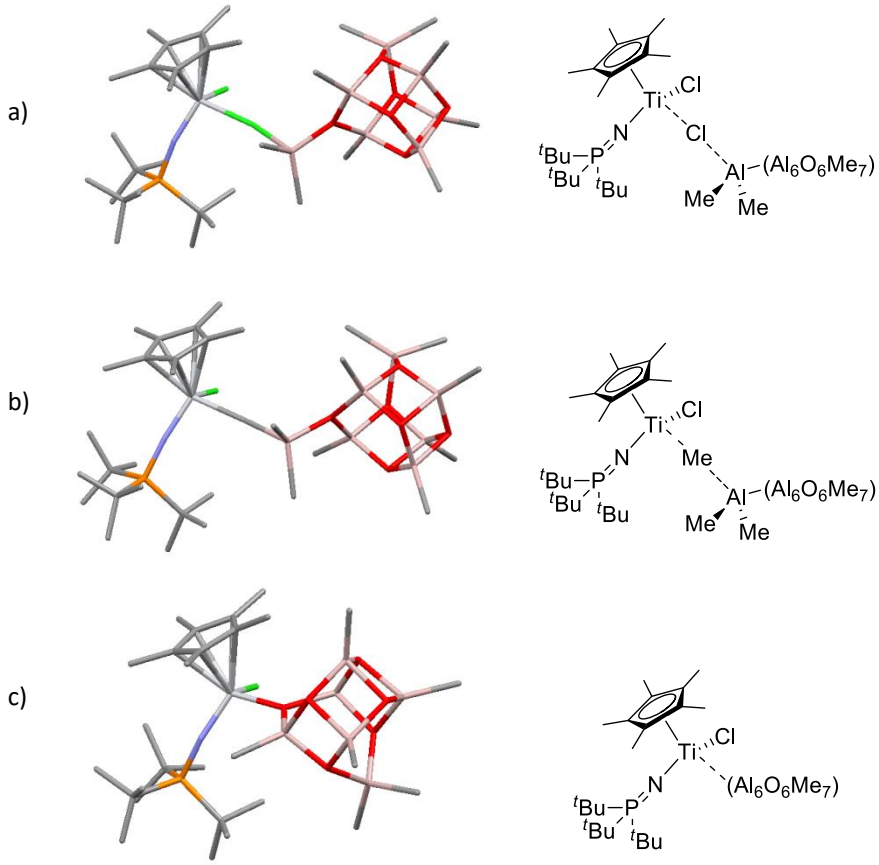

Figure 5.10 – DFT optimized model structures for **14-Cl** (RI-TPSSTPSS/DZ level). Hydrogen atoms omitted for clarity. Analogous structures for **14-Me** were optimized as well, see Table 5.2 for details.

5.2.2.3 - Polymerization of 1-hexene

After addition of 1-hexene to the activated cations **14**, the broad peaks disappear and sharper signals are obtained at 54.0 and 55.5-57.2 ppm (Figure 5.11). This indicates that the monomer displaces the MAO anion from the active pocket to initiate the polymerization.[179, 345] It is interesting to emphasize that also **14-Cl** seems to vanish in the presence of monomer, even though it does not contain a Ti-C bond necessary to be polymerization active. This

suggests that the presence of monomer and the subsequent opening of the ISIP might favor further alkylation reactions with MAO.

Comparison with independent 1-hexene polymerization experiments by using different precursors (*e.g.* **12'-Me$_2$**) and different activators (TTB) gave substantially the same NMR peaks, suggesting that these species have lost the labile ligands (*i.e.* Me or Cl) of the starting complexes and have no direct interaction with the counterion. For instance, we can exclude that one of this peaks corresponds to the cationic chloride complex with coordinated olefin (deriving from **14-Cl**), since the same signals are obtained also when starting from non-chlorinated species. No noticeable changes could be seen after full monomer consumption and after further storing the NMR solutions up to 24h, suggesting that remarkably stable compounds were formed.

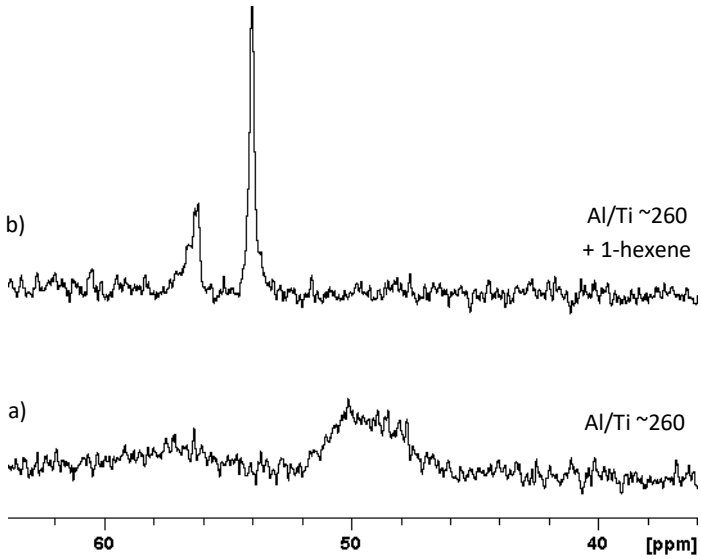

Figure 5.11 – Comparison between ^{31}P NMR (tol-d_8, 298 K) spectra at Al/Ti ~260 before (a) and after (b) addition of 1-hexene. See also Figure 2d,e.

Regarding the identification of these (at least two) species, a few possibilities can be envisaged:

A. the active cation(s) bearing a growing polymeryl;
B. decomposition products deriving from *intermolecular* reactions;
C. decomposition products deriving from *intramolecular* reactions;
D. dormant species obtained under polymerization conditions.

Concerning option (A), it might be that the two peaks correspond to agostic reactive intermediates bearing primary and secondary Ti-polymeryls. Unfortunately, this hypothesis is quite difficult to prove, since the broad and intense ^{1}H NMR peaks of hexene polymers and Ti-polymeryls hamper a detailed structural characterization. The synthesis of model cationic compounds is non-trivial, and it might *not* be of help anyways. For instance, a comparison of ^{31}P NMR resonances would not be conclusive, since all these species have very similar chemical shifts in the typical region of alkyl cations (see also Table 5.1).

Possibility (B) refers to the decomposition of alkyl complexes. For instance, impurities contained in 1-hexene might cause *intermolecular* side reactions with the highly reactive cationic species in the polymerization mixture. The monomer has been carefully dried and purified by distillation, and NMR experiments using different sources of hexene give comparable results. Therefore, even if we cannot rule it out, we believe that this possibility is quite unlikely.

Alternatively, side reactions might also occur *intramolecularly* (C). An example of typical *intramolecular* processes is the formation of metallacycles *via* C-H activation of the Cp-ancillary ligand; although this is more typical of Cp ligands featuring longer alkyl substituents (e.g. C_2[148] or C_3[149, 376]), some examples of Cp-Me activation has been reported.[150] On the one hand, it should be noted that this kind of decomposition reactions is generally favored for Ti-Me rather than longer Ti-alkyl complexes, but none of the species of Figure 5.11b was observed in **14-Me** solutions. On the other hand, stabilizing interactions with the counterion might make **14-Me** less reactive than the corresponding

polymeryl complex; the former gives a quite stable ISIP with MAO, which might become an OSIP in the latter case, due to the bulkier alkyl fragment. Indeed, the analogous Ti-Me complex **12'-Me$^+$** obtained with TTB activator clearly gives an OSIP with the borate anion, and visibly decomposes when stored for a few hours in toluene-d_8 at 298 K; this suggests that the different tightness of the ion pair can be an important factor determining the stability of the alkyl species. No clear indication could be found on whether the decomposition products of **12'-Me$^+$** are comparable to those of Figure 5.11b. However, while addition of hexene to **14-Me** immediately leads to the formation of the observed peaks, the decomposition rate of **12'-Me$^+$** is much lower.

Intramolecular reactions can also lead to dormant rather than inactive species in polymerization (D). A largely debated side reaction is the formation of dormant allyl species *via* β-H transfer to the metal and subsequent C-H activation of the resulting olefin ligand.[377-383] In order to verify this hypothesis, we prepared the diallyl complexes **12'-All$_2$**, a moderately light and temperature sensitive solid. This species exhibits only two signals for the coordinated allyl (quintet at 6.33 ppm and doublet 3.24 ppm in ^{1}H NMR) that is indicative of fluxional behavior, analogously to the corresponding Zr-complex.[190] When it is reacted with 1 eq of TTB, the symmetry of the allyl ligand is lost and the signals of the Cp* broadened, probably indicating hindered rotation of cyclopentadienyl ring due to the formation of relatively tight ion pairs. Only ^{1}H NMR spectrum of the ion pair could be rapidly recorded in toluene-d_8, before most of the product precipitated as a dark oil. Addition of ca. 15 vol/vol % of dichlorobenzene-d_4 allows detailed characterization of the cationic allyl complex but complicates direct comparison with the other experiments. The ^{1}H NMR allyl signals in **12'-All$^+$** appear between 5.6 and 3.2 ppm, *i.e.* in a relative clean region of the spectrum also in the presence of 1-hexene, and therefore they served to prove that no detectable traces of allyl cation are found in

reaction mixture of Figure 5.11b. Moreover, reaction of **12'-All$_2$** with only 20 eq of dMAO/BHT already leads to fast decomposition of the allyl complexes and only traces of monoallyl cation. This suggests that allyl species of phosphinimide titanium complexes are unstable in presence of MAO.

Also secondary monomer insertion has often been associated with the formation of dormant sites,[94, 384] but we have shown in Chapter 4 that this does not seem to apply to phosphinimide catalysts. Rather, secondary alkyls are characterized by very weak Ti-C bonds, potentially leading to solvent activation *via* homolytic cleavage. Although this reactivity seems to be particularly evident at higher temperatures, it might be possible that chain transfer to solvent occurs also at 298 K. Insertion barrier in the resulting Ti-Bn bond is predicted to be higher than in Ti-^{i}Pr (Figure 5.12), possibly enough to make **12'-Bn^{+}** a dormant species on the polymerization timescale at 298 K, but not enough to

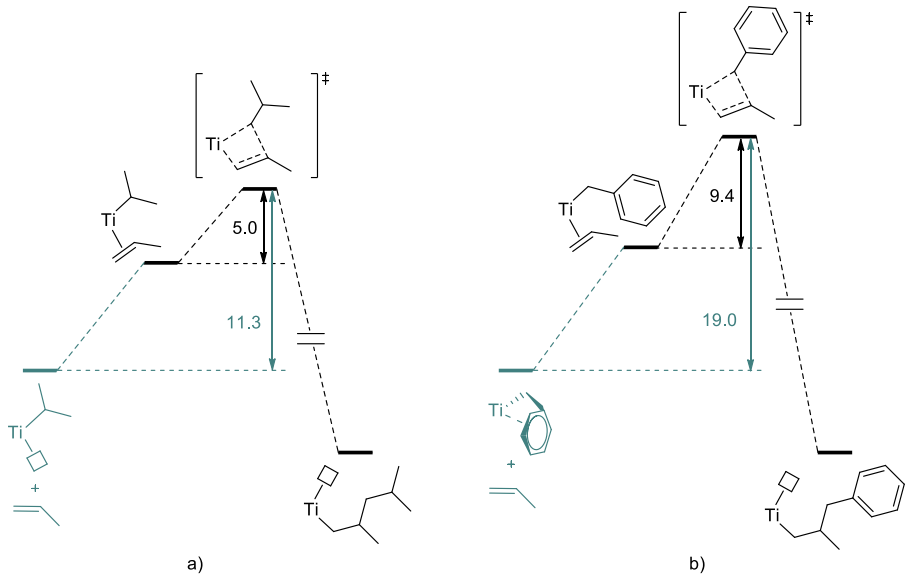

Figure 5.12 – Calculated insertion barriers of propene insertion in (a) Ti-iPr and (b) Ti-Bn at 298 K, $\Delta G^{‡}$ in kcal/mol, calculated at the M06-2X(PCM)/TZ//RI-TPSSTPSS/DZ level. η^2-coordinated benzyl is considered for **12'Bn^{+}** (see main text).

justify its NMR observation in presence of 1-hexene. Formation of benzyl chain ends in the polymer at 383 K (Chapter 4) clearly shows that **12'-Bn$^+$** must be polymerization active, at least at high temperature. Nonetheless, were interested in exploring the chemistry of benzyl complexes, also to get insight in the formation of benzyl terminated polymers, as more extensively discussed in the following sections.

5.2.3 – The chemistry of cationic Ti-benzyl complex

The benzyl cation **12'-Bn$^+$** was first prepared by reaction of the dibenzyl precursor **12'-Bn$_2$** and 1 eq. of TTB activator. The resulting ion pair is poorly soluble in aromatic solvents like benzene-d_6 and toluene-d_8, and tends to precipitate as a dark oil in the NMR tube. For this reason, the oil was separated from the supernatant and redissolved in chlorobenzene-d_5 to allow full characterization of reasonably pure **12'-Bn$^+$**.

The benzylic CH_2 appears as a singlet at 3.65 ppm in the ^{1}H and at 82.0 ppm in the ^{13}C spectrum in C_6D_5Cl. Figure 5.13 reports a selection of NOESY crosspeaks, clearly showing the spatial proximity of the CH_2 to the *tert*-butylphosphinimide and cyclopentadienyl ancillary ligands, as well as to the ortho-H of the phenyl group. ^{1}H-^{13}C heterocorrelation experiments are in line with this interpretation. Thanks to this detailed characterization, it was possible to identify the corresponding resonances in diluted C_6D_6 solutions, which served for comparison with other experiments.

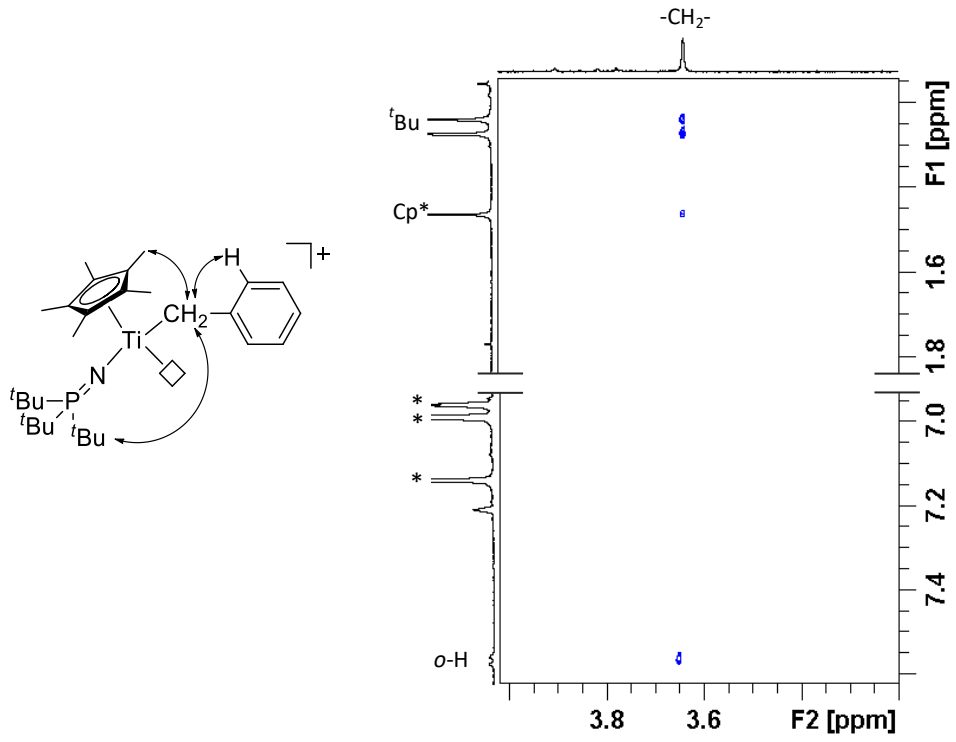

Figure 5.13 – NOESY maps (C_6D_5Cl, 298 K) of **12'-Bn$^+$** obtained from **12'-Bn$_2$** + TTB. * solvent peaks. Arrows highlight NOE contacts.

It is known that η^2-coordination of the benzyl ligand stabilizes the cation and it is often preferred over the η^1-binding mode.[177, 385] Our DFT calculations confirm that the former is expected to be ~14 kcal/mol more stable than the latter in the case of naked **12'-Bn$^+$**; explicit modeling of coordinated benzene and chlorobenzene solvent molecules reduces this preference to about 12 and 5 kcal/mol respectively (Figure 5.14). Typically, η^2-coordination reduces the mobility of the benzyl ligand and generates two distereotopic benzylic CH.[177, 385] In our case, the CH_2 appears as a singlet in the ^{1}H NMR spectrum, which might indicate η^1-coordination or a rapid equilibrium on the NMR time scale between two η^2-configurations.

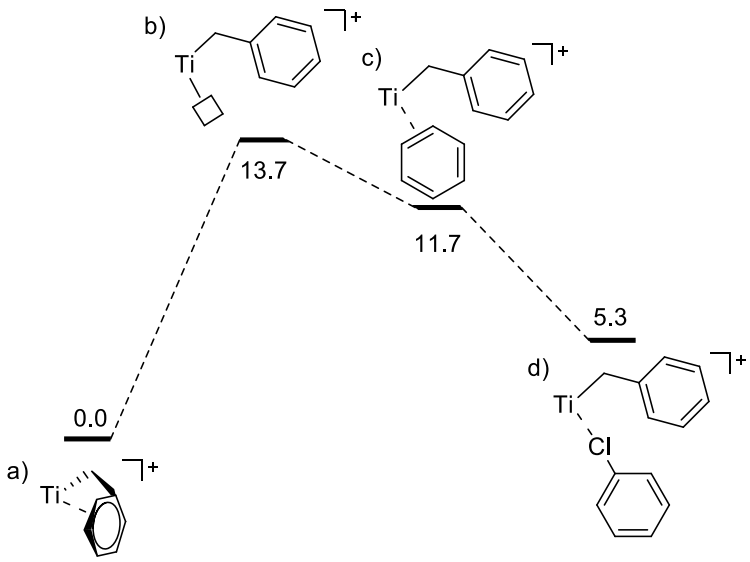

Figure 5.14 – Relative stability of (a) naked η^2-coordinated benzyl cation, (b) naked η^1-benzyl cation and corresponding structures with explicitly modeled (c) benzene and (d) chlorobenzene coordinated solvent molecule. Numbers are relative Δ*G* in kcal/mol, calculated at the M06-2X(PCM)/TZ//RI-TPSSTPSS/DZ level.

5.2.3.1 – Cationic Ti-benzyl complex, dormant or active species?

Once full assignments of NMR signals had been accomplished, we tried to verify if **12'-Bn$^+$** represents an active species under the aforementioned polymerization conditions. Progressive addition of dMAO/BHT to **12'-Bn$_2$** in toluene-d_8 showed that no dimer nor ISIP with MAO are formed in this case, as only sharp peaks corresponding to the precatalysts and the final cationic species are observed (Figure 5.15). This further supports the hypothesis of η^2-coordination of the benzyl ligand stabilizing the monomeric cation.

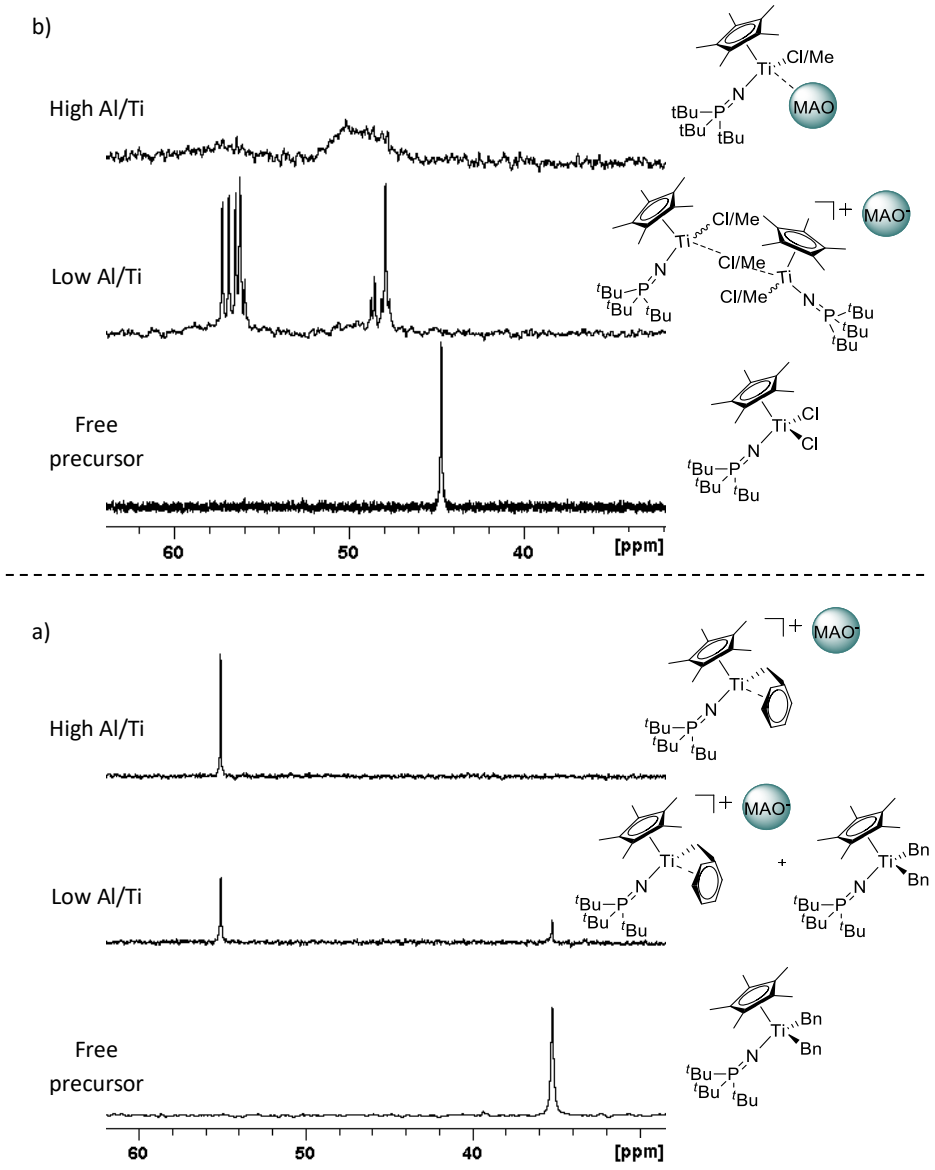

Figure 5.15 – Qualitative comparison between ^{31}P NMR (tol-d_8, 298 K) spectra of activation of (a) dibenzyl and (b) dichloride precursors with dMAO/BHT.

Addition of 1-hexene to the fully activated benzyl cation leads to the disappearance of the ^{31}P benzyl signal at 54.4 ppm, and the typical two peaks around 55.7 and 53.5 ppm are observed (Figure 5.16). This clearly demonstrate that **12'-Bn$^+$** is catalytically active under our conditions, as expected. Insertion in

the Ti-Bn bond appears to be easy, as **12'-Bn**$^+$ is completely consumed by the time the first spectrum is recorded after hexene addition. No quantitative considerations on the comparison with other Ti-alkyl species can be made at this stage.

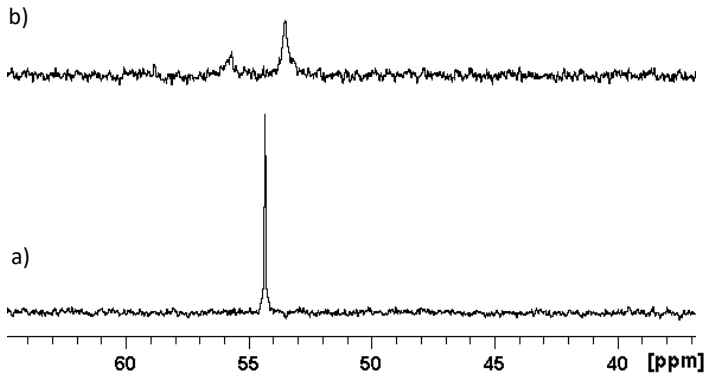

Figure 5.16 - Comparison between ^{31}P NMR (tol-d_8, 298 K) spectra of **12'-Bn$_2$** + dMAO/BHT (a) before and (b) after addition of 1-hexene.

5.2.3.2 – Connections with the chain transfer to solvent mechanism

The above results demonstrate that **12'-Bn**$^+$ does not accumulate during polymerization, but it still interesting to verify if this species can be formed by solvent activation under our conditions. The ^{31}P signal of **12'-Bn**$^+$ shift is quite similar to other alkyl cations such as **12'-Me**$^+$ (55.6 ppm in toluene-d_8 with borate counterion) and therefore it is not diagnostic enough to prove unequivocally the presence of benzyl cations in complex reaction mixtures. Rather, the ^{1}H NMR signal of the benzylic CH_2 would be particularly symptomatic, but activation of the toluene-d_8 solvent would lead to a deuterated benzyl group that cannot be detected by ^{1}H NMR.

Thus, we designed two specific experiments aiming to prove the formation of **12'-Bn$^+$** starting from Ti-polymeryls. First, we performed a polymerization experiment (A) by reacting **12'-Me$_2$**, TTB and 1-hexene in neat toluene under analogous conditions to those described earlier for NMR experiments. After stirring the resulting mixture for ~15 min at 298 K, all the volatiles were removed under vacuum and the resulting solid residue redissolved in C_6D_6. HSQC and NOESY NMR experiments unambiguously demonstrated that a sizable amount of **12'-Bn$^+$** is formed. The ^{31}P NMR spectrum obtained in this attempt is reported in Figure 5.17; it highlights the presence of the new benzyl peak at 55.0 ppm along with the typical ones around 54 and 57 ppm. It should be noted here, that also two more peaks at 69.1 and 64.2 ppm were found after drying; they both correspond to unknown products, although the one at 69.1 ppm is typical of the reactivity of the methyl cation **12'-Me$^+$** and was likely formed before injection of monomer.

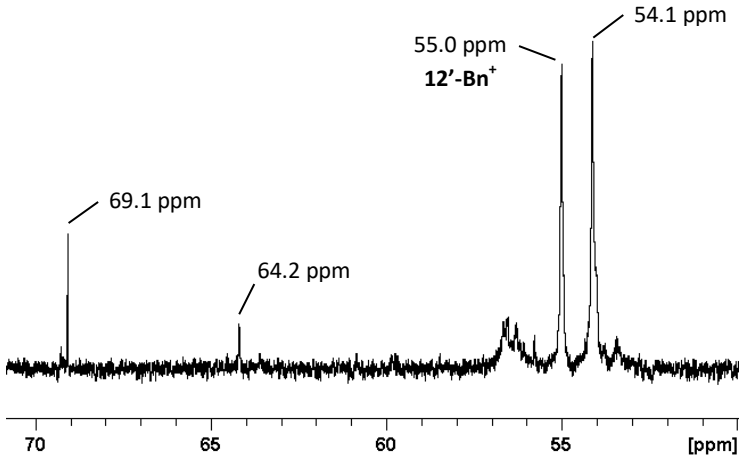

Figure 5.17 – ^{31}P NMR spectrum (298 K, C_6D_6) of **12'-Me$_2$** + TTB + 1-hexene in toluene, dried after ~15 min and redissolved in benzene-*d*$_6$ (Experiment A).

Analogously, a second experiment (B) was carried out by activating **12'-Me$_2$** with TTB in a ~6:1 vol/vol mixture of non-deuterated toluene and benzene-*d*$_6$, and then adding a small amount of 1-hexene. The reaction was monitored

by ^{1}H and ^{31}P NMR and no evidence for benzyl complex was observed. After full conversion of hexene we stored the solution for about 16h at room temperature, trying to verify if the cation alkyl complex slowly decomposes giving **12'-Bn^{+}**. In absence of free olefin, it should still be possible to obtain **12'-Bn^{+}** *via* Ti-C homolysis, benzylic CH activation and radical recombination, while chain reinitiation (*i.e.* **12'-Bn^{+}** consumption) is impossible with no available monomer. However, no notable changes in the solution and specifically no evidence for benzyl cation formation was detected, not even after gently warming up for a few minutes.

This somewhat contradictory results might suggest that benzyl formation in experiment (A) occurs as a consequence of the drying process, although no obvious explanation could be found. A possibility might be that the radical process is favored by the increase of concentration of Ti-species during solvent removal. It should be noted here that the sample was dried at temperature ≤303K, stored overnight under nitrogen and shielded from light before being redissolved in C_6D_6; traces of leftover toluene were detected by NMR.

In any case, this observation represents an important finding in the demystification of the chain transfer to solvent mechanism. Indeed, it might prove that **12'-Bn^{+}** is a reaction intermediate, yielding head- rather than tail-functionalized chains. Furthermore, although further studies would be necessary to prove the radical mechanism (*e.g.* identifying other key minor products such as bibenzyl), these results are in line with the hypothesis of homolysis being a potential decomposition route also at 298 K, although not as easy as at higher temperature.

5.2.3.3 - Chemical estimation of acidic sites on MAO clusters.

It is generally known that the number of strongly acidic sites on MAO clusters is limited, but it is hard to accurately quantify them.[159, 165, 180, 346] We have previously shown that reaction of **12'-Bn_2** with dMAO/BHT affords a single well-defined species **12'-Bn^+**, giving a sharp singlet at 54.4 ppm (Figure 5.15). This signal can be integrated more accurately than the broad one obtained for the analogous species **14-Me** forming ISIP with MAO, and we tried to exploit this feature to quantitatively monitor the activation of **12'-Bn_2** with dMAO/BHT. In this way, we obtained a rough estimation of the ratio between the number of acidic sites of $(AlOMe)_n$ that are capable to abstract a benzyl group and the overall number of Al centers. In particular, we estimate that oligomeric MAO in dMAO/BHT has one effective acidic site every ~60 Al atoms, if we neglect the contribution of $MeAl(bht)_2$.

In a recent combined experimental and computational paper, Stellbrink, Linnolahti and Bochmann have estimated the number of acidic Al centers per MAO cage to be in the range 30-60 atoms.[346] If we assume that after the first abstraction each cage becomes anionic and loses its abstracting power (*i.e.* no more than one 'working' acidic site per cage),[159, 165] and that the effect of BHT on acidic sites of oligomeric MAO is negligible, our measurements are in good agreement.

The higher Al/Ti ratios necessary in the case of **12'-Cl_2** (initial ISIP formation observed at Al/Ti~110, full conversion to ISIP between 180 and 260) are likely due the double alkylating/abstracting role carried out by MAO. Anyway, also in this case, our quantifications are comparable with other literature works on activation of dichlorides by 'TMA-depleted' MAO. For instance, UV-vis studies by Cramail and coworkers showed that unsaturated cations first appears around Al/Ti ~100 and that higher ratios of approximately 200 are needed for full activation.[180]

5.2.4 - Consequences of TMA removal on formation of dormant sites

Our results demonstrate that activation of **12'-Cl_2** with TMA-free MAO initially (Al/Ti = 40-110) produces homodinuclear rather than Ti/Al heterodinuclear adducts, while at higher Al/Ti (> 180) ISIP are formed rather than MAO-derived OSIP. Bryliakov and Bochmann suggested that the relative preference between OSIP and ISIP can also be a function of the steric hindrance of the ancillary ligand, since sterically open CGC preferentially interacts with the more stabilizing MAO even in presence of aluminum trimethyl.[350] However, this considerations likely do not apply to our case, since the bulkiness of Cp* and tri-*tert*-butyl phosphinimide ligand is quite pronounced.

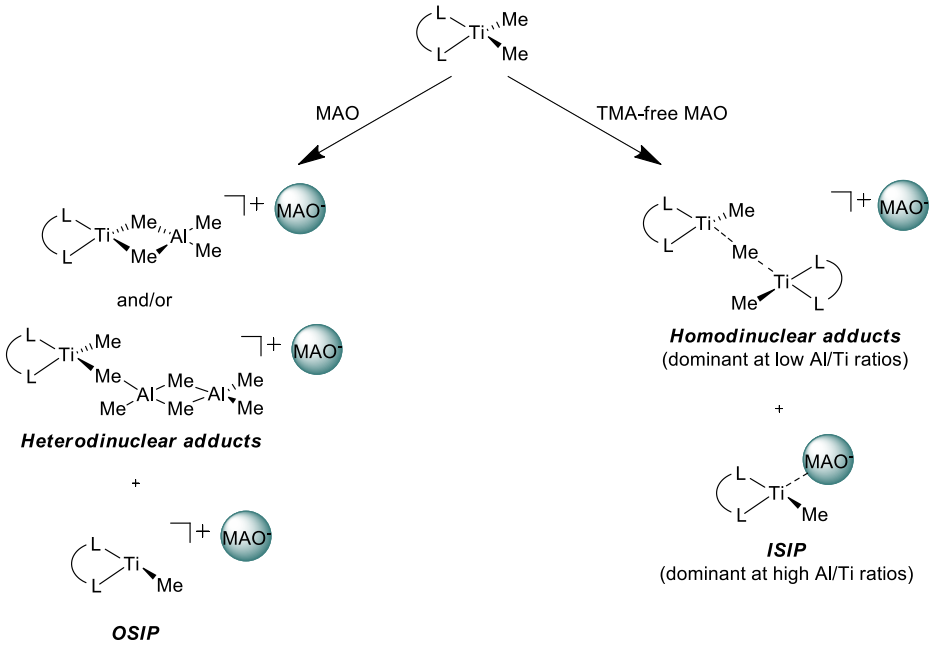

Scheme 5.3 – General representation of the major species obtained by reaction of dimethyl Ti-complexes with MAO in presence and absence of TMA.

Heterodinuclear adducts have often been proposed as some of the most common dormant species that can be obtained upon activation of group IV precatalysts with commercial MAO.[176, 179-180] Trapping TMA prevents their formation and, therefore, it is interesting to comment on its potential consequences on the active fraction of metal centers.

In principle, both homodinuclear dimers and ISIP with MAO might represent dormant species. At first, we explored the catalytic properties of homobinuclear adducts. An NMR solution of **12'-Cl_2** and dMAO/BHT was prepared so to reproduce the conditions of Figure 5.8a, *i.e*. large amounts of **13-Cl_3^+** and **13-Me/Cl^+** and minor amounts of monocations **14-Cl** and **14-Me**. When 1-hexene is added, most of the methylated adducts **13-Me/Cl^+** rapidly disappear from the ^{31}P NMR spectrum, while **13-Cl_3^+** remain substantially unchanged. The same peaks of Figure 5.11b around 54 and 56 ppm are observed.

While there is no available Ti-C bond in **13-Cl_3^+, 13-Me/Cl^+** can easily dissociate to give neutral methyl-chloride **12'-ClMe** or dichloride **12'-Cl_2** complex, and cationic **12'-Me^+**, with the latter being suitable for olefin coordination and subsequent chain propagation (Scheme 5.4). Coordinatively saturated **12'-ClMe** and **12'-Cl_2** should *not* be able to enter the catalytic cycle (Scheme 5.4), but we did not detect any of them after addition of 1-hexene. An analogous experiment was performed by adding 1-hexene to a mixture of fully methylated dimers **13-Me_3^+**, obtained by reaction of **12'-Me_2** and ½ eq of TTB. In this case, it could be clearly seen that **13-Me_3^+** reacts with 1-hexene and the neutral dimethyl precursor **12'-Me_2** is restored. The different observations with dMAO/BHT might suggest that, after dimer dissociation, neutral species **12'-ClMe** and **12'-Cl_2** might become more prone to reaction with MAO since they are not involved in the interaction with the naked cations anymore. The same cannot happen with TTB since the trityl cation is quantitatively consumed in the

preparation of **13-Me$_3^+$** (*i.e.* well before the addition of hexene), while non-stoichiometric amounts of MAO are used.

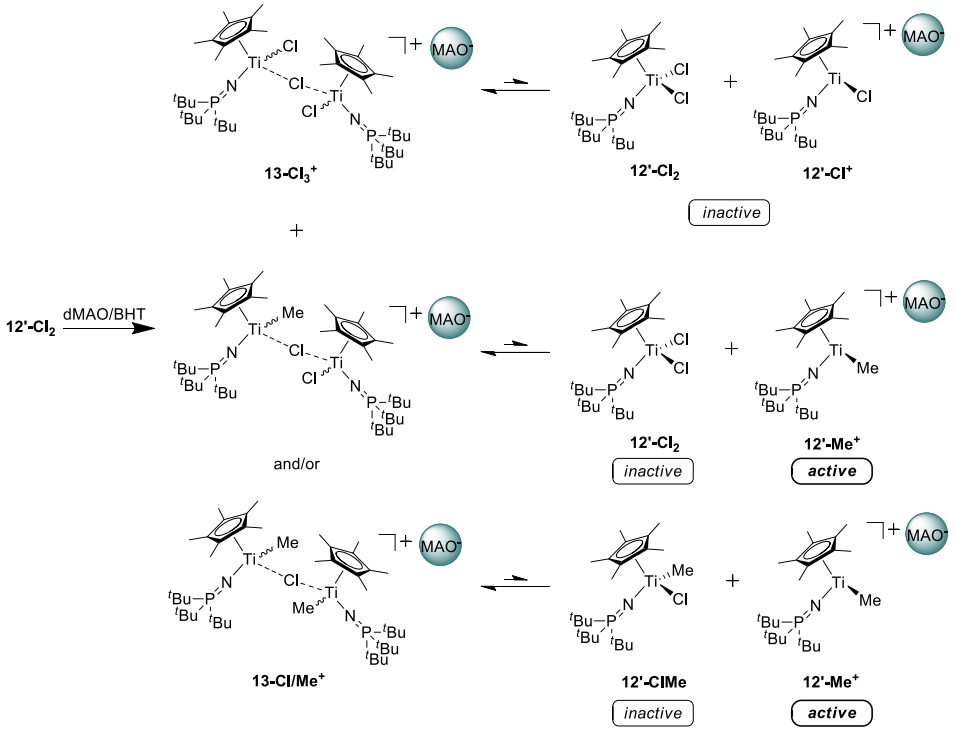

Scheme 5.4 – Schematic representation of relevant dissociation equilibria for **13-Cl$_3^+$** and **13-Me/Cl$^+$** leading to active or inactive species.

In summary, even though they do not take part in the catalytic cycle directly, homodinuclear adducts are affected by the presence of monomer, provided that the Ti-centers are alkylated. On the one hand, they are symptomatic of ineffective/incomplete activation, but on the other hand, mild interactions between the two subunits might play a positive role in stabilizing the more reactive naked cation in absence of coordinated monomer, preventing deactivation.[373] The overall quantitative effect on activity is unfortunately difficult to determine.

The second type of possible dormant sites is related to the formation of ISIP with MAO. This kind of ion pair is generally obtained when activation

occurs *via* direct abstraction by a tricoordinated aluminum of oligomeric $(AlMeO)_n$.[345-348] The resulting cationic Ti-complex can interact with different sites on MAO, namely tricoordinated Al atoms or bridging oxygen atoms on MAO clusters, with the latter being often proposed as dormant sites.[163, 165, 178, 345, 348, 375]

Experimentally, we clearly observed by ^{31}P NMR that at least most of ISIPs easily dissociate to allow monomer coordination and initiate polymerization. However, we cannot exclude that the fraction of ion pairs bearing stronger Ti-O-MAO interaction remained associated even in presence of monomer, since low concentration and broadness of the corresponding peaks might have made them undetectable under our conditions.

5.3 – Concluding Remarks

Trapping the free TMA with an hindered phenol and removig the toluene solvent under vacuum provided a *dried*-MAO/BHT powder with good solubility properties in typical deuterated solvents. This cocatalyst was used to activate the half-titanocene **12'-Cl_2** at 298 K, follow the activation by NMR, and react the activated catalyst with 1-hexene. This is one of the few examples of NMR activation studies that explored the chemistry of the enigmatic oligomeric fraction of MAO in rigorous absence of free aluminum alkyl.

NMR spectroscopy in combination with DFT, revealed that at low Al/Ti ratios, rather stable homodinuclear adducts are formed. These result from the stabilizing interaction between unsaturated cationic species obtained after addition of MAO and corresponding neutral precursors. Structural characterization indicates the presence of various isomers, and their relative stability was explored by 2D NMR and DFT calculations. Their reactivity towards olefinic monomers was evaluated as well, showing that methylated dimers easily dissociate in presence of 1-hexene, releasing the alkyl cation that initiates the chain growth. This proves that these homodinuclear species do not necessarily represent dormant sites. Addition of monomer seems to have beneficial effects also on the alkylation of chlorinated species, likely because it induces dissociation of the dimers, making the neutral precursor more prone to react with MAO. Analogous heterodinuclear adducts with $AlMe_3$ are generally expected be more stable these homodinuclear species, but no signals compatible with Ti-Me-Al fragments could be found, further confirming the effectiveness of the TMA removal.

At Al/Ti around 260, the abstraction process is complete and the dimers are fully converted to ISIP with MAO. Also in this case, addition of 1-hexene rapidly leads to dissociation of the ion pair, showing that close binding of MAO to the transition metal cation is not always associated with dormancy. We

cannot exclude however that a fraction of ISIP -especially the one featuring strong Ti-O-Al interactions- remains associated in presence of monomer, since it might be undetectable by NMR under our conditions. The species formed after addition of monomer seem to be independent from the precatalyst and the activator used. They probably correspond to cationic Ti-alkyl complexes, although no definitive proof could be found. At this stage, we can safely exclude that they correspond to **12'-Bn**$^+$ and **12'-All**$^+$, based on comparison with independently synthesized compounds, and to heterodinuclear adducts with TMA for the above reasoning. Ti-hydride species should not be stable enough to be detected since they should rapidly react with hexene and/or activate the toluene solvent.[331] Side reactions with impurities in 1-hexene seems unlikely, while intramolecular decomposition processes such as CH activation of the Cp* ligand might be plausible.

Finally, interesting insights were obtained by exploring the chemistry of the metal cation **12'-Bn**$^+$. Insertion in the Ti-Bn bond is easy also at low temperatures. Attempts to prove that benzyl cations form *via* solvent activation by a Ti-polymeryl, showed that **12'-Bn**$^+$ can be obtained at 298 K starting from activated **12'-Me**$^+$ after reaction with 1-hexene, although only under rather peculiar conditions (*i.e.* after vacuum drying the polymerization mixture). This might prove that **12'-Bn**$^+$ is a reaction intermediate of the formation of benzyl terminated polymer described in Chapter 4, and that homolysis is a competitive process in olefin polymerization also at relatively low temperature, although not as easy as at 383 K.

The sharp and well defined ^{31}P NMR peaks of cationic **12'-Bn**$^+$ allowed tentative estimation of acidic sites of MAO. The results obtained here, suggest an average cage size of oligomeric MAO of about 60 Al atoms, which is in line with previous experimental estimates.

5.4 – Experimental Part

The same general methodological considerations reported in Section 4.3 apply in this case. NMR samples were prepared in J-Young tubes by dissolving the solid reagents in the deuterated solvent. All manipulations were carried out under nitrogen in glove boxes with O_2 and H_2O levels <0.1 ppm. A large part of the NMR experiments described in this Chapter were performed on a Bruker Avance III HD 400 instrument equipped with a smartprobe at the University of Perugia.

5.4.1 – Synthetic procedures

Precatalysts, **12'-X_2** (X = Me, All, Bn; for the synthesis of X = Cl see Section 4.4.2). A solution of XMgCl in diethyl ether (2.7 mmol) was added dropwise to a stirred solution of **12'-Cl_2** (0.9 mmol) in toluene (15 mL) at 0°C. After 10 min, the resulting suspension was allowed to warm up to room temperature and stirred for 16h. In the case of **12'-All_2** the mixture was shielded from light. The suspension was filtered, dried under vacuum and recrystallized in toluene/pentane at -30°C to afford the pure products (yields 40-70%). **12'-Me_2**. ^{1}H NMR (400 MHz, tol-d_8): 2.05 (s, 15H, Cp-CH_3), 1.35 (d, 27H, J_{PH} = 12.7 Hz, C(CH_3)$_3$), 0.33 (s, 6H, Ti-CH_3) ppm. ^{13}C NMR (100 MHz, tol-d_8): 117.6 (C_5Me_5), 42.9 (Ti-CH_3), 41.1 (d, J_{PC} = 45.0 Hz, C(CH_3)$_3$), 29.6 (C(CH$_3$)$_3$), 11.8 (Cp-CH_3) ppm. ^{31}P NMR (161 MHz, tol-d_8): 31.1 ppm.

12'-All_2. ^{1}H NMR (400 MHz, tol-d_8): 6.44 (q, 2H, J^3 = 11.0 Hz, CH_2CHCH_2), 3.34 (d, 8H, CH_2CHCH_2), 2.05 (s, 15H, Cp-CH_3), 1.32 (d, 27H, J_{PH} = 12.8 Hz, C(CH_3)$_3$) ppm. ^{13}C NMR (100 MHz, tol-d_8): 146.4 (CH_2CHCH_2), 119.5 (C_5Me_5), 86.9 (CH_2CHCH_2), 41.7 (d, J_{PC} = 46.0 Hz, C(CH_3)$_3$), 30.1 (C(CH$_3$)$_3$), 12.4 (Cp-CH_3) ppm. ^{31}P NMR (161 MHz, tol-d_8): 33.6 ppm.

12'-Bn$_2$. ^{1}H NMR (400 MHz, tol-d_8): 7.20 (m, 4H, aromatic CH) 7.15 (m, 4H, aromatic CH), 6.91 (m, 2H, aromatic CH), 2.74 (d, 2H, J^2 = 11.0 Hz, Ti-CH$_2$-Ph), 2.40 (d, 2H, Ti-CH$_2$-Ph), 1.89 (s, 15H, Cp-CH$_3$), 1.26 (d, 27H, J_{PH} = 12.8 Hz, C(CH$_3$)$_3$) ppm. ^{13}C NMR (100 MHz, tol-d_8): 152.8 (quaternary aromatic C), 128.2 (aromatic CH), 127.7 (aromatic CH), 121.3 (aromatic CH), 120.3 (C_5Me$_5$), 72.5 (Ti-CH$_2$), 41.6 (d, J_{PC} = 46.0 Hz, C(CH$_3$)$_3$), 30.1 (C(CH$_3$)$_3$), 12.4 (Cp-CH$_3$) ppm. ^{31}P NMR (161 MHz, tol-d_8): 34.5 ppm.

Monomeric cations, **12'-X$^+$** (X = Me, All, Bn). These compounds were synthesized on an NMR scale by adding 0.6 mL of a suitable deuterated solvent to the solid mixture of the corresponding precursor **12'-Me$_2$** and 1 eq. of TTB. **12'-Me$^+$**. ^{1}H NMR (400 MHz, tol-d_8): 1.67 (s, 15H, Cp-CH$_3$), 0.87 (d, 27H, J_{PH} = 13.8 Hz, C(CH$_3$)$_3$) ppm. ^{13}C NMR (100 MHz, tol-d_8): 128.9 (C_5Me$_5$), 40.6 (d, J_{PC} = 40.0 Hz, C(CH$_3$)$_3$), 28.3 (C(CH$_3$)$_3$), 10.9 (Cp-CH$_3$) ppm. ^{31}P NMR (161 MHz, tol-d_8): 55.6 ppm.

12'-All$^+$. ^{1}H NMR (400 MHz, 15 v/v% C$_6$D$_4$Cl$_2$/tol-d_8): 5.69 (m, 1H, Ti-CH$_2$CHCH$_2$), 4.94 (dq, 4H, J^2 = 1.8 Hz, J^3 = 17.0 Hz, Ti-CH$_2$CHCH_2), 4.86 (dq, 4H, J^3 = 10.3 Hz, Ti-CH$_2$CHCH_2), 3.31 (d, 2H, Ti-CH_2CHCH$_2$), 1.61 (s, 15H, Cp-CH$_3$), 1.18 (d, 27H, J_{PH} = 13.6 Hz, C(CH$_3$)$_3$) ppm. ^{13}C NMR (100 MHz, 15 v/v% C$_6$D$_4$Cl$_2$/tol-d_8): 129.6 (C_5Me$_5$), 116.8 (Ti-CH$_2$CHCH_2), 93.5 (Ti-CH$_2$CHCH$_2$), 45.6 (Ti-CH_2CHCH$_2$), 42.0 (d, J_{PC} = 42.0 Hz, C(CH$_3$)$_3$), 29.0 (C(CH$_3$)$_3$), 11.5 (Cp-CH$_3$) ppm. ^{31}P NMR (161 MHz, 15 v/v% C$_6$D$_4$Cl$_2$/tol-d_8): 54.5 ppm.

12'-Bn$^+$. ^{1}H NMR (400 MHz, C$_6$D$_5$Cl): 7.57 (d, 2H, J^3 = 7.7 Hz, *o*-aromatic CH), 6.95 (m, 3H, aromatic CH), 3.65 (s, 2H, Ti-CH$_2$-Ph), 1.47 (s, 15H, Cp-CH$_3$), 1.26 (d, 27H, J_{PH} = 13.8 Hz, C(CH$_3$)$_3$) ppm. ^{13}C NMR (100 MHz, C$_6$D$_5$Cl): 146.4 (quaternary C), 134.27 (aromatic CH), 128.1 (C_5Me$_5$), 118.2 (*o*-aromatic CH), 82.0 (Ti- CH$_2$-Ph), 41.9 (d, J_{PC} = 40.0 Hz, C(CH$_3$)$_3$), 29.1 (C(CH$_3$)$_3$), 11.2 (Cp-CH$_3$) ppm. ^{31}P NMR (161 MHz, C$_6$D$_5$Cl): 55.2 ppm. Alternatively, ^{1}H NMR (400 MHz, C$_6$D$_6$): 7.41 (d, 2H, J^3 = 8.0 Hz, *o*-aromatic CH), 6.77 (m, 3H, aromatic CH), 3.56 (s, 2H, Ti-CH$_2$-

Ph), 1.30 (s, 15H, Cp-CH_3), 1.05 (d, 27H, J_{PH} = 13.7 Hz, $C(CH_3)_3$) ppm. ^{31}P NMR (161 MHz, C_6D_5Cl): 54.9 ppm.

Homodinuclear adducts, **13-Me_3^+/$[B(C_6F_5)]_4^-$.** These compounds were synthesized on an NMR scale by adding 0.6 mL of a suitable deuterated solvent to the solid mixture of the corresponding precursor **12'-X_2** and 0.5 eq. of TTB.

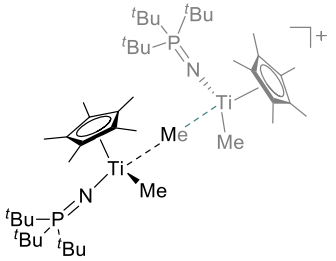

13-Me_3^+/$[B(C_6F_5)]_4^-$, ***meso* c/d**. ^1H NMR (400 MHz, tol-d_8): 1.86 (s, 15H, Cp-CH_3), 1.79 (s, 15H, Cp-CH_3), 1.25 (d, 27H, J_{PH} = 13.4 Hz, $C(CH_3)_3$), 1.18 (d, 27H, J_{PH} = 13.4 Hz, $C(CH_3)_3$), 0.64 (s, 3H, Ti-CH_3), 0.54 (s, 3H, Ti-CH_3), -0.79 (s, 3H, Ti-CH_3-Ti) ppm. ^{13}C NMR (100 MHz, tol-d_8): 122.0 (C_5Me_5), 121.8 (C_5Me_5), 55.4 (Ti-CH_3), 52.1 (Ti-CH_3), 41.1 (d, J_{PC} = 43.0 Hz, $C(CH_3)_3$), 40.9 (d, J_{PC} = 46.0 Hz, $C(CH_3)_3$), 37.2 (Ti-CH_3-Ti), 29.3 ($C(CH_3)_3$), 29.1 ($C(CH_3)_3$), 12.1 (Cp-CH_3), 12.0 (Cp-CH_3) ppm. ^{31}P NMR (161 MHz, tol-d_8): 45.2, 45.1 ppm.

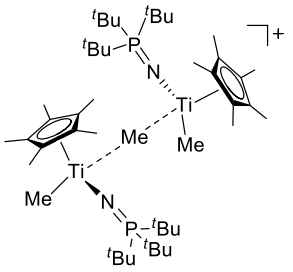

13-Me_3^+/$[B(C_6F_5)]_4^-$, ***rac* c**. ^1H NMR (400 MHz, tol-d_8): 1.88 (s, 30H, Cp-CH_3), 1.19 (d, 54H, J_{PH} = 13.6 Hz, $C(CH_3)_3$), 0.53 (s, 6H, Ti-CH_3), -0.72 (s, 3H, Ti-CH_3-Ti) ppm. ^{13}C NMR (100 MHz, tol-d_8): 122.1 (C_5Me_5), 54.0 (Ti-CH_3), 40.8 (d, J_{PC} = 44.0 Hz, $C(CH_3)_3$), 33.3 (Ti-CH_3-Ti), 29.4 ($C(CH_3)_3$), 12.2 (Cp-CH_3) ppm. ^{31}P NMR (161 MHz, tol-d_8): 44.9 ppm.

Homodinuclear adducts, **13-Me_3^+/MAO$^-$**. Pentane (5mL) was added to a solid mixture of **12'-Me_2** (25 µmol) and ~20 eq. of dMAO/BHT. After vigorously stirring the resulting suspension for 5 min, the mixture was decanted and the supernatant removed. The solid was washed three more times with pentane to remove $MeAl(bht)_2$ and excess **12'-Me_2**, dried under vacuum and redissolved in toluene-d_8 for characterization.

13-Me_3^+/MAO$^-$, ***meso* c/d**. ^1H NMR (400 MHz, tol-d_8): 2.03 (s, 15H, Cp-CH_3), 1.87

(s, 15H, Cp-CH_3), 1.42 (d, 27H, J_{PH} = 13.3 Hz, C(CH_3)$_3$), 1.31 (d, 27H, J_{PH} = 13.3 Hz, C(CH_3)$_3$), 0.71 (s, 3H, Ti-CH_3), 0.60 (s, 3H, Ti-CH_3), -0.69 (s, 3H, Ti-CH_3-Ti) ppm. ^{13}C NMR (100 MHz, tol-d_8): 122.2 (C_5Me_5), 122.2 (C_5Me_5), 55.4 (Ti-CH_3), 52.4 (Ti-CH_3), 41.5 (d, J_{PC} = 43.0 Hz, C(CH_3)$_3$), 41.2 (d, J_{PC} = 48.0 Hz, C(CH_3)$_3$), 37.6 (Ti-CH_3-Ti), 29.7 (C(CH_3)$_3$), 29.4 (C(CH_3)$_3$), 12.5 (Cp-CH_3), 12.2 (Cp-CH_3) ppm. ^{31}P NMR (161 MHz, tol-d_8): 44.7(8), 44.8(5) ppm.

13-Me_3^+/MAO$^-$, ***rac* c**. ^{1}H NMR (400 MHz, tol-d_8): 2.03 (s, 30H, Cp-CH_3), 1.36 (d, 54H, J_{PH} = 13.6 Hz, C(CH_3)$_3$), 0.61 (s, 6H, Ti-CH_3), -0.61 (s, 3H, Ti-CH_3-Ti) ppm. ^{13}C NMR (100 MHz, tol-d_8): 122.4 (C_5Me_5), 54.5 (Ti-CH_3), 41.3 (d, J_{PC} = 45.0 Hz, C(CH_3)$_3$), 33.5 (Ti-CH_3-Ti), 29.4 (C(CH_3)$_3$), 12.6 (Cp-CH_3) ppm. ^{31}P NMR (161 MHz, tol-d_8): 44.6 ppm.

5.4.2 – Computational details

The same protocol described in Chapter 4 was used, *i.e.* optimization at the RI-TPSSTPSS/cc-pVDZ-(PP) level (RI = Resolution of Identity),[333-336] followed by single point energy calculation at the M06-2X(PCM)/cc-pVTZ-(PP) level. NMR chemical shifts predictions were performed with the GIAO method[362-365] at the TPSSTPSS level in combination with basis sets optimized for this method, *i.e.* aug-cc-pVTZ-J basis set[366-370] for Ti and IGLO-III[371-386] for all other atoms. Calculated chemical shifts are internally referred to **12'-Cl_2**.

Chapter 6

Conclusion and Outlook

This thesis represents a contribution to the development of a rational approach to catalyst design in olefin polymerization. We explored some of the most intriguing aspects related to molecular olefin polymerization catalysis, trying to elucidate their origins and/or to provide novel tools for their investigation.

Factors determining comonomer affinity in ethene/α-olefin copolymerization are a prominent example. In Chapter 2, we showed that an appropriate choice of functional and basis set allows to accurately predict the polymerization parameter r_e by straightforward static DFT calculations. Trends seem to be dominated by the enthalpic preference for ethene *vs.* comonomer insertion, although some exceptions are found. For instance, an especially small entropy contribution for CGC might be the origin of its remarkable comonomer incorporation capability at high operating temperature. This type of information might prove particularly useful in the context of *in silico* catalysts pre-screening by HTC to identify high performing systems for commercial applications.

While investigating the more intricate copolymerization parameter, r_c, we identified a backbone rearrangement (BBRA) motion of the ancillary ligand occurring in the late stages of monomer capture as a potential rate limiting step for chain propagation. Barriers for BBRA were found to be competitive with those for insertion for all the variously substituted bis-indenyl *ansa*-zirconocenes explored and for the prototypical CGC. Including this process in the modeling leads to a remarkably good agreement between theory and experiments, and allows to interpret the occasionally non-trivial temperature dependence of copolymerization statistics and the role of steric bulk far from the active pocket. In summary, this computational study proved the effectiveness of the computational protocol developed within the *Laboratory of Stereoselective Polymerization* in calculating accurate barriers for monomer

insertion; furthermore, the identification of BBRA transition states contributes to the long-standing debate on the real rate determining step for chain propagation, and it can be potentially applied to the understanding of many other catalysts properties, such as MW capability.

Within the field of olefin polymerization, copolymerization is definitely the major area of application for molecular catalysts. Along with the design of novel copolymer architectures, the identification of selective ethene oligomerization catalysts for the production of comonomer feedstock is becoming a challenge of growing interest, in order to address the increasing commercial demand for advanced thermoplastics. In the realm of oligomerization Cr-catalysts, those based on BIMA ligands represent an intriguing case of selectivity, giving alternating distribution of LAOs. In Chapter 3, we described the interpretation proposed by the group of Britovsek for this peculiar product distribution, and summarized some pressure dependence studies providing supporting experimental evidence for this model. The proposed competition between single and double monomer insertion in the growing metallacycle might help in the interpretation of other catalyst systems as well (such as the Sasol PNP catalysts) and possibly in the identification of novel highly selective active species.

Finally, activity and thermal stability are two key properties to consider in catalyst development. They are generally rather difficult to rationalize, due to their strong dependence on the features of both catalyst and cocatalyst, and on the complex interactions between them. In the second part of the thesis, we focused on phosphinimide half-titanocenes, which served as interesting case study to explore some of the factors presiding over these two important properties.

Chapter 4 discussed the weak Ti-polymeryl bonds obtained during polymerization, and the role of regioerrors in further facilitating the breakage

of these Ti-C bonds *via* homolysis. This appears to be a relevant and general deactivation route, especially -but not only- for Ti-systems at high temperatures. In the case of phosphinimide catalysts in propene polymerization, we suggest that such deactivation leading to Ti(III) can be reversible, and it represents part of an unprecedented chain transfer to solvent mechanism, leading to benzyl terminated polymers when toluene is used as a solvent. The polymeryl radical obtained by Ti-C bond homolysis abstracts an H from toluene and the resulting benzyl radical recombines with Ti(III) giving a polymerization active Ti(IV)-Bn species. The DFT estimated relative barriers for insertion *vs.* further homolysis of this Ti-Bn bond correlates with the amount of benzyl chain ends obtained with different phosphinimide catalysts. The probability of Ti(III)/benzyl radical recombination is significantly affected by the nature of the cocatalyst, with MAO/BHT being a particularly favorable case.

Steric hindrance deriving from ancillary ligands, regioerrors, monomer and/or anion coordination is expected to trigger Ti-polymeryl bond cleavage and initiate the abovementioned process; the ease of homolysis with respect to propagation after 2,1 insertion determines the percentage of regioerrors leading to chain termination, affecting polymer MW. In cases were Ti(III) reduction is not reversible, homolysis leads to catalyst decay, as it is probably the case for Cp_2TiCl_2.

On the one hand, this reactivity exemplifies the complexity of the chemical processes determining catalyst activity. On the other hand, it shows some of the unexploited potentialities of molecular catalysts; for instance, the mechanism of chain transfer to solvent might allow catalytic chain end functionalization of polyolefin by group IV catalysts. Although our preliminary attempts to incorporate halogenated toluene were unsuccessful, this might represent an important contribution to the development of commercial processes for the production of novel high-performing materials.

In order to further elucidate the mechanism of this unprecedented termination process, we undertook an NMR study on the reactivity of phosphinimide complexes with dried-MAO/BHT (reported in Chapter 5). This provided experimental indications of cationic Ti-benzyl complexes deriving from solvent activation by Ti-polymeryl being a plausible reaction intermediate. Furthermore, with the help of ^{31}P NMR, we successfully to monitored the activation of dichloride complexes at increasing Al/Ti ratio and after addition of 1-hexene. In absence of TMA, and consequently of heterodinuclear Ti-(μ-Me)-Al adducts, homodinuclear Ti-(μ-Me/Cl)-Ti dimers are obtained at low MAO/BHT loadings, while ISIP rather than OSIP with MAO anions are observed after full precatalyst activation. Addition of 1-hexene demonstrated that Ti-dimers and OSIP do not necessarily represent dormant species in polymerization, although we cannot exclude that the fraction of OSIP bearing strong Ti-O-MAO bonds remains associated also in the presence of monomer. This study represents one of the few examples of NMR investigation of the oligomeric fraction of MAO under rigorous absence of TMA, and allowed us to estimate an average $(AlOMe)_n$ cage size containing roughly 60 Al-atoms, in agreement with previous reports.

In conclusion, factors determining catalytic performance are many and complex, and despite six decades of continuous progress, the mechanistic understanding of olefin polymerization related reactions is still too limited to allow catalyst design 'from scratch'. This work provides an overview of some of the most challenging topics related to the understanding of olefin polymerization, showing how advances in both experimental and computational technologies are offering the possibility of further significant improvement.

References

1. Leach, Bruce. E., Industrial Catalysis: Chemistry applied to your life-style and environment, In Applied industrial catalysis, vol 1, New York, Academic press, Inc., **1983**.
2. Anastas, P. T.; Kirchhoff, M. M.; Williamson, T. C. *Appl. Cat. A: Gen.* **2001,** *221* (1), 3-13.
3. Sauter, D.; Taoufik, M.; Boisson, C. *Polymers* **2017,** *9* (6), 185.
4. Fawcett, E.W.; Gibson, R.O. Patent GB471590, **1937**.
5. Sailors, H. R.; Hogan, J. P. *J. Macromol. Sci. A - Chem.* **1981,** *15* (7), 1377-1402.
6. Ziegler, K.; Holzkamp, E.; Breil, H.; Martin, H. *Angew. Chem.* **1955,** *67* (16), 426-426.
7. Natta, G.; Pino, P.; Corradini, P.; Danusso, F.; Mantica, E.; Mazzanti, G.; Moraglio, G. *J. Am. Chem. Soc.* **1955,** *77* (6), 1708-1710.
8. Bailey, G.C.; Reid, J.A. U.S. Patent 2381198, **1945**.
9. Hogan, J.P.; Banks, R.L. U.S. Patent 2825721, **1958**.
10. Stürzel, M.; Mihan, S.; Mülhaupt, R. *Chem. Rev.* **2016,** *116* (3), 1398-1433.
11. Data from Remco Koster, Presentation at PEPP2015.
12. Pasquini, N., Ed. Polypropylene Handbook, 2nd ed.; Hanser Publishers: Munich, **2005**.
13. Vittoria, A.; Meppelder, A.; Friederichs, N.; Busico, V.; Cipullo, R. *ACS Catal.* **2017,** *7* (7), 4509-4518.
14. Credendino, R.; Liguori, D.; Fan, Z.; Morini, G.; Cavallo, L. *ACS Catal.* **2015,** *5* (9), 5431-5435.
15. D'Amore, M.; Thushara, K. S.; Piovano, A.; Causà, M.; Bordiga, S.; Groppo, E. *ACS Catal.* **2016,** *6* (9), 5786-5796.
16. Morra, E.; Giamello, E.; Van Doorslaer, S.; Antinucci, G.; D'Amore, M.; Busico, V.; Chiesa, M. *Angew. Chem. Int. Ed.* **2015,** *54* (16), 4857-4860.
17. Busico, V. In Giulio Natta and the Development of Stereoselective Propene Polymerization in Polyolefins: 50 years after Ziegler and Natta; Kaminsky, W., Ed.; Springer: Heidelberg, Germany, **2013**; Vol. 257, pp 37−58.
18. Tabone, M. D.; Cregg, J. J.; Beckman, E. J.; Landis, A. E. *Environ. Sci. Technol.* **2010,** *44* (21), 8264-8269.
19. Simpson, D. M.; Vaughan, G. A., *Encyclopedia of Polymer Science and Technology*. 4th ed.; John Wiley & Sons, Inc., Hoboken, N. J: **2014**; Vol. 5.
20. Bohm, L. L.; Enderle, H. F.; Fleißner, M. *Adv. Mater.* **1992,** *4* (3), 234-238.
21. Porter, R. S.; Kanamoto, T.; Zachariades, A. E. *Polymer* **1994,** *35* (23), 4979-4984.

22. Stevens, J. C., Constrained geometry and other single site metallocene polyolefin catalysts: A revolution in olefin polymerization. In *Studies in Surface Science and Catalysis*, Joe W. Hightower, W. N. D. E. I.; Alexis, T. B., Eds. Elsevier: **1996**; Vol. Volume 101, pp 11-20.
23. Natta, G.; Pino, P.; Mazzanti, G.; Giannini, U. *J. Am. Chem. Soc.* **1957,** *79* (11), 2975-2976.
24. Chien, J. C. W.; Wang, B.-P. *J. Polym. Sci. A: Polym. Chem.* **1988,** *26* (11), 3089-3102.
25. Sinn, H.; Patat, F. *Angew. Chem.* **1963,** *75* (18), 805-813.
26. Long, W. P.; Breslow, D. S. *J. Am. Chem. Soc.* **1960,** *82* (8), 1953-1957.
27. Breslow, D. S.; Newburg, N. R. *J. Am. Chem. Soc.* **1957,** *79* (18), 5072-5073.
28. Andresen, A.; Cordes, H.-G.; Herwig, J.; Kaminsky, W.; Merck, A.; Mottweiler, R.; Pein, J.; Sinn, H.; Vollmer, H.-J. *Angew. Chem. Int. Ed. Eng.* **1976,** *15* (10), 630-632.
29. Sinn, H.; Kaminsky, W.; Vollmer, H.-J.; Woldt, R. *Angew. Chem. Int. Ed. Eng.* **1980,** *19* (5), 390-392.
30. Kaminsky, W.; Steiger, R. *Polyhedron* **1988,** *7* (22), 2375-2381.
31. Kaminsky, W. *Macromolecules* **2012,** *45* (8), 3289-3297.
32. Severn, J.; Robert, L. In Handbook of Transition Metal Polymerization Catalysts; Hoff, R., Mathers, R. T., Eds.; John Wiley and Sons: New York, 2010; p 157.
33. Kaminsky, W. *J. Polym. Sci. A: Polym. Chem.* **2004,** *42* (16), 3911-3921.
34. Alt, H. G.; Köppl, A. *Chem. Rev.* **2000,** *100* (4), 1205-1222.
35. Kaminsky, W. *Macromol. Symp.* **2016,** *360* (1), 10-22.
36. Britovsek, G. J. P.; Gibson, V. C.; Wass, D. F. *Angew. Chem. Int. Ed.* **1999,** *38* (4), 428-447.
37. Gibson, V. C.; Spitzmesser, S. K. *Chem. Rev.* **2003,** *103* (1), 283-316.
38. Baier, M. C.; Zuideveld, M. A.; Mecking, S. *Angew. Chem. Int. Ed.* **2014,** *53* (37), 9722-9744.
39. Stevens, J. C.; Timmers, F. J.; Wilson, D. R.; Schmidt, G. F.; Nickias, P. N.; Rosen, R. K.; Knight, G. W.; Lai, S.-y. Eur. Pat. Appl. 0 416 815 A2, **1991**.
40. Stevens, J. C.; Neithamer, D. R. Eur. Pat. Appl. 0 418044 A2, **1991**.
41. Canich, J. A. M. U.S. Patent 5,026,798, **1991**.
42. Canich, J. A. M.; Licciardi, G. F. U.S. Patent 5,057,475, **1991**.
43. McKnight, A. L.; Waymouth, R. M. *Chem. Rev.* **1998,** *98* (7), 2587-2598.
44. Klosin, J.; Fontaine, P. P.; Figueroa, R. *Acc. Chem. Res.* **2015,** *48* (7), 2004-2016.
45. Dilworth, J. R.; de Liefde Meijer, H. J.; Teuben, J. H. *J. Organomet. Chem.* **1978,** *159* (1), 47-52.
46. Stephan, D. W.; Stewart, J. C.; Guérin, F.; Spence, R. E. v. H.; Xu, W.; Harrison, D. G. *Organometallics* **1999,** *18* (7), 1116-1118.

47. Stephan, D. W. *Macromol. Symp.* **2001,** *173* (1), 105-116.
48. Stephan, D. W. *Organometallics* **2005,** *24* (11), 2548-2560.
49. Stephan, D. W.; Steward, J. C.; Brown, S. J.; Swabey, J. W.; Wang, Q. EP0881233 (A1), **1998**.
50. Von Haken Spence, R. E.; Stephan, D.; Brown, S. J.; Jeremic, D.; Wang, Q. EP1112276 (A1) **2001**.
51. Brown, S. J.; Dobbin, C. J. B.; Elston, C. T.; Aubee, N. D. J.; Arnould, G. A.; Marshall, S.; Kale, L. T.; Weber, M. US2004086671 (A1), **2004**.
52. Hoang, P. P. M.; Baar, C.; Chisholm, P. S.; Patel, R. D. WO2013026131 (A1), **2013**.
53. Severn, J. R.; Berthoud, R.; Kidd, T. J. WO2015059280 (A1), **2015**.
54. Severn, J. R.; Berthoud, R.; Kidd, T. J. WO2015059268 (A1), **2015**.
55. Windmuller, P.; Doremaele Van, G. US2011021732 (A1), **2011**.
56. Ferreira, M. J.; Martins, A. M. *Coord. Chem. Rev.* **2006,** *250* (1), 118-132.
57. J. McMeeking, X. Gao, R. E. v.H. Spence, S. J. Brown, D. Jeremic, WO 99/14250, **1999**.
58. E.G. Ijpeij, P. J. H.Windmuller, H. J. Arts, F. van der Burgt, G. H. J. van Doremaele, M.A. Zuideveld, (DSM), WO 2005/090418 A1, **2005**;
59. P. J.H. Windmuller, G. H. J. van Dore-maele, WO2005/005496 A2, **2005**;
60. van Doremaele, G.; van Duin, M.; Valla, M.; Berthoud, A. *J. Polym. Sci. A: Polym. Chem.* **2017,** *55* (18), 2877-2891.
61. Cozzi, P. G.; Gallo, E.; Floriani, C.; Chiesi-Villa, A.; Rizzoli, C. *Organometallics* **1995,** *14* (11), 4994-4996.
62. Makio, H.; Terao, H.; Iwashita, A.; Fujita, T. *Chem. Rev.* **2011,** *111* (3), 2363-2449.
63. T. Fujita,Y. Thoi, M. Mitani, S. Matsui, J. Saito,M. Nitabaru,K. Sugi, H. Makio, T. Tsutsui, (Mitsui Chemicals), EP 0 874 005 B1, **1997**.
64. Wenzel, T. T.; Arriola, D. J.; Carnahan, E. M.; Hustad, P. D.; Kuhlman, R. L., Chain Shuttling Catalysis and Olefin Block Copolymers (OBCs). In *Metal Catalysts in Olefin Polymerization*, Guan, Z., Ed. Springer Berlin Heidelberg: Berlin, Heidelberg, **2009**; pp 65-104.
65. Britovsek, G. J. P.; Cohen, S. A.; Gibson, V. C.; van Meurs, M. *J. Am. Chem. Soc.* **2004,** *126* (34), 10701-10712.
66. Britovsek, G. J. P.; Cohen, S. A.; Gibson, V. C.; Maddox, P. J.; van Meurs, M. *Angew. Chem. Int. Ed.* **2002,** *41* (3), 489-491.
67. Hustad, P. D. *Science* **2009,** *325* (5941), 704-707.
68. Cossee, P. *J. Catal.* **1964,** *3* (1), 80-88.
69. Brookhart, M.; Green, M. L. H. *J. Organomet. Chem.* **1983,** *250* (1), 395-408.
70. Margl, P.; Deng, L.; Ziegler, T. *J. Am. Chem. Soc.* **1999,** *121* (1), 154-162.
71. Resconi, L.; Camurati, I.; Sudmeijer, O. *Top. Catal.* **1999,** *7* (1), 145-163.

72. Busico, V.; Cipullo, R.; Mingione, A.; Rongo, L. *Ind. Eng. Chem. Res.* **2016,** *55* (10), 2686-2695.
73. High Throughput Screening inCatalysis, eds.A.Hagemeyer, P. Strasser and A. F. Volpe, Jr.,Wiley-VCH,Weinheim, **2004**.
74. Busico, V. *Dalton Trans.* **2009,** (41), 8794-8802.
75. Möhring, P. C.; Coville, N. J. *Coord. Chem. Rev.* **2006,** *250* (1–2), 18-35.
76. Cruz, V. L.; Martinez, S.; Ramos, J.; Martinez-Salazar, J. *Organometallics* **2014,** *33* (12), 2944-2959.
77. Rappé, A. K.; Skiff, W. M.; Casewit, C. J. *Chem. Rev.* **2000,** *100* (4), 1435-1456.
78. Angermund, K.; Fink, G.; Jensen, V. R.; Kleinschmidt, R. *Chem. Rev.* **2000,** *100* (4), 1457-1470.
79. Rappè, A. K.; Casewit, C. J. Molecular Mechanics Across Chemistry; University Science Books: Sausalito, CA, **1997**.
80. Corradini, P.; Guerra, G.; Cavallo, L. *Acc. Chem. Res.* **2004,** *37* (4), 231-241.
81. Guerra, G.; Longo, P.; Cavallo, L.; Corradini, P.; Resconi, L. *J. Am. Chem. Soc.* **1997,** *119* (19), 4394-4403.
82. Jolly, C. A.; Marynick, D. S. *J. Am. Chem. Soc.* **1989,** *111* (20), 7968-7974.
83. Kawamura-Kuribayashi, H.; Koga, N.; Morokuma, K. *J. Am. Chem. Soc.* **1992,** *114* (7), 2359-2366.
84. Kawamura-Kuribayashi, H.; Koga, N.; Morokuma, K. *J. Am. Chem. Soc.* **1992,** *114* (22), 8687-8694.
85. Yoshida, T.; Koga, N.; Morokuma, K. *Organometallics* **1995,** *14* (2), 746-758.
86. Lohrenz, J. C. W.; Woo, T. K.; Ziegler, T. *J. Am. Chem. Soc.* **1995,** *117* (51), 12793-12800.
87. Margl, P.; Deng, L.; Ziegler, T. *Organometallics* **1998,** *17* (5), 933-946.
88. Margl, P.; Deng, L.; Ziegler, T. *J. Am. Chem. Soc.* **1998,** *120* (22), 5517-5525.
89. Wondimagegn, T.; Wang, D.; Razavi, A.; Ziegler, T. *Organometallics* **2009,** *28* (5), 1383-1390.
90. Flisak, Z.; Ziegler, T. *Proc. Nat. Ac. Sci.* **2006,** *103* (42), 15338-15342.
91. Yoshida, T.; Koga, N.; Morokuma, K. *Organometallics* **1996,** *15* (2), 766-777.
92. Froese, R. D. J.; Musaev, D. G.; Morokuma, K. *J. Mol. Struc. THEOCHEM* **1999,** *461–462*, 121-135.
93. Corradini, P.; Busico, V.; Cavallo, L.; Guerra, G.; Vacatello, M.; Venditto, V. *J. Mol. Cat.* **1992,** *74* (1), 433-442.
94. Resconi, L.; Cavallo, L.; Fait, A.; Piemontesi, F. *Chem. Rev.* **2000,** *100* (4), 1253-1346.

95. Talarico, G.; Blok, A. N. J.; Woo, T. K.; Cavallo, L. *Organometallics* **2002,** *21* (23), 4939-4949.
96. Falivene, L.; Cavallo, L.; Talarico, G. *ACS Catal.* **2015,** *5* (11), 6815-6822.
97. Scuseria, G. E.; III, H. F. S. *J. Chem. Phys.***1989,** *90* (7), 3700-3703.
98. J. Cížek, in Advances in Chemical Physics, Ed. P. C. Hariharan, Vol. 14 (Wiley Interscience, New York, **1969**) 35.
99. Wang, D.; Tomasi, S.; Razavi, A.; Ziegler, T. *Organometallics* **2008,** *27* (12), 2861-2867.
100. Talarico, G.; Busico, V.; Cavallo, L. *Organometallics* **2004,** *23* (25), 5989-5993.
101. Talarico, G.; Busico, V.; Cavallo, L. *J. Am. Chem. Soc.* **2003,** *125* (24), 7172-7173.
102. Kohn, W.; Sham, L. J. *Phys. Rev.* **1965,** *140* (4A), A1133-A1138.
103. Hohenberg, P.; Kohn, W. *Phys. Rev.* **1964,** *136* (3B), B864-B871.
104. Ehm, C.; Budzelaar, P. H. M.; Busico, V. *J. Organomet. Chem.* **2015,** *775*, 39-49.
105. Ehm, C.; Antinucci, G.; Budzelaar, P. H. M.; Busico, V. *J. Organomet. Chem.* **2014,** *772–773*, 161-171.
106. Correa, A.; Cavallo, L. *J. Am. Chem. Soc.* **2006,** *128* (33), 10952-10959.
107. Schnutenhaus, H.; Brintzinger, H. H. *Angew. Chem. Int. Ed. Eng.* **1979,** *18* (10), 777-778.
108. Ewen, J. A. *J. Am. Chem. Soc.* **1984,** *106* (21), 6355-6364.
109. Corradini, P.; Barone, V.; Fusco, R.; Guerra, G. *Eur. Polym. J.* **1979,** *15* (12), 1133-1141.
110. Kaminsky, W.; Külper, K.; Brintzinger, H. H.; Wild, F. R. W. P. *Angew. Chem. Int. Ed. Eng.* **1985,** *24* (6), 507-508.
111. Erker, G.; Nolte, R.; Aul, R.; Wilker, S.; Krueger, C.; Noe, R. *J. Am. Chem. Soc.* **1991,** *113* (20), 7594-7602.
112. Ewen, J. A. *J. Mol. Cat. A: Chem.* **1998,** *128* (1), 103-109.
113. Busico, V.; Cipullo, R. *Prog. Polym. Sci.* **2001,** *26* (3), 443-533.
114. Yoder, J. C.; Bercaw, J. E. *J. Am. Chem. Soc.* **2002,** *124* (11), 2548-2555.
115. Busico, V.; Cipullo, R. *J. Am. Chem. Soc.* **1994,** *116* (20), 9329-9330.
116. Busico, V.; Cipullo, R.; Talarico, G.; Segre, A. L.; Chadwick, J. C. *Macromolecules* **1997,** *30* (16), 4786-4790.
117. Miller, S. A.; Bercaw, J. E. *Organometallics* **2006,** *25* (15), 3576-3592.
118. Talarico, G.; Budzelaar, P. H. M. *Organometallics* **2016,** *35* (1), 47-54.
119. De Rosa, C.; Di Girolamo, R.; Talarico, G. *ACS Catal.* **2016,** *6* (6), 3767-3770.
120. Talarico, G.; Budzelaar, P. H. M. *Organometallics* **2014,** *33* (21), 5974-5982.

121. Domski, G. J.; Eagan, J. M.; De Rosa, C.; Di Girolamo, R.; LaPointe, D. A. M.; Lobkovsky, E. B.; Talarico, G.; Coates, G. W. *ACS Catal.* **2017**, *7* (10), 6930-6937.
122. Talarico, G.; Budzelaar, P. H. M. *Macromolecules* **2017,** *50* (14), 5332-5336.
123. Talarico, G.; Budzelaar, P. H. M. *J. Am. Chem. Soc.* **2006,** *128* (14), 4524-4525.
124. Naga, N.; Ohbayashi, Y.; Mizunuma, K. *Macromol. Rapid Commun.* **1997,** *18* (9), 837-851.
125. Seraidaris, T.; Kaminsky, W.; Seppälä, J. V.; Löfgren, B. *Macromol. Chem. Phys.* **2005,** *206* (13), 1319-1325.
126. Tynys, A.; Saarinen, T.; Hakala, K.; Helaja, T.; Vanne, T.; Lehmus, P.; Löfgren, B. *Macromol. Chem. Phys.* **2005,** *206* (10), 1043-1056.
127. Wondimagegn, T.; Wang, D.; Razavi, A.; Ziegler, T. *Organometallics* **2008,** *27* (24), 6434-6439.
128. Laine, A.; Linnolahti, M.; Pakkanen, T. A.; Severn, J. R.; Kokko, E.; Pakkanen, A. *Organometallics* **2011,** *30* (6), 1350-1358.
129. Stehling, U.; Diebold, J.; Kirsten, R.; Roell, W.; Brintzinger, H. H.; Juengling, S.; Muelhaupt, R.; Langhauser, F. *Organometallics* **1994,** *13* (3), 964-970.
130. Talarico, G.; Budzelaar, P. H. M. *Organometallics* **2008,** *27* (16), 4098-4107.
131. Friederichs, N.; Wang, B.; Budzelaar, P. H. M.; Coussens, B. B. *J. Mol. Cat. A: Chem.* **2005,** *242* (1–2), 91-104.
132. Fan, W.; Waymouth, R. M. *Macromolecules* **2001,** *34* (25), 8619-8625.
133. Schneider, M. J.; Suhm, J.; Mülhaupt, R.; Prosenc, M.-H.; Brintzinger, H.-H. *Macromolecules* **1997,** *30* (11), 3164-3168.
134. Burfield, D. R. *Macromolecules* **1987,** *20* (12), 3020-3023.
135. Alizadeh, A.; Richardson, L.; Xu, J.; McCartney, S.; Marand, H.; Cheung, Y. W.; Chum, S. *Macromolecules* **1999,** *32* (19), 6221-6235.
136. Xu, X.; Xu, J.; Feng, L.; Chen, W. *J. Appl. Polym. Sci.* **2000,** *77* (8), 1709-1715.
137. Bensason, S.; Minick, J.; Moet, A.; Chum, S.; Hiltner, A.; Baer, E. *J. Polym. Sci. B: Polym. Phys.* **1996,** *34* (7), 1301-1315.
138. Piel, C.; Starck, P.; Seppälä, J. V.; Kaminsky, W. *J. Polym. Sci. A: Polym. Chem.* **2006,** *44* (5), 1600-1612.
139. Dankova, M.; Waymouth, R. M. *Macromolecules* **2003,** *36* (11), 3815-3820.
140. Reybuck, S. E.; Meyer, A.; Waymouth, R. M. *Macromolecules* **2002,** *35* (3), 637-643.
141. Kunz, K.; Erker, G.; Kehr, G.; Fröhlich, R.; Jacobsen, H.; Berke, H.; Blacque, O. *J. Am. Chem. Soc.* **2002,** *124* (13), 3316-3326.

142. Lehmus, P.; Kokko, E.; Härkki, O.; Leino, R.; Luttikhedde, H. J. G.; Näsman, J. H.; Seppälä, J. V. *Macromolecules* **1999,** *32* (11), 3547-3552.
143. Klosin, J.; Kruper, W. J.; Nickias, P. N.; Roof, G. R.; De Waele, P.; Abboud, K. A. *Organometallics* **2001,** *20* (13), 2663-2665.
144. Xu, Z.; Vanka, K.; Ziegler, T. *Organometallics* **2004,** *23* (1), 104-116.
145. Lanza, G.; Fragalà, I. L.; Marks, T. J. *Organometallics* **2002,** *21* (25), 5594-5612.
146. Laine, A.; Coussens, B. B.; Hirvi, J. T.; Berthoud, A.; Friederichs, N.; Severn, J. R.; Linnolahti, M. *Organometallics* **2015,** *34* (11), 2415-2421.
147. Schrock, R. R.; Bonitatebus, P. J.; Schrodi, Y. *Organometallics* **2001,** *20* (6), 1056-1058.
148. Yang, X.; Stern, C. L.; Marks, T. J. *J. Am. Chem. Soc.* **1994,** *116* (22), 10015-10031.
149. Zuccaccia, C.; Tensi, L.; Kuhlman, R. L.; Gies, A. P.; Macchioni, A. *ACS Catal.* **2017,** *7* (1), 563-567.
150. Chen, Y.-X.; Marks, T. J. *Organometallics* **1997,** *16* (16), 3649-3657.
151. Zhang, S.; Piers, W. E. *Organometallics* **2001,** *20* (10), 2088-2092.
152. Bochmann, M.; Cuenca, T.; Hardy, D. T. *J. Organomet. Chem.* **1994,** *484* (1-2), c10-c12.
153. Rocchigiani, L.; Busico, V.; Pastore, A.; Macchioni, A. *Organometallics* **2016,** *35* (9), 1241-1250.
154. Rios, I. G.; Novarino, E.; van der Veer, S.; Hessen, B.; Bouwkamp, M. W. *J. Am. Chem. Soc.* **2009,** *131* (46), 16658-16659.
155. Wu, F.; Dash, A. K.; Jordan, R. F. *J. Am. Chem. Soc.* **2004,** *126* (47), 15360-15361.
156. Flisak, Z. *J. Phys. Chem. A* **2012,** *116* (5), 1464-1468.
157. Chen, E. Y.-X.; Marks, T. J. *Chem. Rev.* **2000,** *100* (4), 1391-1434.
158. Zijlstra, H. S.; Harder, S. *Eur. J. Inorg. Chem.* **2015,** *2015* (1), 19-43.
159. Linnolahti, M.; Severn, J. R.; Pakkanen, T. A. *Angew. Chem.* **2008,** *120* (48), 9419-9423.
160. Linnolahti, M.; Severn, J. R.; Pakkanen, T. A. *Angew. Chem. Int. Ed.* **2006,** *45* (20), 3331-3334.
161. Falls, Z.; Tymińska, N.; Zurek, E. *Macromolecules* **2014,** *47* (24), 8556-8569.
162. Boudene, Z.; De Bruin, T.; Toulhoat, H.; Raybaud, P. *Organometallics* **2012,** *31* (23), 8312-8322.
163. Tymińska, N.; Zurek, E. *ACS Catal.* **2015,** *5* (11), 6989-6998.
164. Zurek, E.; Ziegler, T. *Prog. Polym. Sci.* **2004,** *29* (2), 107-148.
165. Zurek, E.; Ziegler, T. *Organometallics* **2002,** *21* (1), 83-92.
166. Zurek, E.; Woo, T. K.; Firman, T. K.; Ziegler, T. *Inorg. Chem.* **2001,** *40* (2), 361-370.

167. Harlan, C. J.; Bott, S. G.; Barron, A. R. *J. Am. Chem. Soc.* **1995,** *117* (24), 6465-6474.
168. Mason, M. R.; Smith, J. M.; Bott, S. G.; Barron, A. R. *J. Am. Chem. Soc.* **1993,** *115* (12), 4971-4984.
169. Trefz, T. K.; Henderson, M. A.; Wang, M. Y.; Collins, S.; McIndoe, J. S. *Organometallics* **2013,** *32* (11), 3149-3152.
170. Zijlstra, H. S.; Stuart, M. C. A.; Harder, S. *Macromolecules* **2015,** *48* (15), 5116-5119.
171. Cam, D.; Giannini, U. *Makromol. Chem.* **1992,** *193* (5), 1049-1055.
172. Siedle, A. R.; Newmark, R. A.; Lamanna, W. M.; Schroepfer, J. N. *Polyhedron* **1990,** *9* (2), 301-308.
173. Tritto, I.; Sacchi, M. C.; Li, S. *Macromol. Rapid Commun.* **1994,** *15* (3), 217-223.
174. Tritto, I.; Sacchi, M. C.; Locatelli, P.; Li, S. X. *Macromol. Symp.* **1995,** *97* (1), 101-108.
175. Theurkauff, G.; Bondon, A.; Dorcet, V.; Carpentier, J.-F.; Kirillov, E. *Angew. Chem. Int. Ed.* **2015,** *54* (21), 6343-6346.
176. Ehm, C.; Cipullo, R.; Budzelaar, P. H. M.; Busico, V. *Dalton Trans.* **2016,** *45* (16), 6847-6855.
177. Bochmann, M.; Lancaster, S. J. *Angew. Chem. Int. Ed. Eng.* **1994,** *33* (15-16), 1634-1637.
178. Babushkin, D. E.; Semikolenova, N. V.; Zakharov, V. A.; Talsi, E. P. *Macromol. Chem. Phys.* **2000,** *201* (5), 558-567.
179. Song, F.; Cannon, R. D.; Bochmann, M. *J. Am. Chem. Soc.* **2003,** *125* (25), 7641-7653.
180. Pédeutour, J.-N.; Radhakrishnan, K.; Cramail, H.; Deffieux, A. *J. Mol. Cat. A: Chem.* **2002,** *185* (1–2), 119-125.
181. Resconi, L.; Bossi, S.; Abis, L. *Macromolecules* **1990,** *23* (20), 4489-4491.
182. Ghiotto, F.; Pateraki, C.; Severn, J. R.; Friederichs, N.; Bochmann, M. *Dalton Trans.* **2013,** *42* (25), 9040-9048.
183. Kickham, J. E.; Guérin, F.; Stewart, J. C.; Stephan, D. W. *Angew. Chem. Int. Ed.* **2000,** *39* (18), 3263-3266.
184. Kickham, J. E.; Guérin, F.; Stewart, J. C.; Urbanska, E.; Stephan, D. W. *Organometallics* **2001,** *20* (6), 1175-1182.
185. Yang, X.; Stern, C. L.; Marks, T. J. *J. Am. Chem. Soc.* **1991,** *113* (9), 3623-3625.
186. Ewen, J. A.; Elder, M. J., Eur. Patent Appl. 0,427,697, **1991**.
187. Scollard, J. D.; McConville, D. H.; Rettig, S. J. *Organometallics* **1997,** *16* (8), 1810-1812.
188. Wondimagegn, T.; Xu, Z.; Vanka, K.; Ziegler, T. *Organometallics* **2005,** *24* (9), 2076-2085.

189. Wondimagegn, T.; Xu, Z.; Vanka, K.; Ziegler, T. *Organometallics* **2004,** *23* (16), 3847-3852.
190. Yue, N.; Hollink, E.; Guérin, F.; Stephan, D. W. *Organometallics* **2001,** *20* (21), 4424-4433.
191. Guérin, F.; Stewart, J. C.; Beddie, C.; Stephan, D. W. *Organometallics* **2000,** *19* (16), 2994-3000.
192. Arndt, P.; Jäger-Fiedler, U.; Klahn, M.; Baumann, W.; Spannenberg, A.; Burlakov, V. V.; Rosenthal, U. *Angew. Chem. Int. Ed.* **2006,** *45* (25), 4195-4198.
193. Busico, V.; Cipullo, R.; Cutillo, F.; Friederichs, N.; Ronca, S.; Wang, B. *J. Am. Chem. Soc.* **2003,** *125* (41), 12402-12403.
194. Busico, V.; Cipullo, R.; Pellecchia, R.; Talarico, G.; Razavi, A. *Macromolecules* **2009,** *42* (6), 1789-1791.
195. Machat, M. R.; Jandl, C.; Rieger, B. *Organometallics* **2017,** *36* (7), 1408-1418.
196. Tanaka, R.; Kawahara, T.; Shinto, Y.; Nakayama, Y.; Shiono, T. *Macromolecules* **2017,** *50* (15), 5989-5993.
197. Macchioni, A. *Chem. Rev.* **2005,** *105* (6), 2039-2074.
198. Alonso-Moreno, C.; Lancaster, S. J.; Wright, J. A.; Hughes, D. L.; Zuccaccia, C.; Correa, A.; Macchioni, A.; Cavallo, L.; Bochmann, M. *Organometallics* **2008,** *27* (21), 5474-5487.
199. Song, F.; Lancaster, S. J.; Cannon, R. D.; Schormann, M.; Humphrey, S. M.; Zuccaccia, C.; Macchioni, A.; Bochmann, M. *Organometallics* **2005,** *24* (6), 1315-1328.
200. Wass, D. F. *Dalton Trans.* **2007,** (8), 816-819.
201. van Leeuwen, P. W. N. M.; Clément, N. D.; Tschan, M. J. L. *Coord. Chem. Rev.* **2011,** *255* (13–14), 1499-1517.
202. Boffa, L. S.; Novak, B. M. *Chem. Rev.* **2000,** *100* (4), 1479-1494.
203. Lin, W.; Dong, J.; Chung, T. C. M. *Macromolecules* **2008,** *41* (22), 8452-8457.
204. Lee, J.-Y.; Tsai, J.-C. *J. Polym. Sci. A: Polym. Chem.* **2011,** *49* (17), 3739-3750.
205. Aaltonen, P.; Fink, G.; Löfgren, B.; Seppälä, J. *Macromolecules* **1996,** *29* (16), 5255-5260.
206. Imuta, J.-i.; Kashiwa, N.; Toda, Y. *J. Am. Chem. Soc.* **2002,** *124* (7), 1176-1177.
207. Yang, X.-H.; Liu, C.-R.; Wang, C.; Sun, X.-L.; Guo, Y.-H.; Wang, X.-K.; Wang, Z.; Xie, Z.; Tang, Y. *Angew. Chem. Int. Ed.* **2009,** *48* (43), 8099-8102.
208. Johnson, L. K.; Mecking, S.; Brookhart, M. *J. Am. Chem. Soc.* **1996,** *118* (1), 267-268.
209. Rieth, L. R.; Eaton, R. F.; Coates, G. W. *Angew. Chem. Int. Ed.* **2001,** *40* (11), 2153-2156.
210. Boaen, N. K.; Hillmyer, M. A. *Chem. Soc. Rev.* **2005,** *34* (3), 267-275.

211. Kawahara, N.; Saito, J.; Matsuo, S.; Kaneko, H.; Matsugi, T.; Kashiwa, N., Polymer Hybrids Based on Polyolefins – Syntheses, Structures, and Properties. In *New Frontiers in Polymer Synthesis*, Kobayashi, S., Ed. Springer Berlin Heidelberg: Berlin, Heidelberg, **2008**; pp 79-119.
212. Britovsek, G. J. P.; McGuinness, D. S.; Wierenga, T. S.; Young, C. T. *ACS Catal.* **2015,** *5* (7), 4152-4166.
213. Britovsek, G. J. P.; Malinowski, R.; McGuinness, D. S.; Nobbs, J. D.; Tomov, A. K.; Wadsley, A. W.; Young, C. T. *ACS Catal.* **2015,** *5* (11), 6922-6925.
214. Losio, S.; Stagnaro, P.; Motta, T.; Sacchi, M. C.; Piemontesi, F.; Galimberti, M. *Macromolecules* **2008,** *41* (4), 1104-1111.
215. Arriola, D. J.; Bokota, M.; Campbell, R. E.; Klosin, J.; LaPointe, R. E.; Redwine, O. D.; Shankar, R. B.; Timmers, F. J.; Abboud, K. A. *J. Am. Chem. Soc.* **2007,** *129* (22), 7065-7076.
216. Koivumaeki, J.; Fink, G.; Seppaelae, J. V. *Macromolecules* **1994,** *27* (22), 6254-6258.
217. Busico, V.; Cipullo, R.; Segre, A. L. *Macromol. Chem. Phys.* **2002,** *203*, 1403-1412.
218. Brintzinger, H. H.; Fischer, D.; Mülhaupt, R.; Rieger, B.; Waymouth, R. M. *Angew. Chem. Int. Ed. Eng.* **1995,** *34* (11), 1143-1170.
219. Curtin, D. Y. *Rec. Chem. Prog.* **1954**, *15*, 111.
220. Coleman, P. C. P. a. M. M., *Essentials of Polymer Science and Engineering*. DEStech Publications, Inc: **2009**.
221. Mayo, F. R.; Lewis, F. M. *J. Am. Chem. Soc.* **1944,** *66* (9), 1594-1601.
222. Fineman, M.; Ross, S. D. *Journal of Polymer Science* **1950,** *5* (2), 259-262.
223. Kakugo, M.; Naito, Y.; Mizunuma, K.; Miyatake, T. *Macromolecules* **1982,** *15* (4), 1150-1152.
224. Randall, J. C. *Journal of Macromolecular Science, Part C* **1989,** *29* (2-3), 201-317.
225. Forlini, F.; Tritto, I.; Locatelli, P.; Sacchi, M. C.; Piemontesi, F. *Macromol. Chem. Phys.* **2000,** *201* (4), 401-408.
226. Ehm, C.; Budzelaar, P. H. M.; Busico, V. *J. Catal.* **2017,** *351*, 146-152.
227. Ehm, C.; Budzelaar, P. H. M.; Busico, V. *Eur. J. Inorg. Chem.* **2017,** *2017* (27), 3343-3349.
228. Tomasi, J. *Theor. Chem. Acc.* **2004,** *112* (4), 184-203.
229. Galimberti, M.; Piemontesi, F.; Fusco, O.; Camurati, I.; Destro, M. *Macromolecules* **1998,** *31* (11), 3409-3416.
230. Zambelli, A.; Grassi, A.; Galimberti, M.; Mazzocchi, R.; Piemontesi, F. *Makromol. Chem., Rapid Commun.* **1991,** *12* (8), 523-528.
231. Galimberti, M.; Piemontesi, F.; Mascellani, N.; Camurati, I.; Fusco, O.; Destro, M. *Macromolecules* **1999,** *32* (24), 7968-7976.

232. Kissin, Y., *Alkene Polymerization Reactions with Transition Metal Catalysts*. Elsevier, Amsterdam, The Netherlands: **2008**.
233. Nomura, K.; Oya, K.; Imanishi, Y. *J. Mol. Cat. A: Chem.* **2001,** *174* (1–2), 127-140.
234. Nomura, K.; Fujita, K.; Fujiki, M. *J. Mol. Cat. A: Chem.* **2004,** *220* (2), 133-144.
235. Galimberti, M.; Mascellani, N.; Piemontesi, F.; Camurati, I. *Macromol. Rapid Commun.* **1999,** *20* (4), 214-218.
236. Castro, L.; Kirillov, E.; Miserque, O.; Welle, A.; Haspeslagh, L.; Carpentier, J.-F.; Maron, L. *ACS Catal.* **2015,** *5* (1), 416-425.
237. Grimme, S.; Ehrlich, S.; Goerigk, L. *J. Comput. Chem.* **2011,** *32* (7), 1456-1465.
238. Grimme, S.; Antony, J.; Ehrlich, S.; Krieg, H. *J. Chem. Phys.***2010,** *132* (15), 154104.
239. Heiland, K.; Kaminsky, W. *Makromol. Chem.* **1992,** *193* (3), 601-610.
240. Suhm, J.; Schneider, M. J.; Mülhaupt, R. *J. Polym. Sci. A: Polym. Chem.* **1997,** *35* (4), 735-740.
241. Suhm, J.; Schneider, M. J.; Mülhaupt, R. *J. Mol. Cat. A: Chem.* **1998,** *128* (1–3), 215-227.
242. Lu, L.; Niu, H.; Dong, J.-Y.; Zhao, X.; Hu, X. *J. Appl. Polym. Sci.* **2010,** *118* (6), 3218-3226.
243. Margl, P.; Deng, L.; Ziegler, T. *J. Am. Chem. Soc.* **1998,** *121* (1), 154-162.
244. Sauriol, F.; Wong, E.; Leung, A. M. H.; Donaghue, I. E.; Baird, M. C.; Wondimagegn, T.; Ziegler, T. *Angew. Chem. Int. Ed.* **2009,** *48* (18), 3342-3345.
245. O'Connor, J. M.; Casey, C. P. *Chem. Rev.* **1987,** *87* (2), 307-318.
246. Gridnev, I. D. *Coord. Chem. Rev.* **2008,** *252* (15–17), 1798-1818.
247. Calhorda, M. J.; Veiros, L. s. F. *Coord. Chem. Rev.* **1999,** *185–186*, 37-51.
248. Gaussian 09, Revision B.01, Frisch, M. J.; Trucks, G. W.; Schlegel, H. B.; Scuseria, G. E.; Robb, M. A.; Cheeseman, J. R.; Scalmani, G.; Barone, V.; Mennucci, B.; Petersson, G. A.; Nakatsuji, H.; Caricato, M.; Li, X.; Hratchian, H. P.; Izmaylov, A. F.; Bloino, J.; Zheng, G.; Sonnenberg, J. L.; Hada, M.; Ehara, M.; Toyota, K.; Fukuda, R.; Hasegawa, J.; Ishida, M.; Nakajima, T.; Honda, Y.; Kitao, O.; Nakai, H.; Vreven, T.; Montgomery, J. A., Jr.; Peralta, J. E.; Ogliaro, F.; Bearpark, M.; Heyd, J. J.; Brothers, E.; Kudin, K. N.; Staroverov, V. N.; Kobayashi, R.; Normand, J.; Raghavachari, K.; Rendell, A.; Burant, J. C.; Iyengar, S. S.; Tomasi, J.; Cossi, M.; Rega, N.; Millam, M. J.; Klene, M.; Knox, J. E.; Cross, J. B.; Bakken, V.; Adamo, C.; Jaramillo, J.; Gomperts, R.; Stratmann, R. E.; Yazyev, O.; Austin, A. J.; Cammi, R.; Pomelli, C.; Ochterski, J. W.; Martin, R. L.; Morokuma, K.; Zakrzewski, V. G.; Voth, G. A.; Salvador, P.; Dannenberg, J. J.; Dapprich, S.; Daniels, A. D.; Farkas, Ö.; Foresman, J. B.; Ortiz, J. V.; Cioslowski, J.; Fox, D. J. Gaussian, Inc., Wallingford CT, 2009.
249. J. Baker, 2.4 ed., Parallel Quantum Solutions, Fayetteville, AR, 2001.

250. Baker, J. *J. Comput. Chem.* **1986,** *7* (4), 385-395.
251. Budzelaar, P. H. M. *J. Comput. Chem.* **2007,** *28* (13), 2226-2236.
252. Peng, C.; Ayala, P. Y.; Schlegel, H. B.; Frisch, M. J. *J. Comput. Chem.* **1996,** *17* (1), 49-56.
253. Peng, C.; Bernhard Schlegel, H. *Isr. J. Chem.* **1993,** *33* (4), 449-454.
254. Tao, J.; Perdew, J. P.; Staroverov, V. N.; Scuseria, G. E. *Phys. Rev. Letters* **2003,** *91* (14), 146401.
255. Dunning, T. H. *J. Chem. Phys.* **1989,** *90* (2), 1007-1023.
256. Kendall, R. A.; Dunning, T. H.; Harrison, R. J. *J. Chem. Phys.* **1992,** *96* (9), 6796-6806.
257. Woon, D. E.; Dunning, T. H. *J. Chem. Phys.* **1995,** *103* (11), 4572-4585.
258. Peterson, K. A.; Dunning, T. H. *J. Chem. Phys.* **2002,** *117* (23), 10548-10560.
259. Woon, D. E.; Dunning, T. H. *J. Chem. Phys.* **1993,** *98* (2), 1358-1371.
260. Wilson, A. K.; Woon, D. E.; Peterson, K. A.; Dunning, T. H. *J. Chem. Phys.* **1999,** *110* (16), 7667-7676.
261. Peterson, K. A.; Yousaf, K. E. *J. Chem. Phys.* **2010,** *133* (17), 174116.
262. Feller, D. *J. Comput. Chem.* **1996,** *17* (13), 1571-1586.
263. Schuchardt, K. L.; Didier, B. T.; Elsethagen, T.; Sun, L. S.; Gurumoorthi, V.; Chase, J.; Li, J.; Windus, T. L. *J. Chem. Inf. Model.* **2007,** *47* (3), 1045-1052.
264. Schwerdtfeger, P. *ChemPhysChem* **2011,** *12* (17), 3143-3155.
265. Figgen, D.; Rauhut, G.; Dolg, M.; Stoll, H. *Chem. Phys.* **2005,** *311* (1-2), 227-244.
266. Metz, B.; Stoll, H.; Dolg, M. *J. Chem. Phys.* **2000,** *113* (7), 2563-2569.
267. Metz, B.; Schweizer, M.; Stoll, H.; Dolg, M.; Liu, W. J. *Theor. Chem. Acc.* **2000,** *104* (1), 22-28.
268. Zhao, Y.; Truhlar, D. G. *Theor. Chem. Acc.* **2008,** *120* (1-3), 215-241.
269. Zaccaria, F.; Cipullo, R.; Budzelaar, P. H. M.; Busico, V.; Ehm, C. *J. Polym. Sci. A: Polym. Chem.* **2017,** *55* (17), 2807-2814.
270. Tobisch, S.; Ziegler, T. *J. Am. Chem. Soc.* **2004,** *126* (29), 9059-9071.
271. Dunlop-Brière, A. F.; Budzelaar, P. H. M.; Baird, M. C. *Organometallics* **2012,** *31*, 1591-1594.
272. Raucoules, R.; de Bruin, T.; Raybaud, P.; Adamo, C. *Organometallics* **2009,** *28* (18), 5358-5367.
273. Forestière, A.; Olivier-Bourbigou, H.; Saussine, L. *Oil & Gas Sci. Technol. - Rev. IFP* **2009,** *64* (6), 649-667.
274. Speiser, F.; Braunstein, P.; Saussine, L. *Acc. Chem. Res.* **2005,** *38* (10), 784-793.
275. Keim, W. *Angew. Chem. Int. Ed.* **2013,** *52* (48), 12492-12496.
276. Agapie, T. *Coord. Chem. Rev.* **2011,** *255* (7–8), 861-880.
277. Fischer, K.; Jonas, K.; Misbach, P.; Stabba, R.; Wilke, G. *Angew. Chem. Int. Ed. Eng.* **1973,** *12* (12), 943-953.

278. Ziegler, K.; Gellert, G. H.; Holzkamp, E.; Wilke, G.; *Brennst. Chem.*, **1954**, *35*, 321-325
279. Ziegler, K.; *Brennst. Chem.*, **1954**, *35*, 193
280. Johnson, L. K.; Killian, C. M.; Brookhart, M. *J. Am. Chem. Soc.* **1995,** *117* (23), 6414-6415.
281. Killian, C. M.; Johnson, L. K.; Brookhart, M. *Organometallics* **1997,** *16* (10), 2005-2007.
282. O'Connor, K. S.; Lamb, J. R.; Vaidya, T.; Keresztes, I.; Klimovica, K.; LaPointe, A. M.; Daugulis, O.; Coates, G. W. *Macromolecules* **2017**.
283. Musaev, D. G.; Froese, R. D. J.; Svensson, M.; Morokuma, K. *J. Am. Chem. Soc.* **1997,** *119* (2), 367-374.
284. Rose, J. M.; Cherian, A. E.; Coates, G. W. *J. Am. Chem. Soc.* **2006,** *128* (13), 4186-4187.
285. Stapleton, R. A.; Chai, J.; Nuanthanom, A.; Flisak, Z.; Nele, M.; Ziegler, T.; Rinaldi, P. L.; Soares, J. B. P.; Collins, S. *Macromolecules* **2007,** *40* (9), 2993-3004.
286. Al-Sa'doun, A. W. *Appl. Cat. A: Gen.* **1993,** *105* (1), 1-40.
287. Al-Jarallah, A. M.; Anabtawi, J. A.; Siddiqui, M. A. B.; Aitani, A. M.; Al-Sa'doun, A. W. *Catal. Today* **1992,** *14* (1), 1-121.
288. Robinson, R.; McGuinness, D. S.; Yates, B. F. *ACS Catal.* **2013,** *3* (12), 3006-3015.
289. R. M. Manyik, W. E. Walker and T. P. Wilson, Union Carbide Corporation, US Pat., 3 300 458 , **1967**.
290. Reagen, W. K.; McDaniel, M. P. US5438027, **1995.**
291. Dixon, J. T.; Green, M. J.; Hess, F. M.; Morgan, D. H. *J. Organomet. Chem.* **2004,** *689* (23), 3641-3668.
292. Bollmann, A.; Blann, K.; Dixon, J. T.; Hess, F. M.; Killian, E.; Maumela, H.; McGuinness, D. S.; Morgan, D. H.; Neveling, A.; Otto, S.; Overett, M.; Slawin, A. M. Z.; Wasserscheid, P.; Kuhlmann, S. *J. Am. Chem. Soc.* **2004,** *126* (45), 14712-14713.
293. Manyik, R. M.; Walker, W. E.; Wilson, T. P. *J. Catal.* **1977,** *47* (2), 197-209.
294. Briggs, J. R. *J. Chem. Soc., Chem. Commun.* **1989,** (11), 674-675.
295. McGuinness, D. S. *Chem. Rev.* **2011,** *111* (3), 2321-2341.
296. Jabri, A.; Mason, C. B.; Sim, Y.; Gambarotta, S.; Burchell, T. J.; Duchateau, R. *Angew. Chem. Int. Ed.* **2008,** *47* (50), 9717-9721.
297. Vidyaratne, I.; Nikiforov, G. B.; Gorelsky, S. I.; Gambarotta, S.; Duchateau, R.; Korobkov, I. *Angew. Chem. Int. Ed.* **2009,** *48* (35), 6552-6556.
298. McGuinness, D. S.; Chan, B.; Britovsek, G. J. P.; Yates, B. F. *Aust. J. Chem.* **2014,** *67* (10), 1481-1490.
299. Budzelaar, P. H. M. *Can. J. Chem.* **2009,** *87* (7), 832-837.

300. Tomov, A. K.; Gibson, V. C.; Britovsek, G. J. P.; Long, R. J.; van Meurs, M.; Jones, D. J.; Tellmann, K. P.; Chirinos, J. J. *Organometallics* **2009,** *28* (24), 7033-7040.
301. Agapie, T.; Labinger, J. A.; Bercaw, J. E. *J. Am. Chem. Soc.* **2007,** *129* (46), 14281-14295.
302. Tomov, A. K.; Chirinos, J. J.; Jones, D. J.; Long, R. J.; Gibson, V. C. *J. Am. Chem. Soc.* **2005,** *127* (29), 10166-10167.
303. Tenza, K.; Hanton, M. J.; Slawin, A. M. Z. *Organometallics* **2009,** *28* (16), 4852-4867.
304. Tomov, A. K.; Chirinos, J. J.; Long, R. J.; Gibson, V. C.; Elsegood, M. R. J. *J. Am. Chem. Soc.* **2006,** *128* (24), 7704-7705.
305. Britovsek, G. J. P.; McGuinness, D. S.; Tomov, A. K. *Catal. Sci. Technol.* **2016,** *6* (23), 8234-8241.
306. Britovsek, G. J. P.; McGuinness, D. S. *Chem. Eur. J.* **2016,** *22* (47), 16891-16896.
307. Tomov, A. K.; Nobbs, J. D.; Chirinos, J. J.; Saini, P. K.; Malinowski, R.; Ho, S. K. Y.; Young, C. T.; McGuinness, D. S.; White, A. J. P.; Elsegood, M. R. J.; Britovsek, G. J. P. *Organometallics* **2017,** *36* (3), 510-522.
308. Flory, P. J. *J. Am. Chem. Soc.* **1936,** *58* (10), 1877-1885.
309. Ystenes, M. *J. Catal.* **1991,** *129* (2), 383-401.
310. Marques, M. M.; Dias, A. R.; Costa, C.; Lemos, F.; Ramôa Ribeiro, F. *Polymer Int.* **1997,** *43* (1), 77-85.
311. Kelly, W. M.; Wang, S.; Collins, S. *Macromolecules* **1997,** *30* (11), 3151-3158.
312. Young, C. T. Ethylene Oligomerization and Polymerization: Catalyst Synthesis, Mechanism and Product Analysis. PhD Thesis, Imperial College London (UK), **2017**.
313. Cariou, R.; Chirinos, J. J.; Gibson, V. C.; Jacobsen, G.; Tomov, A. K.; Britovsek, G. J. P.; White, A. J. P. *Dalton Trans.* **2010,** *39* (38), 9039-9045.
314. Kubler, P.; Sundermeyer, J. *Dalton Trans.* **2014,** *43* (9), 3750-3766.
315. Dellinger, D. J.; Sheehan, D. M.; Christensen, N. K.; Lindberg, J. G.; Caruthers, M. H. *J. Am. Chem. Soc.* **2003,** *125* (4), 940-950.
316. Hoang, P. P. M.; Lam, P.; Ker, V.; Shaw, B. M.; Baar, C. CA2742454 (A1), **2012**.
317. Lam, P.; Ker, V.; Carter, C. A. G.; Shaw, B. M.; Baar, C.; Kazakov, A.; McKay, I. D.; Jeremic, D. US2012238720 (A1), **2012**.
318. Stephan, D. W.; Stewart, J. C.; Guérin, F.; Courtenay, S.; Kickham, J.; Hollink, E.; Beddie, C.; Hoskin, A.; Graham, T.; Wei, P.; Spence, R. E. v. H.; Xu, W.; Koch, L.; Gao, X.; Harrison, D. G. *Organometallics* **2003,** *22* (9), 1937-1947.
319. Von Haken Spence, R. E.; Kock, L.; Jeremic, D.; Berown, S. J. US6234950 (B1), **2001**.

320. Ehm, C.; Cipullo, R.; Passaro, M.; Zaccaria, F.; Budzelaar, P. H. M.; Busico, V. *ACS Catal.* **2016,** *6* (11), 7989-7993.
321. Passaro, M. Solvent Activation by Ti(IV) organometallic species. Master Thesis in Chemical Sciences, University of Naples Federico II, **2016**.
322. Bryliakov, K. P.; Babushkin, D. E.; Talsi, E. P.; Voskoboynikov, A. Z.; Gritzo, H.; Schröder, L.; Damrau, H.-R. H.; Wieser, U.; Schaper, F.; Brintzinger, H. H. *Organometallics* **2005,** *24* (5), 894-904.
323. Lindeman, L. P.; Adama, J. Q. *Anal. Chem.* **1971,** *43* (10), 1245-1252.
324. Cipullo, R.; Mellino, S.; Busico, V. *Macromol. Chem. Phys.* **2014,** *215* (18), 1728-1734.
325. Jeske, G.; Schock, L. E.; Swepston, P. N.; Schumann, H.; Marks, T. J. *J. Am. Chem. Soc.* **1985,** *107* (26), 8103-8110.
326. Bunel, E.; Burger, B. J.; Bercaw, J. E. *J. Am. Chem. Soc.* **1988,** *110* (3), 976-978.
327. Barrera Galland, G.; Da Silva, L. P.; Dias, M. L.; Crossetti, G. L.; Ziglio, C. M.; Filgueiras, C. A. L. *J. Polym. Sci. A: Polym. Chem.* **2004,** *42* (9), 2171-2178.
328. Lü, C.; Zhang, Y.; Mu, Y. *J. Mol. Cat. A: Chem.* **2006,** *258* (1), 146-151.
329. Ruiz-Orta, C.; Fernandez-Blazquez, J. P.; Anderson-Wile, A. M.; Coates, G. W.; Alamo, R. G. *Macromolecules* **2011,** *44* (9), 3436-3451.
330. Luo, Y. R. Comprehensive Handbook of Chemical Bond Energies; CRC Press: Boca Raton, FL, **2007**.
331. Ma, K.; Piers, W. E.; Gao, Y.; Parvez, M. *J. Am. Chem. Soc.* **2004,** *126* (18), 5668-5669.
332. Ma, K.; Piers, W. E.; Parvez, M. *J. Am. Chem. Soc.* **2006,** *128* (10), 3303-3312.
333. Whitten, J. L. *J. Chem. Phys.***1973,** *58*, 4496.
334. Baerends, E. J.; Ellis, D. E.; Ros, P. *Chem. Phys.* **1973,** *2* (1), 41-51.
335. Feyereisen, M.; Fitzgerald, G.; Komornicki, A. *Chem. Phys. Letters* **1993,** *208* (5), 359-363.
336. Vahtras, O.; Almlöf, J.; Feyereisen, M. W. *Chem. Phys. Letters* **1993,** *213* (5), 514-518.
337. Fong, A.; Peters, B.; Scott, S. L. *ACS Catal.* **2016,** *6* (9), 6073-6085.
338. van Leeuwen, P. W. N. M.; Chadwick, J. C. In Homogeneous Catalysts; Wiley−VCH Verlag GmbH & Co. KGaA: Weinheim, Germany, **2011**.
339. Bochmann, M. *J. Organomet. Chem.* **2004,** *689* (24), 3982-3998.
340. Ciancaleoni, G.; Fraldi, N.; Cipullo, R.; Busico, V.; Macchioni, A.; Budzelaar, P. H. M. *Macromolecules* **2012,** *45* (10), 4046-4053.
341. Crabtree, R. H. *Chem. Rev.* **2015,** *115* (1), 127-150.
342. Song, F.; Cannon, R. D.; Lancaster, S. J.; Bochmann, M. *J. Mol. Cat. A: Chem.* **2004,** *218* (1), 21-28.
343. Jüngling, S.; Mülhaupt, R.; Stehling, U.; Brintzinger, H.-H.; Fischer, D.; Langhauser, F. *Macromol. Symp.* **1995,** *97* (1), 205-216.

344. Landis, C. R.; Sillars, D. R.; Batterton, J. M. *J. Am. Chem. Soc.* **2004,** *126* (29), 8890-8891.
345. Kuklin, M. S.; Hirvi, J. T.; Bochmann, M.; Linnolahti, M. *Organometallics* **2015,** *34* (14), 3586-3597.
346. Ghiotto, F.; Pateraki, C.; Tanskanen, J.; Severn, J. R.; Luehmann, N.; Kusmin, A.; Stellbrink, J.; Linnolahti, M.; Bochmann, M. *Organometallics* **2013,** *32* (11), 3354-3362.
347. Hirvi, J. T.; Bochmann, M.; Severn, J. R.; Linnolahti, M. *ChemPhysChem* **2014,** *15* (13), 2732-2742.
348. Zurek, E.; Ziegler, T. *Inorg. Chem.* **2001,** *40* (14), 3279-3292.
349. Tritto, I.; Donetti, R.; Sacchi, M. C.; Locatelli, P.; Zannoni, G. *Macromolecules* **1997,** *30* (5), 1247-1252.
350. Bryliakov, K. P.; Talsi, E. P.; Bochmann, M. *Organometallics* **2004,** *23* (1), 149-152.
351. Pédeutour, J.-N.; Radhakrishnan, K.; Cramail, H.; Deffieux, A. *Macromol. Rapid Commun.* **2001,** *22* (14), 1095-1123.
352. Reddy, S. S.; Shashidhar, G.; Sivaram, S. *Macromolecules* **1993,** *26* (5), 1180-1182.
353. Ioku, A.; Hasan, T.; Shiono, T.; Ikeda, T. *Macromol. Chem. Phys.* **2002,** *203* (4), 748-755.
354. Michiue, K.; Jordan, R. F. *J. Mol. Cat. A: Chem.* **2008,** *282* (1–2), 107-116.
355. Hasan, T.; Ioku, A.; Nishii, K.; Shiono, T.; Ikeda, T. *Macromolecules* **2001,** *34* (10), 3142-3145.
356. Rocchigiani, L.; Busico, V.; Pastore, A.; Macchioni, A. *Dalton Trans.* **2013,** *42* (25), 9104-9111.
357. Panchenko, V. N.; Zakharov, V. A.; Danilova, I. G.; Paukshtis, E. A.; Zakharov, I. I.; Goncharov, V. G.; Suknev, A. P. *J. Mol. Cat. A: Chem.* **2001,** *174* (1–2), 107-117.
358. Stellbrink, J.; Niu, A.; Allgaier, J.; Richter, D.; Koenig, B. W.; Hartmann, R.; Coates, G. W.; Fetters, L. J. *Macromolecules* **2007,** *40* (14), 4972-4981.
359. Cabrera, L.; Hollink, E.; Stewart, J. C.; Wei, P.; Stephan, D. W. *Organometallics* **2005,** *24* (6), 1091-1098.
360. Friesen, D. M.; Piers, W. E.; Parvez, M. *Organometallics* **2008,** *27* (24), 6596-6604.
361. Smith, J. C.; Ma, K.; Piers, W. E.; Parvez, M.; McDonald, R. *Dalton Trans.* **2010,** *39* (42), 10256-10263.
362. McWeeny, R. *Phys. Rev.* **1962,** *126* (3), 1028-1034.
363. Ditchfield, R. *Molecular Physics* **1974,** *27* (4), 789-807.
364. Wolinski, K.; Hinton, J. F.; Pulay, P. *J. Am. Chem. Soc.* **1990,** *112* (23), 8251-8260.

365. Cheeseman, J. R.; Trucks, G. W.; Keith, T. A.; Frisch, M. J. *J. Chem. Phys.***1996,** *104* (14), 5497-5509.
366. Enevoldsen, T.; Oddershede, J.; Sauer, S. P. A. *Theor. Chem. Acc.* **1998,** *100* (5), 275-284.
367. Sauer, S. P. A.; Raynes, W. T. *J. Chem. Phys.***2000,** *113* (8), 3121-3129.
368. Sauer, S. P. A.; Raynes, W. T.; Nicholls, R. A. *J. Chem. Phys.***2001,** *115* (13), 5994-6006.
369. Provasi, P. F.; Aucar, G. A.; Sauer, S. P. A. *J. Chem. Phys.***2001,** *115* (3), 1324-1334.
370. Barone, V.; Provasi, P. F.; Peralta, J. E.; Snyder, J. P.; Sauer, S. P. A.; Contreras, R. H. *J. Phys. Chem. A* **2003,** *107* (23), 4748-4754.
371. Schindler, M.; Kutzelnigg, W. *J. Chem. Phys.* **1982,** *76* (4), 1919-1933.
372. Kutzelnigg, W.; Fleischer, U.; Schindler, M. The IGLOMethod: Ab Initio Calculation Interpretation of NMR Chemical Shifts Magnetic Susceptibilities; Springer-Verlag: Heidelberg, Germany, **1990**; 23
373. Beck, S.; Prosenc, M.-H.; Brintzinger, H.-H.; Goretzki, R.; Herfert, N.; Fink, G. *J. Mol. Cat. A: Chem.* **1996,** *111* (1), 67-79.
374. Babushkin, D. E.; Brintzinger, H.-H. *J. Am. Chem. Soc.* **2002,** *124* (43), 12869-12873.
375. Tritto, I.; Sacchi, M. C.; Locatelli, P.; Li, S. X. *Macromol. Symp.* **1995,** *89* (1), 289-298.
376. Gies, A. P.; Kuhlman, R. L.; Zuccaccia, C.; Macchioni, A.; Keaton, R. J. *Organometallics* **2017,** *36* (18), 3443-3455.
377. Jeske, G.; Lauke, H.; Mauermann, H.; Swepston, P. N.; Schumann, H.; Marks, T. J. *J. Am. Chem. Soc.* **1985,** *107* (26), 8091-8103.
378. Eshuis, J. J. W.; Tan, Y. Y.; Meetsma, A.; Teuben, J. H.; Renkema, J.; Evens, G. G. *Organometallics* **1992,** *11* (1), 362-369.
379. Lieber, S.; Prosenc, M.-H.; Brintzinger, H.-H. *Organometallics* **2000,** *19* (4), 377-387.
380. Margl, P. M.; Woo, T. K.; Ziegler, T. *Organometallics* **1998,** *17* (23), 4997-5002.
381. Vatamanu, M. *J. Catal.* **2015,** *323*, 112-120.
382. Vatamanu, M.; Stojcevic, G.; Baird, M. C. *J. Am. Chem. Soc.* **2008,** *130* (2), 454-456.
383. Chen, C.-H.; Shih, W.-C.; Hilty, C. *J. Am. Chem. Soc.* **2015,** *137* (21), 6965-6971.
384. Flisak, Z.; Ziegler, T. *Proc. Nat. Ac. Sci.* **2006,** *103* (42), 15338-15342.
385. Bochmann, M.; Lancaster, S. J. *Organometallics* **1993,** *12* (3), 633-640.
386. Kutzelnigg, W.; Fleischer, U.; Schindler, M. The IGLOMethod: Ab Initio Calculation Interpretation of NMR Chemical Shifts Magnetic Susceptibilities; Springer-Verlag: Heidelberg, Germany, **1990**; 23

Appendix - PhD Course Activity Summary

Candidate: Francesco Zaccaria **Supervisor:** Prof. Vincenzo Busico

1) Attended Courses (6 minimum, 8 hours each):

- *Computational Chemistry* (Prof. Nadia Rega, March-June 2015).
- *Advanced Mass Spectrometry* (Prof. Piero Pucci, June-July 2015).
- *Origins of Chirality and Asymmetric Synthesis* (Prof. Giovanni Palumbo, October 2015).
- *Neutron Scattering* (Prof. Reiner Zorn, October 2015).
- *Chemical Reactors for Solid–Gas Processes Aimed at Energy Production* (Prof. Fabio Montagnaro, February 2016).
- *Techniques of Solid-Liquid Extraction Used in the Preparation of Samples for Chemical Analysis and Production of Extracts for Industrial Uses* (Prof. Daniele Naviglio, March 2016).

2) Attended Seminars:

Title	Speaker	Date	Place
Advanced Technology for Life Sciences by Using TEM	Dr. Paolo Grianti	24/11/2014	DSC-UniNa
Characterization of Complex Ethylene-Propylene Copolymers – A Journey Inside the Analytical Techniques	Dr. Benjamin Monrabal	27/11/2014	DSC-UniNa
Le Fitotossine: un'Avventura Lunga 40 Anni	Prof. Antonio Evidente	10/12/2014	DSC-UniNa
New Chiral Catalysis Derived from Iron(II) and Bismuth(III) for Asymmetric Synthesis	Prof. Thierry Ollevier	15/12/2014	DSC-UniNa
Enhanced Sampling Techniques Aimed at Characterizing Protein-Ligand Binding for Drug Design Applications	Dr. Walter Rocchia	22/12/2014	DSC-UniNa
On the Conformational Stability of Globular Protein	Prof. Giuseppe Graziano	06/02/2015	DSC-UniNa
Multiscale Modeling of Soft Materials: Atoms, Beads and Fields	Prof. Giuseppe Milano	19/02/2015	DSC-UniNa

In Searching of the Chemical Basis of the Origin of Life: from Experiments to the Space missions (I)	Prof. Guido Barone	23/02/2015	DSC-UniNa
In Searching of the Chemical Basis of the Origin of Life: from Experiments to the Space missions (II)	Prof. Guido Barone	27/02/2015	DSC-UniNa
European Large Facilities: Neutron and Synchroton Sources	Prof. Serge Perez	06/05/2015	DSC-UniNa
La Normativa di Riferimento per la Professione del Chimico	Prof. Luigi Romano	13/05/2015	DSC-UniNa
Pharmaceutical Companies: External Manufacturing and Quality Assurance	Dr. Domenico Demasi	25/05/2015	DSC-UniNa
Biosensing and Bioelectronics Based on Organic Electrochemical Devices: from Monitoring Drug Dynamics to Hybrid Bio-organic Memristive Devices	Dr. Salvatore Iannota	11/06/2015	DSC-UniNa
Transglutaminases from Polyamine to Bioplastics	Prof. Raffaele Porta	30/06/2015	DSC-UniNa
Effect of Graphene Oxide in Disentangled Polyethylene and LLDPE	Dr. Sara Ronca	17/07/2015	DSC-UniNa
Disentangled UHMWPE: Synthesis to Mechanical Properties	Dr. Sara Ronca	17/07/2015	DSC-UniNa
Bleaching Systems in Domestic Laundry Detergents	Dr. Giulia Bianchetti	29/10/2015	DSC-UniNa
Scientific Calculator	Prof. Michele Vacatello	11/11/2015	DSC-UniNa
Multimodal Approaches for Preclinical Molecular Imaging	Dr. Menichetti and Dr. Chiariello	05/02/2016	DSC-UniNa
Basics of Detergents Formulations and Challenges	Dr. Giulia Bianchetti	16/03/2016	DSC-UniNa
Progettazione, Risk-assesment e Controllo Qualità del Packaging Alimentare: il ruolo inatteso del Chimico	Dr. Vincenzo Benessere	17/03/2016	DSC-UniNa
The versatility of Mesoscopic Solar Cells	Prof. Anders Hagfeldt	14/04/2016	DSC-UniNa

Supramolecular Chemistry of Chiral Calixarenes	Prof. Mauro Mocerino	13/01/2017	DSC-UniNa
Modified Nucleotides and oligonucleotides for Biomedical Applications	Prof. Daniela Montesarchio	18/01/2017	DSC-UniNa
Using ab-initio methods to describe ground and excited state reactivity	Dr. Ilaria Ciofini	31/10/2017	DSC-UniNa

DSC-UniNa = Dept. of Chemical Sciences – University of Naples Federico II

3) Attended Integration Exams (for candidates not graduated in Chemical Science):

Title	Professor	Date
-	-	-

4) Visiting periods in Institutions different from the University of Naples Federico II:

Host Institution	Country	Start Date	End Date
University of Perugia	Italy	16/11/2016	25/11/2016
Imperial College London	United Kingdom	03/04/2017	06/07/2017
University of Perugia	Italy	19/09/2017	22/09/2017

5) Publications (include submitted and in preparation):

- Ehm, C.; Cipullo, R.; Passaro, M.; Zaccaria, F.; Budzelaar, P. H. M.; Busico, V., Chain Transfer to Solvent in Propene Polymerization with Ti Cp-phosphinimide Catalysts: Evidence for Chain Termination via Ti–C Bond Homolysis. *ACS Catal.* **2016**, *6*, 7989-7993.
- Zaccaria, F.; Ehm, C.; Budzelaar, P. H. M.; Busico, V., Accurate Prediction of Copolymerization Statistics in Molecular Olefin Polymerization Catalysis: The Role of Entropic, Electronic, and Steric

Effects in Catalyst Comonomer Affinity. *ACS Catal.* **2017**, *7*, 1512-1519.

- Zaccaria, F.; Cipullo, R.; Budzelaar, P. H. M.; Busico, V.; Ehm, C., Backbone rearrangement during olefin capture as the rate limiting step in molecular olefin polymerization catalysis and its effect on comonomer affinity. *J. Polym. Sci. Part A*, **2017**, *55*, 2807-2814.

6) Attended congresses/workshops/summer schools:

- *National School of Nuclear Magnetic Resonance - Basic Module,* University of Turin (I), August 2015.
- *10th International School of Organometallic Chemistry,* University of Camerino (I), September 2015.
- *Bioeconomy in the Circular Economy*, University of Naples (I), January 2016.
- *Dutch Polymer Institute Research Training Course in Polyolefins Block 1. Chemistry / Catalysis / Polymer Microstructure – Advanced Module,* Sorrento (I), June 2016.
- *4th Blue Sky Conference on Catalytic Olefin Polymerization*, Sorrento (I), July 2016.
- *National School of Nuclear Magnetic Resonance - Advanced Module,* University of Turin (I), September 2016.
- *6thEuCheMS Chemistry Congress*, Seville (E), September 2016.
- *EuCheMS International Organometallic Conference XXII*, Amsterdam (NL), July 2017.

7) Other Activities:

- *PhD delegate at the Students Orientation Commission of the Department of Chemical Sciences* - University of Naples Federico II, February 2016 – October 2017.